Imperial College of Science, Technology and Medicine
Department of Physics

Intertwined Order in Strongly Correlated Quantum Systems

Milan Rakic

Submitted in partial fulfillment of the requirements for the degree of Doctor of Philosophy in Physics of Imperial College of Science, Technology and Medicine
August 2024

"Some days I'm walking backwards.
Truth be told, I don't mind"

Abstract

Supersolids are a fascinating quantum phase of matter that have both superfluid and solid properties, and are in some ways an extension of a superfluid, in that it possesses an additional rich and dynamic set of phenomenological features. Supersolids are an example of strongly correlated intertwined order, which is the notion that systems can form phases of matter that are more than the sum of its parts. Put simply, a supersolid is not a superfluid + solid. This intertwined order generates new and exciting physics which looks a little like its constituent components, but also not at all.

In this thesis we develop a homogenisation technique, which begins with a microscopic theory of a supersolid and ends with a phenomenological Lagrangian. By doing this we marry two opposite ends of supersolid theory, providing the phenomenological toolset to study supersolids, but rooted in the foundation of microscopic theory.

We derive the mathematical framework necessary to employ homogenisation, apply it to the Gross-Pitaevskii Lagrangian, elucidate crucial contributions from the thermodynamic ensemble of a supersolid, and obtain an effective theory of the Goldstone modes. We conduct numerics on a soft-core bosonic system, applying homogenisation to our simulated supersolids, and verify our results with Bogoliubov theory.

We find an unexpected result that the supersolid has two distinct values for bulk compressibility, which takes it outside of the class of materials for which this thermodynamic relation holds. To the best of our knowledge, this is the first such example of this particular physical feature in any material.

We then extend homogenisation to include beyond-meanfield effects, in order to apply it to a dipolar BEC. The dipolar BEC has a considerably richer phase diagram, in which we find several exciting results.

Statement of Originality

I declare that the following is entirely my own work except where explicitly stated otherwise. Contributions from collaborators have been acknowledged using standard referencing practices.

Reuse & Permissions

Where third party material has been used or adapted, I have obtained the necessary permission and reproduced it at the end of this thesis. Material which is under public domain or copyright licenses that do not require permission have been indicated appropriately.

Copyright Declaration

The copyright of this thesis rests with the author. Unless otherwise indicated, its contents are licensed under a Creative Commons Attribution-Non Commercial 4.0 International Licence (CC BY-NC). Under this licence, you may copy and redistribute the material in any medium or format. You may also create and distribute modified versions of the work. This is on the condition that: you credit the author and do not use it, or any derivative works, for a commercial purpose. When reusing or sharing this work, ensure you make the licence terms clear to others by naming the licence and linking to the licence text. Where a work has been adapted, you should indicate that the work has been changed and describe those changes. Please seek permission from the copyright holder for uses of this work that are not included in this licence or permitted under UK Copyright Law.

Acknowledgements

Firstly, I would like to thank my supervisors Dr Derek Lee and Dr Andrew Ho. Thank you both for the helpful discussions, expertise and advice. Thank you for the support you both offered, the kindness you showed and the patience (and sometimes urgency) you gave me. Thank you for the zoom calls over a very sudden and unexpected lockdown which went on for longer than any of us thought. Thank you for the long meetings in which we passionately discussed research, before having a chat about whatever was going on in the world that day, and then returning back to physics again. Thank you for all your support and guidance.

Thank you to Kim, Matthew, Carolyn, Juraci, and Beth for making the group so welcoming and for all your pastoral care. Thank you to Félix for the coffee.

To all the students at CMTH, but particularly Krishnan, Matthieu, Peru and Halvard, thank you for the friendship. You all made the office somewhere I wanted to be, especially if I wanted to get no work done. I'm grateful for the camaraderie, the laughs we shared, the heated physics debates and the deranged chats we had. I'll miss the office, and I truly hope we stay in touch.

Thank you to Joe, Shuqiu and Qiangqiang for making me feel so welcome. Thank you to Anubha for being a great co-worker.

Thank you to Beth and Tash, Ivet and Natasha, Kristjan, Katy, Naomi and Asel for putting up with me and being the best friends I could ask for. You guys are great.

Thank you to James, James, Joe and Tom for continuing the tradition of our scheduled bi-annual drinks. It's always a pleasure.

Thank you to Adam, Augi and Josh for your friendship and our calls over lockdown. I hope you guys know how much it meant to me, and how much I miss it. Thank you again to Adam and Augi for your continued and cherished friendship over these years, and for being the groomsmen at my wedding. A special thank you goes to Rory, who not only put together a fantastic stag do (and truly is the best man), but is one of the best people I know. You're like brothers to me, and I wish I could see you all more.

Thank you to Jack, Ivy, Nicole and Rosanne for being my second family. I couldn't have asked for a better one.

Hvala mama, tata i Jelena. Bez vas ja ne bih mogao ovo završiti. Vi ste uvek bili moji najveći navijači, kad sam trebao pomoć vi ste bili pored mene, i niste nikad dozvolili da ja spuštam sebe previše. Ovaj doktorat je vaš isto kao što je moj.

Thank you finally to my ~~girlfriend~~ ~~fiancée~~ wife Kelly, I can't express how much you mean to me. Your endless patience and infinite support has been the foundation of everything I do.

Contents

1 *Introduction* 19

2 *Supersolid Experiments* 25

1 *Bulk Helium* 25

2 *He-on-C* 27

3 *Dipolar BECs* 28

4 *Commonalities* 31

3 *Concepts around Superfluidity and BECs* 33

1 *Single condensate at $p = 0$* 33

2 *GPE Numerically* 42

3 *Condensates at finite momenta* 47

4 *Homogenisation Framework* 53

1 *Elastic background* 53

2 *Homogenisation for Elasticity* 57

3 *U(1) Phase field* 61

4 *Tensor differentiation* 62

5 *Expanding the Lagrangian* 65

1 *Expanding the U(1) component of the Lagrangian* 65

2 *Elasticity Theory* 68

2.1 *Numerics* 74

3 *Tying it together* 76

6 *Dynamics* 81

1 *Free energy and Grand Canonical ensemble* 81

2 *Effective supersolid Lagrangian* 83

3 *Bogoliubov Dispersion* 86

7 *Results* 93

1 *Thermodynamic Anomaly* 93

8 *Extending the Gross-Pitaevskii equation* 99

1 *Introduction* 99

2 *Theoretical set-up* 100

9 *Homogenisation for dipolar BECs* 105

1 *Homogenisation adapted for the LHY term* 105

2 *Results* 110

10 *Closing Remarks* 117

List of Figures

1.1 Liquid ^{4}He in the superfluid phase. Picture by Alfred Leitner, in the public domain. 19

1.2 The changing of the moment of inertia of a torsional oscillator with temperature as filling fraction of a helium deposit on a graphene substrate is changed. The legend indicates the different number densities for the helium film coverages. The key signal of supersolidity is that the scaling of the NCRI as a function of temperature is not accurately described by assuming that the adsorbed helium forms a superfluid; the authors showed that a triangular supersolid ansatz correctly describes the temperature scaling of the superfluid fraction. Image and data taken from [8] with permission. 20

1.3 Dispersion relation for a 2D triangular supersolid generated by a Heaviside potential, showing a trace in k-space over high-symmetry points in the Brillouin zone. Two Goldstone modes appear due to the broken continuous translational symmetry and are degenerate at the K point; a feature of triangular lattice symmetry. The lowest mode is the Bogoliubov mode appearing due to the broken $U(1)$ symmetry. All three modes may be mixed, and the elementary excitations consist of fluctuations in both the elastic displacement as well as the $U(1)$ phase. We find that the shear mode is initially decoupled from the phase field, and the two longitudinal branches are mixed modes, though this is only true at the Γ point. A derivation of the band structure is shown in section 6.3 and section 9.2. 21

1.4 Image of the superconducting gap function forming a PDW (top) and charge density profile forming a CDW (bottom) taken in UTe_2 with scanned Josephson tunneling microscopy (SJTM) experiments. The PDW is globally π out of phase with the CDW, and it is believed the CDW generates the PDW phase. Image and data taken from [14] under CC BY permission. 21

1.5 Cartoon illustration of a 2D triangular supersolid and its three Goldstone modes. The wavevector is in the direction of the blue and green arrows. The blue arrow is the slow longitudinal mode, which is mostly the Bogoliubov mode and pumps number density up and down. The green arrow is the fast longitudinal mode which is mostly the elastic mode, responsible for moving the peaks relative to each other along the direction of propagation. The red arrow is the shear mode, which also moves the peaks but perpendicular to the direction of propagation. 22

1.6 Experimental [23] (top) and theoretical (bottom) density profiles of a dipolar BEC in a 2D optical lattice at an initial time (left) and after a 36ms time of flight measurement (right). Bland et al. performed numerics by using an extended Gross-Pitaevskii equation (eGPE) which includes the trap potential, beyond-meanfield effects and also thermal noise in the system. Note that the experimental figure is averaged over 68 different trials of the experiment. Figure and results taken from [23] with permission. 23

2.1 Figure illustrating the resonant period of the Vycor disk in the Kim and Chan experiment. The authors drove the disk (which contained the sample of solid Helium) at a range of different velocities (indicated by the legend) and measured the resonant period as a response. They found that a drop in the resonant period occurred around $\sim 0.18K$, which suggests that there is a sudden change in the rotational inertia of the sample and hence signifying a transition into the supersolid phase. It would later transpire that the signal was a feature of an elastic anomaly (in this particular case it was a shear-stiffening) of solid Helium which shifted the rotational inertia due to the geometry of the cell containing the sample. Image taken from [17] with permission. 26

2.2 (a) Illustration of the experimental setup. Helium is deposited on the graphite substrate and the NCRI is measured using the torsional oscillator shown. (b) Ansatz used for the ground state of supersolid helium on graphite in k-space. The authors showed that a triangular lattice described by the Fourier components shown accurately describes the superfluid fraction scaling as determined by NCRI measurements. (c) Change in the resonant frequency of the torsional oscillator as a function of temperature for a range of filling densities (indicated by the legend which lists the number demsity of the helium film coverage). Assuming the NCRI is due to a change in the superfluid fraction, this atypical result is explained by the ansatz in (b). Image adapted from [8] with permission. 28

2.3 Phase diagram of ^{166}Er and ^{164}Dy dipolar BECs contained in a cigar trap. (a) is an illustration of the experiment geometry, (b) shows the averge density profile as a function of the Feschbach scattering length a_s with (c), (d), (e) showing an insulating droplet phase, supersolid phase and typical BEC phase respectively. (f) and (g) show the phase diagrams for ^{166}Er and ^{164}Dy respectively. BEC indicates a typical Bose-Einstein condensate phase, ID refers to insulating droplets which are regions of high and low density in space but do not possess phase coherence from droplet to droplet. SSP is the supersolid phase of interest, where there are regions of high and low density **and** phase coherence across them. Figure obtained from [25] under CCA4 license. 29

2.4 Illustrating the difference between a solid and a supersolid. In (a) and (b) figures display the norm of the Fourier transform of their density profiles from time-of-flight imaging for a supersolid and solid respectively. The grey lines illustrate the many individual images whereas the thick coloured line displays the complex average. The existence of a modulated form in the **complex average** for a supersolid illustrates coherence. This is further illustrated in figures (c) (the supersolid phase) and (d) (the solid phase) which are representations in the complex plane of the value of the complex phase Φ associated with the first peak of the Fourier transform amplitude. The tighter spread in the values of the complex phase for the supersolid indicate phase coherence, which is notably absent in the regular solid phase. Figure obtained from [62]. 30

3.1 A cursory diagram detailing a two particle scattering process via some interaction potential $U(\mathbf{r} - \mathbf{r}')$. Though this is not meant to be interpreted literally, it does provide some intuitive basis for how we arrive at the Gross-Pitaevskii equation. 34

3.2 A set of diagrams for the types of interactions, where time is going downwards. 37

3.3 The dispersion relation for superfluid ^{4}He with a top-hat interaction at various Λ (where Λ is a dimensionless parameter that describes interaction strength and will be introduced later). We see that the existence of the roton minimum is dependent on the strength of the interaction, and in fact we can get a phase transition prior to the roton minimum touching $E = 0$ [36]. 41

3.4 Top figure showcases a triangular supersolid in Cartesian space; bottom figure is the same supersolid but represented in the parallelogram basis. 44

3.5 The '13 point stencil' for the parallelogram basis. In order to calculate the Laplacian at the central point, one employs a finite differencing scheme over the nearest 12 points with α the weight for the nearest 6 and β for the next-nearest 6. The central point has a weighting of $-6(\alpha+\beta)$. This picture is drawn in Cartesian space and will look different in the parallelogram basis but importantly will have the exact same α and β. 45

3.6 The phase diagram for the multi condensate system. The red line between (010) and (101) indicates a *first order* phase transition, whereas the blue and purple lines indicate *second order* transitions, with the distinction between blue and purple being that purple also has a broken $Z(2)$ symmetry. The dashed line indicates the asymptote of the (abc) state as $v_2 \to \infty$. 50

4.1 A schematic of the deformation procedure. The leftmost image depicts an undeformed system with a basis $\mathbf{r}$, which then undergoes an *active* transformation given by some strain to become the middle system. The rightmost image depicts the system after the *passive* transformation, such that the final coordinate system $\mathbf{r}''$ coincides exactly with $\mathbf{r}$, but now there are additional curvatures in the space. 58

5.1 The reduction ϱ/n in the superfluid fraction as a function of interaction strength Λ, exhibiting a discontinuous jump at the transition. This value can potentially be used as an order parameter for the supersolid phase transition. 67

5.2 A comparison of the various elastic constants obtained via homogenisation to those from numerics (homogenisation constants are shown in solid markers, numerics in crosses). The top figure shows the bulk modulus and shear modulus, the middle figure shows the pressure, and the bottom figure shows the absolute value of μ_1. The agreement between homogenisation and numerics is very strong on the whole, but falls apart in the phase transition region. This is likely due to numerical instabilities close to the phase transition which affect the numerically obtained constants but not the homogenisation constants. 76

6.1 Top: excitation velocities for all available sound modes of a system governed by a Heaviside interaction of strength Λ with a phase transition at $\Lambda \sim 38$, as calculated via homogenisation. Velocities are in units of $\hbar/\sqrt{n}ma^2$. Bottom: the eigenvector angle θ for the available longitudinal modes. Both diagrams indicate a superfluid phase at low Λ and a supersolid phase at high Λ, in agreement with earlier results. We see several interesting behaviours in the relative modes; notably the shear mode velocity appears to be linearly dependent on Λ, whereas the other two modes seem to have a dip close to the transition before exhibiting linear behaviour. In the eigenvector angle, there is an interesting maxima in the Bogoliubov mode, whereas the elastic mode seems to tend to a value of $\sim$ 2.8 radians in the large Λ limit. The eigenvector angle should be related to the thermal transport properties of the modes. 86

6.2 Band structure for a supersolid at $\Lambda = 50$. The three Goldstone modes are highlighted as a fast longitudinal, slow longitudinal and shear mode. The velocities of the Goldstone modes are obtained by calculating the slope of the three bands at the Γ point; we typically find agreement to about $\sim 1\%$ with homogenisation. Note also that the two elastic modes (the fast longitudinal and shear modes) are degenerate at the K point due to triangular symmetry. Consequently, one can deduce that the bands do not cross but rather only touch, by examining the $N \to \Gamma$ dispersion relation and noting that Goldstone velocities should be isotropic in a crystal lattice, hence the shear mode must have the same velocity in either the $\Gamma \to K$ section or $M \to \Gamma$ section, and therefore the bands do not cross at K. 89

7.1 Compressibility ratio $\mathcal{R}$ for a system governed by a soft-core interaction of strength Λ. The expected value of $\mathcal{R} = 1$ is obtained in the superfluid phase, but is starkly different in the supersolid regime. 95

8.1 Experimental setup for a planar dipolar BEC supersolid system. Here the atoms have their magnetic dipoles aligned along the z axis and are confined with a harmonic trap in the z direction. Because of the aligned magnetic dipoles along z, the atoms will assemble into a gaussian in the z direction that is much tighter than the gaussian of a harmonic oscillator. There is no trap in the planar field, with the atoms free to self-assemble. The subsequent theory and analysis of the supersolid is conducted inside the xy plane. Image taken from [60] with permission. 100

8.2 Figure depicting the phase diagram of a planar dipolar BEC with an LHY term as a function of scaled density na_{dd}^2 and scaled Feschbach scattering length a_s/a_{dd}, where a_{dd} is the dipole-dipole scattering length. There are four distinct phases: the uniform phase, honeycomb phase, stripe phase and triangular phase. The regions are shaded by their relative contrast

$$C \equiv \frac{\rho_{max} - \rho_{min}}{\rho_{max} + \rho_{min}} \quad .$$

The red line indicates the roton boundary (where the roton mode softens). Several points on the phase diagram are highlighted by text; we will later be examining some of these points in the honeycomb and triangular phases. Image adapted from [60] with permission. 102

8.3 Illustration of the k-space interactions for both the soft-core and dipolar systems, with the approximate condensate momenta illustrated, scales in arbitrary units and the dipolar interaction has $a_s < a_{dd}$. In the soft-core system there are natural minima in the interaction landscape in k-space, around which the density condenses at a finite momenta (not strictly at the minima, due to the kinetic term in the energy). In contrast, there are no such minima in the dipolar interaction, which tends to a value of $U \to \sqrt{8\pi}/\sigma(a_s - a_{dd})$ as $k \to \infty$. This generates many options for how to distribute the finite momenta condensates, which is why the phase diagram for the dipolar system is much richer in comparison to the soft-core system. 103

8.4 From left to right: stripe phase, honeycomb phase, triangular phase. Regions of low density are shown as black in this heatmap. The rich phase diagram of the dipolar BEC lends itself to interesting phenomena; there are two distinct isotropic phases (triangular and honeycomb) and one anisotropic phase (stripe) which means that the excitations can be either isotropic or anisotropic. Consequently, driving the system across a phase transition from the stripe phase to e.g. the honeycomb phase may create interesting dynamics. Note here that the simulations were conducted in the parallelogram basis outlined in section 3.2. 104

9.1 Figure showing the bulk modulus (top row), shear modulus (middle row) and pressure (bottom row) for both the triangular (left column) and honeycomb (right column) phases over a range of points in the phase diagram. There is a strong indication that the bulk modulus and pressure for the honeycomb phases are significantly higher than the triangular phase, while the shear modulus is lower than in the triangular phase. In both phases the shear modulus is significantly smaller than both the bulk modulus and pressure, owing to the malleable nature of the dipolar BEC. An explanation for why the shear modulus is higher in the triangular phase than the honeycomb phase, but the bulk modulus and pressure are **lower** in the triangular phase than in the honeycomb phase, may possibly be arrived at by considering the superfluid-to-solid transition and how it affects the elastic constants. N.B. Lines shown are interpolated for ease of viewing. 111

9.2 Figure showing the velocities for the fast longitudinal mode (top row), shear mode (middle row) and slow longitudinal mode (bottom row) for the triangular (left column) and honeycomb (right column) phases. The fast longitudinal mode is consistently much faster in the honeycomb phase than the triangular phase, which is somewhat to be expected as the bulk modulus is also much higher in the honeycomb phase. Importantly, even though the shear modulus is several orders of magnitude lower than the bulk modulus, the velocity of the shear mode is only one order of magnitude slower than the fast longitudinal mode, and is actually comparable to the slow longitudinal mode. Interesting behaviour is observed in the inverted relationship of the shear and slow longitudinal speeds in the triangular phase; in the honeycomb phase both the shear and slow longitudinal velocities are constantly increasing as the superfluid fraction decreases (though note that the slow longitudinal mode increases much slower), while in the triangular phase the slow longitudinal mode **decreases**. Note again that lines are interpolated across data points for viewing ease. 112

9.3 Left figure shows a triangular supersolid state at $a_s = 0.769 a_{dd}$ and $n = 0.0886/a_{dd}^2$ with a lattice spacing $\sim 600 a_{dd}$, right figure shows the Bogoliubov band structure of the supersolid (units of ω scaled up from $\sim 10^{-9}$). This specific point in the phase diagram may look like a typical triangular supersolid, but it is actually one of the triangular phases which has the peculiar property of the shear mode being slower than the slow longitudinal mode. At about $2/3$ of the way between the Γ and K point one can see that the two lowest bands apparently cross over. In this figure we have also included some of the higher bands as they also cross over with the fast longitudinal mode. 114

9.4 Figure illustrating the ratio of the shear velocity v_G to the slow longitudinal velocity v_{sl} (top row) and the respective supersolid fraction ϱ (bottom row) for the triangular phases (left column) and honeycomb phases (right column). One can see that in the triangular phase there is a signicant variation in both the speed ratio and the supersolid fraction as one scans over the density na_{dd}^2, in contrast to the honeycomb phase which is relatively stable in both metrics. The circled point on the left column corresponds to the phase shown in Fig. 9.3 which possesses a band degeneracy, predicted first by homogenisation (as the ratio is less than unity and therefore the shear mode must cross through the slow longitudinal mode) and then shown conclusively by the Bogoliubov band structure. 115

Note to reader

In this thesis I will make use of several different environments in both the side margins and the main text. The side margin environments are used for important notes, additional information, and the main text will sometimes contain chapter summaries if deemed pertinent. Each of these environments will have their own colour scheme, which I will now illustrate.

To the right is an example of a **"note well"** environment in a light green shade, which will contain information that the reader should pay particular attention to. Just below it is an example of an **"additional information"** environment in a light blue shade, which will contain additional information that may add flavour and context to the passage. The blue environments are to be treated as footnotes that are not strictly necessary for the understanding of the text, whereas the green environments are to be treated as important notes that the reader should pay attention to, as they may recall useful information or alert the reader to important subtleties.

Finally, directly beneath this text is a **"chapter summary"** environment in a light orange shade, which will contain a brief summary of the chapter that the reader has just completed. The chapter summary will be used to help the reader remember the key points of the chapter, and may not be present in every chapter.

Note Well

In this environment I will point to information that may have been discussed previously and is relevant to the current context. I will also alert the reader to important subtleties that may not be immediately obvious. This environment may also draw on "general knowledge" that is not explicitly stated in the text, or be used as a reminder of important concepts.

Additional information

In this environment I will provide additional information that is not strictly necessary for the understanding of the text, but may be of interest to the reader. This information may be tangentially related to the text, historical context, or some additional insight that may be useful.

Chapter Summary

In this environment I will provide a summary of the chapter that the reader has just completed. This will be a brief overview of the main points discussed in the chapter, and will be used to help the reader remember the key points of the chapter. Note that not every chapter will have a summary.

1 *Introduction*

Following the discovery of superconductivity in 1911 by Kamerlingh Onnes [1], there was a flurry of activity in the field of low temperature physics. While substantial theoretical and experimental progress in superconducting physics was made over the following two decades, it wasn't until 1937 that superfluids were first discovered by Kapitza [2], and independently by Allen and Misener [3].

Superconductors are characterised by 'free flow', known as *superflow*, of current across the material (i.e. zero electrical resistance), and superfluids by superflow of the fluid (i.e. zero viscosity). The two phenomena are linked by the fact that they are both macroscopic quantum features of the system which occur below some critical temperature T_c, and are both characterised by a broken symmetry.

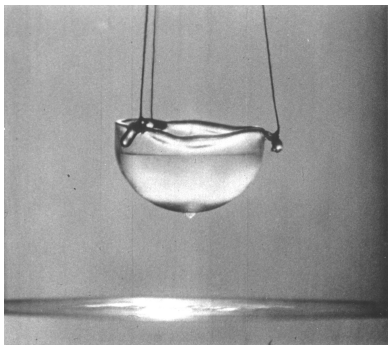


Fig. 1.1: Liquid ^{4}He in the superfluid phase. Picture by Alfred Leitner, in the public domain.

An incredibly successful phenomenological theory of superconductivity was developed by Ginzburg and Landau [4], who were able to explain the Meissner effect and the existence of a critical temperature T_c. It was also Landau who developed the phenomenological theory of superfluidity [5] in 1941 by considering the minimum energy required to excite a sound wave in a superfluid via scattering processes. While both theories were able to explain qualitative features of superconductors and superfluids respectively, they were unable to provide insight into the mechanism through which these phenomena would arise. A comprehensive microscopic theory for both superfluids and superconductors is still an active area of research.

Ginzburg and Landau achieved this by considering an expansion of the free energy in terms of a function labelled the order parameter, which is a complex scalar field. The ground-state value of the order parameter is set by an additional two phenomenological parameters α and β, in what is now known to be an example of spontaneous symmetry breaking.

A key consideration in traditional superfluids and superconductors is that they are *spatially uniform* in the density profile. A superfluid would obviously contain no density modulations, and a superconductor has a uniform order parameter (barring the existence of vortices in the material).

In 1969, Thouless [6] and Andreev & Lifshitz [7] independently proposed the existence of a new phase of matter, which they called a supersolid. The authors suggested that a supersolid might be some material which has both solid and superfluid properties in the same phase. This material would showcase new phenomena, including the existence of additional Goldstone modes (Fig. 1.3), due to the

N.B. this distinguishes a superconductor from a supersolid; while a superconductor is most certainly a solid, the 'super' refers to the behaviour of the electrons, not the atom lattice. A 'superconducting supersolid' would be a material which exhibits crystallinity in the phase that has superflow, i.e. the condensate of Cooper pairs.

additional broken symmetries of translational invariance (the solid component) and $U(1)$ phase invariance (the superfluid component).

The theoretical principle developed by the authors was that a supersolid would be a solid with vacancies (namely, lattice sites which should be occupied but are instead empty) that can exhibit exchange interactions with neighbours via quantum tunnelling. More specifically, if this tunnelling can occur across a macroscopic distance, then below a certain temperature the solid would display superflow properties in the vacancies. Since the lattice sites are distributed in a lattice and have a crystalline structure, any superflow in the vacancies would classify this as a supersolid.

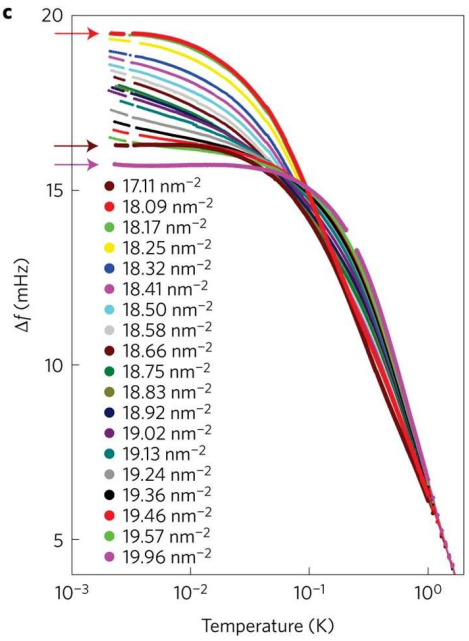


Fig. 1.2: The changing of the moment of inertia of a torsional oscillator with temperature as filling fraction of a helium deposit on a graphene substrate is changed. The legend indicates the different number densities for the helium film coverages. The key signal of supersolidity is that the scaling of the NCRI as a function of temperature is not accurately described by assuming that the adsorbed helium forms a superfluid; the authors showed that a triangular supersolid ansatz correctly describes the temperature scaling of the superfluid fraction. Image and data taken from [8] with permission.

The macroscopic behaviour can be characterised by:

- The existence of a superfluid fraction, which is the fraction of the system that is able to flow without dissipation.
- The existence of a non-classical rotational inertia (NCRI); in a regular fluid, as the container is rotated so too is the fluid. A superfluid on the other hand does not contribute any rotational inertia at all to the system, i.e. it does not rotate with the walls of the container. NCRI is when only some fraction of the system (not 0 or 1) contributes to the rotational inertia
- At least one additional Goldstone mode due to the spontaneous breaking of a continuous symmetry, plus D many dimensional acoustic phonons where D is the dimensionality of the system.

N.B. a supersolid is often stated as a state that spontaneously breaks continuous translational symmetry and some global gauge symmetry. This is unfortunately not enough, as BECs break the global $U(1)$ phase but do not always exhibit superfluidity, as we will discuss in section 3.1.

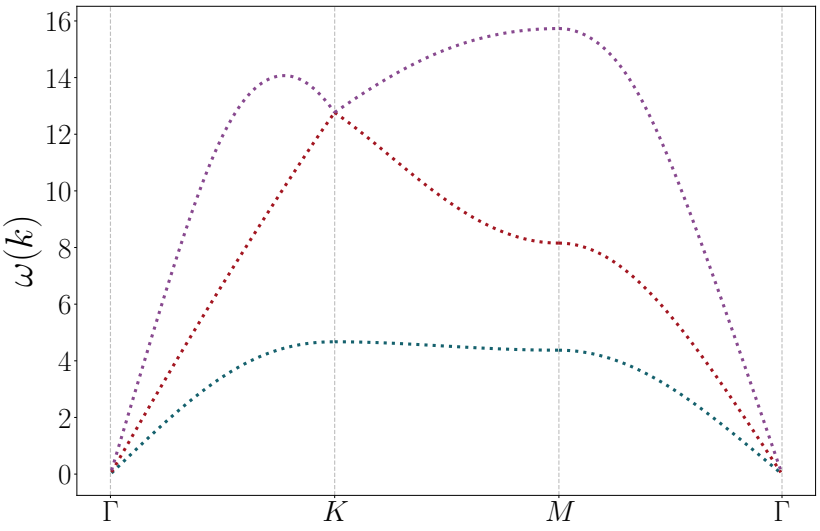


Fig. 1.3: Dispersion relation for a 2D triangular supersolid generated by a Heaviside potential, showing a trace in k-space over high-symmetry points in the Brillouin zone. Two Goldstone modes appear due to the broken continuous translational symmetry and are degenerate at the K point; a feature of triangular lattice symmetry. The lowest mode is the Bogoliubov mode appearing due to the broken $U(1)$ symmetry. All three modes may be mixed, and the elementary excitations consist of fluctuations in both the elastic displacement as well as the $U(1)$ phase. We find that the shear mode is initially decoupled from the phase field, and the two longitudinal branches are mixed modes, though this is only true at the Γ point. A derivation of the band structure is shown in section 6.3 and section 9.2.

A more general interpretation of a supersolid is that it is a phase of matter that displays both crystalline order and superfluidity in the form of non-classical rotational inertia (NCRI).

The simultaneous breaking of continuous translational symmetry and a $U(1)$ gauge is predicted to generate a supersolid [9, 10, 11]. This can arise via spatial modulation in the superfluid order parameter, which itself has an interesting history. The long-searched Fulde-Ferrel Larkin-Ovchinnikov (FFLO) phase also generates a spatially modulated *superconducting* order parameter in the presence of a magnetic field [12, 13]. This occurs due to an applied external B-field inducing a split in the energy levels of $|\uparrow\rangle$ and $|\downarrow\rangle$ electrons at the Fermi level which then form Cooper pairs, leading to Cooper pairs with finite momenta. Consequently, the order-parameter of the superconducting phase is spatially modulated, similar to a supersolid but with the key difference that the FFLO phase exists only under an external magnetic field.

The FFLO phase is part of a broader class of phases known as pair density waves (PDWs); these are phases with a well defined periodic modulation in the Cooper pair density profile. The FFLO phase is special in that it requires a magnetic field to stabilise, PDWs in general can exist even at zero external B field. These are observed through either scanned tunnelling microscopy (STM) or scanned Josephson tunnelling microscopy (SJTM) measurements of the superconducting gap function. Interestingly, most PDWs coexist alongside charge density waves (CDWs), which are periodic modulations in the charge density of a material. It is widely believed that the CDW induces the PDW in most materials that exhibit this behaviour, with

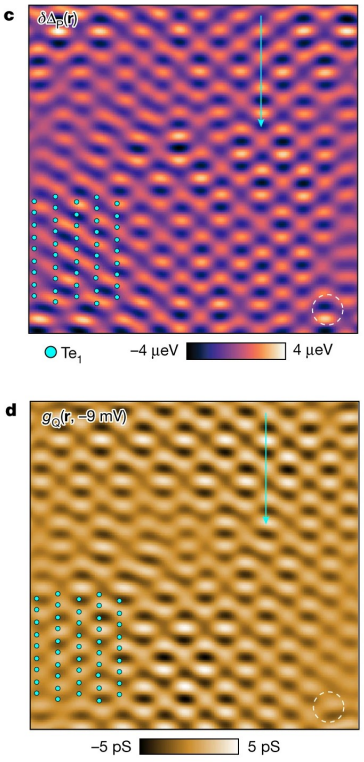


Fig. 1.4: Image of the superconducting gap function forming a PDW (top) and charge density profile forming a CDW (bottom) taken in UTe_2 with scanned Josephson tunneling microscopy (SJTM) experiments. The PDW is globally π out of phase with the CDW, and it is believed the CDW generates the PDW phase. Image and data taken from [14] under CC BY permission.

While PDWs are distinct from supersolids in that they exhibit periodic density modulation in the Cooper-pair field, whereas supersolids are periodically modulated BECs, both phases are examples of *intertwined order*, and should be considered (to some degree) on equal footing. Though the mechanism of generating PDWs may be very different from those generating supersolids, they should exhibit many of the same phenomenological and macroscopic properties, and PDWs may be broadly considered as charged supersolids.

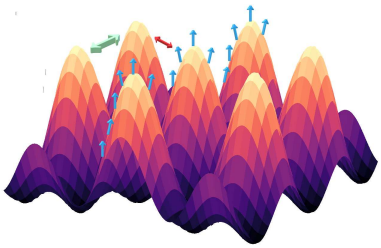


Fig. 1.5: Cartoon illustration of a 2D triangular supersolid and its three Goldstone modes. The wavevector is in the direction of the blue and green arrows. The blue arrow is the slow longitudinal mode, which is mostly the Bogoliubov mode and pumps number density up and down. The green arrow is the fast longitudinal mode which is mostly the elastic mode, responsible for moving the peaks relative to each other along the direction of propagation. The red arrow is the shear mode, which also moves the peaks but perpendicular to the direction of propagation.

N.B. some claim that since ^{4}He only exhibits such a behaviour on a substrate, it is not a true supersolid as it does not form spontaneously. Counter arguments to this claim are that the ^{4}He crystal structure is incommensurate to the underlying substrate, and hence the substrate only stabilises the supersolid phase, but does not cause it.

the PDW usually being π out of phase relative to the CDW [15]. However, recent observations in $Bi_2Sr_2CaCu_2O_{+x}$ [16] have identified nematic PDWs in the absence of a CDW, suggesting that PDW formation may be more complex than initially anticipated.

Supersolids and PDWs are both examples of a new type of macroscopic superfluid or superconducting phase, respectively. The development of a spontaneously formed crystal lattice in the order-parameter and the thermodynamic properties of these phases are not well understood. Developing an understanding of these open questions may provide greater insight into the theories of superfluids and superconductors. While PDWs have recently been observed in various solid-state superconductors [16, 14], it is very difficult to access certain properties of the PDW phase. On the other hand, the search for a supersolid has been conducted over various different media.

In 2004, Kim and Chan [17, 18] conducted experiments which showed behaviour that suggested the existence of a supersolid. The experiments were conducted on ^{4}He, which is a bosonic superfluid, and the results claimed to show that the material had a NCRI, which indicates that there was superflow through only a fraction of the system. Later experiments [19] showed that there were systematic errors in the Kim & Chan experiments, and that the results were not indicative of true supersolidity. This anomalous result in the end turned out to be due to a peculiar shear stiffening of solid Helium, which manifested itself as a shift in the inertia of the sample due to the geometry of the cell containing the Helium [20].

While the Kim & Chan experiments were not a discovery of supersolids, they inspired a new wave of theoretical and experimental work on the subject. Phenomenological approaches were developed by Nozières [21] and Dorsey et al [22], and Son [9] has described a theory of the low energy excitations which are allowed based on symmetry constraints.

Experimental work to discover supersolids has been conducted on bulk ^{4}He, bulk ^{3}He, ^{4}He on substrates, and dipolar BECs (Bose-Einstein Condensates). While the first experiments were conducted on bulk ^{4}He, later experiments considered ^{4}He specifically on a graphene substrate coupled to a torsional oscillator [8] and found signals of NCRI.

More recently, supersolidity has been proposed in dipolar BECs, and in Rydberg-dressed BECs [24]. Ferlaino [25], Bottcher [26] and Tanzi [27] et al. have all conducted experiments on dipolar BECs which show evidence of supersolidity. More precisely, they used either Dysprosium or Erbium which possess magnetic dipole interactions and have found a phase coherent state with density modulation

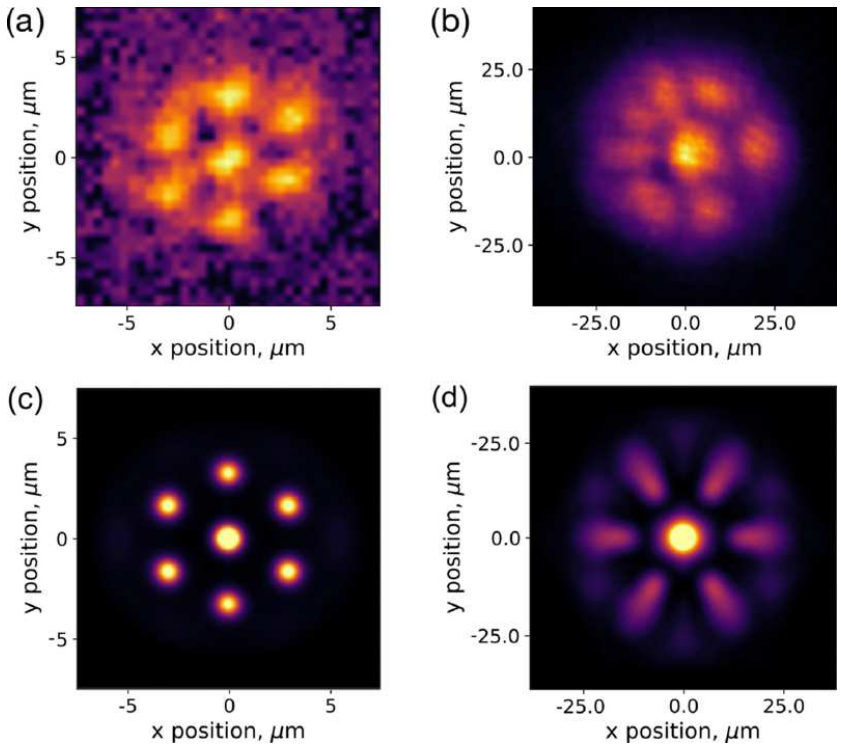


Fig. 1.6: Experimental [23] (top) and theoretical (bottom) density profiles of a dipolar BEC in a 2D optical lattice at an initial time (left) and after a 36ms time of flight measurement (right). Bland et al. performed numerics by using an extended Gross-Pitaevskii equation (eGPE) which includes the trap potential, beyond-meanfield effects and also thermal noise in the system. Note that the experimental figure is averaged over 68 different trials of the experiment. Figure and results taken from [23] with permission.

and measured two branches in the excitation spectrum corresponding to the broken symmetries, which some argue is sufficient evidence for the existence of a supersolid. Later work by Tanzi et al [28] has shown a NCRI in the system, providing strong evidence that it is in fact a supersolid.

Though the above experiments have shown some evidence of supersolidity, there are still many questions to be answered about the arisal and behaviour of supersolids. Namely, what is the nature of superfluidity in the system? What is the Landau critical velocity of a supersolid, and how does it compare to the critical velocity of a superfluid? What is the origin of the crystalline order? What can we expect their thermal transport and entropy dissipation to look like now that we have coupled diffusive and ballistic modes?

An avenue to answer these questions may exist using a phenomenological theory, but any such approach necessarily requires free parameters in the theory. One such example of this is the following phenomenological Lagrangian,

$$\begin{aligned}\mathcal{L} = &\frac{1}{2}\left(\rho_n(\partial_\tau u_\alpha)^2 + \lambda_{\alpha\beta\gamma\delta}u_{\alpha\beta}u_{\gamma\delta}\right)\\ &+\frac{1}{2}\left(\kappa(\partial_\tau\theta)^2 + \rho_s^{\alpha\beta}\partial_\alpha\theta\partial_\beta\theta\right) + ia_{\alpha\beta}u_{\alpha\beta}\partial_\tau\theta\end{aligned} \tag{1.0.1}$$

Symbols in (1.0.1) are as follows: ρ_n is the density of the normal fraction, $\lambda_{\alpha\beta\gamma\delta}$ is the effective elastic tensor, κ is the superfluid compressibility, $\rho_s^{\alpha\beta}$ is the superfluid stiffness tensor and $a_{\alpha\beta}$ is the coupling tensor. The fields are the linearised strain tensor $u_{\alpha\beta}$, which represents the elastic displacement of the materials, and the superfluid phase ϕ, which is the gradient of the phase of the superfluid order parameter.

which was proposed by Ye [11]. Note that phenomenological theories may be able to describe the low-energy excitations of the system, but in order to do so quantitatively, one needs to *a posteriori* fit the free parameters.

N.B. This is one of many effective Lagrangians which are allowed by symmetry constraints. By considering the symmetries imposed on a supersolid, Son [9] was able to derive a family of effective Lagrangians which may describe the low-energy dynamics of a theoretical supersolid, as well as consider interactions between vortices and phonons. The Lagrangian chosen by Ye was selected primarily to consider Goldstone modes.

In this work, the author uses equation (1.0.1) to describe the low energy excitations of a supersolid and calculate some bulk properties. However, in order to obtain results which match experiments, one would need to fit the phenomenological parameters $\{\rho_n, \lambda_{\alpha\beta\gamma\delta}, \kappa, \rho_s^{\alpha\beta}, a_{\alpha\beta}\}$ to the system.

Unfortunately, experiments are not at the stage where they are able to measure these parameters directly. Consequently, an important field of research is then obtaining phenomenological behaviour starting from a microscopic (or as close to microscopic as we can get) theory.

The microscopic nature of supersolids is still an active area of research. There are two main approaches to this problem. The first is to use Monte-Carlo techniques with real interaction potentials [29, 30, 31] to find the ground state wave function. The second is to employ a mean-field approach using some variation of the effective Gross-Pitaevskii equation (eGPE) [32, 33] for a system with some effective interaction potential. In the case of dipolar gases, theoretical work is studied using the eGPE with a beyond-meanfield correction called the LHY (Lee-Huang-Yang) term [34, 23, 25, 35].

The advantage of Monte Carlo techniques is that they are able to more accurately simulate realistic systems, and can give more conclusive answers about whether a particular supersolid phase is stable. The disadvantage is the extensive computational cost in comparison to eGPE methods, and the comparitive difficulty in obtaining excitation spectra and dynamic properties.

In this thesis I will be focusing on using an eGPE approach to study the pattern formation of a supersolid. More precisely, I will build on previous work by Josserand et al [10, 36, 37] to develop the technique of homogenisation in a supersolid. This technique allows us to obtain a phenomenological Lagrangian of the form (1.0.1), but with variables obtained from the microscopic eGPE. I then analyse the nature of the excitations described by this effective Lagrangian, and comment on certain bulk properties of the system.

This is the first result where macroscopic properties of supersolids are calculated from a microscopic theory, and used to develop a phenomenological theory. Interestingly, I find that supersolids have a peculiar feature in the bulk moduli; specifically the thermodynamic definition of the bulk modulus is a different value to the elastic definition, i.e. $B_T \neq B_E$, where the following definitions apply:

$$B_T = -n\frac{\partial P}{\partial n}\bigg|_V \quad ; \quad B_E = \frac{\partial P}{\partial V}\bigg|_N \tag{1.0.2}$$

This is a novel feature that has not been observed in any other material, and would be a clear indicator of the purported supersolidity of a material. Moreover, this finding may pave the way for further scrutiny of otherwise accepted thermodynamic relations.

2 *Supersolid Experiments*

In this section we will conduct a short review of the experimental history of the search for supersolids. This will range from initial studies on bulk solid ^{4}He, through to ^{4}He deposition on graphite, and finally concluding with contemporary studies on cold dipolar gases.

2.1 Bulk Helium

In 2004 Kim and Chan [17] designed an experiment to probe for supersolidity in bulk ^{4}He. They filled an annular cell with solid helium and attached it to a torsional oscillator. The experiment was then set up to probe the resonant frequency of the torsional oscillator.

If the helium sample were to exhibit supersolidity, the experimentalists would expect to see a drop in the resonant period as the moment of inertia would reduce due to a superfluid fraction. This is the NCRI (sometimes called fractional rotational inertia) predicted as a key signal for supersolidity; the solid helium would exhibit a fraction of the system which is completely decoupled from the rotational inertia as a whole. Such a signal would be a so-called 'smoking gun' sign of supersolidity, and indeed was what Kim and Chan observed (see Fig. 2.1).

The resonant frequency of a torsional oscillator is given by

$$\tau = 2\pi\sqrt{I/\kappa}$$

with $\{\tau, I, \kappa\}$ the resonant period, moment of inertia of the sample and torsional spring constant respectively.

This immediately sparked a sharp increase in experimental studies around supersolids. A considerable amount of experimental work was conducted in trying to confirm the results of Kim and Chan, most notably verifying that the rotational anomalies [38, 39, 40, 41, 42, 43], elastic anomalies [19, 44, 45, 46] and specific heat signatures [47, 48] were all present.

Viscosity is a measure of the resistance of a fluid to flow. It is typically measured in units of $Pa \cdot s$ or $N \cdot s/m^2$. The viscosity of a fluid is a measure of the internal friction of the fluid, and is typically a function of temperature and pressure. A superfluid is a material which has zero viscosity, and hence flows without any resistance, which is why it has no effect on the resonant period of the torsional oscillator.

The subsequent experimental studies also found a few key features that suggested the picture painted by the Kim and Chan experiments were incomplete. Rittner and Reppy [38] found that annealing the samples **drastically** reduced the NCRI (and hence supersolidity) of the system, which suggested that crystal structure/disorder played a significant role in the development of supersolidity. They also found that changes in the shear modulus of the sample were extremely

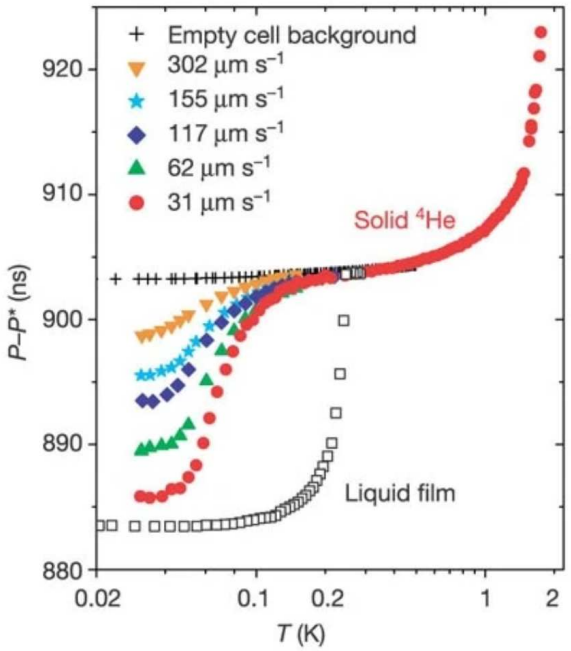


Fig. 2.1: Figure illustrating the resonant period of the Vycor disk in the Kim and Chan experiment. The authors drove the disk (which contained the sample of solid Helium) at a range of different velocities (indicated by the legend) and measured the resonant period as a response. They found that a drop in the resonant period occurred around $\sim 0.18K$, which suggests that there is a sudden change in the rotational inertia of the sample and hence signifying a transition into the supersolid phase. It would later transpire that the signal was a feature of an elastic anomaly (in this particular case it was a shear-stiffening) of solid Helium which shifted the rotational inertia due to the geometry of the cell containing the sample. Image taken from [17] with permission.

A helpful cartoon image for thinking of the vacancy based supersolid is that of a little wooden magic square puzzle, where the goal is to order the numbered squares given some random configuration and at least one missing square (which is our vacancy). The puzzle can be solved by essentially moving the missing square around in such a way as to push the numbered squares into their correct order. This is a lot like the vacancy based supersolid; if your crystal has vacancies and they are superfluid then you can move the vacancies around in such a way as to reduce the energy cost of a rotation. Of course you can't completely remove the effect of rotation from the whole crystal as there aren't enough vacancies, this is why we get NCRI.

well correlated with measurements of the NCRI, suggesting that the origins of the elastic anomalies were closely tied with those of supersolidity.

Moreover, follow up studies from Rittner et al [38, 39] also found that quenching the sample (which should increase the amount of disorder in the lattice) greatly **increased** the amount of supersolidity indicated by the experiment, at times allowing samples to have an NCRI fraction of $\sim$ 20% compared to the usual $\sim$ 1% Kim and Chan were reporting. This furthered the notion that supersolidity had its roots in disorder, which led some theorists to believe that supersolidity is a vacancy based phenomenon.

These experimental advances were pre-empted well ahead of schedule by both Thouless [6] and Andreev & Lifshitz [7] in 1969. Both papers presented a central thesis where the supersolidity was driven by superfluidity in the *vacancies*. They hypothesised that if there were

1. Sufficiently large amounts of vacancies in the crystal

2. Sufficiently strong correlations between the vacancies

then it could be possible for the vacancies to form a BEC. If the vacancies were interacting in a repulsive manner, they would generate the kind of dispersion relation that could potentially lead to a superfluid. What would be left would be a crystal with superflow, a supersolid.

As usual with theoretical predictions based around energetic arguments, the gold standard test comes from Monte Carlo simulations. Over the course of a few years, several studies independently showed [49, 50, 51] that the cost of creating vacancies was about $10K$ (Kelvin being used as a measure of energy here), which was much larger than the temperatures of $0.1K$ that supersolidity was purported to arise at. This was a harsh blow to the vacancy-based supersolid thesis, and suggested that some experimental results, particularly those based around quenching which would *introduce* disorder, and comparatively annealing which would *reduce* disorder, would have to be reconsidered with greater care.

On energetic grounds, the argument was relatively straightforward: a delocalised vacancy minimises the ∇^2 term in the Hamiltonian, but has to 'beat' the potential energy gained by placing an atom in the interatomic potential $U(r - r')$. This balance struck between the delocalisation favouring kinetic term and the localisation favouring interacting term was central to the argument. It is already well known that solid Helium is a considerably 'quantum' crystal, with the zero-point motion of Helium at ambient pressure being very large. This lended some credence to the notion that delocalisation of crystal defects may generate supersolidity in solid Helium.

The final piece of evidence against supersolid bulk ^{4}He was provided by Chan himself in collaboration with his postdoc D. Y. Kim [20]. Together, by altering the geometry of the cell that contained the sample, they redesigned the experiment in such a way as to remove the effect of any elastic anomaly which may or may not arise in Helium at the 'supersolid' temperature on the torsional oscillator. What they found was a complete absence of any signal of supersolidity within the measurement capabilities of their experiment. It would appear that the anomalous shear stiffening of solid Helium at this temperature was ultimately responsible for the NCRI signal, and that what they observed was an interesting and unexpected phenomena, but unfortunately not supersolidity.

2.2 *He-on-C*

While the search for bulk supersolidity in ^{4}He slowed down, a new avenue was explored in a 2-dimensional direction. John Saunders' group at RHUL experimented with thin film depositions of ^{4}He on a graphite substrate [8]. By controlling the amount of Helium placed on the graphite and the temperature of the experiment, they were able to determine the NCRI by using a torsional oscillator to measure the resonant frequency of the combined system.

The hexagonal lattice of the graphite imposes a repulsive potential for the helium substrate; one would expect a commensurate layer of solid helium directly above the graphite. The interesting physics occurs upon the population of the the second layer of helium. Saunders' group found that as they increased the filling fraction of the helium on the second layer, the NCRI emerged at a range of helium densities at about $1K$.

An immediate explanation can be given by suggesting that the second layer of helium forms a liquid superfluid whilst the first layer remains a commensurate solid. However, the scaling behaviour of the normal fraction does not line up accurately with this hypothesis.

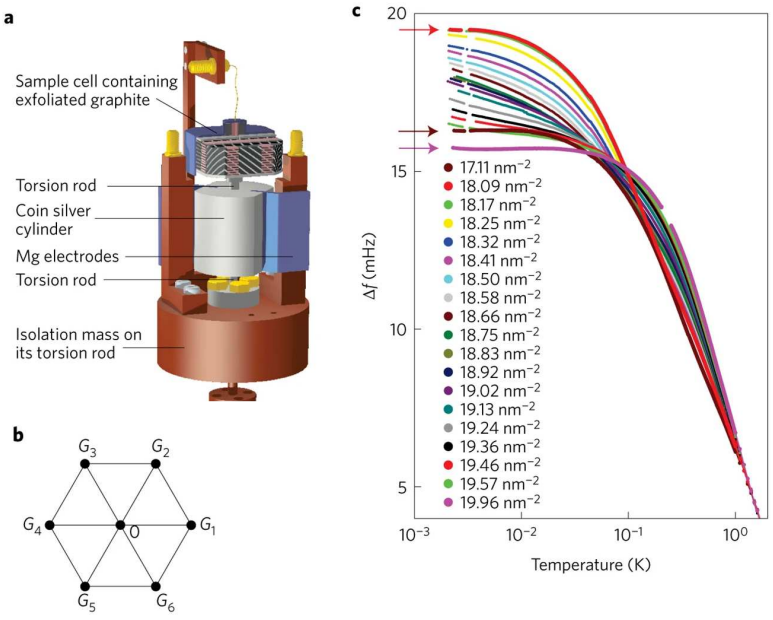


Fig. 2.2: (a) Illustration of the experimental setup. Helium is deposited on the graphite substrate and the NCRI is measured using the torsional oscillator shown. (b) Ansatz used for the ground state of supersolid helium on graphite in k-space. The authors showed that a triangular lattice described by the Fourier components shown accurately describes the superfluid fraction scaling as determined by NCRI measurements. (c) Change in the resonant frequency of the torsional oscillator as a function of temperature for a range of filling densities (indicated by the legend which lists the number demsity of the helium film coverage). Assuming the NCRI is due to a change in the superfluid fraction, this atypical result is explained by the ansatz in (b). Image adapted from [8] with permission.

While this does appear to be strong evidence of supersolidity, it is unclear whether the translational symmetry is *spontaneously* broken in the second layer, as the graphite is necessary to generate this phase and so one may argue that the supersolid is generated by the graphite. One counter argument as to whether this is a true supersolid is that the authors claim the second layer is incommensurate with the underlying graphite lattice, and as such it is *only stabilised by the graphite*, hence it **is spontaneously generated**.

Instead, the authors found that by considering the second layer as composed of softened roton-like modes at finite momentum in a triangular lattice, they were able to reproduce the scaling behaviour shown in the experiment. This is strong evidence that the second layer of helium forms an *intertwined* phase, where there exists both superfluidity and spontaneously broken translational symmetry.

Furthermore, while the NCRI signal is explained by the existence of a supersolid-like phase, it has not been entirely ruled out that the NCRI is a result of some other phenomena. Attempts at theoretically simulating the system have been mostly conducted using Monte Carlo techniques [52, 53, 54, 55]. As of now it is still largely unclear whether the Saunders experiment has been 'verified' computationally.

2.3 *Dipolar BECs*

While the aforementioned systems are relatively easy to construct, it is difficult to have a high degree of control over the system and to directly observe the sample. Over the course of $\sim$ 10 years or so between the Kim and Chan experiment and the Saunders experiment, significant advances were made in the field of ultracold atomic gases. Most notably, the degree of control over the laser trap and coherence times of these experiments greatly increased, opening a new avenue

for potential supersolid research.

Prior to the devlopment of such experimental studies, preliminary theoretical analysis was conducted on the viability of generating supersolid phases in such an environment. One such study used an extended Gross-Pitaevskii equation (eGPE) and predicted that, under the meanfield approximation necessary to derive the eGPE, any supersolid state is unstable and would collapse [56]. This was done by considering the contact potential that arises from a dipolar interaction, which is actually attractive. This study showed that the attractive contact interaction in a supersolid state would lead to points of infinite density and hence that state would be unstable.

While this was initially discouraging, later work showed that the state would actually stabilise upon inclusion of a beyond mean-field correction (by calculating one-loop corrections) known as the Lee-Huang-Yang (LHY) term [34], provided that the trap could be tightened and the number density sufficiently large [57, 58].

Experiments are also currently being built on molecular BECs. These will be able to access a much wider range of supersolid behaviour, providing an exciting experimental avenue in the future.

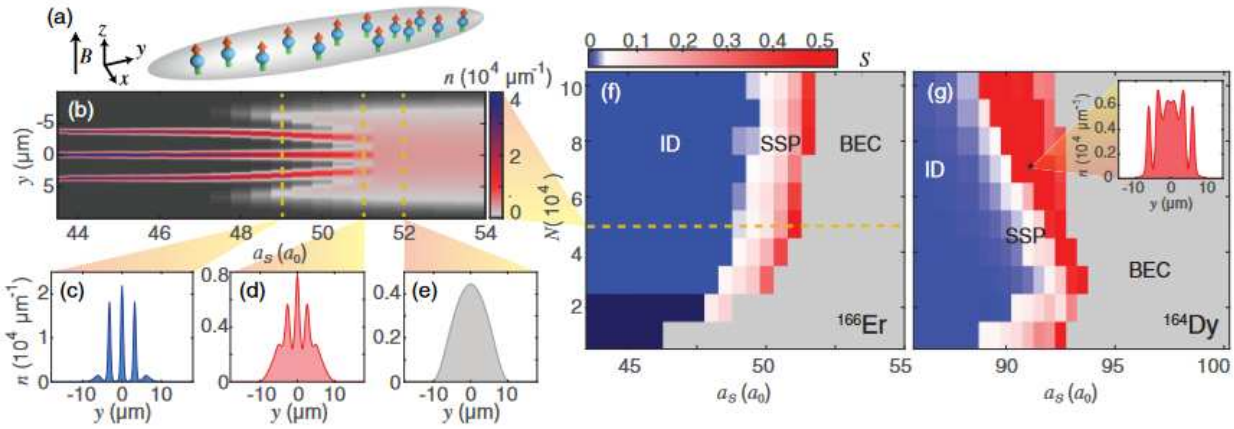


Fig. 2.3: Phase diagram of ^{166}Er and ^{164}Dy dipolar BECs contained in a cigar trap. (a) is an illustration of the experiment geometry, (b) shows the averge density profile as a function of the Feschbach scattering length a_s with (c), (d), (e) showing an insulating droplet phase, supersolid phase and typical BEC phase respectively. (f) and (g) show the phase diagrams for ^{166}Er and ^{164}Dy respectively. BEC indicates a typical Bose-Einstein condensate phase, ID refers to insulating droplets which are regions of high and low density in space but do not possess phase coherence from droplet to droplet. SSP is the supersolid phase of interest, where there are regions of high and low density **and** phase coherence across them. Figure obtained from [25] under CCA4 license.

This encouraged experimentalists greatly, leading to several ultracold gas specialists applying their expertise to supersolids [24, 35, 26, 27]. It is also important to note that work has also been done in constructing supersolids using optical pumps [59, 14], whereby the gas is optically pumped in two directions. This creates a potential landscape where atoms are led to attract/repel. If you can also create a global phase coherence between the atoms, it is possible to obtain superfluidity across the system whilst possessing a spatially modulated density profile. This is quite a different 'style' of supersolid, and we will focus more on magnetic dipole BECs.

By populating an optical trap with atoms that have a strong magnetic dipole interaction and a large total angular momentum, it is possible to create an environment where atoms have long-range

interactions (via the dipole-dipole interaction), tunable scattering interactions (through Feschbach resonances via angular momentum channels) and a confined system (due to the optical trap). The combination of these various features *should be able to create a supersolid*, as the atoms can be sufficiently cooled to below the BEC temperature and can be shown to spatially modulate their density profile [58, 60].

Time-of-flight imaging is essentially LADAR. It operates by shing a laser on different sections of your sample and recording the time it takes for the signal to bounce back. One can reproduce an image which consists of particle positions quite accurately.

It is possible to directly image the density profile of the BEC gas through time of flight imaging, which provides the fourier spectrum as well as the phases on the fourier transform. From this one can see immediately if a density modulation exists, and separately over many repeated experiments one can check for global phase coherence by tracking the value of the phase on the fourier amplitude of the first non-zero peak. For further details see Fig. 2.4.

Three independent experiments [27, 25, 26] showed that a spatial modulation can coexist with a global phase coherence in a 'cigar' trap (i.e. in $1D$). This was immediately followed by measurements of the NCRI [28], as well as measurements of the Goldstone modes [61]. The field has since been extended to the second dimension [23, 35], with visible triangular lattices forming in conjunction with global phase coherence and a measured NCRI.

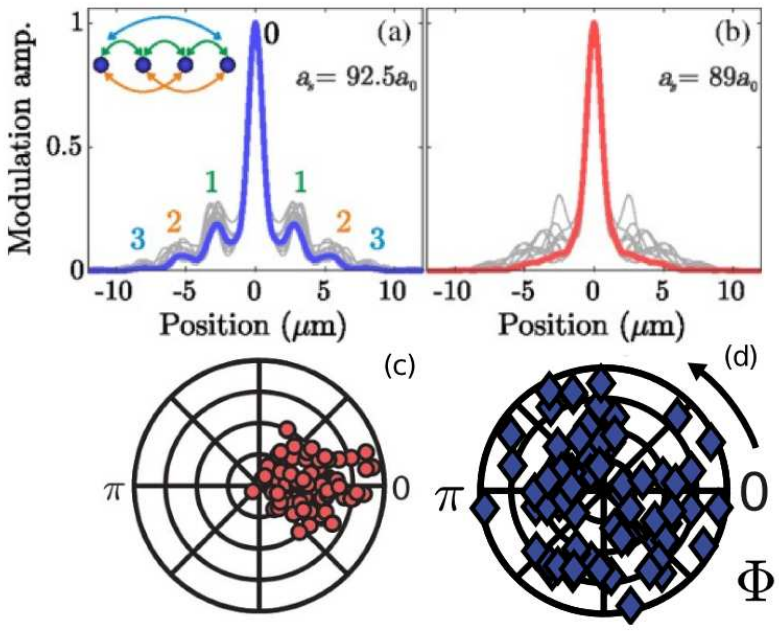


Fig. 2.4: Illustrating the difference between a solid and a supersolid. In (a) and (b) figures display the norm of the Fourier transform of their density profiles from time-of-flight imaging for a supersolid and solid respectively. The grey lines illustrate the many individual images whereas the thick coloured line displays the complex average. The existence of a modulated form in the **complex average** for a supersolid illustrates coherence. This is further illustrated in figures (c) (the supersolid phase) and (d) (the solid phase) which are representations in the complex plane of the value of the complex phase Φ associated with the first peak of the Fourier transform amplitude. The tighter spread in the values of the complex phase for the supersolid indicate phase coherence, which is notably absent in the regular solid phase. Figure obtained from [62].

While these are certainly supersolids, in that they exhibit both superfluidity and a crystal lattice, it should be noted that these phases of matter are not strictly stable and spontaneous. They often

have a relatively short lifetime before thermal noise destroys the state as is typical in ultracold atomic gases.

2.4 *Commonalities*

There are several common features to note.

- It appears to be necessary to have momentum dependent interactions between the particles. This leads to minima at finite momenta in the dispersion relation, and since the dynamics describing these ground states are non-linear the value of these minima are usually highly dependent on the average density of particles. Consequently, by increasing the number density one may form roton minima which will eventually be populated in a first order phase transition.

Finite momentum minima are crucial, but so too is a long-wavelength repulsion in order to ensure a finite non-negative compressibility.

- The additional broken translational symmetry in the supersolid phase creates new Goldstone modes. In some experimental set ups it is possible to measure the Goldstone modes, but it is currently unclear how the introduction of these additional modes affects features of superfluidity in the supersolid. More precisely, is there a new formulation of Landau's critical velocity in this system?

The eGPE is typically solved using a finite-differencing scheme applied to a Runge-Kutta algorithm. This is described in some detail starting on page 42.

Finally, it is difficult to numerically simulate the Saunders experiment, and increasingly difficult to obtain dynamical responses of the supersolid. By comparison, the eGPE is a relatively straightforward numerical problem, and has been shown to predict experimental results (at least in terms of a phase diagram) to good accuracy [23]. However, there is still no complete effective theory of supersolids which emerges from a microscopic theory.

This will be the goal of this thesis, to attempt to describe supersolidity using a meanfield approximation and to subsequently derive the dynamic responses of a supersolid.

3 Concepts around Superfluidity and BECs

In this chapter we will first start by going through basic superfluid theory in order to apply the techniques we develop to supersolids. We will then extend the theory to a first approximation of a supersolid, discuss the insights we gain and the physics we miss out on due to the approximation.

3.1 Single condensate at $p = 0$

While Bose-Einstein Condensates (BECs) are often talked about in literature regarding superfluids, it is important to note that a superfluid is **not** a BEC. Though most of the time a superfluid has a BEC component, superfluids **do not require** a BEC to exist, and conversely not all BECs are superfluid.

One of the most important features of superfluids is their dispersion relation. If we take a standard non-interacting Bose gas which has a dispersion relation

$$\epsilon(\mathbf{p}) = \frac{\mathbf{p}^2}{2m} \tag{3.1.1}$$

and substitute it into the Landau criterion,

$$v_c = \min_p \frac{\epsilon(\mathbf{p})}{p}, \tag{3.1.2}$$

then we see that $v_c \propto \mathbf{p}$, and if we choose minimal values of $\mathbf{p}$ (i.e. $\mathbf{p} = 0$) then there is no critical velocity v_c, and we will always have flow with dissipation (friction). This implies that interactions **must** be necessary to produce a superfluid system, and simply having a BEC or other type of long range order (quasi or otherwise) is insufficient and not even necessary.

To come to a picture which describes superfluids accurately, we must start by including interactions. We begin by considering a system of atoms which form a BEC state, and apply the Hartree approximation

$$\Psi(\mathbf{r}_1, \mathbf{r}_2, \ldots, \mathbf{r}_N) = \phi(\mathbf{r}_1)\phi(\mathbf{r}_2)\ldots\phi(\mathbf{r}_N) \tag{3.1.3}$$

Explicitly, a superfluid is defined by macroscopic properties, namely, it is a fluid which flows without viscosity. This means that there are no accessible excitations of the fluid at the velocity it is flowing at. The Landau criterion can be derived via arguments concerning Galilean invariance, and briefly is summarised as

$$\epsilon(\mathbf{p}) + \mathbf{v}\cdot\mathbf{p} < 0$$

where $\epsilon(\mathbf{p})$ is the dispersion relation at momentum $\mathbf{p}$ and $\mathbf{v}$ is the flow velocity. So long as the flow velocity is less than some critical value

$$v_c = \min_p \frac{\epsilon(\mathbf{p})}{p},$$

(where the minimum indicates calculating over all values of $\mathbf{p}$) then there is insufficient energy to create an excitation of the fluid. It is also **not** necessary to have some form of long ranged order in a superfluid, though one does usually exist and is most often provided by a BEC component. However, in low-dimension ($d \leq 2$) systems no BEC can exist (due to impossibility of SSB by Hohenberg-Wagner Theorem) but we can still have a form of quasi-long ranged order due to the BKT transition.

N.B. We assume that from this point our system is at 0*K*, and is completely in a condensate (i.e. there is no normal fraction).

which, when applied to a BEC where all the particles are in the same state, greatly reduces the complexity of the wavefunction.

We continue by applying the many body Hamiltonian

$$H = -\frac{\hbar^2}{2m}\sum_i \nabla_i^2 + V_{ext}(\mathbf{r}_i) \tag{3.1.4}$$

which considers the many-body kinetic energy and the many-body potential energy due to some external potential V_{ext}. We find that

$$\begin{aligned}\langle\Psi|\,\hat{H}\,|\Psi\rangle &= \int \prod_i \phi^*(\mathbf{r}_i)\left[-\frac{\hbar^2}{2m}\sum_i \nabla_i^2 + V_{ext}(\mathbf{r}_i)\right]\prod_i \phi(\mathbf{r}_i)\;\mathrm{d}\mathbf{r}_1\ldots\mathrm{d}\mathbf{r}_N \\ &= \sum_i \int \frac{\hbar^2}{2m}|\nabla_i\phi(\mathbf{r}_i)|^2\left(\prod_{i\neq j}|\phi(r_j)|^2\right) + \phi^*(\mathbf{r}_i)V_{ext}(\mathbf{r}_i)\phi(\mathbf{r}_i)\;\mathrm{d}\mathbf{r}_1\ldots\mathrm{d}\mathbf{r}_N\end{aligned} \tag{3.1.5}$$

where we then use the fact that $\int |\phi(\mathbf{r}_i)|^2\,\mathrm{d}\mathbf{r}_i = 1$ to obtain

$$\langle\Psi|\,\hat{H}\,|\Psi\rangle = N\int\left[\frac{\hbar^2}{2m}|\nabla\phi(\mathbf{r})|^2 + V_{ext}(\mathbf{r})|\phi(\mathbf{r})|^2\right]\mathrm{d}\mathbf{r}\,. \tag{3.1.6}$$

We then rescale the mean-field wavefunction $\phi = (1/\sqrt{N})\psi$ to then obtain

$$\langle\Psi|\,\hat{H}(\mathbf{r},t)\,|\Psi\rangle = \frac{\hbar^2}{2m}\int|\nabla\psi(\mathbf{r},t)|^2\,\mathrm{d}\mathbf{r} + \int V_{ext}(\mathbf{r},t)|\psi(\mathbf{r},t)|^2\,\mathrm{d}\mathbf{r} \tag{3.1.7}$$

which is now a single-particle Hamiltonian in a classical field theory. This describes a BEC in an external potential with no self-interaction, under a meanfield approximation.

We have already concluded that superfluids need interactions, so we now add an interaction term which arises from a two body scattering process.

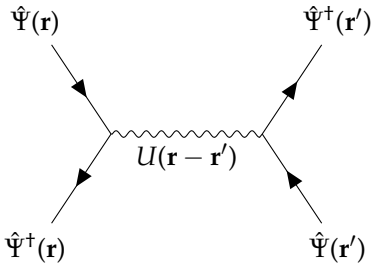


Fig. 3.1: A cursory diagram detailing a two particle scattering process via some interaction potential $U(\mathbf{r}-\mathbf{r}')$. Though this is not meant to be interpreted literally, it does provide some intuitive basis for how we arrive at the Gross-Pitaevskii equation.

We can consider a generic interaction potential $U(\mathbf{r}-\mathbf{r}')$, whose form we do not define precisely yet, but with the key bosonic feature that it is symmetric under exchange of coordinates. With this we define the interaction potential as:

$$\sum_{i<j} U(\mathbf{r_i}-\mathbf{r_j}) \tag{3.1.8}$$

where the summation indicates that we are summing over both i and j but with the distinction that i must be less than j in order to not have self interactions.

This can be easily rewritten by instead considering a summation s.t. $i \neq j$ and observing that terms like $U(\mathbf{r}_\gamma - \mathbf{r}_\kappa) = U(\mathbf{r}_\kappa - \mathbf{r}_\gamma)$, which allows us to then write the interaction potential as

Note that this is an effective interaction; as such we are allowed a little freedom in selecting various different interactions.

$$\hat{U} = \frac{1}{2}\sum_{i\neq j} U(\mathbf{r_i} - \mathbf{r_j}). \tag{3.1.9}$$

It is important to note that this is a two body operator, and therefore it must be sandwiched between two number operators. Consequently, we want the interaction energy

$$\langle n|\,\hat{U}\,|n\rangle = \frac{1}{2}\sum_i \int \prod_i |\phi(\mathbf{r}_i)|^2 \sum_{j\neq i} \int U(\mathbf{r}_i - \mathbf{r}_j) \prod_{j\neq i} |\phi(\mathbf{r}_j)|^2 \,\mathrm{d}\mathbf{r}_j\,\mathrm{d}\mathbf{r}_i\,, \tag{3.1.10}$$

which we then rescale to ψ and obtain

$$\begin{aligned}\langle n|\,\hat{U}\,|n\rangle &= \frac{1}{2}\sum_i \int |\phi(\mathbf{r}_i)|^2 \sum_{j\neq i} \int U(\mathbf{r}_i - \mathbf{r}_j)|\phi(\mathbf{r}_j)|^2 \,\mathrm{d}\mathbf{r}_j\,\mathrm{d}\mathbf{r}_i \\ &= \frac{1}{2}N(N-1)\int |\phi(\mathbf{r})|^2 \left(U * |\phi|^2\right)(\mathbf{r})\,\mathrm{d}\mathbf{r} \\ &= \frac{1}{2}(1-\frac{1}{N})\int |\psi(\mathbf{r})|^2 \left(U * |\psi|^2\right)(\mathbf{r})\,\mathrm{d}\mathbf{r}\,.\end{aligned} \tag{3.1.11}$$

The notation $(A * B)(\mathbf{r})$ denotes the convolution of two functions A and B, and is a function of $\mathbf{r}$. Here we use the normalisation property of the wavefunction $\int |\phi|^2\,\mathrm{d}\mathbf{r} = 1$ to simplify the expression.

Finally, we make the assumption that N is large and therefore $1/N \to 0$, which results in

$$\langle n|\,\hat{U}\,|n\rangle = \frac{1}{2}\int |\psi(\mathbf{r})|^2 \left(U * |\psi|^2\right)(\mathbf{r})\,\mathrm{d}\mathbf{r}\,. \tag{3.1.12}$$

This is a general expression for any arbitrary interaction potential $U(\mathbf{r})$. We now make a final step to obtain the end goal, the Gross-Pitaevskii equation (GPE), by selecting the interaction potential as

$$U(\mathbf{r} - \mathbf{r}') = g\delta^{(3)}(\mathbf{r} - \mathbf{r}') \tag{3.1.13}$$

which is known as the contact potential.

We can simplify the interaction term in the particular case of the contact potential (via propeties of the Dirac delta) and find that

The GPE is a particular variety of *non-linear Schrödinger equation* (NLSE), where the more general NLSE has any particular interaction $U(\mathbf{r} - \mathbf{r}')$ and the GPE has the contact potential.

$$\begin{aligned}\langle \Psi|\,\hat{H}(\mathbf{r},t)\,|\Psi\rangle = \int \Big[&-\frac{\hbar^2}{2m}\psi^*(\mathbf{r},t)\nabla^2\psi(\mathbf{r},t) + V_{ext}(\mathbf{r},t)|\psi(\mathbf{r},t)|^2 \\ &+\frac{g}{2}|\psi(\mathbf{r},t)|^2|\psi(\mathbf{r},t)|^2\Big]\,\mathrm{d}^3\mathbf{r}\end{aligned} \tag{3.1.14}$$

which is the full interacting meanfield Hamiltonian. We then employ the Schrödinger equation

$$\hat{H}\,|\Psi\rangle = i\hbar\frac{\partial}{\partial t}\,|\Psi\rangle \equiv i\hbar\frac{\partial}{\partial t}\psi(\mathbf{r},t) \tag{3.1.15}$$

and assume that ψ is a state completely in the condensate which has a unitary time evolution described by

$$\psi(\mathbf{r}, t) = e^{-i\mu t/\hbar}\psi(\mathbf{r}) \tag{3.1.16}$$

such that we then find

$$\langle \Psi(\mathbf{r}, t)| \hat{H} |\Psi(\mathbf{r}, t)\rangle = \int \mu |\psi(\mathbf{r}, t)|^2 \, \mathrm{d}^3\mathbf{r} \quad . \tag{3.1.17}$$

Minimizing the energy with respect to the wavefunction (by using variational calculus), we find

$$\left[-\frac{\hbar^2}{2m}\nabla^2 + V_{ext}(\mathbf{r}, t) + g|\psi(\mathbf{r})|^2 - \mu \right] \psi(\mathbf{r}) = 0 \tag{3.1.18}$$

which is the differential form of the Gross-Pitaevskii equation.

N.B. The system described by this equation is superfluid (as we will later see) but does not contain rotons.

We now move on to determining quantum fluctuations in the system. Here we will employ both the Bogoliubov approximation and the Bogoliubov transformation to obtain a dispersion relation which describes excitations in this quantum fluid.

Let us first start by taking the interaction potential and transferring it over to k-space. Recall that the field operator is

$$\hat{\Psi}(\mathbf{r}) = \frac{1}{\sqrt{V}} \sum_{\mathbf{p}} \hat{a}_{\mathbf{p}} e^{-i\mathbf{p}\cdot\mathbf{r}} \quad . \tag{3.1.19}$$

We can then consider the many body interaction energy in the k-space basis by performing a Fourier transform and obtain

$$\langle \Psi| \hat{U} |\Psi\rangle \equiv \langle \hat{U} \rangle = \frac{g}{2} \langle \Psi| \sum_{\mathbf{p}_1, \mathbf{p}_2, \mathbf{q}} \hat{a}^\dagger_{\mathbf{p}_1+\mathbf{q}} \hat{a}^\dagger_{\mathbf{p}_2-\mathbf{q}} \hat{a}_{\mathbf{p}_1} \hat{a}_{\mathbf{p}_2} |\Psi\rangle \quad . \tag{3.1.20}$$

In this following short section I will omit the $\langle\psi| \ldots |\psi\rangle$ for brevity.

We then want to consider the effects the interaction potential would have when it involves the condensate. As we have only three momentum variables and must have momentum conservation, when we set one of the variables to $\mathbf{p} = 0$ (the condensate momentum) then it implies that we must have interactions where:

There are some important features to note. Firstly, the interaction potential, when Fourier transformed looks like

$$\mathcal{F}\left[\frac{g}{2}\delta^{(3)}(\mathbf{r} - \mathbf{r}')\right] = \frac{g}{2}\delta_{\mathbf{p}\mathbf{p}'}$$

where $\delta_{\mathbf{p}\mathbf{p}'}$ is the Kronecker delta. This allows us to perform the summation over only three variables $(\mathbf{p_1}, \mathbf{p_2}, \mathbf{q})$. The second important feature is the fact that, due to momentum conservation, the two created particles must have total equivalent momentum to the two annihilated particles, hence why they have momentums $\mathbf{p_1} + \mathbf{q}$ and $\mathbf{p_2} - \mathbf{q}$ respectively. Note that this is exactly equivalent to a elastic scattering problem.

- The condensate interacts only with itself

$$\langle \hat{U} \rangle = \hat{a}^\dagger_0 \hat{a}^\dagger_0 \hat{a}_0 \hat{a}_0 \tag{3.1.21}$$

  which is just two-particle scattering and only has one unique Feynman diagram (diagram (a) in Fig. 3.2).

- Total momentum before and after = 0

$$\langle \hat{U} \rangle = \sum_{\mathbf{p}\neq 0} \left[\hat{a}^\dagger_{\mathbf{p}} \hat{a}^\dagger_{-\mathbf{p}} \hat{a}_0 \hat{a}_0 + \hat{a}^\dagger_0 \hat{a}^\dagger_0 \hat{a}_{\mathbf{p}} \hat{a}_{-\mathbf{p}} \right] \tag{3.1.22}$$

  which corresponds to two unique Feynman diagrams where either two excitations exit the condensate or two excitations enter the condensate. Note that these processes are just the time reversed version of each other, as can be seen in diagram (b) in Fig. Fig. 3.2.

- Total momentum before and after $\neq 0$

$$\sum_{\mathbf{p}\neq 0}\left[\hat{a}^\dagger_{\mathbf{p}}\hat{a}^\dagger_0\hat{a}_0\hat{a}_{\mathbf{p}} + \hat{a}^\dagger_{\mathbf{p}}\hat{a}^\dagger_0\hat{a}_{\mathbf{p}}\hat{a}_0 + \hat{a}^\dagger_0\hat{a}^\dagger_{\mathbf{p}}\hat{a}_{\mathbf{p}}\hat{a}_0 + \hat{a}^\dagger_0\hat{a}^\dagger_{\mathbf{p}}\hat{a}_0\hat{a}_{\mathbf{p}}\right] \tag{3.1.23}$$

  which can correspond to two different scenarios where either the excitation scatters off the condensate or it pushes out a condensate particle and replaces it. This is shown by diagrams (c) and (d) in Fig. 3.2 respectively. We note that because we can flip the time direction, we obtain the different ordering of the operators.

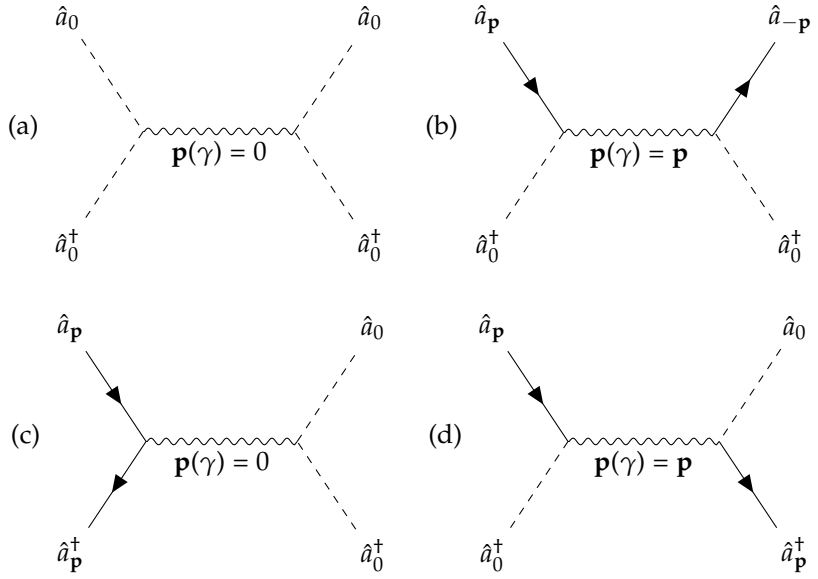


Fig. 3.2: A set of diagrams for the types of interactions, where time is going downwards.

We can then consider the commutation relation between the operators, and the nature of the $\mathbf{p} = 0$ operators. Firstly, we note that we have a standard bosonic commutation relation, i.e. $\left[\hat{a}_{\mathbf{p}}, \hat{a}^\dagger_{\mathbf{p}'}\right] = \delta_{\mathbf{p}\mathbf{p}'}$, and so our expressions can be re-ordered freely. This is used mostly in the third diagram to pack the operators together and obtain a combinatorial factor of 4. We then perform the Bogoliubov approximation, where we say that the condensate is effectively a reservoir. This means that applying a creation/annihilation operator to the state actually doesn't affect it at all (approximately). Note that this is equivalent to saying that the condensed state is coherent.

We are hence able to replace the operators relating to ψ_0 with their c-numbers, in this case $\hat{a}_0 \to a_0 = \sqrt{N}$ where N is the macroscopic fraction of occupation of the condensate. This then allows us to rewrite our total contribution to the interaction potential (when considering either condensate/condensate or condensate/excitation interactions) to be

The $|\mathbf{p}\rangle$ states are forward moving excitations of the condensate (and similarly $|-\mathbf{p}\rangle$ are backward moving excitations).

$$\langle U\rangle = \frac{gN}{2}\sum_{\mathbf{p}}\left[\hat{a}^\dagger_{\mathbf{p}}\hat{a}^\dagger_{-\mathbf{p}} + \hat{a}_{\mathbf{p}}\hat{a}_{-\mathbf{p}} + 4\hat{a}^\dagger_{\mathbf{p}}\hat{a}_{\mathbf{p}}\right] \quad . \tag{3.1.24}$$

It is important to note that this interaction term leads to particle mixing between states $|\mathbf{p}\rangle$ and $|-\mathbf{p}\rangle$, and hence the $|\pm\mathbf{p}\rangle$ states are not eigenstates of the Hamiltonian. Our task is to then find a basis which diagonalises the Hamiltonian, which of course means finding the eigenbasis. This is done via the Bogoliubov transformation.

This is splitting up real particles into quasiparticles with positive and negative momenta.

The Bogoliubov transformation is defined as

$$\hat{a}_{\mathbf{p}} = u_{\mathbf{p}}\hat{b}_{\mathbf{p}} + v^*_{-\mathbf{p}}\hat{b}^\dagger_{-\mathbf{p}}\,, \quad \hat{a}^\dagger_{\mathbf{p}} = u^*_{\mathbf{p}}\hat{b}^\dagger_{\mathbf{p}} + v_{-\mathbf{p}}\hat{b}_{-\mathbf{p}} \tag{3.1.25}$$

where the key feature of the Bogoliubov transformation then lies in the commutation relation of the new Bogoliubov operators $\hat{b}$ and $\hat{b}^\dagger$.

We impose that the operators have a standard boson commutation relation, i.e. that $\left[\hat{b}_{\mathbf{p}}, \hat{b}^\dagger_{\mathbf{p}'}\right] = \delta_{\mathbf{p}\mathbf{p}'}$. Using that and the commutation relation for the $\hat{a}$ and $\hat{a}^\dagger$ operators, we can easily see that we require

$$\left|u_{\mathbf{p}}\right|^2 - \left|v_{-\mathbf{p}}\right|^2 = 1 \tag{3.1.26}$$

which can be satisfied if we represent these amplitudes as hyperbolic functions. More specifically,

$$u_{\mathbf{p}} = \cosh\left(\alpha_{\mathbf{p}}\right), \quad v_{-\mathbf{p}} = \sinh\left(\alpha_{\mathbf{p}}\right), \tag{3.1.27}$$

where the parameter $\alpha_{\mathbf{p}}$ will be chosen such that the non-diagonal terms in the Hamiltonian go to zero.

After performing the maths we can find

$$\coth\left(2\alpha_{\mathbf{p}}\right) = -\frac{p^2/2m + gn}{gn} \implies u_{\mathbf{p}}, v_{-\mathbf{p}} = \pm\left[\frac{p^2/2m + gn}{2\epsilon(p)} \pm \frac{1}{2}\right] \tag{3.1.28}$$

where $\epsilon(p)$ is the dispersion relation defined by

$$\mathcal{H} = E_0 + \sum_{\mathbf{p}} \epsilon(p)\hat{b}^\dagger_{\mathbf{p}}\hat{b}_{\mathbf{p}}\,. \tag{3.1.29}$$

Here, E_0 is the ground state energy of the system (not relevant) and the explicit form of the dispersion relation is

$$\epsilon(p) = \left[\frac{gn}{m}p^2 + \left(\frac{p^2}{2m}\right)^2\right]^{\frac{1}{2}} \tag{3.1.30}$$

While this does explain the phenomena of superfluidity (at least in a weakly interacting BEC gas), we still have some unexplained features in the theory. For instance, the critical velocity is actually significantly lower than the one predicted by the Bogoliubov treatment. One reason for this is the appearance of a roton in the dispersion relation, illustrated in Fig. 3.3, which we will discuss later.

which is the famous Bogoliubov dispersion relation.

Analysing the behaviour of $\epsilon(p)$ at small and large p, we see that

$$\lim_{p\to\infty}\epsilon(p) \sim \frac{p^2}{2m} \quad ; \quad \lim_{p\to 0}\epsilon(p) \sim \sqrt{\frac{gn}{m}}\,p \tag{3.1.31}$$

i.e. that at large p the dispersion relation is approximately quadratic, and at small p it is linear. If we reconsider the Landau criterion (3.1.2) we can recall that in order for there to exist flow without dissipation,

we would need at most linear dependence on p in the dispersion relation. Since this is achieved with the Bogoliubov treatment, our superfluid behaviour is explained.

An alternative method of applying the Bogoliubov transformation will be shown (note that this is how we will apply the Bogoliubov transformation later in this thesis). We first use a Legendre transformation to convert the Hamiltonian to a Lagrangian, and then we apply the Madelung transformation

$$\psi(\mathbf{r},t) = \sqrt{\rho(\mathbf{r},t)}e^{i\phi(\mathbf{r},t)} \tag{3.1.32}$$

The Madelung transformation makes the Lagrangian look considerably more 'hydrodynamic'.

which converts the complex wavefunction ψ into a density and phase representation.

The combination of these two transformations converts the Hamiltonian into the following Lagrangian

$$\begin{aligned}\mathcal{L} = -\int_\Omega \Bigg[&\hbar\rho\frac{\partial\phi}{\partial t} + \frac{\hbar^2}{2m}\left(\rho(\nabla\phi)^2 + \frac{1}{4\rho}(\nabla\rho)^2\right) \\ &+\frac{1}{2}\rho(\mathbf{r})\int_\Omega U(|\mathbf{r}-\mathbf{r}'|)\rho(\mathbf{r}')\,\mathrm{d}\mathbf{r}'\Bigg]\,\mathrm{d}\mathbf{r}\end{aligned} \tag{3.1.33}$$

Note here we are back to considering a general interaction potential $U(\mathbf{r}-\mathbf{r}')$.

where the global minus sign is a conventional choice.

The GPE can then be found by minimizing the Lagrangian variationally. The Euler-Lagrange equations that arise for the field ρ and ϕ are

$$\partial_t\rho + \frac{\hbar}{m}\boldsymbol{\nabla}\cdot(\rho\boldsymbol{\nabla}\phi) = 0 \tag{3.1.34}$$

$$\frac{\hbar^2}{4m}\left(\frac{(\nabla\rho)^2}{2\rho^2} - \frac{\nabla^2\rho}{\rho}\right) + U*\rho + \frac{\hbar^2}{2m}(\nabla\phi)^2 + \hbar\partial_t\phi = \mu\,. \tag{3.1.35}$$

The notation $a*b$ refers to a convoluted with b, i.e.

$$[a*b](\mathbf{r}) \equiv \int_\Omega a(\mathbf{r}-\mathbf{r}')b(\mathbf{r}')\,\mathrm{d}\mathbf{r}'$$

and is equivalent, via Plancherel's theorem, to

$$[a*b](\mathbf{r}) \equiv \mathcal{F}^{-1}\left[\mathcal{F}[a]\cdot\mathcal{F}[b]\right](\mathbf{r})$$

where $\mathcal{F}[g]$ and $\mathcal{F}^{-1}[\hat{g}]$ denotes the Fourier transform of g and inverse Fourier transform of $\hat{g}$, respectively.

Upon inspection of the Lagrangian (3.1.33), we note that the Lagrangian is maximised by setting $\nabla\phi = \partial_t\phi = 0$, i.e. there is no spatial or temporal variation in the $U(1)$ phase. The ground state must then be found by solving (3.1.35) with the above constraint, which generates

$$\frac{\hbar^2}{4m}\left(\frac{(\nabla\rho)^2}{2\rho^2} - \frac{\nabla^2\rho}{\rho}\right) + U*\rho - \mu = 0\,. \tag{3.1.36}$$

The solution of this equation for ρ given a U and some μ will provide the ground state density $\rho_0(\mathbf{r},t)$.

This Lagrangian can generate supersolid phases provided the effective interaction has at least some negative components at $\mathbf{k}\neq 0$ [32], and is sufficiently strong to incur a quantum phase transition.

One interaction that has been shown to generate a modulated density is the Heaviside interaction (sometimes called the *soft-core*

If you want an interaction that will generate a supersolid, you need something that has attractive interactions at the ordering wavevector, but repulsive interactions at long-wavelength in order to ensure finite non-negative compressibility.

boson model) [36, 10]

$$U(\mathbf{r}-\mathbf{r}') = \Theta(a - |\mathbf{r}-\mathbf{r}'|) = \begin{cases} U_0 & |\mathbf{r}-\mathbf{r}'| < a \\ 0 & |\mathbf{r}-\mathbf{r}'| \geq > a \end{cases} \tag{3.1.37}$$

where r is the radial coordinate, and a is the interaction range.

Consider the Bogoliubov dispersion relation for this interaction potential. An alternative formulation of the Bogoliubov technique is created by choosing the excitations to be $\delta\rho$ and ϕ, and linearising the equations of motion. One then arrives at the following equations for ϕ and $\delta\rho$

$$\begin{aligned} \partial_t \delta\rho &= -\frac{\hbar}{m}\nabla\cdot(\rho\nabla\phi) \\ -\hbar\partial_t\phi &= -\frac{\hbar^2}{4m\rho}\nabla\cdot\left(\rho\nabla\left(\frac{\delta\rho}{\rho}\right)\right) + U * \delta\rho \quad . \end{aligned} \tag{3.1.38}$$

It is useful to Fourier transform these equations; using the plane wave basis $e^{i\mathbf{k}\cdot\mathbf{x}-\omega t}$ we obtain the following equations

Note here the use of the convolution theorem.

$$\begin{aligned} -i\omega\delta\rho &= \frac{\hbar}{m}\rho k^2\phi \\ i\hbar\omega\phi &= \frac{\hbar^2}{4m\rho}k^2\delta\rho + U_{\mathbf{k}}\delta\rho \end{aligned} \tag{3.1.39}$$

where $U_{\mathbf{k}}$ is the Fourier transform of the interaction potential $U(\mathbf{r}-\mathbf{r}')$.

Recalling that $E = \hbar\omega$ and $p = \hbar k$, by substituting the equations into each other we find

$$E^2\delta\rho = \left(\frac{p^2}{2m}\right)^2\delta\rho + \frac{p^2}{m}\rho U_{\mathbf{k}}\delta\rho \tag{3.1.40}$$

which is a general wave equation for the excitations. Consequently, one can then find the dispersion relation of any homogeneous BEC described by the GPE

$$E(p) = \sqrt{\left(\frac{p^2}{2m}\right)^2 + \frac{p^2}{m}\rho U_k} \tag{3.1.41}$$

which is valid for any interaction potential $U(\mathbf{r}-\mathbf{r}')$ (given that the ground state density is a constant ρ).

In order to see the appearance of supersolid phases in a Heaviside potential system, consider defining a dimensionless ground-state energy density. We begin by rescaling so that a is now our length scale, i.e. $a = 1$, which allows us to express the energy per particle as

$$\bar{\mathcal{E}} = \frac{1}{|\Omega|}\int_\Omega \frac{1}{8\rho}(\nabla\rho)^2 + \frac{\Lambda}{2}\rho\,\bar{U} * \rho \; \mathrm{d}^2\mathbf{r} \quad . \tag{3.1.42}$$

Recall that a is defined in (3.1.37) and is the length scale of the soft-core interaction.

This is a general energy density valid in any dimension; we will conduct our research in $2D$ primarily, and for $2D$ we find

$$\Lambda = \frac{ma^2}{\hbar^2} n\pi a^2 U_0 \tag{3.1.43}$$

where n is the average density of particles.

As the ground state of the system is the density distribution ρ which minimises the above energy per particle, we can see that the quantum phase transition will be determined entirely by Λ. By solving the dispersion relation in (3.1.41), we can observe the emergence of a roton minima Fig. 3.3.

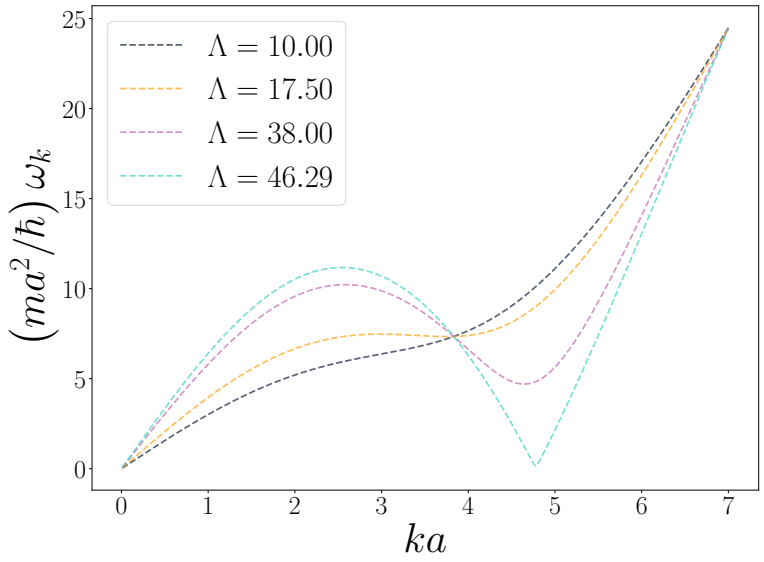


Fig. 3.3: The dispersion relation for superfluid ^{4}He with a top-hat interaction at various Λ (where Λ is a dimensionless parameter that describes interaction strength and will be introduced later). We see that the existence of the roton minimum is dependent on the strength of the interaction, and in fact we can get a phase transition prior to the roton minimum touching $E = 0$ [36].

Depending on the value of Λ, the dispersion relation can show inflection points, local minima or even degenerate global minima at finite momenta. As a consequence the system can lower its energy by distributing density at finite momenta, which leads to the formation of the supersolid phase. It is crucial to recognise that this is a feature of an interaction potential with non-trivial k-space dependency. More specifically, there must be an attractive $k \neq 0$ component of the interaction at the very least.

The value of the roton minima in some sense drives the phase transition. Previous work [36] has shown that prior to the softening of the roton mode a first order phase transition is possible, and appears to agree relatively well with numerical simulations of the GPE, which brings us to our next section.

Softening of the roton mode refers to the roton minima touching the $E = 0$ line.

3.2 GPE Numerically

The GPE is sometimes called the non-linear Schrödinger equation, on account of the Euler-Lagrange equation (3.1.18)

$$\left[-\frac{\hbar^2}{2m}\nabla^2 + V_{ext}(\mathbf{r},t) + g|\psi|^2 - \mu\right]\psi = 0 \tag{3.2.1}$$

having the same functional form as the Schrödinger equation but with the additional $|\Psi|^2$ term rendering the differential equation non-linear. Consequently, there is no general analytical solution which can be expressed for arbitrary external potential or interaction potential. One must then tackle the equation numerically, which we will detail here.

Consider the time-dependent GPE for a general interaction potential U in zero external potential

$$\left[-\frac{\hbar^2}{2m}\nabla^2 + U * |\psi|^2 - \mu\right]\psi = i\hbar\partial_t\psi \tag{3.2.2}$$

where we have imposed a constrained number of particles, set by the Lagrange multiplier μ. We then perform a Wick rotation on the time variable $t = -i\tau$, which transforms the above equation into

$$\left[-\frac{\hbar^2}{2m}\nabla^2 + U * |\psi|^2 - \mu\right]\psi = -\hbar\partial_\tau\psi \quad . \tag{3.2.3}$$

This allows us to find a solution to GPE by propagating this imaginary time diffusion equation to $\tau = \infty$.

Given some initial wavefunction $\psi(\tau_0)$, in order to find $\psi(\tau + \delta\tau)$, one can use a Runge-Kutta time propagation technique. Given some initial function $\psi(\mathbf{x}, t)$ and some equation which determines the rate of change of ψ with respect to time, i.e. the non-linear Schrödinger equation represented like so

$$\partial_t\psi = F(t, \psi(t)) \tag{3.2.4}$$

one can define the following functions assuming some initial time t and some finite time step δt

$$\begin{aligned} k_1 &= F(t, \psi) \\ k_2 &= F\left(t + \delta t/2, \psi + k_1 \cdot \delta t/2\right) \\ k_3 &= F\left(t + \delta t/2, \psi + k_2 \cdot \delta t/2\right) \\ k_4 &= F\left(t + \delta t, \psi + k_3 \cdot \delta t\right) \end{aligned} \tag{3.2.5}$$

with the conclusive statement then being

$$\psi(t + \delta t) = \psi(t) + \frac{\delta t}{6}\left(k_1 + 2k_2 + 2k_3 + k_4\right) \tag{3.2.6}$$

This is a nifty little trick in quantum mechanics; imagine picking some initial random Ψ, which we then express as a function of time like so

$$\Psi(t) = \sum_n^\infty \psi_n e^{-iE_n t/\hbar}$$

where ψ_n are the eigenfunctions of your Hamiltonian and E_n are their energies. By performing a Wick rotation this transforms Ψ into

$$\Psi(\tau) = \sum_n^\infty \psi_n e^{-E_n \tau/\hbar} \quad .$$

Consider now the effect of pushing $\tau \to \infty$. Assuming there is a unique ground state, if you divide the wavefunction by $e^{-E_o\tau/\hbar}$ you obtain

$$\Psi(\tau)/e^{-E_0\tau/\hbar} = \psi_0 + \mathcal{O}(e^{-(E_1-E_0)\tau/\hbar})$$

and now by pushing τ to ∞ we see that all the non-ground state eigenwaves are truncated by an $e^{-\infty}$ term. What remains is only the ground state. In essence by going to infinite imaginary time you have decayed away any superposition of non-ground state eigenwaves in your initial random distribution.

which specialises the broad class of Runge-Kutta family to the specific RK4 technique.

In this way we can approximate $\psi(t+\delta t)$ given some $\psi(t)$ relatively well. The Runge-Kutta techniques are famously subject to careful constraints on the time step in order to ensure convergence of the technique [63, 64].

Combining this with a Wick rotation, we are able to notionally solve the GPE. The final condition to impose is self consistency, i.e. that $\psi(\tau+\delta\tau)=\psi(t)$, in other words $\partial_\tau\psi=0$, which is the statement that we have reached the ground state. This is done quite simply by calculating the fractional difference between iterative wavefunctions

$$f(\tau,\delta\tau)=\frac{\|\psi(\tau+\delta\tau)-\psi(\tau)\|}{\|\psi(\tau)\|} \tag{3.2.7}$$

where $\|\psi\|$ is the Frobenius norm of ψ i.e.

$$\|M\| = \sqrt{\sum_{i,j}|M_{ij}|^2} \tag{3.2.8}$$

and stating that the algorithm is converged once the fractional difference drops below some user-specified tolerance. In this way we are able to satisfy (3.1.36) and hence find the ground state density ρ.

Consider the general GPE given by (3.1.36); we have shown that we *can* solve it, but how have we chosen to actually implement the linear operations defined in this system? The most straightforward answer is by discretising a spatial grid, employing periodic boundary conditions, and using finite differencing techniques.

This is a relatively standard procedure which we assume the reader is familiar with, so we will not describe it in explicit detail except for one particular feature.

- A $2D$ supersolid with a soft-core interaction forms a triangular lattice in periodic boundary conditions.
- Triangular lattices are characterised by the following set of reciprocal lattice vectors

$$G_i = G\cdot\left[(0,1),\left(\frac{\sqrt{3}}{2},\frac{1}{2}\right),\left(\frac{\sqrt{3}}{2},-\frac{1}{2}\right)\right] \tag{3.2.9}$$

  where G is the reciprocal lattice spacing.
- If you discretise your physical space (and have a finite box size, which causes your reciprocal space to be discretized) it is impossible to have reciprocal lattice discretisations which are centered on integer values of G as well as irrational values of G due to irrational numbers not being represented as fractions

Consider each of these terms in the context of a time derivative. Here we can see that k_1 is the slope at time t, k_2 is the approximate slope at the midpoint between t and $t+\delta t$ using k_1 as the derivative, k_3 is *also the slope at the midpoint* but this time calculated using k_2, and finally k_4 is the slope at the end. The RK4 technique calculates slopes at various points in the interval $[t,t+\delta t]$ via (3.2.5), then averages them with a weighting in (3.2.6) in order to obtain a good approximation for the objective function ψ at the time $t+\delta t$.

Note here that we are now treating ψ as a matrix because it is discretized on a grid.

N.B. This is just the 'first ring' of the supersolid reciprocal lattice vectors. Higher harmonics extend much farther out but are all linear superpositions of the lattice vectors defined here. Note also that the third lattice vector is a combination of the first two and is only included for posterity.

- Consequently, any discretisation in Cartesian space cannot perfectly represent a triangular lattice as the reciprocal lattice will always be slightly deformed.

In order to solve this problem one must search for non-Cartesian spaces which can accurately describe triangular lattices. In our work we elected to use a so-called 'parallelogram' basis.

Called the 'parallelogram basis' because the unit cell is a parallelogram.

We want to find a basis such that the lattice vectors which are

$$\mathbf{u} = \left(\frac{\sqrt{3}}{2}, \frac{1}{2}\right) \quad ; \quad \mathbf{v} = (0, 1) \tag{3.2.10}$$

in Cartesian space are represented by the vectors $(1, 0)$ and $(0, 1)$ in the basis given by $\mathbf{a}$ and $\mathbf{b}$. In other words we want to convert a unit cell given by the Cartesian coordinates

$$(0, 0) \to \left(\frac{\sqrt{3}}{2}, \frac{1}{2}\right) \to \left(\frac{\sqrt{3}}{2}, \frac{3}{2}\right) \to (0, 1) \tag{3.2.11}$$

into a unit cell given by the coordinates

$$(0, 0) \to (0, 1) \to (1, 1) \to (1, 1) \tag{3.2.12}$$

in the $\{\mathbf{a}, \mathbf{b}\}$ basis. See Fig. 3.4 for an illustration.

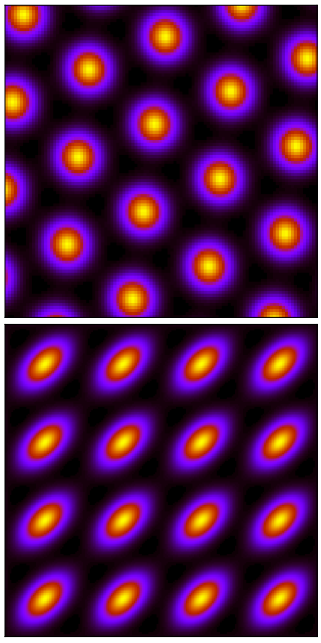


Fig. 3.4: Top figure showcases a triangular supersolid in Cartesian space; bottom figure is the same supersolid but represented in the parallelogram basis.

One can show that such a basis is given by

$$\mathbf{a} = \frac{2}{\sqrt{3}}\mathbf{x} \quad ; \quad \mathbf{b} = \mathbf{y} - \frac{1}{\sqrt{3}}\mathbf{x} \tag{3.2.13}$$

and the corresponding reciprocal space basis is

$$\mathbf{k_a} = \frac{\sqrt{3}}{2}\mathbf{k_x} + \frac{1}{2}\mathbf{k_y} \quad ; \quad \mathbf{k_b} = \mathbf{k_y} \tag{3.2.14}$$

where x and y refer to the Cartesian basis.

This transformation of the space induces a few changes into the typical numerical recipe of finite differencing. Firstly, it introduces a simple Jacobian into your integrals, s.t.

$$\int_\Omega \mathrm{d}x\, \mathrm{d}y \to \int_{\Omega'} \frac{\sqrt{3}}{2}\, \mathrm{d}a\, \mathrm{d}b \tag{3.2.15}$$

which can readily be included easily into any integrals. Secondly, it changes the finite-differencing derivative operator.

Note that while using this particular spatial basis favours triangular lattice formation, we first scan the space in the Cartesian basis and then if the supersolid is triangular, we re-run the simulation in the parallelogram basis to obtain optimal results.

Consider now the following: if we construct a square grid of discrete points in the parallelogram basis, the nearest neighbours at any point $\{u_i, v_i\}$ (where u_i and v_i are the two coordinates in the parallelogram discretisation) are now no longer given by

$$\Big\{(u_{i+1}, v_i), (u_i, v_{i+1}), (u_{i-1}, v_i), (u_i, v_{i-1})\Big\}. \tag{3.2.16}$$

In fact the point now has 6 nearest neighbours given by

$$\Big\{(u_{i+1}, v_i), (u_{i+1}, v_{i+1}), (u_i, v_{i+1}), (u_{i-1}, v_i), (u_{i-1}, v_{i-1}), (u_i, v_{i-1})\Big\} \tag{3.2.17}$$

and therefore we have to reconsider our finite differencing scheme. In order to correctly construct a finite-differencing Laplacian that respects the geometry of this space, we have to derive a $C(6)$ invariant Laplacian.

We could use a '7 point stencil' which calculates the Laplacian over the nearest 6 neighbours, but for better numerical accuracy we use a Laplacian with next-nearest-neighbours; this means taking derivatives across the 12 nearest points. We call this the '13 point stencil' (see Fig. 3.5), defined by the weights α and β.

The following discussion centers on the Laplacian specifically, but the same point applies to any arbitrary derivative too (and we had to derive the correct derivatives for the numerics).

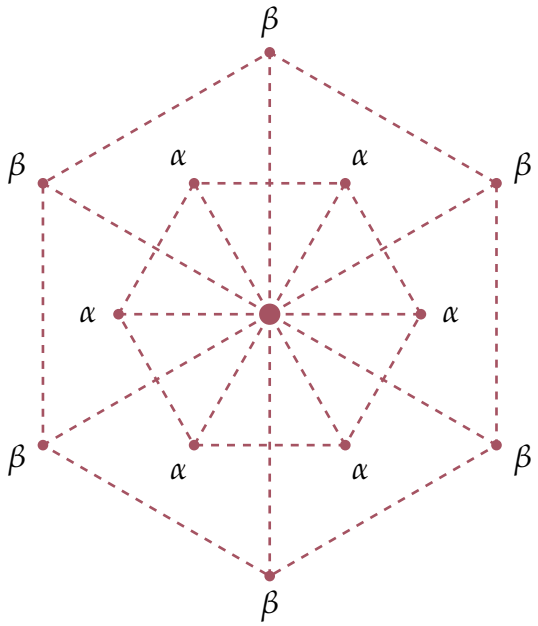


Fig. 3.5: The '13 point stencil' for the parallelogram basis. In order to calculate the Laplacian at the central point, one employs a finite differencing scheme over the nearest 12 points with α the weight for the nearest 6 and β for the next-nearest 6. The central point has a weighting of $-6(\alpha+\beta)$. This picture is drawn in Cartesian space and will look different in the parallelogram basis but importantly will have the exact same α and β.

These weights are found by Taylor expanding the Laplacian operator under a finite differencing scheme. Consider that the Laplacian operator $\hat{L}$ on a function f at position x_0 is given by

$$h^2 \hat{L} f(x_0) \approx \sum_i f(\delta_i)\alpha_i - f(x_0)\sum_i \alpha_i \tag{3.2.18}$$

where h is the discretisation spacing (assumed equal in both axes), δ_i are the various positions of the neighbours (currently unspecified how many) and α_i are the coefficients in this Taylor expansion.

Now consider expanding the summation up to the second nearest neighbour, while also recognising that

$$f(\delta_i) = r^\mu \partial_\mu f|_0 + r^\mu r^\nu \partial_\mu \partial_\nu f|_0 + \dots \tag{3.2.19}$$

i.e. expressing the value of a function as the inner product of its derivatives with the distances. By noting that the odd-order terms should disappear due to inversion symmetry, and truncating the sum up to fourth order derivatives, one can show

$$\begin{aligned} h^2 \hat{L} f = & \frac{3h^2}{2} (\nabla^2 f) \cdot (\alpha + 3\beta) \\ & + \frac{9h^4}{96} (\alpha + 9\beta) \left[\partial_x^4 f + \partial_y^4 f + 2\partial_x^2 \partial_y^2 f \right] \end{aligned} \tag{3.2.20}$$

We truncate at fourth order derivatives simply because we decided that sixth order derivatives, which would have a power of $\mathcal{O}(h^6)$ and hence a contributing error term to the Laplacian of $\mathcal{O}(h^4)$, was a sufficiently small error for our grid and the purposes of our calculation.

where α is α_i for $i \in [1, 6]$ and β is α_i for $i \in [7, 12]$.

We can find the values of α and β by ensuring that the factor in front of the Laplacian on the RHS is 1 and that the factor in front of the fourth order derivatives is 0. This gives us $\alpha = 1/h^2$ and $\beta = -1/(9h^2)$.

The combination of these various features allows us to generate 'true' triangular supersolids in the context of a finite differencing scheme.

3.3 *Condensates at finite momenta*

The previous section introduced the framework for studying superfluids in a meanfield context, derived some of the basic results relevant to the research in this thesis, and ended with a general Lagrangian which can generate supersolid behaviour.

In this section we will study a 1D model of a supersolid by extending the GPE to include condensate components at $p \neq 0$ with various approximations.

We start by considering a 1D system which now has the existence of 3 condensates; the standard one at $p = 0$ and two new ones at $p = \pm\mathbf{G}$, with energies $\epsilon_{p=0} = 0$ and $\epsilon_{p=\pm G} = \epsilon_G \neq 0$, respectively. Note that here we will interchange p with k freely and often.

We can construct a Hamiltonian $\mathcal{H}$ which contains the 'kinetic' terms and also the inter-condensate scattering terms, written in the Bogoliubov basis

$$\mathcal{H} = \epsilon_G \left(b_G^\dagger b_G + b_{-G}^\dagger b_{-G} \right) + \frac{1}{2L} \sum_{k,k',q} v_q b_{k-q}^\dagger b_{k'+q}^\dagger b_{k'} b_k \tag{3.3.1}$$

Note that this is exactly analogous to equation (3.1.20) with a key difference being that we are now considering scattering between **condensates** and not **excitations**.

where L is the length of the system (tends to ∞ in the thermodynamic limit), v_q is the interaction strength at momentum q (i.e. the Fourier component of the interaction potential at q) and the summation variables $\{k, k', q\} \in \{-G, 0, +G\}$ (i.e. we are only considering interactions between some set of condensates).

We can construct a trial wavefunction which is a coherent state:

$$|\Psi\rangle = \exp\left\{ \alpha_0 b_0^\dagger + \alpha_1 b_1^\dagger + \alpha_{-1} b_{-1}^\dagger \right\} |\text{vac}\rangle \tag{3.3.2}$$

where the subscripts $\{0, \pm 1\}$ correspond to $\{0, \pm G\}$ respectively. This state and the coefficients contained within are subject to the standard normalisation conditions, namely:

$$|\alpha_0|^2 + |\alpha_1|^2 + |\alpha_{-1}|^2 = N \tag{3.3.3}$$

where N is the particle number, and each coefficient α_i is in general $\mathbb{C}$ and represented by $\alpha_i = \sqrt{Ln_i} e^{i\theta_i}$ with n_i the particle density at momentum/wavelength i.

We can intuitively think of each of these terms as interactions by inspection. Each 'unit' of $\sqrt{n_i}$ is a condensate term, coefficients of v_i provide information on momentum transfer, and the phase (if it exists) tells you if there is net transfer of particles between condensates. E.g. the 'Josephson' (cos) term can be thought of as two particles leaving the single $k = 0$ condensate and entering the $\pm G$ condensates.

We can then write the mean-field energy density $E_{MF} = \langle \Psi | \mathcal{H} | \Psi \rangle$ as:

$$\begin{aligned} E_{MF} = \frac{v_0}{2}\bar{n}^2 + (\epsilon_G + v_1 n_0)(n_1 + n_{-1}) + v_2 n_1 n_{-1} \\ + 2v_1 n_0 \sqrt{n_1 n_{-1}} \cos(\theta_1 + \theta_{-1} - 2\theta_0) \end{aligned} \tag{3.3.4}$$

where $\bar{n} = n_0 + n_1 + n_{-1}$.

In order to find the ground state solution we need to minimise E_{MF}, and regardless of the distribution of condensate populations,

this means we must minimise the Josephson term, which is achieved by setting

$$\theta_1 + \theta_{-1} - 2\theta_0 = m\pi\,, \quad \text{m even for } v_1 < 0\,;\ \text{m odd for } v_1 > 0 \tag{3.3.5}$$

i.e. depending on the sign of v_1 we want the Josephson term to either be minimised or maximised, and adjust the requirement on the phases and the integer that connects them accordingly.

It is important to note that the Josephson term only exists for $n_1, n_{-1}, n_0 \neq 0$, and it will later turn out that this is only possible for a negative v_1 (i.e. an attractive interaction between the $k = 0$ and $k = \pm G$ condensates). There is an intuitive reason for this; if $v_1 > 0$ (repulsive interaction) then the system gains nothing by populating multiple states and it is instead favourable to populate the lowest energy state ($k = 0$) exclusively. We can use this fact to simplify the equation by rewriting the Josephson term with $-|v_1|$ as the coefficient and by placing the aforementioned restrictions on the phases s.t. $\theta_1 - \theta_0 = 2\pi m - (\theta_{-1} - \theta_0)$.

We elect to rewrite this equation using the parameters $n_+ = n_1 + n_{-1}$ and $n_- = n_1 - n_{-1}$, which make explicit the (a)symmetry of the system by representing the total in the non-zero momentum condensates (n_+) and the asymmetry of the occupation (n_-). We can then obtain:

$$\begin{aligned} E_{MF} = \frac{v_0}{2}\bar{n}^2 + (\epsilon_G + v_1\bar{n})n_+ - v_1 n_+^2 + \frac{v_2}{4}(n_+^2 - n_-^2) \\ - |v_1|(\bar{n} - n_+)\sqrt{n_+^2 - n_-^2} \end{aligned} \tag{3.3.6}$$

from which we can obtain the ground state of the system dependent on the parameter choice.

Consider the minimisation procedure. We have 3 free dynamical variables in $\{n_0, n_1, n_{-1}\}$ which we have replaced with $\{n_0, n_+, n_-\}$ and used the constraint that $\bar{n} = n_0 + n_1 + n_{-1}$, which means we only have 2 dynamical variables in $\{n_+, n_-\}$. Thus in order to find the ground state we need to find stationary points in **both** $\{n_+, n_-\}$. This involves solving a set of simultaneous equations:

$$\frac{\partial E_{MF}}{\partial n_+} = 0 \qquad \text{and} \qquad \frac{\partial E_{MF}}{\partial n_-} = 0 \tag{3.3.7}$$

s.t. we find an $\{\tilde{n}_+, \tilde{n}_-\}$ which satisfies both requirements.

Note that we cannot necessarily find all the phase boundaries by just solving the differential equations, as this may miss out on any first order transitions. In order to correctly identify the phase boundaries then we need to directly consider the E_{MF} of each distribution and derive the restrictions on the parameter space accordingly. In general, this should be done all the time anyway as it's the only foolproof way to determine the correct phase boundaries.

We can classify the distributions relatively simply with a straightforward notational system: $\{n_{-1}, n_0, n_1\} \to \{a, b, c\}$. The following distributions are possible:

- (010) condensate - The system is exclusively condensed at $k = 0$
- (101) condensate - The system has equivalent condensation at $k = \pm G$ with no condensation at $k = 0$
- (aba) condensate - The system has a symmetric distribution of condensate populations with some finite fractions a and b
- (abc) condensate - The system has an asymmetric distribution with finite fractions $\{a, b, c\}$ for the $\{-G, 0, +G\}$ condensates respectively. N.B. We suspect this phase is just an artefact.

and by imposing these requirements on the minimisation conditions, we can analyse each type of system independently.

Let us begin by analysing 'left-right symmetric' systems where $n_- = 0$, and separate the problem into quadrants of v_1 and v_2. First let us rewrite equation (3.3.6) with $n_- = 0$.

$$E_{MF} = \frac{v_0}{2}\bar{n}^2 + n_+\left(\epsilon_G + \frac{v_2}{4}n_+\right) + n_+(v_1 - |v_1|)(\bar{n} - n_+) \tag{3.3.8}$$

We can then note that when $v_1 > 0$ the term $v_1 - |v_1| = 0$ and when $v_1 < 0$ then $v_1 - |v_1| = -2|v_1|$. First we start with $v_1 > 0$ and we can immediately observe that for $\{v_1, v_2\} > 0$, E_{MF} is minimised by taking $n_+ \to 0$. Hence the top-right quadrant has only a (010) distribution possible.

Note that $\epsilon_G \geq 0$ and $v_0 \geq 0$ for physicality and boundedness/-compressibility respectively.

If we can allow $v_2 < 0$ then we can observe a (101) state. Consider the $n_+(\epsilon_G + \frac{v_2}{4}n_+)$ term; we immediately see that E_{MF} is minimised by setting $n_+ = 0$ whenever $\epsilon_G + \frac{v_2}{4}n_+ > 0$. If, however, $\epsilon_G + \frac{v_2}{4}n_+ < 0$ then we can reduce E_{MF} by increasing n_+, i.e. occupying the non-zero momentum states. This would correspond to a supersolid phase. Consider further the inequality

$$\epsilon_G + \frac{v_2}{4}n_+ < 0 \tag{3.3.9}$$

and ask when it is satisfied.

If $v_2 < 0$ and we can freely vary v_2, then it is natural to ask when this condition is *first true*. We can immediately see that if there exists a v_2 s.t. this condition is true for some $\tilde{n}_+$ but not true at $n_+ < \tilde{n}_+$ then there is a first order transition possible. In fact the first case where this is possible is for a v_2 s.t.

$$\epsilon_G + \frac{v_2}{4}\bar{n} = 0 \quad . \tag{3.3.10}$$

In this way we can immediately see that in the local area of $v_2 = -\frac{4\epsilon_G}{\bar{n}}$ that a first order transition can occur. For a less negative v_2, the system is minimised by having zero occupation in $\pm G$ states. However, at and below this critical value, the system can reduce its E_{MF} by immediately fully occupying the $\pm G$ states.

This is an example of a phase transition that would have been missed out if we had not studied E_{MF} directly. Since the change in n_+ is discontinuous at this point in phase space, the transition is first order.

Consider now the case where $v_1 < 0$. We can then express (3.3.8) as

$$E_{MF} = \frac{v_0}{2}\bar{n}^2 + n_+\left[\epsilon_G - 2|v_1|\bar{n} + n_+\left(\frac{v_2}{4} + 2|v_1|\right)\right] \tag{3.3.11}$$

and we can now separate the two instances for $v_2 > 0$ and $v_2 < 0$, starting with v_2 positive.

Given $v_2 > 0$, the term $\left(\frac{v_2}{4} + 2|v_1|\right)$ is automatically always positive, therefore there is an obstruction to occupying the n_+ states freely. We can immediately note that if $\epsilon_G - 2|v_1|\bar{n} > 0$ then there can be no occupation of the $\pm G$ states, thus implying that if $v_1 > -\epsilon_G/(2\bar{n})$ then only a (010) state is possible.

If we now also allow $v_2 < 0$ then it is possible to achieve a (101) state. In order to find the parameter configuration we simply require that E_{MF} is minimised at $n_+ = \bar{n}$. Thus we write

$$\left.\frac{\partial E_{MF}}{\partial n_+}\right|_{n_+=\bar{n}} = 0 \tag{3.3.12}$$

and obtain

$$v_2 = 4v_1 - \frac{2}{\bar{n}}\epsilon_G \tag{3.3.13}$$

where we note this holds only in the region where $v_1 < -\epsilon_G/2\bar{n}$.

Note that this is a second order phase boundary, as with v_1 less than the critical value we can occupy some fraction of the system into the $\pm G$ states and have it be the minimal solution. Thus this is a second order phase transition between (010) and (*aba*).

Finally we can consider when the distribution is *asymmetric*, i.e. $n_- \neq 0$ and we have an (*abc*) solution. The way to attack the region where this distribution holds is to simultaneously minimise for both n_+, n_- plug the solutions back in to E_{MF} and assert that $E_{MF}(abc) < E_{MF}(aba)$. This will give you the parameter space where the system transitions to (*abc*). The mathematics is long but not particularly difficult, so it will be omitted here. The end result is the requirement that

$$v_2 > \frac{2v_1\left(\epsilon_G - 2v_1\bar{n}\right)}{v_1\bar{n} + \epsilon_G} \tag{3.3.14}$$

which notably has a singularity at $v_1 = -\epsilon_G/\bar{n}$.

This set of restrictions on the parameter space can be represented by a phase diagram, pictured in Fig. 3.6. We can discuss briefly

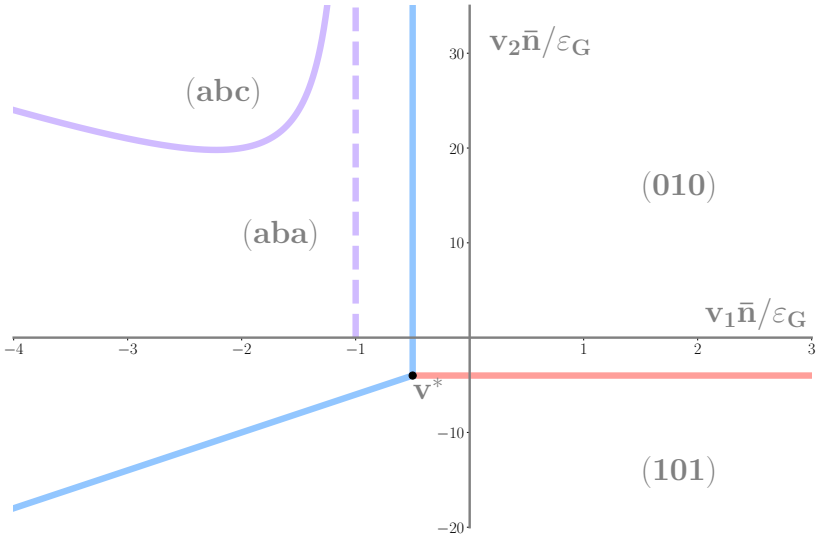


Fig. 3.6: The phase diagram for the multi condensate system. The red line between (010) and (101) indicates a *first order* phase transition, whereas the blue and purple lines indicate *second order* transitions, with the distinction between blue and purple being that purple also has a broken $Z(2)$ symmetry. The dashed line indicates the asymptote of the (*abc*) state as $v_2 \to \infty$.

the manifold of states which occur at each of these phases. In doing so we refer to equation (3.3.2), where the state is a coherent wavefunction with coefficients α_i that are in general $\mathbb{C}$ and represented as $\sqrt{Ln_i}e^{i\theta_i}$ where n_i is the density and θ_i the phase.

Beginning with the (010) state, we have unique condensation at the $k = 0$ state, and so we expect a singular phase which can be chosen spontaneously. The state is expressed as

$$|\Psi\rangle = \exp\left[\sqrt{L\bar{n}}e^{i\theta_0}b_0^\dagger\right]|\text{vac}\rangle \quad ; \quad \theta \in [0, 2\pi) \tag{3.3.15}$$

and we note that this is a standard superfluid with a spontaneously broken $U(1)$ symmetry.

We can move over to the (101) state, which is slightly more complicated as we now have two phases to consider (one from each $k = \pm G$ condensation). We note that we can write

$$\{\theta_{-1}, \theta_1\} \to \{\theta - \chi, \theta + \chi\} \implies e^{i\theta}\left[e^{-i\chi}b_{-1}^\dagger + e^{i\chi}b_1^\dagger\right] \tag{3.3.16}$$

and that the manifold of states is then

$$|\Psi\rangle = \exp\left[\sqrt{L\frac{\bar{n}}{2}}e^{i\theta}\left[e^{-i\chi}b_{-1}^\dagger + e^{i\chi}b_1^\dagger\right]\right]|\text{vac}\rangle \tag{3.3.17}$$

where $\theta \in [0, 2\pi)$, $\chi \in [0, \pi)$.

It is important to note that $\chi \in [0, \pi)$ as when $\chi = \pi$ the phase shift can be absorbed into θ. Namely, when $\chi \to \chi + \pi$, then

$$e^{i\theta}\left[e^{-i\chi}b_{-1}^\dagger + e^{i\chi}b_1^\dagger\right]$$
$$\downarrow$$
$$e^{i\theta}\cdot e^{i\pi}\left[e^{-i\chi}b_{-1}^\dagger + e^{i\chi}b_1^\dagger\right]$$

and then θ absorbs the phase shift s.t. $\theta \to \theta + \pi$.

If we look at the (*aba*) system, we can also draw a manifold of states. We note that there are now 3 phases to consider, but the condition on minimising the Josephson term allows us to put a constraint on $\{\theta_{-1}, \theta_0, \theta_1\}$ allowing us to again represent our state like so

$$|\Psi\rangle = \exp\left(\sqrt{L}e^{i\theta_0}\left[\sqrt{\bar{n} - n_+}b_0^\dagger + \sqrt{\frac{n_+}{2}}\left(e^{-i\chi}b_{-1}^\dagger + e^{i\chi}b_1^\dagger\right)\right]\right)|\text{vac}\rangle \tag{3.3.18}$$

with $\{\theta_0, \chi\} \in [0, 2\pi)$. We note the key difference now that θ_0 does *not* absorb the phase shift in χ, and as such χ can now vary all the way to 2π.

Finally we can consider the manifold of states for the (*abc*) system, where the same constraint on the phases applies. However now there is an asymmetry in the distributions. We represent this with two parameters $\{\psi, \Upsilon\}$ where

$$n_+ = \sin^2(\psi)\,,\; n_- = n_+\sin(\Upsilon) \tag{3.3.19}$$

with $\psi \in [0, \pi/2]$ and $\Upsilon \in [-\pi/2, \pi/2]$. In this formalism we see that ψ represents the fraction in the $\pm G$ states, and Υ represents the 'skew' of the distribution. The state can then be written as

$$|\Psi\rangle = \exp\left(\sqrt{L\bar{n}}\Gamma^\dagger\right)|\text{vac}\rangle \tag{3.3.20}$$

where $\Gamma^\dagger$ is defined as

$$\begin{aligned}\Gamma^\dagger e^{-i\theta_0} = \cos(\psi)b_0^\dagger + \sin(\psi)\Bigg(&e^{-i\chi}\sin\left(\frac{\pi}{4} \mp \frac{\Upsilon}{2}\right)b_{-1}^\dagger \\ &+e^{+i\chi}\cos\left(\frac{\pi}{4} \mp \frac{\Upsilon}{2}\right)b_1^\dagger\Bigg)\end{aligned} \tag{3.3.21}$$

and is introduced solely for neatness.

Concepts around Superfluidity and BECs: Key Points

In this chapter we introduced a few key pieces of the framework for studying supersolids. We began with a short introduction to superfluid theory in a meanfield context.

- We derived the Gross-Pitaevskii Lagrangian, and converted it to a density-phase representation given by

$$\mathcal{L} = -\int_\Omega \left[\hbar\rho\frac{\partial\phi}{\partial t} + \frac{\hbar^2}{2m}\left(\rho(\nabla\phi)^2 + \frac{1}{4\rho}(\nabla\rho)^2\right) + \frac{1}{2}\rho(\mathbf{r})\int_\Omega U(|\mathbf{r}-\mathbf{r}'|)\rho(\mathbf{r}')\,\mathrm{d}\mathbf{r}'\right]\mathrm{d}\mathbf{r} \quad . \tag{3.3.22}$$

  To minimise the Lagrangian we use variational calculus and find the Euler-Lagrange equations

$$\partial_t\rho + \frac{\hbar}{m}\boldsymbol{\nabla}\cdot(\rho\boldsymbol{\nabla}\phi) = 0 \tag{3.3.23}$$

$$\frac{\hbar^2}{4m}\left(\frac{(\nabla\rho)^2}{2\rho^2} - \frac{\nabla^2\rho}{\rho}\right) + U*\rho + \frac{\hbar^2}{2m}(\nabla\phi)^2 = \mu\,. \tag{3.3.24}$$

- We introduced a scaled ground-state energy density

$$\bar{\mathcal{E}} = \frac{1}{|\Omega|}\int_\Omega \frac{1}{8\rho}(\nabla\rho)^2 + \frac{\Lambda}{2}\rho\,\bar{U}*\rho\;\mathrm{d}^2\mathbf{r} \tag{3.3.25}$$

  with a single dimensionless parameter Λ, which will control the quantum phase transition. We will later show the supersolid behaviour of this system as a function of Λ.

- We described how to solve the GPE numerically for any general interaction U; by using an RK4 algorithm in imaginary time we are able to find the ground state given some initial random distribution. We have also recognised that the ground state for 2D supersolids is typically triangular, hence we need to accomodate for a triangular geometry in our simulations. We do this by converting to the 'parallelogram basis', which allows us to represent triangular supersolid states very effectively. As a result, we have had to define finite differencing operators and Jacobians which correspond to this geometry.

- We illustrated superfluid behaviour by introduction of the Bogoliubov transformation

$$\hat{a}_\mathbf{p} = u_\mathbf{p}\hat{b}_\mathbf{p} + v^*_{-\mathbf{p}}\hat{b}^\dagger_{-\mathbf{p}}\,, \quad \hat{a}^\dagger_\mathbf{p} = u^*_\mathbf{p}\hat{b}^\dagger_\mathbf{p} + v_{-\mathbf{p}}\hat{b}_{-\mathbf{p}} \tag{3.3.26}$$

  with the requirement that the Bogoliubov operators have a bosonic commutation relation. This generates the necessary condition

$$|u_\mathbf{p}|^2 - |v_{-\mathbf{p}}|^2 = 1 \tag{3.3.27}$$

  from which we can find the dispersion relation of the system.

We then studied a simple 1D model of a supersolid, and showed that the ground-state phase of the system is dependent on the scattering coefficients between the condensates. We subsequently derived a phase diagram Fig. 3.6 and briefly studied the ground states at various points in the phase diagram.

4 Homogenisation Framework

In this chapter we will derive the framework for a homogenisation calculation. The aim of the following work is to bridge a microscopic theory of supersolids (in so far as the GPE, which is a meanfield theory, can be considered microscopic) with a macroscopic hydrodynamic theory. This will allow us to use a powerful hydrodynamic framework to describe the dynamics of the system, which should be quantitatively valid due to the microscopic basis of the theory.

We will begin by describing an elastic deformation and outlining the expected result from elasticity theory. This is extended to a geometry argument from which we will obtain the required terms in the theory. We will then derive the form of the phase perturbation, as well as the necessary responses in the chemical potential.

We refer to this as a homogenisation calculation as we will be applying perturbations at every length scale in the system and then integrating out the short length scales (i.e. taking the long-wavelength response) to obtain a macroscopic theory.

Homogenisation essentially takes a heterogeneous system (like a supersolid) and averages out the microscopic details to obtain a homogeneous macroscopic theory.

4.1 Elastic background

This section closely follows the calculation done by Bavaud et al [65]. The aim of this section is to define an elastic deformation $u_{\alpha\beta}$ which perturbs the position of fields in the theory and obtain the analytic expansion of the theory in terms of this perturbative parameter henceforth known as the strain.

We describe a general field theory which has a free energy F that is a function of some set of undescribed fields which, importantly, are a function of position x_α. This field theory has support over a spatial domain Ω.

Note that the index α goes over the spatial dimensions in this section, and we assume Einstein notation.

We define an analytic expansion in the free energy of our system around a deformation $x'_\alpha = \left(\delta_{\alpha\beta} - u_{\alpha\beta}\right) x_\beta$ with a mapping $\Omega \mapsto \Omega'$

$$F(\Omega') = F(\Omega) - |\Omega|\pi_{\alpha\beta}(\Omega)u_{\alpha\beta} + |\Omega|\frac{1}{2}A_{\alpha\beta\gamma\delta}(\Omega)u_{\alpha\beta}u_{\gamma\delta} \tag{4.1.1}$$

where

$$\pi_{\alpha\beta}(\Omega) = \frac{1}{|\Omega|}\frac{\partial F(\Omega')}{\partial\left(-u_{\alpha\beta}\right)}\bigg|_{u=0} = -\frac{1}{|\Omega|}\frac{\partial F(\Omega')}{\partial u_{\alpha\beta}}\bigg|_{u=0} \tag{4.1.2}$$

and similarly

$$A_{\alpha\beta\gamma\delta}(\Omega) = \frac{1}{|\Omega|}\frac{\partial^2 F(\Omega')}{\partial u_{\alpha\beta}u_{\gamma\delta}}\bigg|_{u=0} \quad . \tag{4.1.3}$$

In principle, one can expand the free energy to arbitrary order in the strain $u_{\alpha\beta}$, but the study of terms beyond order $\mathcal{O}(u^2)$ is known as *non-linear elastic theory*.

To clarify, we map between spaces $\Omega \mapsto \Omega'$ through the transformation $\mathbf{x} \mapsto \mathbf{x}'$.

Studying the terms $\pi_{\alpha\beta}$ and $A_{\alpha\beta\gamma\delta}$, we can recognise the stress tensor $\pi_{\alpha\beta}$ immediately, but it is important to note that the tensor $A_{\alpha\beta\gamma\delta}$ is **not** the elastic tensor. It is the expansion of the free energy due to the deformation, whereas the elastic tensor strictly connects the stress tensor to the strain.

What we are searching for is a generalised form of Hooke's Law [66] which maps strain in a deformed point to strain in an undeformed point. This can be expressed formally with the equation

$$\pi_{ik}(\Omega') = \pi_{ik}(\Omega) - B_{iklm}(\Omega)u_{lm} \quad . \tag{4.1.4}$$

which can be interpreted as $F_1 = F_0 + kx$ in the style of Hooke's law.

An important additional feature of the elastic tensor B_{iklm} is that, for a sufficiently symmetric system, it has certain symmetry properties as described by Landau & Lifshitz [67], whereas the expansion tensor A_{iklm} **does not** necessarily have these symmetries.

In order to derive the functional form of B_{iklm}, we first define an additional two deformations, u' and u'' such that

$$x''_\alpha = \left(\delta_{\alpha\beta} - u'_{\alpha\beta}\right)x'_\beta \quad ; \quad x''_\alpha = \left(\delta_{\alpha\beta} - u''_{\alpha\beta}\right)x_\beta \tag{4.1.5}$$

To clarify; we have an initial space Ω which we can deform with the transformation $\mathbf{u}$ into the space Ω'. We can then deform from $\Omega' \mapsto \Omega''$ with the deformation $\mathbf{u}'$, and we can *also* deform to the Ω'' space from the *original space* like $\Omega \mapsto \Omega''$ with the deformation $\mathbf{u}''$. We can combine the deformations to find the relation

$$u''_{\alpha\beta} = u_{\alpha\beta} + u'_{\alpha\beta} - u'_{\alpha\sigma}u_{\sigma\beta} \quad . \tag{4.1.6}$$

We then use the above relation to expand the stress tensor that connects the Ω' and Ω'' space. Examining the expansion of the free energy from the Ω' space to the Ω'' space, we find

$$F(\Omega'') = F(\Omega') - \left|\Omega'\right|\pi_{\alpha\beta}(\Omega')u'_{\alpha\beta} + \frac{|\Omega'|}{2}A_{\alpha\beta\gamma\delta}(\Omega')u'_{\alpha\beta}u'_{\gamma\delta}\,. \tag{4.1.7}$$

Expanding $\pi_{\alpha\beta}(\Omega')$ and using (4.1.2) and (4.1.6), we find

$$\begin{aligned}\pi_{\alpha\beta}\left(\Omega'\right) &= -\frac{1}{|\Omega'|}\frac{\partial F(\Omega'')}{\partial u'_{\alpha\beta}}\bigg|_{u'=0} \\ &= -\frac{1}{|\Omega'|}\frac{\partial F(\Omega'')}{\partial u''_{\gamma\epsilon}}\frac{\partial u''_{\gamma\epsilon}}{\partial u'_{\alpha\beta}}\bigg|_{u'=0} \\ &= -\frac{1}{|\Omega'|}\frac{\partial F(\Omega'')}{\partial u''_{\gamma\epsilon}}\left(\delta_{\gamma\alpha}\delta_{\beta\epsilon}-\delta_{\gamma\alpha}\delta_{\beta\sigma}u_{\sigma\epsilon}\right)\bigg|_{u'=0} \\ &= -\frac{1}{|\Omega'|}\left(\delta_{\beta\epsilon}-u_{\beta\epsilon}\right)\frac{\partial F(\Omega'')}{\partial u''_{\alpha\epsilon}}\bigg|_{u'=0}.\end{aligned} \tag{4.1.8}$$

It is interesting to note the principal result of this process (4.1.14) is arrived at essentially through repeated application of the chain rule, whilst the same result is derived much later (6.1.6) through judicious consideration of work done on the environment by an excitation.

We can now turn our attention to the derivative in the above expression. Namely, since the derivative actually does not depend on u' explicitly (recall that we can map from $\Omega \mapsto \Omega''$ through u'' without needing u' at all), we can remove the evalutation at $u' = 0$. As such, the derivative is now not a number, but a function instead!

This function describes the energy response of the mapping $\Omega \mapsto \Omega''$ through u'' for any arbitrary Ω'' and u''. That means it **must be equivalent** to the function which maps from $\Omega \mapsto \Omega'$ through u. Thus we can write

$$\frac{\partial F(\Omega'')}{\partial u''_{\alpha\epsilon}}\bigg|_{u'=0} = \frac{\partial F(\Omega')}{\partial u_{\alpha\epsilon}} \tag{4.1.9}$$

and the final result from (4.1.8) becomes

$$\pi_{\alpha\beta}\left(\Omega'\right) = -\frac{1}{|\Omega'|}\left(\delta_{\beta\epsilon}-u_{\beta\epsilon}\right)\frac{\partial F(\Omega')}{\partial u_{\alpha\epsilon}} \quad . \tag{4.1.10}$$

Since the derivative is no longer evaluated at $u = 0$, we now substitute in (4.1.1) to find

$$\frac{\partial F(\Omega')}{\partial u_{\alpha\epsilon}} = -|\Omega|\pi_{\alpha\epsilon}(\Omega) + |\Omega|A_{\alpha\epsilon\gamma\delta}(\Omega)u_{\gamma\delta} \quad . \tag{4.1.11}$$

We now also expand the $1/|\Omega'|$ term to find

$$\frac{1}{|\Omega'|} = \frac{1}{|\Omega|}\frac{1}{\det(\mathbb{1}-\mathbf{U})} = \frac{1}{|\Omega|}\left(1+\delta_{xy}u_{xy}+\mathcal{O}(u^2)\right) \tag{4.1.12}$$

where the indices x and y are tensor indices of the same nature as α, β etc.

Again note that we are discarding terms of $\mathcal{O}(u^2)$ or higher as we are trying to derive Hooke's law, i.e. $F = kx$, and we do not want anharmonic terms.

We can now combine the results of (4.1.11) and (4.1.12) into (4.1.10) (discarding $\mathcal{O}(u_{ik}^2)$ terms) to find

$$\pi_{\alpha\beta}(\Omega') = \pi_{\alpha\beta} - \left(A_{\alpha\beta\gamma\delta}+\delta_{\gamma\beta}\pi_{\alpha\delta}-\delta_{\gamma\delta}\pi_{\alpha\beta}\right)u_{\gamma\delta} \tag{4.1.13}$$

where everything on the RHS is a function of Ω. This is the expression of Hooke's Law as described in (4.1.4)! We can therefore find that

$$B_{iklm} = A_{iklm} + \pi_{im}\delta_{kl} - \pi_{ik}\delta_{lm} \tag{4.1.14}$$

with now the final task being to relate π_{ik} to the pressure tensor P_{ik}. Recalling that the stress tensor is just the negative of the pressure, we can write the final expression as

$$B_{iklm} = A_{iklm} + P_{ik}\delta_{lm} - P_{im}\delta_{kl} \tag{4.1.15}$$

which is the Cauchy elastic tensor. For the case of C_3 symmetry, we have the relation [67]:

$$B_{xxxx} = B_{xxyy} + 2B_{xyxy}\,. \tag{4.1.16}$$

Landau & Lifshitz [67] showed that one can identify the bulk modulus K and shear modulus G with B_{xxyy} and B_{xyxy} respectively.

This was shown by considering that an applied force in certain directions relative to the orientation of a C_3 symmetric crystal will result in the same response, and therefore the elastic tensor must be symmetric under these transformations.

The key result is that in order to discuss *forces* after a deformation, we have to consider additional contributions from the pressure to the analytic expansion of the free energy. This will be extremely important later as we derive an effective Lagrangian for low-energy excitations which makes careful use of this fact.

4.2 *Homogenisation for Elasticity*

The spontaneously broken translational symmetry in a supersolid means that the system must possess Goldstone modes which are the elastic modes. In this section, we will build on the work of [10, 36, 68] to derive the elastic response of the system. The goal here is to consider an elastic deformation on the ground state, e.g. stretching/shearing as described by some strain tensor, and then to expand the Lagrangian to second order in said strain tensor and recover the elastic moduli through the generalised Hooke's law.

We follow the metholodology of Josserand et al [10, 36], but our results have some key differences. Namely, we believe some key terms were missed which skews the elastic constants to ones that do not agree with simple calculations in the superfluid limit and lead to physically inconsistent elastic moduli. More specifically, the Cauchy elastic tensor does not obey internal symmetries consistent with a triangular lattice, and possesses negative elastic moduli which suggest an unstable state. Moreover, we conduct a different treatment of the system with regard to the canonical ensemble and the degrees of expansion in the strain tensor.

Notably, we believe that previous work [10] did not correctly include relevant terms generated by the elastic deformation in both the derivative and Jacobian, missed out crucial changes to the chemical potential, and did not correctly note the difference between B_{iklm} and A_{iklm}.

The analysis will take the following structure: we will first carefully define the notion of an elastic deformation on the system and provide the basis for the calculation. We then expand the Lagrangian to second-order in the elastic strain tensor. We demand that the deformed system also be a ground state, and therefore solve the Euler-Lagrange equations for the new system, which will allow us to determine elastic constants.

We begin by describing a physical deformation by considering the displacement of points in the material. The displacement can be written as

$$\mathbf{r}' = \mathbf{r} - \mathbf{u}(\mathbf{r})\,, \tag{4.2.1}$$

moving points $\mathbf{r}$ (over some domain Ω) in the undeformed ground state to points $\mathbf{r}'$ (with some domain Ω'). This basis describes the deformed material in the lab frame of an external observer.

To clarify, this is considered an *active* transformation which physically acts on the material and changes the domain of the system in the lab frame. The basis $\mathbf{r}'$ is a Cartesian coordinate system in the lab frame of the external observer, but is a non-Cartesian coordinate system in the frame of the material. This is the same general deformation utilised in (4.1.1).

We then define an inverse *passive* transformation which maps the coordinate system $\mathbf{r}'$ to the coordinate system $\mathbf{r}''$, which is a non-Cartesian basis in the material frame that has the same domain as the inital $\mathbf{r}$ (domain Ω). This transformation is of the form

$$\mathbf{r}'' = \mathbf{r}' + \mathbf{u}'(\mathbf{r}')\,, \tag{4.2.2}$$

where the basis $\mathbf{r}''$ coincides identically with the basis $\mathbf{r}$ in the material frame, i.e. $\mathbf{r}'' = \mathbf{r}$, but now the space has additional components in its gradients, as well as a Jacobian associated with its volume element. These extra curvatures are necessary to describe the full

effect of the displacement procedure on the system. We now relabel the basis $\mathbf{r}''$ as $\mathbf{r}$, for convenience, where again we must stress that even though the coordinate systems $\mathbf{r}$ and $\mathbf{r}''$ coincide, the space is no longer Cartesian and has an associated Jacobian and curvature. This procedure is illustrated schematically in Fig. 4.1.

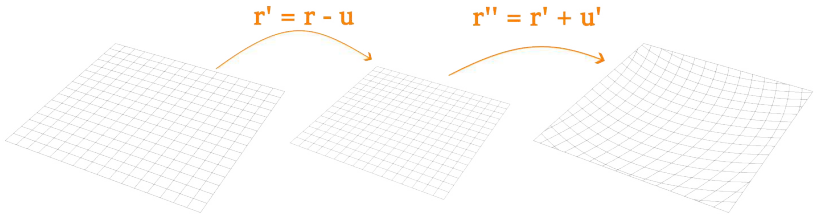


Fig. 4.1: A schematic of the deformation procedure. The leftmost image depicts an undeformed system with a basis $\mathbf{r}$, which then undergoes an *active* transformation given by some strain to become the middle system. The rightmost image depicts the system after the *passive* transformation, such that the final coordinate system $\mathbf{r}''$ coincides exactly with $\mathbf{r}$, but now there are additional curvatures in the space.

As of now, the above transformation is completely general, but in order to proceed we need to specify a particular class of transformation which allows us to use linear response theory and elasticity theory. We make the distinction that $\mathbf{u}(\mathbf{r})$ is such that all gradients in either space or time are small constants. More specifically, we set $\partial_i u_k \sim \delta$ and $\partial_t u_k \sim \delta \cdot m/s$, with δ an arbitrarily small constant that we choose to track up to $\mathcal{O}(\delta^2)$.

This is referred to as a uniform deformation, in that the gradient of the deformation is constant everywhere and is small, allowing us to treat it as a perturbative parameter.

We now refer to $u_{ik} \equiv \partial_i u_k$ as the *strain tensor*, where u is the displacement field as defined in (4.2.1), and endeavour to expand $\mathcal{L}$ in powers of u_{ik}. In order to employ linear elastic theory we have to keep all terms up to $\mathcal{O}(\delta^2)$ in the Lagrangian. We also need to relate the gradient of the transformation $\mathbf{u}'$ in the primed deformed basis in the lab frame to the gradient of the transformation $\mathbf{u}$ in the material basis. It is relatively easy to show that

$$\partial'_i u'_k = \partial_i u_k + \partial_i u_l \partial_l u_k \equiv u_{ik} + u_{il} u_{lk} \tag{4.2.3}$$

up to $\mathcal{O}(\delta^2)$ in the strain tensor (n.b. we are using the Einstein summation convention). This allows us now to express derivatives in the primed (deformed lab frame) basis in terms of derivatives in the unprimed (deformed material frame) basis to find

$$\partial'_i = \partial_i + (u_{ik} + u_{il} u_{lk})\, \partial_k \quad . \tag{4.2.4}$$

In order to simplify the expressions that we will derive in this thesis, we introduce notation for a set of key tensors that appear regularly.

$$\begin{aligned} \epsilon_{ik} &= -\frac{1}{2}\left(u_{ik} + u_{ki}\right) \quad ; \quad \Delta_{ik} = \frac{1}{2} u_{il} u_{kl} \quad ; \\ \omega_{ik} &= \frac{1}{2} u_{li} u_{lk} \quad ; \quad \chi_{ik} = \frac{1}{2}\left(u_{li} u_{kl} + u_{lk} u_{il}\right) \end{aligned} \tag{4.2.5}$$

Since the deformation actively changes the domain of the system, there is an associated change of volume. We refer to the deformations described in (4.2.1) and (4.2.2) to define the differential volume elements as

$$\int_{\Omega'} \mathrm{d}\mathbf{r}' = \int_{\Omega} \mathcal{J}_{\mathbf{r}'\to\mathbf{r}}\, \mathrm{d}\mathbf{r} \tag{4.2.6}$$

with the Jacobian

$$\mathcal{J}_{\mathbf{r}'\to\mathbf{r}} = \det\left(\frac{\partial r'_i}{\partial r_k}\right) = 1 + \epsilon_{ll} + M_{iklm}\, u_{ik} u_{lm} \quad . \tag{4.2.7}$$

The quantities ϵ_{ll} and $M_{iklm}u_{ik}u_{lm}$ are sometimes called the first and second strain invariants as they are independent of the basis in which the strain tensor is written.

where $M_{iklm} \equiv (\delta_{ik}\delta_{lm} - \delta_{im}\delta_{kl})/2$. A negative ϵ_{ll} corresponds to a reduction in volume. In two dimensions, $M_{iklm}u_{ik}u_{lm} = u_{xx}u_{yy} - u_{xy}u_{yx}$.

We stress now that the coordinate system $\mathbf{r}$ describes the deformed system in the frame of the material: it has the same domain as the undeformed material but is now a non-Cartesian space.

To understand how this deformation affects the Lagrangian, we need to understand how the density changes as a function of the deformation. After the deformation occurs, the particles in the system will reorganise themselves in such a way as to minimise the total energy of the new configuration, leading to a new density described by $\rho(\mathbf{r}')$.

The reorganisation of particles due to a deformation can be expressed as the pre-deformation density plus a component, $\tilde{\rho}$, which completely accounts for all changes. The component $\tilde{\rho}$ covers both local density changes at length scales within a unit cell of the supersolid and also includes the change in average density due to total number conservation and a change in volume.

Note that this new density is written in the $\mathbf{r}'$ basis. We stress that this is not the density in the material frame, but rather the density in the lab frame of the external observer.

We then employ a passive transformation to write the density in the $\mathbf{r}''$ basis, which is the material frame that now has some curvature. Without loss of generality we can express this new density at some point $\mathbf{r}'$ as

$$\rho(\mathbf{r}') = \rho_0(\mathbf{r}'') + \tilde{\rho}(\mathbf{r}'') \quad ; \quad \int_{\Omega'} \rho(\mathbf{r}')\, \mathrm{d}\mathbf{r}' = \int_{\Omega} \rho_0(\mathbf{r}'')\, \mathrm{d}\mathbf{r}'' \tag{4.2.8}$$

where ρ_0 is the pre-deformation ground-state density profile. As of now this is simply a mapping to a scalar function that has been subject to an active transformation.

Note that the elastic deformation has introduced a non-Cartesian space, which therefore must have a metric tensor associated with it. The Jacobian can be derived from this metric tensor, and is a measure of the change in volume due to the deformation. The following analysis will not explicitly define the metric tensor as it is simpler to do so without introducing it, but one could rederive these results using the language of differential geometry.

From this point we drop the $\mathbf{r}''$ notation and refer to the coordinate as $\mathbf{r}$ where now the coordinate system is non-Cartesian and has a Jacobian associated with it.

The general form of $\tilde{\rho}$ is determined by minimising the energy of the deformed system, subject to particle conservation. For linear elastic theory, we only need to consider a perturbative strain on the system and expect that, since the strain is perturbative, the density

change $\tilde{\rho}$ must be analytic in the strain tensor. We truncate the Taylor expansion to $\mathcal{O}(\delta^2)$ in the strain tensor and use the ansatz

$$\tilde{\rho}(\mathbf{r}) = \rho_1^{ik}(\mathbf{r})\,\epsilon_{ik} + \rho_2^{iklm}(\mathbf{r})\,u_{ik}u_{lm} \tag{4.2.9}$$

which we will justify later. This allows us to expand the new normalisation condition for particle conservation.

$$\int_\Omega (\rho_0 + \tilde{\rho})\,(1 + \epsilon_{ll} + M_{iklm}\,u_{ik}u_{lm})\,\mathrm{d}\mathbf{r} = \int_\Omega \rho_0\,\mathrm{d}\mathbf{r} \tag{4.2.10}$$

and after collecting powers of the strain tensor obtain normalisation requirements for the different terms in the expansion

$$\begin{aligned} \int_\Omega \left(\rho_1^{ik} + \rho_0\delta^{ik}\right)\mathrm{d}\mathbf{r} &= 0 \\ \int_\Omega \left[\rho_2^{iklm} + \rho_0\,(M_{iklm} - \delta_{ik}\delta_{lm})\right]\mathrm{d}\mathbf{r} &= 0\,. \end{aligned} \tag{4.2.11}$$

Due to the changing energy of the system (and indeed the change in average density), we can expect to see a change in the chemical potential μ too. In a similar spirit as that of equation (4.2.9), we can analytically expand the new chemical potential in the strain tensor as

$$\mu = \mu_0 + \mu_1^{ik}\,\epsilon_{ik} + \mu_2^{iklm}\,u_{ik}u_{lm} \quad , \tag{4.2.12}$$

where the first term is the chemical potential of the undeformed system, and the constants μ_1^{ik} and μ_2^{iklm} encodes how the chemical potential changes due to the deformation and are to be determined by the least-action principle.

This was a key point that was missed in the analysis of [10]; while the authors had considered a normalisation condition which was strain dependent, they had not considered that the chemical potential should also be strain dependent. These additional energetic contributions turn out to be crucial to an accurate theory of homogenisation.

We additionally need to consider how the displacement field u_{ik} changes the interaction potential U. We note that the interaction is a function of separation between particles, but importantly is originally written in terms of the separation $\Delta r'$ as measured in the *real lab frame coordinates*: $U = U(\Delta r')$. For a uniform strain, we find immediately that the lab-frame separation $\Delta\mathbf{r}'$ can be written in terms of the material-frame separation $\Delta\mathbf{r}$ such that

$$\left(\Delta r'\right)^2 = \left(\delta_{ik} + 2\epsilon_{ik} + 2\Delta_{ik}\right)\left(\Delta r\right)_i\left(\Delta r\right)_k \tag{4.2.13}$$

The tensor $(\delta_{ik} + 2\epsilon_{ik} + 2\Delta_{ik})$ is sometimes referred to as the *finite strain tensor*. This result can also be derived by considering the metric tensor of the deformed space.

which is exactly equivalent to that of Landau & Lifshitz [67].

A Taylor expansion of the interaction for small strain gives

$$\begin{aligned} U(\Delta\mathbf{r}') = U(\Delta\mathbf{r}) &+ (\epsilon_{ik} + \Delta_{ik})\,f_{ik}(\Delta\mathbf{r}) \\ &+ \epsilon_{ik}\epsilon_{lm}W_{iklm}(\Delta\mathbf{r}) \end{aligned} \tag{4.2.14}$$

with

$$\begin{aligned} f_{ik}(\mathbf{r}) &\equiv \frac{r_i r_k}{|\mathbf{r}|}\frac{\partial U(|\mathbf{r}|)}{\partial|\mathbf{r}|} \\ W_{iklm}(\mathbf{r}) &\equiv \frac{r_i r_k r_l r_m}{2|\mathbf{r}|^2}\left(\frac{\partial^2 U}{\partial|\mathbf{r^2}|} - \frac{1}{|\mathbf{r}|}\frac{\partial U}{\partial|\mathbf{r}|}\right)\,. \end{aligned} \tag{4.2.15}$$

4.3 U(1) Phase field

Here we will briefly consider the application of a phase perturbation to the meanfield supersolid, and analyse the coupling of the phase to the strain field.

We begin by specifying the nature of the phase perturbation. We consider imposing a small superflow to the system in the form of a phase gradient. This is applied to the supersolid *in the deformed state*, i.e the lab frame of the deformed material. The system will respond to this long-wavelength perturbation by generating phase fluctuations, $\tilde{\phi}$, at small wavelengths within a unit cell of the supersolid.

As with $\tilde{\rho}$ in the previous section, $\tilde{\phi}$ is a correcting function to the respective perturbation applied to the ground state. Namely, $\tilde{\rho}$ is the function which allows the density to settle into the energetically optimal configuration for a given strain, and $\tilde{\phi}$ is the function which will allow the phase field to settle into the energetically optimal configuration for a given applied phase gradient.

We mathematically represent this as

$$\phi(\mathbf{r}') = \phi_0(\mathbf{r}') + \tilde{\phi}(\mathbf{r}) \tag{4.3.1}$$

where $\phi(\mathbf{r}')$ is the total phase in the lab frame $\mathbf{r}'$, $\phi_0(\mathbf{r}')$ is the applied perturbative phase in the lab frame, and $\tilde{\phi}(\mathbf{r})$ is the phase-correction provided by the material in the material frame of reference. We express $\tilde{\phi}$ in terms of the material frame deformed coordinate system $\mathbf{r}$ in keeping with linear response theory, similar to how we expressed $\tilde{\rho}$ in terms of the material frame coordinate system $\mathbf{r}$.

In order to apply perturbation theory to the phase field, we specify that $\partial_i \phi_0(\mathbf{r}')$ is small and constant within the scope of the unit cell of the supersolid, in a similar way to the strain tensor u_{ik}. We note that since the phase is applied in the deformed frame, the total phase in the material frame can be expanded to obtain

$$\phi(\mathbf{r}') = \phi_0(\mathbf{r}) - \mathbf{u} \cdot \boldsymbol{\nabla} \phi_0(\mathbf{r}) + \tilde{\phi}(\mathbf{r}) \tag{4.3.2}$$

which is the final expression for the phase field in the material frame of reference.

Note here that we will discard time derivatives of $\tilde{\phi}$ or $\tilde{\rho}$. We state that the relaxation time of the fields $\tilde{\phi}$ and $\tilde{\rho}$ are much shorter than $\partial_t \phi_0$ or $\partial_t \mathbf{u}$, and hence they are stationary fields with respect to $\partial_t \phi_0$ or $\partial_t \mathbf{u}$. This is analogous in some ways to the Born-Oppenheimer approximation, which states that the motion of nuclei is much slower than the surrounding electrons. Here we are treating the 'nuclei' as the fields $\partial_t \phi_0$ and $\partial_t \mathbf{u}$, and the 'electrons' as $\tilde{\phi_0}$ and $\tilde{\rho}$, with the understanding that we are interested in the motion of the 'nuclei' rather than the 'electrons', and since the fast field equilibrates much quicker it is stationary with respect to time. In other words, we apply perturbations that are slow compared to the response of the system.

There is an interesting analogue to this approach in the completely different field of tight-binding models [69]. Here the authors found that in order to correct some serious errors to the bulk modulus of a material as calculated via a frozen-phonon calculation, one would have to impose a self-consistency constraint on the charge-density of the material. This is exactly equivalent to what we do in homogenisation, which is calculating correcting fields to a perturbation in a self-consistent manner. Here the Born-Oppenheimer comparison is even more evident; the authors are literally treating the electrons as the self-consistent correcting field and state that it equilibrates much faster than the nuclei.

We now have everything we need to proceed to expand the Lagrangian in terms of the phase field, using the least action principle to find $\tilde{\phi}$ and the associated energy.

4.4 *Tensor differentiation*

This is a short section which will provide information on how to relate tensors in an expansion to the Cauchy elastic tensor. More specifically, once we have that expansion, how do we recover the homogenised tensors as first and second differentives: $\pi_{ik} = \partial F/\partial u_{ik}$ and $A_{iklm} = \partial^2 F/\partial u_{ik}\partial u_{lm}$?

We will now write out explicitly how expressions involving the tensors listed in (4.2.5) differentiate. Consider first $F = F_{ik}u_{ik}$ with $F_{ik} = F_{ki}$, its first derivative is: $\partial F/\partial uik = F_{ik}$. Similarly, the first derivative of $F = F_{ik}\epsilon_{ik}$ is $\partial F/\partial u_{ik} = -F_{ik}$.

Let us now consider second derivatives. Suppose there is a term in the Lagrangian of the form $F = F_{iklm}u_{ik}u_{lm}$. We have the result $\partial^2 F/\partial u_{ik}\partial u_{lm} = 2F_{iklm}$. Consider now $F = F_{ik}\chi_{ik}$ where $\chi_{ik} = \left(u_{li}u_{kl} + u_{lk}u_{il}\right)/2$. Since χ_{ik} is symmetric under $i \leftrightarrow k$, we can impose that F_{ik} is also symmetric under the same exchange.

It is helpful to refer to the definitions of the tensors as written in (4.2.5)

$$\epsilon_{ik} = -\frac{1}{2}\left(u_{ik} + u_{ki}\right)$$
$$\Delta_{ik} = \frac{1}{2}u_{il}u_{kl}$$
$$\omega_{ik} = \frac{1}{2}u_{li}u_{lk}$$
$$\chi_{ik} = \frac{1}{2}\left(u_{li}u_{kl} + u_{lk}u_{il}\right)$$

$$\begin{aligned}\frac{\partial^2\chi_{ik}}{\partial u_{cd}\partial u_{ab}} &= \frac{1}{2}\frac{\partial}{\partial u_{cd}}\left(\delta_{la}\delta_{ib}u_{kl} + \delta_{la}\delta_{kb}u_{il} + \delta_{ka}\delta_{lb}u_{li} + \delta_{ia}\delta_{lb}u_{lk}\right)\\ &= \frac{1}{2}\left(\delta_{ib}\delta_{kc}\delta_{ad} + \delta_{kb}\delta_{ci}\delta_{ad} + \delta_{ka}\delta_{bc}\delta_{id} + \delta_{ia}\delta_{bc}\delta_{kd}\right)\,.\end{aligned} \tag{4.4.1}$$

This allows us to obtain

$$\frac{\partial^2 F}{\partial u_{ik}\partial u_{lm}} = \frac{1}{2}\left(F_{bc}\delta_{ad} + F_{cb}\delta_{ad} + F_{da}\delta_{bc} + F_{ad}\delta_{bc}\right) = F_{kl}\delta_{im} + F_{im}\delta_{kl} \tag{4.4.2}$$

using the symmetry of F_{ik} under exchange of indices. A similar calculation can be done for other tensor contractions involving the tensors in (4.2.5). This is listed in Table 4.1.

Table 4.1: Table relating the terms that appear in an elastic expansion to their contributions to the Cauchy elastic tensor.

F	$F_{iklm}\epsilon_{ik}\epsilon_{lm}$	$F_{ik}\Delta_{ik}$	$F_{ik}\omega_{ik}$	$F_{ik}\chi_{ik}$
$\frac{\partial^2 F}{\partial u_{ik}\partial u_{lm}}$	$2F_{iklm}$	$F_{il}\delta_{km}$	$F_{km}\delta_{il}$	$F_{kl}\delta_{im} + F_{im}\delta_{kl}$

It is important to briefly discuss the symmetry of each of these expressions. For terms that look like $F_{iklm}\epsilon_{ik}\epsilon_{lm}$, these already have all the symmetry properties we would want from our elastic tensors. However, we can immediately see that the contribution from $F_{ik}\Delta_{ik}$, $F_{ik}\omega_{ik}$ and $F_{ik}\chi_{ik}$ **do not** have the requisite symmetries. We instead need to *create* these symmetries from combinations of these tensors. This cannot be achieved a priori by adding in whatever we like. However, if we expect elastic theory to hold, then we would expect any expansion in any strain tensor (including ours) to lead us eventually back to symmetric expressions. This is a good test to check whether the expansion calculation has been done correctly.

Homogenisation Framework: Key points

In this chapter we introduced several key tools to develop a homogenisation theory for supersolids. We began with a discussion on elasticity theory on general:

- We provided a derivation of the Cauchy elastic tensor B_{iklm} and showed that it is not simply the coefficient of the expansion of the Lagrangian to second order, but rather there is an extra contribution to the tensor from the pressure component

$$B_{iklm} = A_{iklm} + P_{ik}\delta_{lm} - P_{im}\delta_{kl}$$

  where

$$A_{iklm}(\Omega) = \frac{1}{|\Omega|}\frac{\partial^2 F(\Omega')}{\partial u_{ik}u_{lm}}\bigg|_{u=0} \quad ; \quad P_{ik} = \frac{1}{|\Omega|}\frac{\partial F(\Omega')}{\partial u_{ik}}\bigg|_{u=0}$$

- We expect that the tensor B_{iklm} must obey certain relations if the ground state possesses certain symmetries, i.e. for a ground state with $C(3)$ symmetry, we should expect to see:

$$B_{xxxx} = B_{xxyy} + 2B_{xyxy}$$

  where one can identify B_{xxyy} with the bulk modulus K and B_{xyxy} with the shear modulus G.

We then rigorously derived a deformation procedure from which we expand the Lagrangian and use elastic theory.

- We define a physical deformation with the general transformation $\mathbf{r}' = \mathbf{r} - \mathbf{u}(\mathbf{r})$, with the constraint that the gradients (in both space and time) of $\mathbf{u}$ are constant and small
- From this we showed how to obtain the geometry of the material frame of reference after the deformation, given by the curvature

$$\partial_i' = \partial_i + \partial_k\left(u_{ik} + u_{il}u_{lk}\right)$$

  and Jacobian

$$\mathcal{J}_{\mathbf{r}'\to\mathbf{r}} = \det\left(\frac{\partial r_i'}{\partial r_k}\right) = 1 + \epsilon_{ll} + M_{iklm}\,u_{ik}u_{lm}$$

  respectively.
- We then defined a correction to the density $\tilde{\rho}$ given by

$$\rho(\mathbf{r}) \to \rho_0(\mathbf{r}) + \tilde{\rho}(\mathbf{r})$$

  from which we defined the following ansatz for $\tilde{\rho}$

$$\tilde{\rho}(\mathbf{r}) = \rho_1^{ik}(\mathbf{r})\,\epsilon_{ik} + \rho_2^{iklm}(\mathbf{r})\,u_{ik}u_{lm}$$

  with the normalisation condition

$$\int_\Omega (\rho_0 + \tilde{\rho})\left(1 + \epsilon_{ll} + M_{iklm}\,u_{ik}u_{lm}\right)\mathrm{d}\mathbf{r} = \int_\Omega \rho_0\,\mathrm{d}\mathbf{r}\,.$$

- We also noted that there must be a corresponding change in the chemical potential, given by

$$\mu = \mu_0 + \mu_1^{ik}\,\epsilon_{ik} + \mu_2^{iklm}\,u_{ik}u_{lm} \quad .$$

  which is a crucial part of the success of homogenisation theory.

- There is a shift in the interaction potential due to the deformation

$$U(\Delta\mathbf{r}') = U(\Delta\mathbf{r}) + (\epsilon_{ik} + \Delta_{ik})\, f_{ik}(\Delta\mathbf{r}) + \epsilon_{ik}\epsilon_{lm} W_{iklm}(\Delta\mathbf{r})$$

  with

$$f_{ik}(\mathbf{r}) \equiv \frac{r_i r_k}{|\mathbf{r}|}\frac{\partial U(|\mathbf{r}|)}{\partial|\mathbf{r}|}$$
$$W_{iklm}(\mathbf{r}) \equiv \frac{r_i r_k r_l r_m}{2|\mathbf{r}|^2}\left(\frac{\partial^2 U}{\partial|\mathbf{r}^2|} - \frac{1}{|\mathbf{r}|}\frac{\partial U}{\partial|\mathbf{r}|}\right) .$$

- We derived the contribution to the Lagrangian from the $U(1)$ phase field, and showed how it couples to the $\mathbf{u}$ displacement field

$$\phi(\mathbf{r}') = \phi_0(\mathbf{r}) - \mathbf{u}\cdot\boldsymbol{\nabla}\phi_0(\mathbf{r}) + \tilde{\phi}(\mathbf{r})$$

We introduced several tensors, and showed how they differentiate to contribute to the Cauchy elastic tensor. For the following definitions

$$\epsilon_{ik} = -\frac{1}{2}\left(u_{ik} + u_{ki}\right) \quad ; \quad \Delta_{ik} = \frac{1}{2}u_{il}u_{kl} \quad ;$$
$$\omega_{ik} = \frac{1}{2}u_{li}u_{lk} \quad ; \quad \chi_{ik} = \frac{1}{2}\left(u_{li}u_{kl} + u_{lk}u_{il}\right)$$

we found

F	$F_{iklm}\epsilon_{ik}\epsilon_{lm}$	$F_{ik}\Delta_{ik}$	$F_{ik}\omega_{ik}$	$F_{ik}\chi_{ik}$
$\dfrac{\partial^2 F}{\partial u_{ik}\partial u_{lm}}$	$2F_{iklm}$	$F_{il}\delta_{km}$	$F_{km}\delta_{il}$	$F_{kl}\delta_{im} + F_{im}\delta_{kl}$

To summarise, we have defined a perturbative deformation which changes the geometry of our system, and have obtained the volume changes and curvature changes due to said deformation. We have also derived a new density and chemical potential, for which we will solve for using the least-action principle. We now have all the ingredients to formulate a theory of linear response of the system to elastic deformations, as we know how to expand the theory and how to relate terms in the expansions to terms in the corresponding elastic theory.

5 Expanding the Lagrangian

In this chapter we will go through the calculation of expanding the Lagrangian using the tools and framework derived in the previous chapter. We will then derive and solve the Euler-Lagrange equations for $\tilde{\rho}$ and $\tilde{\phi}$ respectively. This will result in an effective Lagrangian which describes the long-wavelength response of a unit cell to perturbations in the phase gradient and elastic deformation, but not the Goldstone modes of the system.

We will go through the calculation step by step, justifying our choices, and summarise the results at the end.

5.1 Expanding the U(1) component of the Lagrangian

Using the transformation rules for the Lagrangian (curvature (4.2.4) and Jacobian (4.2.7)) and the ϕ expansion given by (4.3.2), the phase-dependent part of the Lagrangian (3.1.33) can be immediately expanded to $\mathcal{O}(\tilde{\phi}^2)$ as

$$\begin{aligned}\mathcal{L}_\phi = -\int_\Omega \Big\{ &\hbar\rho_0 \partial_t \phi_0 \left(1 + \boldsymbol{\nabla}\cdot\mathbf{u}\right) \\ &+ \frac{\hbar^2\rho_0}{2m}\left[\left(\boldsymbol{\nabla}\phi_0\right)^2 + 2\mathbf{A}\cdot\boldsymbol{\nabla}\tilde{\phi} + \left(\boldsymbol{\nabla}\tilde{\phi}\right)^2\right]\Big\}\,\mathrm{d}\mathbf{r}\end{aligned} \tag{5.1.1}$$

Helpful to recall the derivative

$$\partial_i' = \partial_i + \partial_k\left(u_{ik} + u_{il}u_{lk}\right)$$

and Jacobian

$$\mathcal{J}_{\mathbf{r}'\to\mathbf{r}} = 1 + \epsilon_{ll} + M_{iklm}\,u_{ik}u_{lm}$$

where

$$\mathbf{A} = \boldsymbol{\nabla}\phi_0 + \left(\boldsymbol{\nabla}\phi_0\cdot\boldsymbol{\nabla}\right)\mathbf{u} + \frac{m}{\hbar}\partial_t\mathbf{u}\,. \tag{5.1.2}$$

The vector field $\mathbf{A}$ is a kind of convective flow. Recall that the superfluid velocity is given by $\mathbf{v} = (\hbar/m)\boldsymbol{\nabla}\phi_0$. Also, we can define the material derivative of a field as

$$\frac{D}{Dt} = \partial_t + \mathbf{v}\cdot\boldsymbol{\nabla} \tag{5.1.3}$$

to describe the time derivative of a function which is co-moving with the superfluid velocity field. We can rewrite $\mathbf{A}$ in term of these variables:

$$\mathbf{A} = \frac{m}{\hbar}\left(\mathbf{v} + \mathbf{v}\cdot\boldsymbol{\nabla}\mathbf{u} + \partial_t\mathbf{u}\right) = \frac{m}{\hbar}\left(\mathbf{v} + \frac{D\mathbf{u}}{Dt}\right)\,. \tag{5.1.4}$$

A point of subtlety is that the deformation applied is $\mathbf{r}' = \mathbf{r} - \mathbf{u}$, so $(\hbar/m)\,\mathbf{A} = \mathbf{v} - D(-\mathbf{u})/Dt$ is a relative velocity between the superflow and the motion of the lattice deformations.

This is exactly the form predicted by Son [9] from symmetry based

arguments. In fact, all terms in $\mathcal{L}_\phi$ satisfy the Galilean symmetry requirements imposed by Son. In this way we can show that we have microscopically satisfied the necessary Galilean symmetry requirements imposed on any supersolid system macroscopically.

Our phase Lagrangian $\mathcal{L}_\phi$ in (5.1.1) differs from the analogous form in Josserand et al [10] by the existence of the term $\hbar\rho_0\partial_t\phi_0\boldsymbol{\nabla}\cdot\mathbf{u}$. This term is in fact necessary to ensure that $\mathcal{L}_\phi$ satisfies Galilean symmetry constraints as pointed out by Son [9]. We also note that this affects the velocity of the excitations of the system, and we will see later that our results agree with the results obtained in Bogoliubov theory.

We now solve for the phase response $\tilde{\phi}$ within a unit cell due to superflow and strain. We follow a similar procedure to Ref [10]. By recognising that the externally imposed phase twist and strains $\boldsymbol{\nabla}\phi_0$ and $\partial_i u_k$ are defined as long-wavelength relative to the unit cell, we can treat $\mathbf{A}$ as constant within a unit cell. However, a uniform velocity with non-uniform density does not necessarily obey local mass conservation in equilibrium; we need a correction to the phase field $\tilde{\phi}$ to ensure that our system obeys the continuity equation $\boldsymbol{\nabla}\cdot(\rho\boldsymbol{\nabla}\phi)=0$. The Euler-Lagrange equation for $\tilde{\phi}$ gives

This is a common theme within homogenisation. We're applying a long-wavelength perturbation, solving for short-wavelength responses, in this case the functions K_i, and then integrating out the high frequency modes to obtain an effective response to the long-wavelength perturbation.

$$\tilde{\phi}=K_iA_i \quad \text{with} \quad \partial_i\rho_0+\boldsymbol{\nabla}\cdot(\rho_0\boldsymbol{\nabla}K_i)=0\,. \tag{5.1.5}$$

In general, this equation needs to be solved numerically. We write the differential operators as matrix operators on a vector, and solve it using standard iterative matrix solvers. Note that this equation is solved for a general $\mathbf{A}$, and so the solution is valid for any superflow and strain configuration.

Physically, this result expresses the fact that the phase twist (and therefore superflow) is not uniform within a unit cell because it costs less kinetic energy to introduce phase shifts in regions of low density compared to regions of high density. As such, there are preferential 'channels' for the superflow to occupy, but the additional spatial component of the phase shift costs energy.

Using this solution for $\tilde{\phi}$, it can be shown that the phase-dependent Lagrangian can be written as:

$$\begin{aligned} L_\phi =&|\Omega|\frac{\hbar^2}{2m}\varrho_{ij}A_iA_j-\int_\Omega\Big[\hbar\rho_0\partial_t\phi_0\,(1+\boldsymbol{\nabla}\cdot\mathbf{u})\\ &+\frac{\hbar^2\rho_0}{2m}\left(\boldsymbol{\nabla}\phi_0\right)^2\Big]\,\mathrm{d}\mathbf{r}\end{aligned} \tag{5.1.6}$$

with

$$\varrho_{ij}=-\frac{1}{|\Omega|}\int_\Omega\rho_0\partial_iK_j\,\mathrm{d}\mathbf{r} \tag{5.1.7}$$

which can be interpreted as a correction to the superfluid phase stiffness (see equation (5.3.1)). Figure 5.1 shows the evolution of

This is done via integration by parts. There are several other forms for ϱ_{ij} which are equivalent. Namely

$$\begin{aligned}\varrho_{ij}&\equiv\frac{1}{|\Omega|}\int_\Omega\rho_0\nabla K_i\cdot\nabla K_j\,\mathrm{d}\mathbf{r}\\ &\equiv\frac{-2}{|\Omega|}\int_\Omega\rho_0\left(\partial_iK_j+\nabla K_i\cdot\nabla K_j\right)\mathrm{d}\mathbf{r}\end{aligned}$$

however we use (5.1.7) as it is the most concise form.

this quantity as we increase the interaction strength Λ showing a discontinuous transition at the superfluid-supersolid transition.

To restate the above, by carefully considering the dynamics of both an applied/induced phase and a strain deformation (both of which are long-wavelength relative to the unit cell), we calculate how the phase-dependent dynamics of our system are dependent on the parameters n and ϱ_{ij} given by the form (5.1.6). n is simply the density of *all* particles in the system, and corresponds to the phase-coherent BEC with components at both $\mathbf{k} = 0$ and $\mathbf{k} \neq 0$. ϱ_{ij} is the part of the system that corresponds to the pattern formation, i.e. it only exists when $\psi_{\mathbf{k}\neq 0} \neq 0$. Consequently, we refer to ϱ_{ij} as being the "supersolid fraction" of the system. In this way we have separated out the pattern response to the coupled phase-strain dynamical field from the standard superfluid response.

N.B. The dependence of ϱ_{ij} on Λ is due to the ground state density ρ_0 changing with Λ.

Finally, due to the C_3 symmetry, second-rank tensors representing bulk properties should be isotropic. We therefore make the assumption that $\varrho_{ij} = \varrho\delta_{ij}$, though in principle this is not necessary. We also note that the dependency in (5.1.6) on ϕ_0 and $\mathbf{u}$ can be taken out of the integral (due to the same argument that $\mathbf{A}$ is a constant in the unit cell). Consequently, we find that we can write

$$\begin{aligned}\frac{L_\phi}{|\Omega|} &= -\hbar n\dot{\phi}_0(1+\boldsymbol{\nabla}\cdot\mathbf{u}) \\ &\quad -\frac{\hbar^2}{2m}\left[n\left(\boldsymbol{\nabla}\phi_0\right)^2 - \varrho\left(\boldsymbol{\nabla}\phi_0 + \frac{m}{\hbar}\frac{D\mathbf{u}}{Dt}\right)^2\right]\end{aligned} \tag{5.1.8}$$

where $n = \int_\Omega \rho_0\,\mathrm{d}\mathbf{r}/|\Omega|$ is the average particle density.

This will be the contribution from the phase sector to the effective Lagrangian which describes the Goldstone modes.

The phrase 'supersolid fraction' referring to ϱ_{ij} is an odd one. One would expect this means that when $\varrho_{ij} = 1\delta_{ij}$ that the system is completely supersolid, but, as we will later show, this actually corresponds to a *regular solid* (in as much as a regular solid can be described by a GPE). It is perhaps best to think of ϱ_{ij} as a parameter which smoothly tunes your system from superfluid to regular solid.

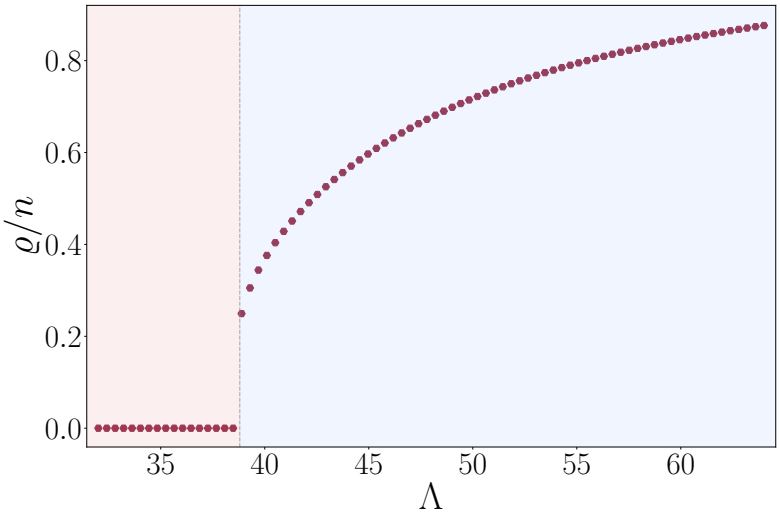


Fig. 5.1: The reduction ϱ/n in the superfluid fraction as a function of interaction strength Λ, exhibiting a discontinuous jump at the transition. This value can potentially be used as an order parameter for the supersolid phase transition.

5.2 *Elasticity Theory*

In this section we will use the expansion rules previously derived to expand and solve the non-$U(1)$ component of the Lagrangian.

We start by expanding the non-interacting, kinetic part of $\mathcal{L}$ using the tools developed. We can express without expansion

$$\left(\nabla'\rho(\mathbf{r}')\right)^2 = \left[\left(\partial_i + \left(u_{ik} + u_{il}u_{lk}\right)\partial_k\right)\left(\rho_0(\mathbf{r}) + \tilde{\rho}(\mathbf{r})\right)\right]^2 \tag{5.2.1}$$

N.B. That $\tilde{\rho}$ has both first *and* second order components of the strain tensor.

where we subsequently drop the coordinates as it is clear everything is in the unprimed basis $\mathbf{r}$. We can re-express the pre-factor

$$\frac{1}{\rho(\mathbf{r}')} = \frac{1}{\rho_0 + \tilde{\rho}} = \frac{1}{\rho_0} - \frac{\tilde{\rho}}{\rho_0^2} + \frac{\tilde{\rho}^2}{\rho_0^3} + \mathcal{O}(\tilde{\rho}^3) \tag{5.2.2}$$

to make it more algebraically pliable. This allows us to write

$$\begin{aligned}\int_{\Omega'} \frac{\hbar^2}{2m}\frac{(\nabla'\rho(\mathbf{r}'))^2}{4\rho(\mathbf{r}')}\,\mathrm{d}\mathbf{r}' = \int_{\Omega}\Bigg\{\frac{\hbar^2}{8m}\left(\frac{1}{\rho_0} - \frac{\tilde{\rho}}{\rho_0^2} + \frac{\tilde{\rho}^2}{\rho_0^3}\right)\left(1 + \epsilon_{ll} + M_{iklm}u_{ik}u_{lm}\right)\\ \times\Big[(\nabla\rho_0)^2 + 2(\boldsymbol{\nabla}\rho_0\cdot\boldsymbol{\nabla}\tilde{\rho}) - 2\epsilon_{ik}\partial_i\rho_0\partial_k\rho_0 + 2\chi_{ik}\partial_i\rho_0\partial_k\rho_0\\ -4\epsilon_{ik}\partial_i\rho_0\partial_k\tilde{\rho} + (\nabla\tilde{\rho})^2 + 2\Delta_{ik}\partial_i\rho_0\partial_k\rho_0\Big]\Bigg\}\,\mathrm{d}\mathbf{r}\end{aligned} \tag{5.2.3}$$

which we can manipulate further.

This section involves a lot of expanding and collecting terms. During this process it is extremely important to keep tracks of the order of the perturbative terms in the expansion. Some of these terms may not be individually 'symmetry conserving', in that they may produce terms in the elastic constant B_{iklm} which do not not obey the crystal symmetry of the lattice. However, one should continue to expand and collect all such terms and trust that they will eventually generate an appropriate Cauchy elastic tensor.

By isolating first and second order (in terms of the strain tensor) parts of the non-interacting Lagrangian, and using the following relation (obtained via integration by parts)

$$\int_{\Omega}\frac{\boldsymbol{\nabla}\tilde{\rho}\cdot\boldsymbol{\nabla}\rho_0}{\rho_0}\,\mathrm{d}\mathbf{r} = \int_{\Omega}\tilde{\rho}\frac{(\nabla\rho_0)^2}{\rho_0^2} - \tilde{\rho}\frac{\nabla^2\rho_0}{\rho_0}\,\mathrm{d}\mathbf{r} \tag{5.2.4}$$

we are able to find the first-order component

$$\mathcal{L}_1 = \frac{\hbar^2}{4m}\left[\left(\frac{(\nabla\rho_0)^2}{2\rho_0^2} - \frac{\nabla^2\rho_0}{\rho_0}\right)\tilde{\rho} + \epsilon_{ik}\left(\frac{(\nabla\rho_0)^2}{2\rho_0}\delta_{ik} - \frac{\partial_i\rho_0\partial_k\rho_0}{\rho_0}\right)\right] \tag{5.2.5}$$

and the second-order component

$$\begin{aligned}\mathcal{L}_2 =& \frac{\hbar^2}{4m}\left[\left(\Delta_{ik} + \chi_{ik}\right)\frac{\partial_i\rho_0\partial_k\rho_0}{\rho_0}\right] +\\ &\frac{\hbar^2}{8m}\Bigg[-4\epsilon_{ik}\frac{\partial_i\rho_0\partial_k\tilde{\rho}}{\rho_0} + \frac{(\nabla\tilde{\rho})^2}{\rho_0} + 2\frac{\boldsymbol{\nabla}\tilde{\rho}\cdot\boldsymbol{\nabla}\rho_0}{\rho_0}\epsilon_{ll} - 2\epsilon_{ik}\frac{\partial_i\rho_0\partial_k\rho_0}{\rho_0}\epsilon_{ll}\\ &+\frac{(\nabla\rho_0)^2}{\rho_0}M_{iklm}u_{ik}u_{lm} - 2\frac{\boldsymbol{\nabla}\tilde{\rho}\boldsymbol{\nabla}\rho_0}{\rho_0^2}\tilde{\rho} + 2\epsilon_{ik}\frac{\partial_i\rho_0\partial_k\rho_0}{\rho_0^2}\tilde{\rho}\\ &-\frac{(\nabla\rho_0)^2}{\rho_0^2}\tilde{\rho}\epsilon_{ll} + \frac{(\nabla\rho_0)^2}{\rho_0^3}\tilde{\rho}^2\Bigg]\end{aligned} \tag{5.2.6}$$

respectively. We now turn to considering the interaction section of the Lagrangian.

Recalling the derivation of (4.2.15)

$$U(\Delta\mathbf{r}') = U(\Delta\mathbf{r}) + (\epsilon_{ik} + \Delta_{ik})\, f_{ik}(\Delta\mathbf{r}) + \epsilon_{ik}\epsilon_{lm} W_{iklm}(\Delta\mathbf{r}) \tag{5.2.7}$$

with

$$f_{ik}(\mathbf{r}) \equiv \frac{r_i r_k}{|\mathbf{r}|}\frac{\partial U(|\mathbf{r}|)}{\partial|\mathbf{r}|} \quad ; \quad W_{iklm}(\mathbf{r}) \equiv \frac{r_i r_k r_l r_m}{2|\mathbf{r}|^2}\left(\frac{\partial^2 U}{\partial|\mathbf{r}^2|} - \frac{1}{|\mathbf{r}|}\frac{\partial U}{\partial|\mathbf{r}|}\right). \tag{5.2.8}$$

This can be used to express the interaction component of $\mathcal{L}$ by combining it with both the density mapping and the Jacobian to obtain

$$U = \frac{1}{2}\int_\Omega (\rho_0 + \tilde{\rho})_{r_1}\left[U(\mathbf{r}_{12}) + (\epsilon_{ik} + \Delta_{ik})\, f_{ik}(\mathbf{r}_{12}) + \epsilon_{ik}\epsilon_{lm} W_{iklm}(\mathbf{r}_{12})\right] (\rho_0 + \tilde{\rho})_{r_2}\left(1 + 2\epsilon_{ll} + \epsilon_{ll}\epsilon_{kk} + 2M_{iklm}u_{ik}u_{lm}\right)\, \mathrm{d}\mathbf{r}_1\, \mathrm{d}\mathbf{r}_2 \tag{5.2.9}$$

N.B. since the convolution is itself an integral, there is a term arising from $(\mathcal{J}_{\mathbf{r}'\to\mathbf{r}})^2$ which generates the bracket which includes $2M_{iklm}$.

where $\mathbf{r}_{12} = \mathbf{r}_1 - \mathbf{r}_2$.

This can be expanded and combined with the non-interacting component of $\mathcal{L}$, and we can fully express the first and second order components of the expansion.

We make use of the Gross-Pitaevskii ground-state equation (3.1.35), as well as the normalisation condition (4.2.10) to simplify our expressions, and we can show that the first order component of the Lagrangian is given by

$$\mathcal{L}_1 = \int_\Omega \left[\rho_0\epsilon_{ll}\,(U * \rho_0 - \mu_0) + \frac{1}{2}\epsilon_{ik}(f_{ik} * \rho_0)\rho_0 + \frac{\hbar^2}{4m}\epsilon_{ik}\left(\frac{(\nabla\rho_0)^2}{2\rho_0}\delta_{ik} - \frac{\partial_i\rho_0\partial_k\rho_0}{\rho_0}\right)\right]\mathrm{d}\mathbf{r} \tag{5.2.10}$$

We can now make a direct connection between the linear component of the expansion and the pressure tensor P_{ik}. Recalling that the first order component of the expansion is the stress tensor, and that the stress tensor is the negative of the pressure, we can write

$$P_{ik} = \frac{1}{|\Omega|}\int_\Omega \left[(\mu_0 - U * \rho_0)\,\delta_{ik} - \frac{1}{2}f_{ik} * \rho_0 - \frac{\hbar^2}{4m}\left(\frac{(\nabla\rho_0)^2}{2\rho_0^2}\delta_{ik} - \frac{\partial_i\rho_0\partial_k\rho_0}{\rho_0^2}\right)\right]\rho_0\,\mathrm{d}\mathbf{r} \tag{5.2.11}$$

which after simplification can be written as

$$P_{ik} = \frac{1}{|\Omega|}\int_\Omega \left[\frac{\hbar^2}{4m}\left(\frac{\partial_i\rho_0\partial_k\rho_0}{\rho_0} - \nabla^2\rho_0\,\delta_{ik}\right) - \frac{1}{2}\rho_0(f_{ik} * \rho_0)\right]\mathrm{d}\mathbf{r} \quad . \tag{5.2.12}$$

In order to simplify the expression for P_{ik} we made use of the GPE (3.1.36) and periodic boundary conditions.

Note that the pressure contains the ground-state density only, and so can be immediately calculated given some on-shell (i.e. solving the GPE) density profile. This is our first key result which is obtaining the pressure of any ground-state system given a specified interaction. We can trivially calculate the expected pressure for a homogeneous superfluid by noting that $\rho_0 \equiv n$ and that $\mu_0 = U_{\mathbf{k}=0} n$ where $U_{\mathbf{k}=0} = \int_\Omega U(\mathbf{r}) d\mathbf{r}$. The pressure simply reduces to $-\frac{1}{2} n^2 \int_\Omega f_{ik}(\mathbf{r})\, \mathrm{d}\mathbf{r}$. Integrating by parts gives the integral over f_{ik} as $-U_{\mathbf{k}=0}\delta_{ik}$. So, we find that $P_{ik} = \frac{1}{2}\mu_0 n \delta_{ik}$, which is the expected result. We can now move on to the more difficult task of solving for the second order components.

It is important to note that since we have allowed $\tilde{\rho}$ to have both first and second order components in u_{ik}, then even single powers of $\tilde{\rho}$ must be taken into consideration for the $\mathcal{O}(u^2)$ components. The above analysis only collected the components of $\tilde{\rho}$ which were of $\mathcal{O}(u)$, but does not remove the singular powers of $\tilde{\rho}$ from the Lagrangian.

It is necessary to calculate the functional form of $\tilde{\rho}$ as there will be terms like $\int_\Omega \tilde{\rho}^2\, \mathrm{d}\mathbf{r}$ that will contribute to the perturbative Lagrangian, and as such we therefore need to solve the equations of motion for $\tilde{\rho}$. It is not enough to simply know the normalisation condition as we did for the $\mathcal{O}(u)$ component.

The first step in solving for $\tilde{\rho}$ is to collect all the terms in which it appears, regardless of first or second order splitting. We take all the terms that contain $\tilde{\rho}$ and call them $\mathcal{L}_{\tilde{\rho}}$, finding

$$\begin{aligned} -\mathcal{L}_{\tilde{\rho}} = \frac{1}{2}\frac{\hbar^2}{4m}\Bigg[& -4\epsilon_{ik}\frac{\partial_i\rho_0\partial_k\tilde{\rho}}{\rho_0} + \frac{(\nabla\tilde{\rho})^2}{\rho_0} + 2\frac{\boldsymbol{\nabla}\tilde{\rho}\cdot\boldsymbol{\nabla}\rho_0}{\rho_0}\epsilon_{ll} - 2\frac{\boldsymbol{\nabla}\tilde{\rho}\cdot\boldsymbol{\nabla}\rho_0}{\rho_0^2}\tilde{\rho} \\ & + 2\epsilon_{ik}\frac{\partial_i\rho_0\partial_k\rho_0}{\rho_0^2}\tilde{\rho} - \frac{(\nabla\rho_0)^2}{\rho_0^2}\tilde{\rho}\,\epsilon_{ll} + \frac{(\nabla\rho_0)^2}{\rho_0^3}\tilde{\rho}^2\Bigg] \\ & + \mu_0\tilde{\rho} + \frac{1}{2}\left((U*\tilde{\rho})\,\tilde{\rho} + 4\epsilon_{ll}\,(U*\rho_0)\,\tilde{\rho} + 2\epsilon_{ik}\,(f_{ik}*\rho_0)\,\tilde{\rho}\right) \end{aligned} \tag{5.2.13}$$

which we can solve by the standard Euler-Lagrange technique. A key detail now is that the new normalisation condition changes the constraints we apply. Specifically, the equation we need to solve is

$$\frac{\partial\mathcal{L}_{\tilde{\rho}}}{\partial\tilde{\rho}} - \partial_i\frac{\partial\mathcal{L}_{\tilde{\rho}}}{\partial\,(\partial_i\tilde{\rho})} + \left(\mu_0 + \mu_1\epsilon_{ll} + \mu_2^{iklm}u_{ik}u_{lm}\right)(1 + \epsilon_{ll} + M_{iklm}u_{ik}u_{lm}) = 0 \tag{5.2.14}$$

which can be shown via the strained normalisation condition (4.2.10).

The process of expanding the chemical potential as a function of strain and combining it with the strained normalisation condition is crucial; without either or both of these features homogenisation would not produce correct excitation spectra or bulk properties.

A straightforward calculation follows of differentiating the $\tilde{\rho}$ dependent Lagrangian and collating all terms. We make use of the zeroth-order equation of motion to simplify our expression and we find

$$L(\tilde{\rho}) = F(\rho_0, \mu_0, \mu_1^{ik}, \mu_2^{iklm}) \tag{5.2.15}$$

with

$$L(\tilde{\rho}) \equiv \frac{\hbar^2}{4m}\boldsymbol{\nabla}\cdot\left(\frac{\boldsymbol{\nabla}\tilde{\rho}}{\rho_0}\right) - U*\tilde{\rho} + \frac{\hbar^2}{4m}\left(\frac{(\nabla\rho_0)^2}{\rho_0^3} - \frac{\nabla^2\rho_0}{\rho_0^2}\right)\tilde{\rho} \tag{5.2.16}$$

and

$$F(\rho_0, \mu_0, \mu_1^{ik}, \mu_2^{iklm}) \equiv -\left(\mu_2^{iklm} + \mu_1^{ik}\delta_{lm} + \mu_0 M_{iklm}\right) u_{ik}u_{lm} + \epsilon_{ik}\left[-\mu_1^{ik} + \frac{\hbar^2}{4m}\left(2\frac{\partial_{ik}\rho_0}{\rho_0} - \frac{\partial_i\rho_0\partial_k\rho_0}{\rho_0^2}\right) + \int_\Omega \left(f_{ik}(\mathbf{r}-\mathbf{r}') + \delta_{ik}U(\mathbf{r}-\mathbf{r}')\right)\rho_0(\mathbf{r}')\,\mathrm{d}\mathbf{r}'\right] \tag{5.2.17}$$

which contains both $\mathcal{O}(u^2)$ and $\mathcal{O}(u)$ terms. We can now begin to separate $\tilde{\rho}$ into first and second order components via (4.2.9), and consider solving the equation component by component. That is to say that we solve the lowest order component first, and then use that solution to solve the next order component, and so on.

We introduce the following definitions for the first and second order components of the equation

$$L\left(\rho_1^{ik}\right) = F_1\left(\rho_0, \mu_1^{ik}\right), \qquad L\left(\rho_2^{iklm}\right) = F_2\left(\mu_0, \mu_1^{ik}, \mu_2^{iklm}\right) \tag{5.2.18}$$

for brevity. We can now find the first order contribution ρ_1^{ik} and find the first order correction to the chemical potential μ_1^{ik} by solving the equation

$$L(\rho_1^{ik}) \equiv \frac{\hbar^2}{4m}\boldsymbol{\nabla}\cdot\left(\frac{\boldsymbol{\nabla}\left(\rho_1^{ik}\epsilon_{ik}\right)}{\rho_0}\right) - U * \left(\rho_1^{ik}\epsilon_{ik}\right) + \frac{\hbar^2}{4m}\left(\frac{(\nabla\rho_0)^2}{\rho_0^3} - \frac{\nabla^2\rho_0}{\rho_0^2}\right)\left(\rho_1^{ik}\epsilon_{ik}\right) \tag{5.2.19}$$

with

$$F_1(\rho_0, \mu_1^{ik}) \equiv \epsilon_{ik}\left[-\mu_1^{ik} + \frac{\hbar^2}{4m}\left(2\frac{\partial_{ik}\rho_0}{\rho_0} - \frac{\partial_i\rho_0\partial_k\rho_0}{\rho_0^2}\right) + \int_\Omega \left(f_{ik}(\mathbf{r}-\mathbf{r}') + \delta_{ik}U(\mathbf{r}-\mathbf{r}')\right)\rho_0(\mathbf{r}')\,\mathrm{d}\mathbf{r}'\right] . \tag{5.2.20}$$

This equation has to be solved numerically; we factor out ϵ_{ik} and solve the set of equations where we have one for each index. As this is an integrodifferential equation we can solve the equation by writing the LHS as a matrix operator on an unraveled vector and applying an iterative matrix solver algorithm which converges on some pre-specified tolerance.

We first state $\rho_1^{ik} \equiv \rho_1^{ik}(\mathbf{r}, \mu_1^{ik})$, i.e. it is now a function of the chemical potential. We specifically choose the functional form $\rho_1^{ik} = \hat{\rho}_1^{ik} + \mu_1^{ik}\rho_1'$, in a kind of 'homogeneous + inhomogeneous'

It is important to note that we do not actually **need** to solve the equation for ρ_2^{iklm} as it only appears in the Lagrangian when multiplied by a constant, thus we can directly use the normalisation condition (4.2.10) and short circuit the task of solving it. We also do not need to find μ_2^{iklm} for a slightly different reason, which is that it appears in the Lagrangian to too high an order and so is always discarded anyway.

In 2D we have 4 equations to solve; in 3D we have 9.

fashion. Namely, we state that

$$L\left(\hat{\rho}_1^{ik}\right) = \frac{\hbar^2}{4m}\left(2\frac{\partial_{ik}\rho_0}{\rho_0} - \frac{\partial_i\rho_0\partial_k\rho_0}{\rho_0^2}\right) + \int_\Omega \left[f_{ik}(\mathbf{r}-\mathbf{r}') + \delta_{ik}U(\mathbf{r}-\mathbf{r}')\right]\rho_0(\mathbf{r}')\,\mathrm{d}\mathbf{r}' \tag{5.2.21}$$

i.e. $\hat{\rho}_1^{ik}$ satisfies the equation of motion without any chemical potential considerations. Then we solve the set of equations

$$L\left(\mu_1^{ik}\rho_1'\right) = -\mu_1^{ik} \;\rightarrow\; L\left(\rho_1'\right) = -1 \tag{5.2.22}$$

simultaneously. We can state this in the notation of (5.2.18)

N.B. We solve each of these equations numerically in the exact same way as for (5.2.15), the operator L remains the same, it's just the target vector (i.e. the RHS) that is changing.

$$L\left(\hat{\rho}_1^{ik}\right) = F_1\left(\rho_0, \mu_1^{ik}=0\right) \quad , \quad L\left(\rho_1'\right) = F_1\left(\rho_0=0, \mu_1^{ik}=1\right) \tag{5.2.23}$$

which we can readily substitute into the 'homogeneous' and 'inhomogeneous' solutions to see that

$$L\left(\hat{\rho}_1^{ik} + \mu_1^{ik}\rho_1'\right) = F_1\left(\rho_0, \mu_1^{ik}\right) \tag{5.2.24}$$

which is the 'general' solution we were looking for. The final task is to now actually calculate μ_1^{ik} which we can do by using the normalisation condition(4.2.10). Since we know what the first-order condition is, we can rearrange to find that

$$\mu_1^{ik} = -\int_\Omega (\rho_0\delta_{ik} + \hat{\rho}_1^{ik})\,\mathrm{d}\mathbf{r} \Big/ \int_\Omega \rho_1'\,\mathrm{d}\mathbf{r} \tag{5.2.25}$$

which is the final ingredient.

We have now fully solved for $\tilde{\rho}$ (and discarded the parts that we don't need), so we can re-express $\mathcal{L}_{\tilde{\rho}}$ using integration by parts. The calculation is relatively straightforward and makes use of the base EoM (3.1.35), allowing one to find

Remember that the $\mathcal{O}(u)$ contributions from $\tilde{\rho}$ have already been included in the pressure (5.2.12)

$$-\mathcal{L}_{\tilde{\rho}} = \frac{1}{2}\left(2\mu_0\rho_2^{iklm}u_{ik}u_{lm} + \rho_1^{lm}\left[\frac{\hbar^2}{4m}\left(2\frac{\partial_{ik}\rho_0}{\rho_0} - \frac{\partial_i\rho_0\partial_k\rho_0}{\rho_0^2}\right) + (f_{ik}+\delta_{ik}U)*\rho_0 + 2\mu_0\delta_{ik} + \mu_1^{ik}\right]\epsilon_{ik}\epsilon_{lm}\right) + \mathcal{O}(\epsilon^3) \tag{5.2.26}$$

which contains all the second-order contributions from $\tilde{\rho}$ (in terms of the strain field u_{ik}, there are terms in here that have come from powers of both $\tilde{\rho}$ *and* $\tilde{\rho}^2$).

We can now combine the contributions from $\tilde{\rho}$ to the other $\mathcal{O}(u^2)$

contributions that **do not contain** $\tilde{\rho}$, and obtain a long expression

$$
\begin{aligned}
-\mathcal{L}_2 = & \\
\frac{1}{2}\Big[& 2\left(U*\rho_0\right)\rho_0 M_{iklm}u_{ik}u_{lm} + \left(\left(U*\rho_0\right)\rho_0\delta_{ik}\delta_{lm} + 2\left(f_{ik}*\rho_0\right)\rho_0\delta_{lm}\right. \\
& \left. + \left(W_{iklm}*\rho_0\right)\rho_0\right)\,\epsilon_{ik}\epsilon_{lm} + \left(f_{ik}*\rho_0\right)\rho_0\Delta_{ik} + \frac{\hbar^2}{2m}\frac{\partial_i\rho_0\partial_k\rho_0}{\rho_0}\left(\Delta_{ik}+\chi_{ik}\right) \\
& - \frac{\hbar^2}{2m}\left(\frac{\partial_i\rho_0\partial_k\rho_0}{\rho_0}\right)\delta_{lm}\epsilon_{ik}\epsilon_{lm} + \frac{\hbar^2}{4m}\frac{\left(\nabla\rho_0\right)^2}{\rho_0}M_{iklm}u_{ik}u_{lm} \\
& + 2\mu_0\rho_0\left(\delta_{ik}\delta_{lm} - M_{iklm}\right)u_{ik}u_{lm} + \rho_1^{lm}\left[\frac{\hbar^2}{4m}\left(2\frac{\partial_{ik}\rho_0}{\rho_0} - \frac{\partial_i\rho_0\partial_k\rho_0}{\rho_0^2}\right)\right. \\
& \left.\left. + \left(f_{ik}+\delta_{ik}U\right)*\rho_0 + 2\mu_0\delta_{ik} + \mu_1^{ik}\right]\,\epsilon_{ik}\epsilon_{lm}\Big]\right]
\end{aligned}
\tag{5.2.27}
$$

N.B. Ths expression can be simplified by quite a bit, but we feel it is important to write out the expression in full for clarity.

which will be used in the calculation of the elastic constants.

To summarise, we have expanded our Lagrangian up to second order in the strain tensor and collected all the terms. We've solved for $\tilde{\rho}$ such that the new state is a ground state with the strained normalisation condition, and subsequently re-expressed the second-order Lagrangian with that solution in hand.

We now use these results by applying them to the definitions obtained from elastic theory (4.1.15), making use of the expression for the pressure (5.2.12) and derivative rules Table 4.1.

We find that $B_{iklm} = |\Omega|^{-1}\int_\Omega b_{iklm}(\mathbf{r})\,\mathrm{d}\mathbf{r}$ where

$$
\begin{aligned}
b_{iklm}(\mathbf{r}) = & + \frac{\hbar^2}{4m}\left(\frac{\partial_i\rho_0\partial_l\rho_0}{\rho_0}\delta_{km} + \frac{\partial_k\rho_0\partial_l\rho_0}{\rho_0}\delta_{im} - \frac{\partial_i\rho_0\partial_k\rho_0}{\rho_0}\delta_{lm}\right) \\
& + \frac{1}{2}\left(f_{il}*\rho_0\right)\rho_0\delta_{km} - \frac{1}{2}\left(f_{ik}*\rho_0\right)\rho_0\delta_{lm} + \frac{1}{2}\left(f_{im}*\rho_0\right)\rho_0\delta_{kl} \\
& + \left[\left(\left(U\delta_{ik}+2f_{ik}\right)\delta_{lm} + W_{iklm}\right)*\rho_0\right]\rho_0 \\
& + \rho_1^{lm}\left[\frac{\hbar^2}{4m}\left(2\frac{\partial_{ik}\rho_0}{\rho_0} - \frac{\partial_i\rho_0\partial_k\rho_0}{\rho_0^2}\right) + \left(f_{ik}+\delta_{ik}U\right)*\rho_0 + \mu_1^{ik}\right]
\end{aligned}
\tag{5.2.28}
$$

N.B. Simply using the differentiation rules Table 4.1 on $\mathcal{L}_2$ will give you the object A_{iklm} instead of B_{iklm}. One has to use

$$B_{iklm} = A_{iklm} + P_{ik}\delta_{lm} - P_{im}\delta_{kl}$$

noting that A_{iklm} is not indicially symmetric in the same way as B_{iklm}.

with $(g*\rho)_{\mathbf{r}} \equiv \int \mathrm{d}\mathbf{r}' g(\mathbf{r}-\mathbf{r}')\rho(\mathbf{r}')$ for any function g and ρ and where f_{ik} and W_{iklm} are defined in (4.2.15).

For a supersolid with C_3 symmetry, we also expect the elastic tensor to obey the indicial symmetries $B_{iklm} = B_{klim} = B_{lkmi} = B_{mlki}$ so that it only contains two independent quantities — the bulk modulus $K = c_{44}$ and the shear modulus $G = c_{66}$:

$$B_{iklm} = K\delta_{ik}\delta_{lm} + G\left(\delta_{il}\delta_{km} + \delta_{im}\delta_{kl}\right)\,. \tag{5.2.29}$$

Elastic theory [67] in 2D posits that the bulk modulus K is given by B_{xxyy}, and the shear modulus G is given by B_{xyxy} (or all equivalent indicially symmetric elements). For a triangular lattice or

a homogeneous system, the tensor also possesses the symmetry: $B_{xxxx} = B_{xxyy} + 2B_{xyxy}$. Note also that we expect the changes to the chemical potential to have the same symmetry as the pressure, i.e. $\mu_1^{ik} = \mu_1 \delta_{ik}$.

Let us check these results for the case of a homogeneous system, where the modulation vanishes and we can check our results against the known results for elastic moduli of a superfluid. We can see that the elastic tensor is greatly simplified by the disappearance of the derivative terms $\partial_i \rho_0$, and the chemical potential is analytically known: $\mu = U * \rho_0$. We can find the convolutions $f_{ik} * \rho_0$ and $W_{iklm} * \rho_0$, solve the equation (5.2.15) and use this to find that

$$B_{iklm} = \mu n \delta_{ik} \delta_{lm} \quad . \tag{5.2.30}$$

Using the definitions of K and G from the Cauchy elastic tensors (5.2.29), we see here that we obtain the expected results of $K = \mu n$ and no shear modulus: $G = 0$.

5.2.2.1 *Numerics*

We will now present the numerical calculation of these homogenisation results for the elastic constants. The results are shown in Fig. 5.2 (solid markers).

In our numerics, we see some small asymmetry, for example $B_{iklm} \approx B_{lmik}$, in the results for the elastic tensor. The discrepancy with the ideal form (5.2.29) decreases as we reduce the discretisation and increase the system size in the numerics. With that in mind, we choose to define the bulk modulus K as the average of the values of B_{xxyy} and B_{yyxx}, the pressure P as the average of P_{xx} and P_{yy}, and the shear modulus G as the average of B_{xyxy}, B_{xyyx}, B_{yxyx} and B_{yxxy}. We then use the minimal and maximal values that the elastic moduli *could have taken* in order to generate 'error bars' for the elastic constants. It should be stressed that these error bars are not measures of some statistical error, but rather a quantification of how much the elastic constants deviate due to the crystal symmetry being only approximately triangular (as opposed to exactly triangular) as a result of discretisation error in our numerics.

In our numerics, we use a spatial discretisation consisting of a triangular lattice as a grid so that the numerical scheme is consistent with the symmetry of the supersolid phase under rotations. Therefore, each "pixel" is a parallelogram and the simulation cell is also a parallelogram with basis vectors $\mathbf{a}$ and $\mathbf{b}$ parallel to $(\sqrt{3}/2, 1/2)$ and $(0, 1)$ in Cartesian coordinates. This will provide some algebraic details on how deformations $\mathbf{V}$ of the simulation cell can be used to extract the elastic tensors numerically using the energy change $F_2 \equiv P u_{ll} + \frac{1}{2} A_{iklm} u_{ik} u_{lm}$ up to second order in the strain.

Let us write all positions and displacements in the basis of the triangular grid: $\mathbf{r} = r_a \mathbf{a} + r_b \mathbf{b}$ and $\mathbf{u} = u_a \mathbf{a} + u_b \mathbf{b}$. The strain tensor in this basis

$$\mathbf{V} = \begin{pmatrix} \partial u_a / \partial r_a & \partial u_a / \partial r_b \\ \partial u_b / \partial r_a & \partial u_b / \partial r_b \end{pmatrix}$$

is related to the strain tensor in the Cartesian basis: $(\mathbf{U})_{ij} \equiv u_{ij}$ by:

$$\mathbf{U} = \mathbf{T}^{-1} \mathbf{V} \mathbf{T} \,, \qquad \text{with} \qquad \mathbf{T} = \begin{pmatrix} \frac{2}{\sqrt{3}} & 0 \\ -\frac{1}{\sqrt{3}} & 1 \end{pmatrix} . \tag{5.2.31}$$

In our numerics, we apply strains diagonal in the triangular-grid basis by deforming the simulation cell in the directions of $\mathbf{a}$ and $\mathbf{b}$. Using the above, we can calculate the energy changes we

should expect to see. There are three deformations that give linearly independent results.

$$\begin{aligned}
\mathbf{V} &= \begin{pmatrix} \epsilon & 0 \\ 0 & 0 \end{pmatrix} : F_2 = P\epsilon + \left(A_{xxxx} + \frac{A_{xyxy}}{3} \right) \frac{\epsilon^2}{2} \\
\mathbf{V} &= \begin{pmatrix} 0 & 0 \\ 0 & \epsilon \end{pmatrix} : F_2 = P\epsilon + \left(A_{yyyy} + \frac{A_{xyxy}}{3} \right) \frac{\epsilon^2}{2} \\
\mathbf{V} &= \begin{pmatrix} \epsilon & 0 \\ 0 & \epsilon \end{pmatrix} : F_2 = 2P\epsilon + \left(\frac{A_{xxxx} + A_{yyyy}}{2} + A_{xxyy} \right) \epsilon^2 .
\end{aligned} \tag{5.2.32}$$

For our system with C_3 symmetry, there are only two independent elastic constants. Using (4.1.15) and (4.1.16), we see that $A_{xxxx} = A_{xxyy} + P + 2A_{xyxy}$. Therefore, we have three equations to solve for the elastic constants and the pressure for a given $\epsilon \ll 1$.

We have calculated these quantities at several values of ϵ to check for the self-consistency of this analysis. This gives a measure of the numerical errors of this technique.

To summarise, we can obtain a purely numerical estimate of the elastic constants by finding how the energy of the ground state of the Gross-Pitaevskii equation changes when we deform the simulation cell at fixed particle number (with periodic boundary conditions). We begin with an undeformed ground-state obtained via numerically solving the Gross-Pitaevskii with some given average density, area and interparticle interaction. We then apply a strain to the system by changing the geometry of the simulation cell by a strain tensor u_{ik}, whilst keeping the total number of particles fixed, and solving the Gross-Pitaevskii equation for the new geometry to find the deformed ground-state. For sufficiently small strain u_{ik}, we expect that such a procedure will yield a ground state with a Lagrangian of the form

A good question to ask is whether or not we are allowed to *a priori* assume the system is symmetric, and whether we are biasing towards a symmetric result. This is a valid question, but really what we are doing is seeking to compare the results we obtain with the analytical theory derived. Importantly, the theory assumes nothing about symmetry, so if the numerics agree with the theory, then this assumption is justified.

$$L = L_0 + P_{ik}u_{ik} + \frac{1}{2}A_{iklm}u_{ik}u_{lm} \tag{5.2.33}$$

where the tensor u_{ik} is now a control parameter in our computational experiment.

By numerically extracting the Lagrangian for a system which has been deformed by some strain u_{ik}, we are able to find the pressure and elastic constants by judicious selection of strains and subsequent fitting of the coefficients.

Our results are presented in Fig. 5.2. These elastic constants should ideally be the same as those obtained via homogenisation theory. In reality, they suffer from numerical errors due to being unable to perform an arbitrarily small strain, as well as convergence errors in the new ground-state when close to the first-order phase transition between the homogeneous superfluid and the supersolid.

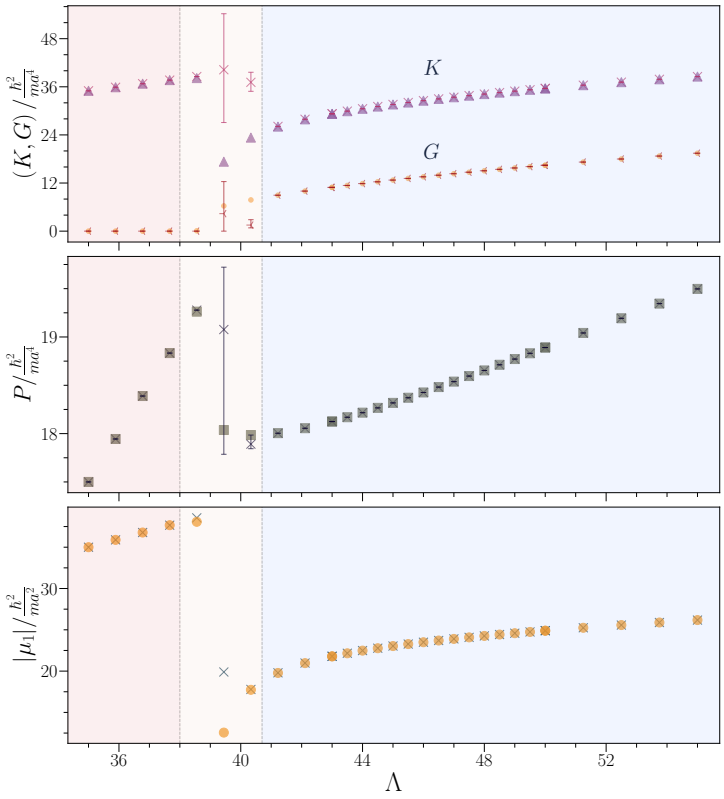


Fig. 5.2: A comparison of the various elastic constants obtained via homogenisation to those from numerics (homogenisation constants are shown in solid markers, numerics in crosses). The top figure shows the bulk modulus and shear modulus, the middle figure shows the pressure, and the bottom figure shows the absolute value of μ_1. The agreement between homogenisation and numerics is very strong on the whole, but falls apart in the phase transition region. This is likely due to numerical instabilities close to the phase transition which affect the numerically obtained constants but not the homogenisation constants.

Scanning across the whole range of the interaction parameter Λ, we find that, outside of a small region where the phase transition occurs, the elastic constants obtained numerically are in excellent agreement with those obtained analytically, with a typical discrepancy of 0.1%.

In Fig. 5.2, we have also shown the shift in the chemical potential for unit strain: $\mu_1^{ik} = \mu_1 \delta_{ik}$.

In summary, we have developed an elastic theory for a supersolid using homogeneration theory and calculated its elastic properties using the solution of the Gross-Pitaevskii equation. Our homogenisation results agree well with results from the numerical simulation of a strained supersolid.

5.3 *Tying it together*

We use this result, along with the elastic expansion (5.2.28), to write out the full Lagrangian density after the homogenisation process as

$$\begin{aligned}\frac{L_{hom}}{|\Omega|} = L_0 - \hbar n \dot{\phi}_0 (1 + \boldsymbol{\nabla} \cdot \mathbf{u}) - P_{ik} u_{ik} - \frac{1}{2} A_{iklm} u_{ik} u_{lm} \\ - \frac{\hbar^2}{2m} (n - \varrho) (\boldsymbol{\nabla} \phi_0)^2 + \hbar \varrho \boldsymbol{\nabla} \phi_0 \cdot \frac{D\mathbf{u}}{Dt} + \frac{1}{2} m \varrho \left(\frac{D\mathbf{u}}{Dt} \right)^2\end{aligned} \tag{5.3.1}$$

This effective Lagrangian contains all the linear responses of the system due to both strain and phase gradients. We can see that the phase stiffness is now given by $n - \varrho$ and ϱ is the inertia associated with the motion of the modulated pattern of the density. In summary, we have followed Ref. [10] and reproduced the same results for the superfluid phase stiffness of the supersolid. Our Lagrangian differs from that reference in the dynamical term. In the next section, we complete the development of an effective low-energy theory for the supersolid by considering the free energy of the system in the grand canonical ensemble. Then, we can finally proceed to discuss the macroscopic dynamics of the system.

Expanding the Lagrangian: Key points

In this chapter we expanded the Lagrangian as a function of a perturbative phase and strain, solved the equations in the corrective fields $\tilde{\phi}$ and $\tilde{\rho}$, and derived a low-energy long-wavelength response to these perturbations.

- We considered a perturbative phase field ϕ_0 and expanded the Lagrangian to $\mathcal{O}(\phi_0^2)$, before solving the corrective equation in $\tilde{\phi}$
- We find that the phase field couples to the strain field in the form of a material derivative given by

$$\mathbf{A} = \boldsymbol{\nabla}\phi_0 + (\boldsymbol{\nabla}\phi_0 \cdot \boldsymbol{\nabla})\,\mathbf{u} + \frac{m}{\hbar}\partial_t \mathbf{u}\,.$$

- The correction to the phase perturbation was found by solving for $\tilde{\phi}$ given the equation

$$\tilde{\phi} = K_i A_i \quad \text{with} \quad \partial_i \rho + \boldsymbol{\nabla}\cdot(\rho \boldsymbol{\nabla} K_i) = 0\,.$$

- After simplification of the Lagrangian, the result was a correction to the superfluid phase stiffness given by

$$\varrho_{ij} = -\frac{1}{|\Omega|}\int_\Omega \rho_0 \partial_i K_j \,\mathrm{d}\mathbf{r}$$

  which is responsible for the non-classical rotational inertia in a supersolid
- We expanded the non-phase component of the Lagrangian up to $\mathcal{O}(u^2)$ in the strain field, and subsequently solved the corrective equation in $\tilde{\rho}$
- We determined the correction to the chemical potential given by

$$\mu = \mu_0 + \mu_1^{ik}\epsilon_{ik} + \mu_2^{iklm} u_{ik} u_{lm}$$

- We found the elastic responses of the supersolid, finding that the pressure is given by

$$P_{ik} = \frac{1}{|\Omega|}\int_\Omega \left[\frac{\hbar^2}{4m}\left(\frac{\partial_i\rho_0\partial_k\rho_0}{\rho_0} - \nabla^2\rho_0\,\delta_{ik}\right) - \frac{1}{2}\rho_0(f_{ik} * \rho_0)\right]\mathrm{d}\mathbf{r}$$

- The corrective equation for $\tilde{\rho}$ (and also the method of finding the shift in the chemical potential) is given by

$$L(\tilde{\rho}) = F(\rho_0, \mu_0, \mu_1^{ik}, \mu_2^{iklm})$$

  with

$$L(\tilde{\rho}) \equiv \frac{\hbar^2}{4m}\boldsymbol{\nabla}\cdot\left(\frac{\boldsymbol{\nabla}\tilde{\rho}}{\rho_0}\right) - U * \tilde{\rho} + \frac{\hbar^2}{4m}\left(\frac{(\nabla\rho_0)^2}{\rho_0^3} - \frac{\nabla^2\rho_0}{\rho_0^2}\right)\tilde{\rho}$$

and

$$\begin{aligned} F(\rho_0, \mu_0, \mu_1^{ik}, \mu_2^{iklm}) \equiv &- \left(\mu_2^{iklm} + \mu_1^{ik}\delta_{lm} + \mu_0 M_{iklm}\right) u_{ik}u_{lm} \\ &+ \epsilon_{ik}\left[-\mu_1^{ik} + \frac{\hbar^2}{4m}\left(2\frac{\partial_{ik}\rho_0}{\rho_0} - \frac{\partial_i\rho_0\partial_k\rho_0}{\rho_0^2}\right)\right. \\ &\left. + \int_\Omega \left(f_{ik}(\mathbf{r}-\mathbf{r}') + \delta_{ik}U(\mathbf{r}-\mathbf{r}')\right)\rho_0(\mathbf{r}')\,\mathrm{d}\mathbf{r}'\right] \end{aligned}$$

- Using these results, we showed the Cauchy elastic tensor to be $B_{iklm} = |\Omega|^{-1}\int_\Omega b_{iklm}(\mathbf{r})\,\mathrm{d}\mathbf{r}$ where

$$\begin{aligned} b_{iklm}(\mathbf{r}) = &+ \frac{\hbar^2}{4m}\left(\frac{\partial_i\rho_0\partial_l\rho_0}{\rho_0}\delta_{km} + \frac{\partial_k\rho_0\partial_l\rho_0}{\rho_0}\delta_{im} - \frac{\partial_i\rho_0\partial_k\rho_0}{\rho_0}\delta_{lm}\right) \\ &+ \frac{1}{2}\left(f_{il} * \rho_0\right)\rho_0\delta_{km} - \frac{1}{2}\left(f_{ik} * \rho_0\right)\rho_0\delta_{lm} + \frac{1}{2}\left(f_{im} * \rho_0\right)\rho_0\delta_{kl} \\ &+ \left[\left(\left(U\delta_{ik} + 2f_{ik}\right)\delta_{lm} + W_{iklm}\right) * \rho_0\right]\rho_0 \\ &+ \rho_1^{lm}\left[\frac{\hbar^2}{4m}\left(2\frac{\partial_{ik}\rho_0}{\rho_0} - \frac{\partial_i\rho_0\partial_k\rho_0}{\rho_0^2}\right) + \left(f_{ik} + \delta_{ik}U\right) * \rho_0 + \mu_1^{ik}\right] \end{aligned}$$

- We verified the elastic constants by performing a numerical simulation using elastic deformations judiciously, and found strong agreement between the constants obtained via homogenisation and numerics Fig. 5.2

- We simplified the Lagrangian and expressed the low-energy response to the perturbative field as

$$\begin{aligned} \frac{L_{hom}}{|\Omega|} = &L_0 - \hbar n\dot{\phi}_0(1 + \boldsymbol{\nabla}\cdot\mathbf{u}) - P_{ik}u_{ik} - \frac{1}{2}A_{iklm}u_{ik}u_{lm} \\ &- \frac{\hbar^2}{2m}\left(n - \varrho\right)\left(\boldsymbol{\nabla}\phi_0\right)^2 + \hbar\varrho\boldsymbol{\nabla}\phi_0\cdot\frac{D\mathbf{u}}{Dt} + \frac{1}{2}m\varrho\left(\frac{D\mathbf{u}}{Dt}\right)^2 \end{aligned}$$

We will now move on to considering the total energy cost of creating a Goldstone mode by considering the work the Goldstone mode has to do on its surroundings.

6 Dynamics

In previous chapters, we developed a homogenised theory of the supersolid in the canonical ensemble at a fixed average particle density of n. We have integrated out the intra-unit-cell dynamics (in that we have taken long-wavelength responses) of the supersolid and have now obtained an effective Lagrangian $L_{hom}(\phi_0, \mathbf{u})$ which describes the system under a given phase gradient and displacements $\mathbf{u}$. We have assumed that all the unit cells responded in the same way, i.e. the response has the same periodicity as the supersolid.

This effective Lagrangian obeys all the necessary requirements of Galilean invariance, rotational invariance and $U(1)$ invariance as specified by Son [9] and Andreev & Lifshitz [7] due to symmetry constraints, so we would expect the dynamics to be phenomenologically correct.

6.1 Free energy and Grand Canonical ensemble

In this section, we will consider the inter-cell dynamics and allow for particle flow between unit cells leading to variations in the density δn across the system at length scales much larger than the size of the unit cells of the supersolid.

It is important to note that the additional energy response due to flow between cells is crucial to obtaining the correct dynamics of the system. If we were to neglect this energy response, we would find that the excitation velocities would be inconsistent with predictions from a Bogoliubov treatment.

We assume that the inter-cell number fluctuation is small, and so we can expand the Lagrangian analytically in δn up to $\mathcal{O}(\delta n^2)$. We now consider the ground state Lagrangian density $\mathcal{E}(n) = -L_0/|\Omega|$ which is a function of the average density n of the undeformed system. Under a change of the local density, this can be expanded as

A similar phenomena was observed in [69], where the authors found that the bulk modulus computed via a homogeneous dilation technique was not in agreement with long-wavelength phonon predictions unless charge redistribution was taken into account.

$$\mathcal{E}(n+\delta n) \simeq \mathcal{E}(n) + \mathcal{E}'\delta n + \frac{1}{2}\mathcal{E}''(\delta n)^2 \tag{6.1.1}$$

and similarly the local pressure can be expanded as

$$P(n+\delta n) \simeq P(n) + P'\delta n\,. \tag{6.1.2}$$

In general, we expect that all terms in the Lagrangian (5.3.1) will be modified by the change in total particle number. However, we only keep track of terms in the Lagrangian up to second order in the total

power of all perturbative fields, and so we only need to track the terms in the above expansion of $\mathcal{E}$ and P.

The coefficients, P' and $\mathcal{E}''$, can be calculated numerically by solving the Gross-Pitaevskii equation at several densities. We can also use $\mathcal{E}' = \mu_0$ and $\mathcal{E}'' = \partial\mu/\partial n$ if we have the density dependence of the chemical potential. In fact, we have already calculated the pressure derivative in terms of the chemical potential shift per unit strain, μ_1, as defined in (4.2.12) with $\mu_1^{ik} = \mu_1\delta_{ik}$. To see this, we note that the pressure, $P = -(\partial E/\partial V)_N$, and the chemical potential, $\mu = (\partial E/\partial N)_V$, are related by a Maxwell relation so that

$$P' = \frac{\partial P}{\partial n} = V\left(\frac{\partial P}{\partial N}\right)_V = -V\left(\frac{\partial \mu}{\partial V}\right)_N = -\mu_1 \,. \tag{6.1.3}$$

since $\delta V/V = u_{kk}$ is the strain. Similarly, we can use $\mathcal{E}'' = \partial\mu/\partial n$ if we have already obtained the density dependence of the chemical potential.

In general, the above analysis is valid for any tensorial quantity, but we have elected to use the symmetry properties of tensors that belong to a triangular lattice (i.e. $P_{ik} = P\delta_{ik}$ and $\mu_1^{ik} = \mu_1\delta_{ik}$) to simplify our calculations. The following analysis also uses this symmetry, but can be generalised to any tensorial quantity.

Finally, we need to include the work done by the change in local density on the local environment. Namely, if a part of the system expands due to an increase in particle number, it does work on the surroundings which must compress. The work done caused by a total volume change of δV is:

$$\delta W = -P\delta V = -P(\epsilon_{ll} + M_{iklm}u_{ik}u_{lm})|\Omega| \,. \tag{6.1.4}$$

In order to describe the dynamics of these density functions, we need to add this work done to the Lagrangian to obtain

$$\frac{L_{dyn}}{|\Omega|} = \frac{L_{hom}}{|\Omega|} - P\left(\epsilon_{ll} + M_{iklm}u_{ik}u_{lm}\right) \,. \tag{6.1.5}$$

Comparing with our form (5.3.1) for L_{hom} and the relation (4.1.15) between the Cauchy tensor B_{iklm} and A_{iklm}, we find that

$$\begin{aligned} &-Pu_{ll} - \frac{A_{iklm}}{2}u_{ik}u_{lm} - P(\epsilon_{ll} + M_{iklm}u_{ik}u_{lm}) \\ &\quad\simeq -\frac{1}{2}B_{iklm}u_{ik}u_{lm} \,. \end{aligned} \tag{6.1.6}$$

Using this, we arrive at an effective quadratic Lagrangian that can describe the dynamics of the low-energy excitations of the supersolid. This is the key result of homogenisation

$$\begin{aligned} \frac{L_{dyn}}{|\Omega|} =& -\mathcal{E} - \mu_0\delta n - \frac{1}{2}\mathcal{E}''(\delta n)^2 - \hbar n\dot{\phi}_0\left(1 + \boldsymbol{\nabla}\cdot\mathbf{u}\right) - \hbar\delta n\dot{\phi}_0 + \mu_1\delta n\boldsymbol{\nabla}\cdot\mathbf{u} \\ &- \frac{1}{2}B_{iklm}u_{ik}u_{lm} - \frac{\hbar^2}{2m}\left(n - \varrho\right)\left(\boldsymbol{\nabla}\phi_0\right)^2 + \hbar\varrho\boldsymbol{\nabla}\phi_0\cdot\dot{\mathbf{u}} + \frac{1}{2}m\varrho\dot{\mathbf{u}}^2 \,. \end{aligned} \tag{6.1.7}$$

In this process we note that we have directly identified the Cauchy elastic tensor in two different ways, firstly by using the result from Bavaud [65], and secondly by directly considering the work the excitations would need to do on their environment.

To summarise, we have a coarse-grained Lagrangian to describe the low-energy excitations of the supersolid. In the next section, we will investigate these dynamics.

6.2 *Effective supersolid Lagrangian*

In the previous sections, we have derived an effective Lagrangian (6.1.7) by integrating out the short-wavelength modes in the unit cell and coarse-graining the system such that a unit cell is now considered a point in the continuous field theory described by the fields $\{\mathbf{u}, n, \phi\}$. This Lagrangian formally describes a low-energy effective field theory wherein the coupled Goldstone modes of the system are the low-lying excitations. We now set out to calculate the normal modes by integrating out the field δN and solving the resulting set of coupled equations.

By minimising the Lagrangian for δn, we find

$$\delta n = \frac{\mu_1}{\mathcal{E}''} \boldsymbol{\nabla} \cdot \mathbf{u} - \frac{\hbar}{\mathcal{E}''} \dot{\phi} \tag{6.2.1}$$

which we substitute back into the Lagrangian to straightforwardly obtain

$$\begin{aligned} L = &- \mathcal{E} - \hbar n \dot{\phi} + \frac{\hbar^2}{2} \left[\frac{\dot{\phi}^2}{\mathcal{E}''} - \frac{n - \varrho}{m} \left(\boldsymbol{\nabla} \phi \right)^2 \right] \\ &+ \frac{1}{2} \left[m \varrho \dot{\mathbf{u}}^2 - \left(B_{iklm} - \frac{\mu_1}{\mathcal{E}''} \mu_1 \delta_{ik} \delta_{lm} \right) u_{ik} u_{lm} \right] \\ &- \hbar \left(n - \varrho + \frac{\mu_1}{\mathcal{E}''} \right) \dot{\phi} \boldsymbol{\nabla} \cdot \mathbf{u} \end{aligned} \tag{6.2.2}$$

This Lagrangian should be able to describe the Goldstone modes for the system.

By counting the number of spontaneously broken continuous symmetries, we are able to predict the number of Goldstone modes that emerge. Since we have broken the $U(1)$ gauge symmetry, we expect to find one Goldstone mode. We also have a triangular lattice, which means we have broken two continuous translational and rotational symmetries, and so we expect to find two Goldstone modes. Therefore we should find three Goldstone modes in total.

One can immediately find the equations of motion for both ϕ and $\mathbf{u}$, but it serves as a useful check to ensure we recover the Lagrangian for a Bogoliubov mode in the superfluid phase. In a superfluid phase, one can show that $B_{iklm} = U_{k=0} n^2 \delta_{ik} \delta_{lm}$, $\mu_1 = -U_{k=0} n$, $\mathcal{E}'' = U_{k=0}$ and $\varrho = 0$. Consequently, the resultant Lagrangian is now

$$L = -\mathcal{E} - \hbar n \dot{\phi} + \frac{\hbar^2}{2} \left[\frac{\dot{\phi}^2}{U_{k=0}} - \frac{n}{m} \left(\boldsymbol{\nabla} \phi \right)^2 \right] \tag{6.2.3}$$

which corresponds exactly with the superfluid Bogoliubov mode.

For the general supersolid case, we derive the equations of motion directly by assuming the fields ϕ and $\mathbf{u}$ are of a plane wave form $\sim e^{i(\mathbf{k} \cdot \mathbf{r} - \omega t)}$. The vector equation for the variable $\mathbf{u}$ can be solved to

This effective Lagrangian is of the form predicted by Ye [11]. A key point to note is that Ye wrote a Lagrangian with an effective B_{iklm} but did not predict an elastic response like the one shown here. Most notably, the feature

$$\Gamma_{iklm} = B_{iklm} - \frac{\mu_1}{\mathcal{E}''} \mu_1 \delta_{ik} \delta_{lm}$$

where Γ_{iklm} is some effective elastic response, exhibits interesting behaviour in that there are effective elastic responses arising from both elastic dynamics B_{iklm} and particle-number dynamics $\mu_1^2 / \mathcal{E}''$. This is an additional insight that has been revealed by homogenisation.

provide both the shear and longitudinal mode. The Euler-Lagrange equation for the variable $\mathbf{u}$ is immediately found to be

$$\begin{aligned} m\varrho\ddot{\mathbf{u}} - \left(K + G - \frac{\mu_1}{\mathcal{E}''}\mu_1\right)\boldsymbol{\nabla}\left(\boldsymbol{\nabla}\cdot\mathbf{u}\right) - G\nabla^2\mathbf{u} \\ - \hbar\left(n - \varrho + \frac{\mu_1}{\mathcal{E}''}\right)\boldsymbol{\nabla}\dot{\phi} = 0 \end{aligned} \tag{6.2.4}$$

where we have used (5.2.29) as we are analysing a triangular lattice.

A similar procedure for isolating the shear mode from the bulk mode was done in Landau & Lifshitz [67]

We can now solve this equation by noting that the vector field $\mathbf{u}$ can be split into longitudinal and transverse elements $\mathbf{u} = \mathbf{u}_l + \mathbf{u}_t$. Taking the curl of (6.2.4) isolates the transverse motion ($\mathbf{u}_t$) giving:

$$\boldsymbol{\nabla}\times\left(m\varrho\ddot{\mathbf{u}}_t - G\nabla^2\mathbf{u}_t\right) = 0 \tag{6.2.5}$$

This is a wave equation for $\boldsymbol{\nabla}\times\mathbf{u}$ from which we obtain the shear velocity

$$c_{\text{shear}} = \sqrt{\frac{G}{m\varrho}} \tag{6.2.6}$$

which is exactly equivalent to the shear velocity predicted in standard solid elasticity.

It may be somewhat surprising that the expression for shear velocity is the exact same as of a standard solid, but recall that the Bogoliubov mode in a superfluid is strictly *longitudinal*, in that the oscillations are parallel to the wavevector. As such, we would expect it to be completely decoupled from the shear mode, and therefore no contribution from the superfluid component should be expected in the shear mode. With regards to the shear mode, the supersolid is just a regular solid.

It should be noted that even though the shear mode is fully decoupled from the $U(1)$ phase at long-wavelengths (i.e. at the Γ point), this may not strictly hold true at shorter wavelengths of these excitations. As will be shown in Fig. 6.2, the shear and fast longitudinal mode are actually *degenerate* at the K point!

We examine longitudinal dynamics ($\mathbf{u}_l$) by taking the divergence of (6.2.4). We find the two coupled equations

$$\hbar\left(\frac{\omega^2}{\mathcal{E}''} - \frac{n-\varrho}{m}\mathbf{k}^2\right)\Phi - i\omega\left(n - \varrho + \frac{\mu_1}{\mathcal{E}''}\right)\boldsymbol{\nabla}\cdot\mathbf{u}_l = 0\,, \tag{6.2.7}$$

$$\begin{aligned} \left[m\varrho\omega^2 - \left(K - \frac{\mu_1}{\mathcal{E}''}\mu_1 + 2G\right)\mathbf{k}^2\right]\boldsymbol{\nabla}\cdot\mathbf{u}_l \\ + i\omega\hbar\mathbf{k}^2\left(n - \varrho + \frac{\mu_1}{\mathcal{E}''}\right)\Phi = 0 \end{aligned} \tag{6.2.8}$$

N.B. these equations are *not valid* if the system is superfluid (i.e. $\varrho = 0$). In this scenario (6.2.8) does not exist at all and is trivially satisfied, and the only equation to solve is that arising from the Lagrangian given in (6.2.3), which generates the correct superfluid dynamics.

in the variables $\mathbf{u}_l$ and ϕ. It can be shown easily that if we are in a superfluid regime the second equation is trivially satisfied, and the first equation finds the Bogoliubov frequency. These equations can be solved for ω as a function of $\mathbf{k}$ and leads to the following dispersion relation

$$\omega^2 = \frac{A \pm D}{2m\varrho}\,\mathbf{k}^2 \tag{6.2.9}$$

with

$$\begin{aligned} A &= K + 2G + \left(n\mathcal{E}'' + 2\mu_1\right)(n-\varrho) \\ D^2 &= A^2 - 4\varrho(n-\varrho)\left[\mathcal{E}''(K+2G) - \mu_1^2\right] . \end{aligned} \tag{6.2.10}$$

Let's briefly examine the two limits of $\varrho = 0$ and $\varrho = n$, i.e. the superfluid and solid limits. We note that, in the case of the homogeneous superfluid ($\varrho = 0$), we obtain the superfluid velocity directly from (6.2.3)

$$\omega^2 = \frac{n\, U_{k=0}}{m}\mathbf{k}^2 \tag{6.2.11}$$

which is exactly equal to the Bogoliubov velocity. In the opposite limit of $\varrho = n$, the two modes have frequencies

$$\omega^2 = \frac{K+2G}{mn}\mathbf{k}^2 \quad \text{and zero.} \tag{6.2.12}$$

The zero mode corresponds to the collapse of the Bogoliubov mode and the linear dispersing mode has a velocity as expected for a normal solid with elastic moduli K and G.

It is interesting to note that, although we expect the Gross-Pitaevskii Lagrangian to struggle with describing a normal solid, the effective phenomenological Lagrangian that emerges actually returns to that of a normal solid in the limit $\varrho \to n$.

We can also now examine the nature of the normal modes of the system. By writing (6.2.7) and (6.2.8) in terms of a matrix equation, we can find the eigenvectors of the system for a given ω. These eigenvectors are the normal modes, and are some composite of the fields ϕ and $\mathbf{u}_l$. We can then subsequently define an eigenvector angle θ which describes the relative contribution of the fields ϕ and $\mathbf{u}_l$ to the normal mode. For example, in the superfluid the eigenvector angle is $\theta = 0$ as the normal mode is purely ϕ, i.e. $\mathbf{e}_n \equiv \mathbf{e}_\phi$. A supersolid with normal mode $\mathbf{e}_n = (0.5, 0.5)$ would have $\theta = \pi/4$ etc. The normal mode composition is illustrated in Fig. 6.1.

An interesting point of note is that the slow longitudinal mode (which is expected to die off in the limit of a solid) is a composite of both ϕ and $\mathbf{u}_l$, but is mostly ϕ at all points in the phase diagram (i.e. θ is small). More importantly, it appears there is a critical point at which the slow longitudinal mode is 'saturated', that is to say that there is a global maximum in the mixing of the slow longitudinal mode (but note that the mode is still mostly ϕ). This feature appears to be absent in the fast longitudinal mode. However, the fast longitudinal mode also exhibits interesting behaviour as the mixing angle does not tend to $\pi/2$ or $3\pi/2$ as one may initially expect (as we would expect the mode to tend to a purely elastic phonon mode in the limit of a solid), but instead tends to approximately $7\pi/8$. This is a curious feature of the fast longitudinal mode, and we are currently investigating the origin of this behaviour.

It is currently unclear whether or not the saturation of the mixing in the slow longitudinal mode has any interesting physical implications. For example, one may choose to think about thermal transport properties of these excitations; what would the thermal transport even look like in a supersolid, and given the answer to that question what (if anything) is special about this particular point where the slow longitudinal mode is maximally mixed?

The above holds for any system described by a Gross-Pitaevskii equation; we can now use these results in the specific case of a soft-core interaction. We find a ground state for the system numerically

and by applying the procedure detailed above we can determine the velocities of all modes that exist. Importantly we note that our Lagrangian is tuned **across the transition**, i.e. a single theory describes both the superfluid and supersolid regime and continuously varies across a first order phase transition. Importantly, symmetry arguments by Son [9] dictate the functional form of any Lagrangian belonging to a supersolid and since our Lagrangian is a subset of those allowed by symmetry, we argue that we completely capture the phenomenological behaviour of the supersolid as described by a Hartree approximation.

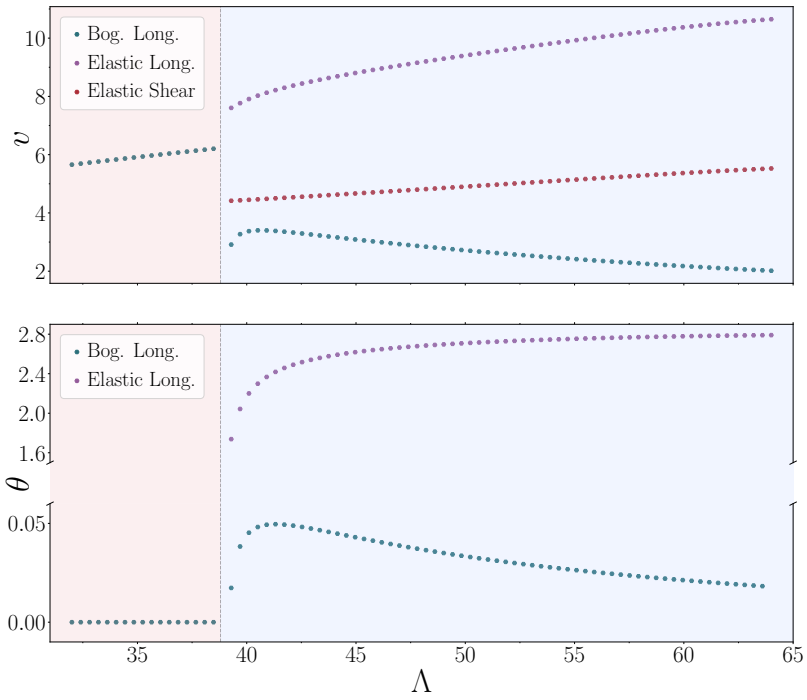


Fig. 6.1: Top: excitation velocities for all available sound modes of a system governed by a Heaviside interaction of strength Λ with a phase transition at $\Lambda \sim 38$, as calculated via homogenisation. Velocities are in units of $\hbar/\sqrt{n}ma^2$. Bottom: the eigenvector angle θ for the available longitudinal modes. Both diagrams indicate a superfluid phase at low Λ and a supersolid phase at high Λ, in agreement with earlier results. We see several interesting behaviours in the relative modes; notably the shear mode velocity appears to be linearly dependent on Λ, whereas the other two modes seem to have a dip close to the transition before exhibiting linear behaviour. In the eigenvector angle, there is an interesting maxima in the Bogoliubov mode, whereas the elastic mode seems to tend to a value of ~ 2.8 radians in the large Λ limit. The eigenvector angle should be related to the thermal transport properties of the modes.

6.3 *Bogoliubov Dispersion*

An alternative technique to finding excitations of the system is to directly apply linearised oscillations in the number density and the phase. Namely, since $\psi = \sqrt{\rho}e^{i\phi}$, we can apply the Bogoliubov fluctuations $\rho \to \rho_0 + \delta\rho$ and ϕ to obtain the Goldstone modes. We expect to recover all the Goldstone modes accessible to the system, and expect the quantitative properties to be the same as those predicted in the elastic theory. More precisely, due to the broken $U(1)$ phase and the broken continuous translational symmetry, we expect to find three Goldstone modes, two of which are longitudinal and one of which

is a shear mode. Since this is a completely independent technique to recovering the Goldstone modes, it serves as an important check of our results.

By following a similar procedure to that outlined in [33], we are able to obtain eigenvalue equations which give the excitation frequencies ω of the Bloch waves in the system. These Bloch waves have a band structure, and the lowest band structure at the Γ point corresponds to the Goldstone modes of the system whose propagation velocities were independently derived in [33].

We begin by directly substituting these fluctuations in to the equations of motion and truncating non-linear terms, leaving us with the set of equations

$$\begin{aligned} \partial_t \delta\rho &= -\frac{\hbar}{m}\boldsymbol{\nabla}\left(\rho_0 \boldsymbol{\nabla}\phi\right) \\ -\hbar\partial_t\phi &= -\frac{\hbar^2}{4m\rho_0}\boldsymbol{\nabla}\left(\rho_0\boldsymbol{\nabla}\left(\frac{\delta\rho}{\rho_0}\right)\right) + U * \delta\rho. \end{aligned} \tag{6.3.1}$$

N.B. This is exactly the same process as that in obtaining (3.1.41) but now with the added distinction that we cannot (and do not) assume ρ_0 is a constant. This complicates things by quite a bit, and it means that we no longer will obtain an analytical expression for the dispersion relation, but instead have to calculate it numerically.

While this would produce the same results, it is a little easier if we choose instead to expand like $\sqrt{\rho} \to \sqrt{\rho_0} + \delta\psi$ instead of $\sqrt{\rho} \to \sqrt{\rho_0 + \delta\rho}$. In doing so we then obtain

$$\begin{aligned} \partial_t \delta\psi &= -\frac{\hbar}{m}\frac{1}{2\sqrt{\rho_0}}\boldsymbol{\nabla}\left(\rho_0\boldsymbol{\nabla}\phi\right) \\ -\hbar\partial_t\phi &= -\frac{\hbar^2}{2m\sqrt{\rho_0}}\nabla^2(\delta\psi) + \frac{\hbar^2}{m}\frac{\nabla^2\left(\sqrt{\rho_0}\right)}{2\rho_0}\delta\psi + 2U * \left(\sqrt{\rho_0}\delta\psi\right) \end{aligned} \tag{6.3.2}$$

which can be simplified further. By noting that

$$\begin{aligned} \frac{\hbar^2}{2m\sqrt{\rho_0}}\nabla^2\left(\sqrt{\rho_0}\right) &= \frac{\hbar^2}{4m}\left(\frac{\nabla^2\rho_0}{\rho_0} - \frac{\left(\boldsymbol{\nabla}\rho_0\right)^2}{2\rho_0^2}\right) \\ &= U * \rho_0 - \mu \end{aligned} \tag{6.3.3}$$

Whilst both techniques access the speeds of sound, the elastic technique also provides elastic moduli and fractional inertia, whereas the bogoliubov technique provides a full band structure. In this way, the two techniques complement each other, as they verify common ground but also provide information that is inaccesible to the other.

by use of the base EoM (3.1.35), the latter equation becomes

$$-\hbar\partial_t\phi = \left[-\frac{\hbar^2}{2m\sqrt{\rho_0}}\nabla^2 + \frac{1}{\sqrt{\rho_0}}\left(U * \rho_0 - \mu\right)\right]\delta\psi + 2U * \left(\sqrt{\rho_0}\delta\psi\right) \tag{6.3.4}$$

which can be re-expressed by use of operator notation.

We apply a local rescaling of the phase s.t. $\Phi \equiv \hbar\sqrt{\rho_0}\phi$ and obtain the set of coupled equations

$$\begin{aligned} \partial_t\delta\psi &= \hat{T}\Phi \\ -\partial_t\Phi &= \left(\hat{T} + \hat{U}\right)\delta\psi \end{aligned} \tag{6.3.5}$$

with

$$\begin{aligned}\hat{T}f &\equiv \left[-\frac{\hbar^2}{2m}\nabla^2 + U * \rho_0 - \mu\right] f \\ \hat{U}f &\equiv 2\sqrt{\rho_0}\left[U * (\sqrt{\rho_0}\delta\psi)\right] \\ &= 2\sqrt{\rho_0}\int U(\mathbf{r}-\mathbf{r}')\sqrt{\rho_0}(\mathbf{r}')f(\mathbf{r}')\,\mathrm{d}\mathbf{r}'\end{aligned} \tag{6.3.6}$$

defined as operators acting on our fluctuations. It is important to note that in the limit of $\rho_0 \to \bar{n}$ these are exactly the Bogoliubov equations.

It is useful to note that the equations (6.3.7) can in principle be solved directly in real space. However, since we are working with periodic crystal lattices, we instead opt to use Bloch's theorem and find a band structure for the Bogoliubov excitations of the system. From the band structure we should expect to recover three Goldstone modes of the same velocities as predicted by the elastic homogenisation theory.

We can immediately solve the simultaneous equations (6.3.5) by direct substitution to obtain either of

$$\begin{aligned}\left[\left(\hat{T}+\hat{U}\right)\hat{T}+\partial_t^2\right]\Phi = 0 \\ \left[\hat{T}\left(\hat{T}+\hat{U}\right)+\partial_t^2\right]\delta\psi = 0\end{aligned} \tag{6.3.7}$$

which provide the excitation spectra of our system.

By applying Bloch's theorem, we note that

$$\Phi(\mathbf{r}) = e^{i\mathbf{k}\cdot\mathbf{r}}\chi_{\mathbf{k}}(\mathbf{r}) \quad ; \quad \delta\psi(\mathbf{r}) = e^{i\mathbf{k}\cdot\mathbf{r}}\eta_{\mathbf{k}}(\mathbf{r}) \tag{6.3.8}$$

and that we can express the operators in $\mathbf{k}$-space as

$$\begin{aligned}\hat{T}^{\mathbf{k}}_{\mathbf{G},\mathbf{G}'} &\equiv \left[\frac{\hbar^2}{2m}(\mathbf{G}+\mathbf{k})^2 - \mu\right]\delta_{\mathbf{G},\mathbf{G}'} + U_{\mathbf{G}-\mathbf{G}'}\rho_{\mathbf{G}-\mathbf{G}'} \\ \hat{U}^{\mathbf{k}}_{\mathbf{G},\mathbf{G}'} &\equiv 2\sum_{\mathbf{G}''}\psi_{\mathbf{G}-\mathbf{G}''}U_{\mathbf{k}+\mathbf{G}''}\psi_{\mathbf{G}''-\mathbf{G}'}\end{aligned} \tag{6.3.9}$$

where they each have an eigenvalue problem

$$\lambda_{\mathbf{k}} f_{\mathbf{G}+\mathbf{k}} = \sum_{\mathbf{G}'} O^{\mathbf{k}}_{\mathbf{G},\mathbf{G}'} f_{\mathbf{G}'+\mathbf{k}} \tag{6.3.10}$$

that we can now solve for. In the above equations, $\mathbf{G}$ is a reciprocal lattice vector at which ψ condenses to. By recognising that the equations (6.3.7) are now eigenvalue problems, and that the time dependency can be Fourier transformed $\partial_t \to i\omega$, we can now express

$$\begin{aligned}\left[-\omega^2 + \left(\hat{T}^{\mathbf{k}}+\hat{U}^{\mathbf{k}}\right)\hat{T}^{\mathbf{k}}\right](\Phi)^{\mathbf{k}} = 0 \\ \left[-\omega^2 + \hat{T}^{\mathbf{k}}\left(\hat{T}^{\mathbf{k}}+\hat{U}^{\mathbf{k}}\right)\right](\delta\psi)^{\mathbf{k}} = 0\end{aligned} \tag{6.3.11}$$

which is simply an eigenvalue problem with $\lambda = \omega^2$. By finding the eigenvalues of either of the equations (9.1.18), we can recover the dispersion relation for the Goldstone modes of the system, as well as a full band structure.

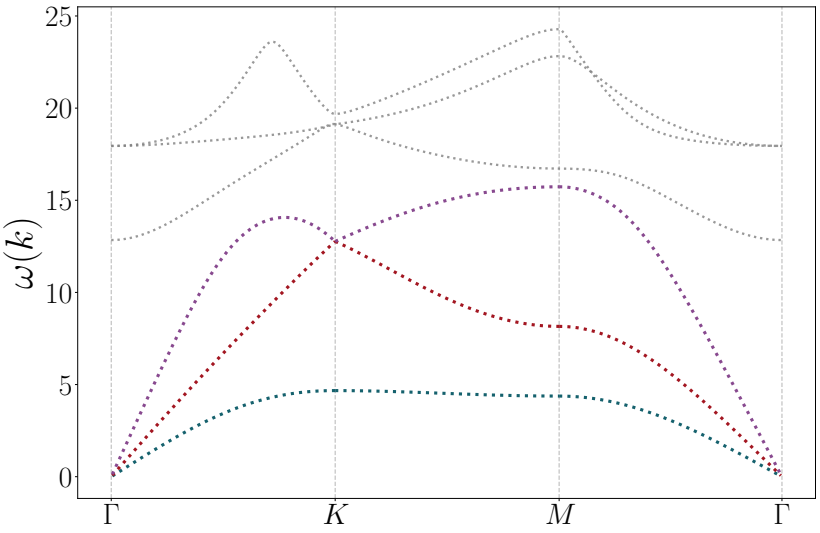


Fig. 6.2: Band structure for a supersolid at $\Lambda = 50$. The three Goldstone modes are highlighted as a fast longitudinal, slow longitudinal and shear mode. The velocities of the Goldstone modes are obtained by calculating the slope of the three bands at the Γ point; we typically find agreement to about $\sim 1\%$ with homogenisation. Note also that the two elastic modes (the fast longitudinal and shear modes) are degenerate at the K point due to triangular symmetry. Consequently, one can deduce that the bands do not cross but rather only touch, by examining the $N \to \Gamma$ dispersion relation and noting that Goldstone velocities should be isotropic in a crystal lattice, hence the shear mode must have the same velocity in either the $\Gamma \to K$ section or $M \to \Gamma$ section, and therefore the bands do not cross at K.

We expect that the band structure obtained from solving these equations should find all the requisite Goldstone modes and that they should have the same velocities as predicted via homogenisation.

Upon recovery of the band structure, one finds exactly $(D + 1)$ Goldstone modes as expected. There is a band crossing at the K point of the fast longitudinal and shear modes, characteristic of a triangular lattice (n.b. this is not actually a crossing but a band touching, as shown by the $M \to \Gamma$ band structure).

For any particular given Λ, both the Bogoliubov and elastic techniques predict all three speeds of sound (if supersolid, only one speed if superfluid), and agree on the speeds with excellent precision. Subsequently, by deriving the excitations of the system in two independent ways and obtaining the same results to excellent numerical precision, we can reliably say we have obtained the correct dynamics.

Dynamics: Key points

In this chapter we

- Considered the additional effect of number-density fluctuations within a unit cell. Prior to this, the effective Lagrangian (5.3.1) had only contained the energetic contributions from the strain u_{ik} and the phase ϕ_0, but this was achieved by treating unit cells with a fixed number-density and in isolation
- Upon the addition of the number-density fluctuations, we saw that they were in fact necessary to recover the correct velocities in the superfluid regime. We find the effective Lagrangian

$$\begin{aligned}\frac{Ł_{dyn}}{|\Omega|} =& -\mathcal{E} - \mu_0\delta n - \frac{1}{2}\mathcal{E}''(\delta n)^2 - \hbar n\dot{\phi}_0\left(1+\boldsymbol{\nabla}\cdot\mathbf{u}\right) - \hbar\delta n\dot{\phi}_0 + \mu_1\delta n\boldsymbol{\nabla}\cdot\mathbf{u}\\ &- \frac{1}{2}B_{iklm}u_{ik}u_{lm} - \frac{\hbar^2}{2m}\left(n-\varrho\right)\left(\boldsymbol{\nabla}\phi_0\right)^2 + \hbar\varrho\boldsymbol{\nabla}\phi_0\cdot\dot{\mathbf{u}} + \frac{1}{2}m\varrho\dot{\mathbf{u}}^2\,.\end{aligned}$$

- We can take the above Lagrangian and find the excitation velocities by integrating out the δn field. We obtain

$$\begin{aligned}L =& -\mathcal{E} - \hbar n\dot{\phi} + \frac{\hbar^2}{2}\left[\frac{\dot{\phi}^2}{\mathcal{E}''} - \frac{n-\varrho}{m}\left(\boldsymbol{\nabla}\phi\right)^2\right]\\ &+\frac{1}{2}\left[m\varrho\dot{\mathbf{u}}^2 - \left(B_{iklm} - \frac{\mu_1}{\mathcal{E}''}\mu_1\delta_{ik}\delta_{lm}\right)u_{ik}u_{lm}\right]\\ &-\hbar\left(n-\varrho+\frac{\mu_1}{\mathcal{E}''}\right)\dot{\phi}\boldsymbol{\nabla}\cdot\mathbf{u}\end{aligned}$$

- The shear velocity is given by

$$c_{\text{shear}} = \sqrt{\frac{G}{m\varrho}}$$

  and the longitudinal velocities are given by

$$\omega^2 = \frac{A\pm D}{2m\varrho}\mathbf{k}^2$$

  with

$$\begin{aligned}A &= K + 2G + \left(n\mathcal{E}'' + 2\mu_1\right)\left(n-\varrho\right)\\ D^2 &= A^2 - 4\varrho(n-\varrho)\left[\mathcal{E}''(K+2G) - \mu_1^2\right]\,.\end{aligned}$$

- We re-derived the Bogoliubov technique for finding supersolid excitations. These were given by the solution of the following equation

$$\begin{aligned}\left[-\omega^2 + \left(\hat{T}^{\mathbf{k}} + \hat{U}^{\mathbf{k}}\right)\hat{T}^{\mathbf{k}}\right](\Phi)^{\mathbf{k}} &= 0\\ \left[-\omega^2 + \hat{T}^{\mathbf{k}}\left(\hat{T}^{\mathbf{k}} + \hat{U}^{\mathbf{k}}\right)\right](\delta\psi)^{\mathbf{k}} &= 0\end{aligned}$$

with the operators defined as

$$\hat{T}^{\mathbf{k}}_{\mathbf{G},\mathbf{G}'} \equiv \left[\frac{\hbar^2}{2m}(\mathbf{G}+\mathbf{k})^2 - \mu\right]\delta_{\mathbf{G},\mathbf{G}'} + U_{\mathbf{G}-\mathbf{G}'}\rho_{\mathbf{G}-\mathbf{G}'}$$
$$\hat{U}^{\mathbf{k}}_{\mathbf{G},\mathbf{G}'} \equiv 2\sum_{\mathbf{G}''}\psi_{\mathbf{G}-\mathbf{G}''}U_{\mathbf{k}+\mathbf{G}''}\psi_{\mathbf{G}''-\mathbf{G}'}$$

we found that they agreed well with the excitation velocities obtained via homogenisation.

- We argue that homogenisation and the Bogoliubov technique make an excellent partnership for the analysis of supersolids. While the Bogoliubov technique provides a full band structure, with additional detail hence contained at high-frequency excitations, it does not generate the bulk quantities that one may be able to measure. Conversely, homogenisation provides a full effective Lagrangian which describes the dynamics of the Goldstone modes, generates a range of bulk quantities which may be measured, and provides insight into the dynamical nature of supersolids. Obviously though, being a long-wavelength theory, it does not provide the high-frequency structure that the Bogoliubov theory does. However, combining the two techniques one can mutually verify their results through the prediction of the Goldstone mode velocities, and obtain a more detailed picture than either technique could on its own.

We now move on to a short section which discusses some of the surprising results we can see.

7 Results

7.1 Thermodynamic Anomaly

In the previous chapters we have verified the technique of homogenisation as a means of recovering the low-lying excitations of the system. This was achieved via means of two completely independent techniques, the results of which both agree to excellent accuracy. An advantage of homogenisation over the Bogoliubov technique is that it also provides the elastic constants of the system, which cannot be obtained via Bogoliubov, as there is a many-to-one relationship between the elastic constants and the Goldstone modes (in that there are 6 elastic constants and three Goldstone modes, so there are always several extra degrees of freedom from which one cannot infer the constants backwards from the modes). Moreover, it provides the fractional inertia of the system, which is a quantity that is of great physical interest. A clear disadvantage however, is that homogenisation does not provide the full spectrum of excitations, only the long-wavelength limit.

We stress that the Bogoliubov technique is completely separate from homogenisation, and so by utilising both techniques one can recover the full band structure from Bogoliubov and supplement it with additional information in the long-wavelength limit from homogenisation.

The effective Lagrangian that is the end result of homogenisation elucidates interesting dynamics. By considering that the flow excitations of the system can be coupled to the strain excitations, we can see that the system is capable of strain-induced flow. Furthermore, by considering the application of an instantaneous strain to the system, we can see that flow will be induced and contribute to the elastic response of the system.

Consider applying a strain and keeping it fixed for a long time so that the flow dissipates. One can see that $\delta n = 0$, and hence there will be a different elastic response as we are now solving the Lagrangian (6.1.7) and not (6.2.2). In this way we can see that the elastic modulus has a time dependence, and that the system is capable of dissipating energy via the flow of the system. This energy dissipation is likely to be via the two longitudinal modes which are coupled crystal and Bogoliubov phonons.

There is an interesting question of defining the compressibility of the system. When one considers the elastic strain, it is natural to define the compressibility of the system as $\kappa = -1/V\,(\partial V/\partial P)$. Typically in a solid, one would simultaneously be able to say $\kappa = 1/n\,(\partial n/\partial P)$, where n is the number density and μ the chemical potential. However, in our analysis, we can show that these two definitions do not agree, and are off by a considerable margin. These two values are defined as $\kappa = 1/B_{xxyy}$ and $\kappa = 1/(n\mu_1)$ in our notation respectively.

The resolution of this seeming dilemma is to revisit the definition

of the two compressibilities. The compressibility $\kappa = 1/B$ where $B = -V(\partial P/\partial V|_N)$ is the elastic bulk modulus of the system, taken at constant particle number. This is the compressibility of the system as defined via elastic theory, and is the one that we will take as the 'true compressibility', and consequently B as the 'true bulk modulus'. Importantly, the derivative is taken under constant particle number. As such, to elucidate this a little further, we write

$$B_e = -V\frac{\partial P}{\partial V}\bigg|_N \tag{7.1.1}$$

where the subscript e denotes that this is the elastic bulk modulus. We can then write the compressibility as $\kappa_e = 1/B_e$. We can subsequently define the thermodynamic bulk modulus (using the typical definition with n but now removing the factor of V which is kept constant) as

$$B_t = N\frac{\partial P}{\partial N}\bigg|_V \tag{7.1.2}$$

and the thermodynamic compressibility accordingly.

A key consideration in understanding why $B_e \neq B_t$ is the fact that we are keeping different variables constant upon taking derivatives. If we want to connect these two definitions, we need to use the cyclic relations of thermodynamics

$$\frac{\partial x}{\partial y}\bigg|_z = -\frac{\partial x}{\partial z}\bigg|_y \frac{\partial z}{\partial y}\bigg|_x \quad . \tag{7.1.3}$$

It is important to note that due to the derivatives being taken w.r.t some other variable being held constant, we have to use the cyclic relations instead of regular chain rule.

We can then write

$$B_e = -V\frac{\partial P}{\partial V}\bigg|_N = V\frac{\partial P}{\partial N}\bigg|_V \frac{\partial N}{\partial V}\bigg|_P \equiv B_t\,\frac{1}{n}\frac{\partial N}{\partial V}\bigg|_P \tag{7.1.4}$$

from which we can consider the following. In a regular material (solid, gas, liquid) we would expect that the derivative of the particle number with respect to the volume under constant pressure is simply the density of the system, and we would recover the thermodynamic bulk modulus $B_t = n(\partial P/\partial n|_V)$ from (7.1.4). We can then examine whether this is the case for our system, i.e. is $1/n(\partial N/\partial V|_P) = 1$?

We can examine this quantity, henceforth denoted as $\mathcal{R}$ and called the 'compressibility ratio', by choosing an initial volume and particle number V_0 and N_0 which will generate a P_0, adjusting the volume around V_0 with some δV, and then varying the particle number $N_0 + \delta N$ until the system reaches P_0. We can then numerically calculate $\mathcal{R}$ by finite differencing. If we expect the difference between the two compressibilities to be due to the fact that $\frac{1}{n}\frac{\partial N}{\partial V}|_P \neq 1$ then we would expect $\mathcal{R} = \frac{\kappa_t}{\kappa_e}$, or equivalently

$$\mathcal{R} = \frac{B_e}{B_t}\,. \tag{7.1.5}$$

Upon performing the numerical determination of $\mathcal{R}$, we find that it is within good agreement of the ratio of the two compressibilities as determined via homogenisation. The percentage error between the homogenisation and numerical $\mathcal{R}$ is typically between 3% and 5%. We believe this is an artifact of the numerical determination of $\mathcal{R}$, and that as the algorithm and precision of simulations for determining $\mathcal{R}$ is improved, the agreement will improve accordingly.

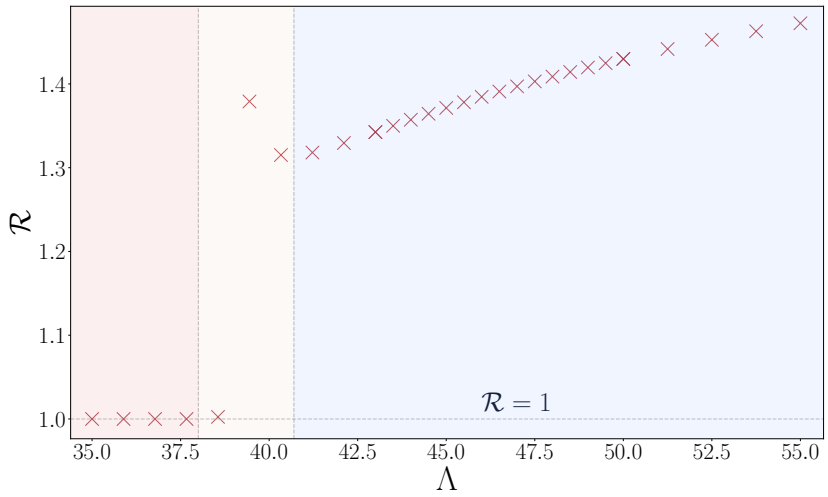


Fig. 7.1: Compressibility ratio $\mathcal{R}$ for a system governed by a soft-core interaction of strength Λ. The expected value of $\mathcal{R} = 1$ is obtained in the superfluid phase, but is starkly different in the supersolid regime.

While we have shown that the compressibility ratio obtained via homogenisation is in good agreement with the numerical determination, we do not yet fully understand the nature of this anomalous result. In our search across the literature we have not found another example of this phenomenon, and we are currently investigating the origin of this effect. A possible explanation for the result is considering a pressure which can be written like $P(n, G(n, V))$, where G is the ordering wavevector.

One can then subsequently show that the difference between bulk moduli can be written as

$$B_e = B_t - V \frac{\partial P}{\partial G}\bigg|_n \frac{\partial G}{\partial V}\bigg|_n \tag{7.1.6}$$

where it is clear that the last term is the anomalous term.

This term vanishes in ordinary materials in various ways. For gases and liquids, there is no ordering vector, so this term never existed to begin with. A regular solid has well-defined atomic positions. So, if the density is specified, the ordering wavevector is also specified. Upon changing the volume, there is no additional change in the ordering wavevector beyond that caused by the change in density. Supersolids are unique in that the ordering vector G experiences a

When we first encountered this anomaly, one of our first attempts to explain this phenomena was considering a mixture of materials in the system. More specifically, if we treated the system as containing roughly $n - \varrho$ superfluid and ϱ solid, and then averaged the compressibility like so

$$B_{eff} = (n - \varrho)B_{\text{sf}} + \varrho B_{\text{solid}}$$

where $B_{\text{sf}} \equiv \mu_0$ and $B_{\text{solid}} \equiv B_{xxyy}$, would you recover the anomalous result? This would seem like a natural guess, however it does not align with either the prediction from homogenisation or the numerics. Consequently, this is a signal of intertwined order rather than just co-existing order.

commensuration effect. For instance, in a one-dimensional system, it needs to be an integer multiple of $2\pi/L$ with L being the length of the system. If we stretch the system by δL much less than the lattice spacing, then the fractional change in the ordering wavevector is $\delta G/G = -\delta L/L$ so that $L\partial G/\partial L = -G$. We believe this is a feature unique to supersolids, due to their ability to exist at a wide range of densities, each of which has their own ordering vector, whereas regular solids only have one density at which they can exist (at some given pressure) and therefore only have one ordering vector. This is (to the best of our knowledge) a new phenomena which could be of great interest to the characterisation of supersolids.

Some currently open questions are as follows. Is this effect unique to the supersolid phase, or is it a more general phenomena? What kind of thermal transport is occurring in the phonon modes of a supersolid? Does the notion of the Landau criterion for superfluidity still hold in the supersolid phase, and if so, how does it change now that we have a band structure? These questions may potentially have avenues to solution via the techniques we've developed.

The successful development of homogenisation techniques for the study of supersolids is a significant step forward in the study of these systems. We have shown that the homogenisation technique is able to accurately capture the behaviour of the supersolid phase through comparison with well established Bogoliubov techniques. We were able to obtain previously unknown elastic properties of these materials as well as an effective Lagrangian which can be used to study the dynamics of the system. In contrast with typical phases of matter which have $\mathcal{R} = 1$, we found that the compressibility ratio of the supersolid phase is $\mathcal{R} > 1$. This is a new phenomena which we predict will arise in supersolids, and of which the origin is currently unknown.

Results: Key points

In this chapter we used the results from previous sections to discover a new phenomena which we've called the 'anomalous compressibility ratio'.

- Regular materials have two equivalent definitions of compressibility

$$B_e = -V\left.\frac{\partial P}{\partial V}\right|_N \equiv B_t = N\left.\frac{\partial P}{\partial N}\right|_V$$

  which are related by the compressibility ratio

$$\mathcal{R} = \frac{B_e}{B_t}$$

- We've shown by homogenisation (and verified numerically) that $\mathcal{R} \neq 1$ in a soft-core supersolid, and takes a value $\mathcal{R} > 1$ in the supersolid phase
- It is not entirely certain why and how this occurs, but it is possible that a supersolid has to have a lattice spacing vector which is commensurate with the system size. As such, one can show that the two compressibilities are related to each other by

$$B_e = B_t - V\left.\frac{\partial P}{\partial G}\right|_n \left.\frac{\partial G}{\partial V}\right|_n$$

  where now it is possible that

$$\left.\frac{\partial G}{\partial V}\right|_n \neq 0$$

  and hence one can obtain an anomalous compressibility ratio
- Physically speaking, a possible explanation arises upon considering a 'regular solid'. If I were to tell you that I have a block of aluminium at room temperature and pressure, you would be able to tell me what the lattice spacing of this crystal is. However, in a supersolid this is not necessarily true, you would also need to be told the density. This additional complication arises because solids, under a single set of externally imposed thermodynamic conditions (i.e. T, P etc.), have a single solution to this problem; there is one valid density and hence one lattice spacing. Supersolids, at a single set of thermodynamic conditions, can form states at a range of densities, each with their own lattice spacing. This extra degree of freedom is what we believe is responsible for the thermodynamic anomaly.
- The implications of this are still unknown, but this is, to the best of our knowledge, the first reporting of such a phenomenon

8 Extending the Gross-Pitaevskii equation

The following chapter was partially done in collaboration with Anubha Bal as part of her UROP (Undergraduate Research Opportunity) project. Anubha and I worked together on developing the ground states for the dipolar BEC. The work on homogenisation and onwards was done entirely by myself.

8.1 Introduction

In previous chapters we considered a meanfield theory of a supersolid in order to develop the technique of homogenisation. While there are certainly experimental applications which can be accurately modelled by the GPE, the current most promising supersolids belong to a class of materials which require a slightly different theory.

While no definitive evidence for supersolidity in Helium has been confirmed yet, the phenomenon has been claimed to be observed in ultracold dipolar Bose-Einstein condensates (BECs). In particular, the interaction between BEC atomic gases and optical resonators [59], light beams to produce a spin-orbit coupling [70], and atomic long-range dipolar interactions [35, 25] have been exploited to produce density patterns that are characteristic of supersolid behaviour.

The theory of supersolid formation in dipolar systems has been well established to arise from the careful balance between atomic contact interactions over short distances, long-range dipole-dipole interactions (DDI), and quantum mechanical fluctuations [62]. We follow on from this work and employ a meanfield theory with a beyond-meanfield correction (the Lee-Huang-Yang, or LHY, term) to study the formation of supersolids in a dipolar BEC.

Previous work has focused on the two-dimensional phase diagram of this system to illustrate the results of varying both the contact potential strength and number density [60] to determine possible ground state phases.

A key difference between a dipolar interaction and a soft-core interaction is the variety of phases that can be formed. The soft-core interaction leads exclusively to a triangular phase [10], whereas the dipolar system can generate stripe and honeycomb phases in addition to triangular [71]. The bulk properties of these supersolid

phases are unexplored, and is the central thesis of this chapter.

8.2 Theoretical set-up

We will study a BEC of particles of mass m with a magnetic dipolar interaction and a beyond-meanfield correction known as the Lee-Huang-Yang (LHY) term. The LHY term is the first order correction to the mean-field energy of interacting bosons. In a dipolar interaction system, it is actually necessary to stabilise the phase, as without it the attractive component of the interaction would cause the particles to collect into a single point which will spike the density profile.

The atoms are unbound in the radial direction (where we assume periodic boundary conditions) and are subject to a harmonic confining potential in the z direction. This system was previously studied by Blakie et al. [60], and we will follow some of the analysis outlined there, as well as show the phase diagram generated by Blakie et al.

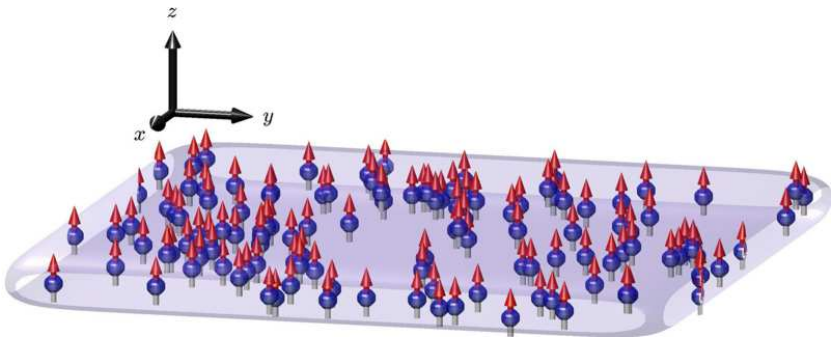


Fig. 8.1: Experimental setup for a planar dipolar BEC supersolid system. Here the atoms have their magnetic dipoles aligned along the z axis and are confined with a harmonic trap in the z direction. Because of the aligned magnetic dipoles along z, the atoms will assemble into a gaussian in the z direction that is much tighter than the gaussian of a harmonic oscillator. There is no trap in the planar field, with the atoms free to self-assemble. The subsequent theory and analysis of the supersolid is conducted inside the xy plane. Image taken from [60] with permission.

The z-direction Hamiltonian is given by

$$H_z = -\frac{\hbar^2}{2m}\nabla_z^2 + \frac{1}{2}m\omega_z^2 z^2 \tag{8.2.1}$$

where ω_z is the trap frequency set by the experiment and ∇_z is the spatial derivative in the z direction. The atoms are subject to a dipolar interaction given by

$$U(\mathbf{r}) = g_s\delta(\mathbf{r}) + \frac{3g_{dd}}{4\pi r^3}\left(1 - 3\cos^2(\theta)\right) \tag{8.2.2}$$

In this experiment we will take the magnetic dipoles to be aligned along the z direction, which therefore means that θ is the angle between the point $\mathbf{r}$ and the z axis.

where the short range component of U is determined by the coupling constant $g_s = 4\pi\hbar^2 a_s/m$, with a_s the s-wave scattering length. The dipole-dipole component of the interaction is determined by $g_{dd} = \mu_0\mu_m^2/3 \equiv 4\pi\hbar^2 a_{dd}/m$ where μ_m is the magnetic moment of the atom.

Following the treatment in Blakie, we apply an ansatz that the wavefunction is separable in z. Specifically, we state

$$\Psi = \sqrt{n}\psi(\mathbf{R})\chi_\sigma(z) \tag{8.2.3}$$

where $\chi_\sigma(z)$ is treated variationally as a Gaussian wavefunction of the form

$$\chi_\sigma(z) = \frac{1}{\pi^{1/4}\sigma^{1/2}} e^{-z^2/2\sigma^2} \tag{8.2.4}$$

which is optimised over the parameter σ. The coordinate $\mathbf{R} \equiv (x, y)$ and n is the average density of particles.

We can analyse the time-dependent energy in a meanfield context by splitting the energy into radial and z components. The energy in the z direction is given by

$$E_z = \frac{1}{4}\left(\frac{\hbar^2}{m\sigma^2} + m\omega_z^2\sigma^2\right) \tag{8.2.5}$$

where we have importantly made the assumption that there are no excitations in the z direction. The parameter ω_z is set by the experiment and is therefore fixed, and the variational parameter σ is optimised to minimise the energy.

Consider here the implication of a variational z-dependent wavefunction. Typically in a harmonic trap we would immediately expect the wavefunction to take the form of a gaussian, the width of which, σ is proportional to the trap frequency ω like $\omega \sim 1/\sqrt{\sigma}$. It is important to note that in the harmonic oscillator there are no interactions, whereas in the z-direction we have aligned magnetic dipoles with strong attractive interactions. Subsequently we impose a variatonal ansatz with the understanding that the profile will be gaussian, but the width will be set by the interactions instead of the trap, hence the variable σ. The trap will still impose some energy on the wavefunction, but it is now not the only consideration.

We will simulate the system for ^{164}Dy atoms, which have a dipolar scattering length of $a_{dd} = 130.8a_0$ where a_0 is the Bohr radius, and a trap frequency $\omega_z/2\pi = 72.4$Hz.

After performing a Madelung transformation $\psi = \rho e^{i\phi}$, we find the mean field time-dependent Lagrangian in the radial plane is given by

$$\begin{aligned}\mathcal{L}_\rho = \int_\Omega \Bigg[\hbar\rho\frac{\partial\phi}{\partial t} + \frac{\hbar^2}{2m}\left(\rho(\nabla\phi)^2 + \frac{1}{4\rho}(\nabla\rho)^2\right) \\ + \frac{1}{2}\rho\,\bar{U} * \rho + \frac{2}{5}g_{QF}\rho^{5/2}\Bigg]\,\mathrm{d}\mathbf{r}\end{aligned} \tag{8.2.6}$$

where Ω is the spatial domain of the radial plane, $\bar{U} * \rho$ is the convolution between the radial dipolar potential $\bar{U}$ and the density ρ, and $g_{QF}\rho^{5/2}$ is the beyond-meanfield correction.

A full derivation of integrating out the planar degrees of freedom is given in Blakie et al. [60].

Blakie has shown that

$$g_{QF} = \frac{128\sqrt{2}}{3\sqrt{5}}\pi^{-1/4}\frac{a_s^{5/2}}{\sigma^{3/2}}\left(1 + \frac{3}{2}\left(\frac{a_{dd}}{a_s}\right)^2\right) \tag{8.2.7}$$

and the fourier transform of $\bar{U}(k) \equiv \mathcal{F}[\bar{U}(r)]$ is

$$\bar{U}(k) = \sqrt{8\pi}\frac{a_s}{\sigma}\left[1 + \frac{a_{dd}}{a_s}\left(2 - 3G_0(\sigma k/\sqrt{2})\right)\right] \tag{8.2.8}$$

with $G_0(q) = \sqrt{\pi}qe^{q^2}\text{erfc}(q)$. Note that r and k are the radial coordinates.

A consequence of the dipolar interaction coupled with tunable Feschbach resonances is that the phase diagram is considerably richer for planar supersolids compared to the soft-core bosonic system. Blakie et al. [60] have generated a phase diagram (see Fig. 8.2) which finds stripe and honeycomb phases in addition to the triangular phase. All three of these phases are shown in Fig. 8.4, but we will only study the triangular and honeycomb phases in this thesis.

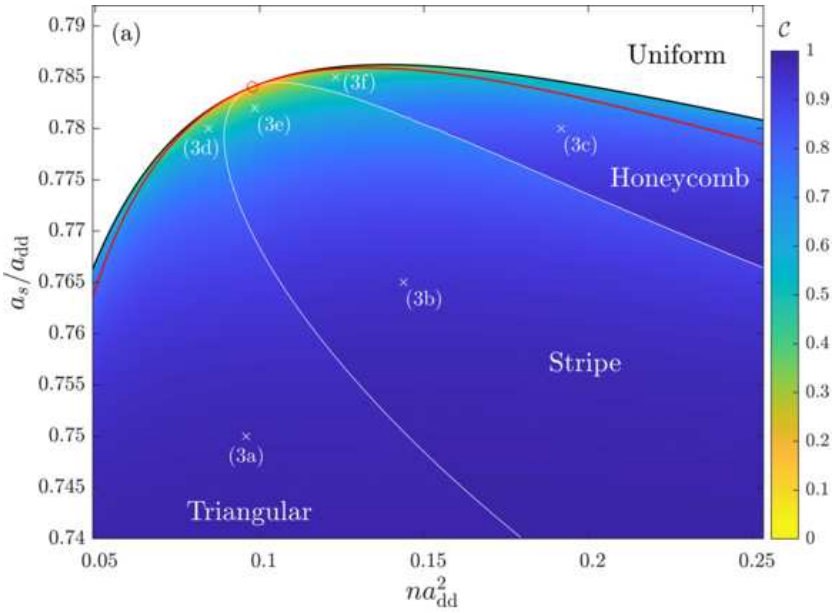


Fig. 8.2: Figure depicting the phase diagram of a planar dipolar BEC with an LHY term as a function of scaled density na_{dd}^2 and scaled Feschbach scattering length a_s/a_{dd}, where a_{dd} is the dipole-dipole scattering length. There are four distinct phases: the uniform phase, honeycomb phase, stripe phase and triangular phase. The regions are shaded by their relative contrast

$$C \equiv \frac{\rho_{max} - \rho_{min}}{\rho_{max} + \rho_{min}} \quad .$$

The red line indicates the roton boundary (where the roton mode softens). Several points on the phase diagram are highlighted by text; we will later be examining some of these points in the honeycomb and triangular phases. Image adapted from [60] with permission.

A key feature of the dipole-dipole interaction is the short range contact potential imposed by both the Feschbach resonance and the natural magnetic dipolar interaction. This real-space contact potential comes from the $k \to \infty$ limit of the fourier interaction. One can split the contact potential from the long-range potential

$$\bar{U}(k) = \frac{\sqrt{8\pi}}{\sigma}(a_s - a_{dd}) + \sqrt{72\pi}\frac{a_{dd}}{\sigma}\left(1 - G_0(\sigma k/\sqrt{2})\right) \tag{8.2.9}$$

which is equivalent to splitting the k-space interaction into a constant plus some k-dependent term. We subsequently define $\bar{U}(k) = \delta + U(k)$

This is equivalent to 'moving the line up to zero' in Fig. 8.3 for the dipolar interaction. This allows us to simplify the treatment of the contact potential as it generates fewer terms to keep track of and to calculate.

with

$$\begin{aligned} \delta =& \frac{\sqrt{8\pi}}{\sigma}\left(a_s - a_{dd}\right) \\ U(k) =& \sqrt{72\pi}\frac{a_{dd}}{\sigma}\left(1 - G_0(\sigma k/\sqrt{2})\right) \end{aligned} \tag{8.2.10}$$

representing the constant and k-dependent parts of the interaction, respectively.

Consequently, we can now express the Lagrangian as

$$\begin{aligned} \mathcal{L}_\rho = \int_\Omega \Bigg[& \hbar\rho\frac{\partial\phi}{\partial t} + \frac{\hbar^2}{2m}\left(\rho(\nabla\phi)^2 + \frac{1}{4\rho}(\nabla\rho)^2\right) \\ & + \frac{1}{2}\rho\, U * \rho + \frac{1}{2}\delta\rho^2 + \frac{2}{5}g_{QF}\rho^{5/2}\Bigg]\, \mathrm{d}\mathbf{r} \end{aligned} \tag{8.2.11}$$

which will now be a little easier to homogenise.

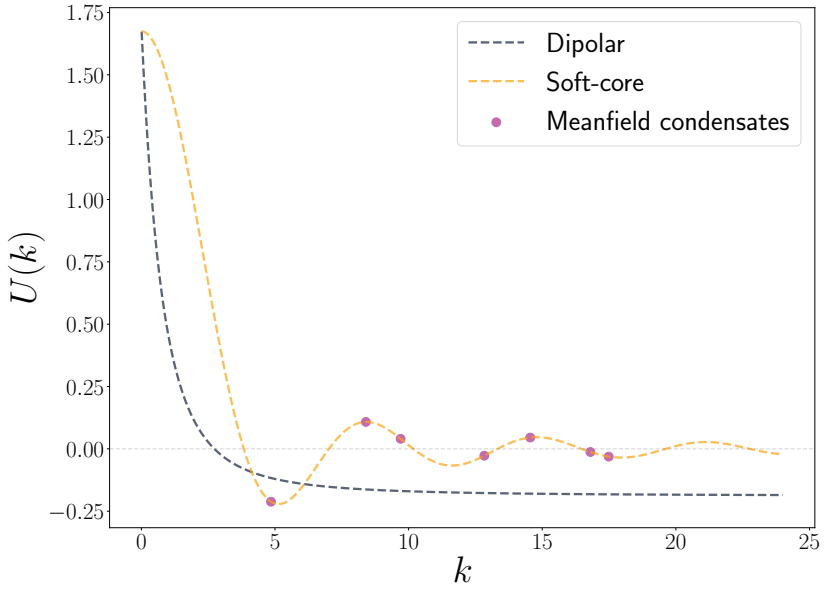


Fig. 8.3: Illustration of the k-space interactions for both the soft-core and dipolar systems, with the approximate condensate momenta illustrated, scales in arbitrary units and the dipolar interaction has $a_s < a_{dd}$. In the soft-core system there are natural minima in the interaction landscape in k-space, around which the density condenses at a finite momenta (not strictly at the minima, due to the kinetic term in the energy). In contrast, there are no such minima in the dipolar interaction, which tends to a value of $U \to \sqrt{8\pi}/\sigma(a_s - a_{dd})$ as $k \to \infty$. This generates many options for how to distribute the finite momenta condensates, which is why the phase diagram for the dipolar system is much richer in comparison to the soft-core system.

There is a constraint on the average number of particles which is imposed by the chemical potential μ, and as such the two equations of motion are

$$\partial_t\rho + \frac{\hbar}{m}\boldsymbol{\nabla}\cdot(\rho\boldsymbol{\nabla}\phi) = 0 \tag{8.2.12}$$

$$\frac{\hbar^2}{4m}\left(\frac{(\nabla\rho)^2}{2\rho^2} - \frac{\nabla^2\rho}{\rho}\right) + U*\rho + \delta\rho + g_{QF}\rho^{3/2} + \frac{\hbar^2}{2m}(\nabla\phi)^2 = \mu\,. \tag{8.2.13}$$

One can subsequently find the ground state of the system given by $\{\rho_0, \phi_0\}$ by noting that $\mathcal{L}$ is trivially minimised by setting $\dot{\phi} = 0$

This is exactly the same as (3.1.36) but with the additional LHY term and the splitting of the dipolar interaction into the contact potential and the long-range potential.

and $\nabla\phi = 0$, which then automatically satisfies (3.1.34). Subsequently, equation (3.1.35) then becomes

$$\frac{\hbar^2}{4m}\left(\frac{(\nabla\rho_0)^2}{2\rho_0^2} - \frac{\nabla^2\rho_0}{\rho_0}\right) + U * \rho_0 + \delta\rho + g_{QF}\rho_0^{3/2} = \mu\,. \tag{8.2.14}$$

which will be used to find the ground state density of the system.

As there are no minima in k-space in the interaction potential, there is an additional degree of freedom in the placement of the condensate momenta. Subsequently, the phase diagram for the dipolar BEC system is considerably richer than that of the soft-core system. One can observe a triangular, honeycomb and stripe phase in the supersolid region of the phase diagram.

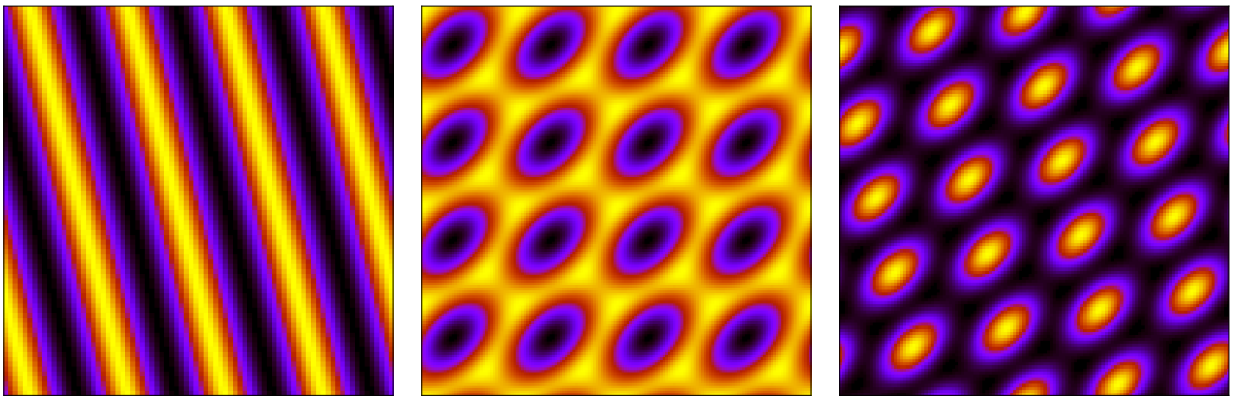


Fig. 8.4: From left to right: stripe phase, honeycomb phase, triangular phase. Regions of low density are shown as black in this heatmap. The rich phase diagram of the dipolar BEC lends itself to interesting phenomena; there are two distinct isotropic phases (triangular and honeycomb) and one anisotropic phase (stripe) which means that the excitations can be either isotropic or anisotropic. Consequently, driving the system across a phase transition from the stripe phase to e.g. the honeycomb phase may create interesting dynamics. Note here that the simulations were conducted in the parallelogram basis outlined in section 3.2.

We will use the above setup to perform a homogenisation technique where we find a long-wavelength effective lagrangian composed of the elastic moduli and various thermodynamic properties of the dipolar BEC. This homogenisation builds on the work in the previous chapters but is now extended to include the beyond-meanfield corrections.

9 *Homogenisation for dipolar BECs*

Using the technique of homogenisation derived in the previous sections, we are able to study the long-wavelength response of a supersolid material, with the caveat that beyond-meanfield corrections are not included in homogenisation currently. This chapter will illustrate the additional work necessary to include the beyond-meanfield correction and employ the same analysis already conducted with a few changes. We will then apply homogenisation with the included beyond meanfield corrections to the planar dipolar BEC supersolid, finding unusual and unexpected results. We will then verify these results with a Bogoliubov technique that now also includes the beyond meanfield terms.

9.1 Homogenisation adapted for the LHY term

The additional component in the Lagrangian coming from the LHY term can be expanded relatively easily

$$\int_\Omega \frac{2}{5} g_{QF} \rho^{5/2} \, \mathrm{d}\mathbf{r} \to \int_\Omega g_{QF} \left(\frac{2}{5} \rho_0^{5/2} + \rho_0^{3/2} \tilde{\rho} + \frac{3}{2} \sqrt{\rho_0} \tilde{\rho}^2 \right) \times (1 + \epsilon_{ll} + M_{iklm} u_{ik} u_{lm}) \, \mathrm{d}\mathbf{r} \tag{9.1.1}$$

The bulk of the homogenisation procedure is the same as outlined in the previous sections, i.e. that the Jacobians, derivatives and expansion of the interaction potentials will be exactly the same. The only changes that arise are the extra LHY terms which are multiplied by the stress tensor in both first and second order, ensuring that it appears in both the pressure and Cauchy elastic tensors. Importantly, the additional LHY contribution also couples to the correction to the density $\tilde{\rho}$ which then leads to an adjustment to the Euler-Lagrange equation for $\tilde{\rho}$, and hence also to μ_1.

Note that the LHY term does not couple to the phase sector of the Lagrangian; thus it does not affect the structure of the effective Lagrangian obtained at the end of the homogenisation procedure, but rather only changes the constants that are obtained in this effective theory.

By using the same expansion rules as defined in Chapter 4, we will expand and collect first and second order terms in the Lagrangian in a similar way. The first task is to collect all terms containing $\tilde{\rho}$ and solve the Euler-Lagrange equation for $\tilde{\rho}$. The Lagrangian consisting

of all elements that contain $\tilde{\rho}$ is (after some simplification) given by

$$\begin{aligned}-\mathcal{L}_{\tilde{\rho}} = \tilde{\rho}\Bigg[&\mu_0\left(1+\epsilon_{ll}\right)+\frac{\hbar^2}{4m}\left(\frac{\partial_i\partial_k\rho_0}{\rho_0}-\frac{\partial_i\rho_0\partial_k\rho_0}{\rho_0^2}\right)\epsilon_{ik}\\&+\left(U*\rho_0\delta_{ik}+f_{ik}*\rho_0\right)\epsilon_{ik}\\&-\frac{1}{2}\Bigg(\frac{\hbar^2}{4m}\nabla\cdot\left(\frac{\nabla\tilde{\rho}}{\rho_0}\right)-\delta\tilde{\rho}-U*\tilde{\rho}\\&-\frac{3}{2}g_{QF}\sqrt{\rho_0}\tilde{\rho}+\frac{\hbar^2}{4m}\left(\frac{(\nabla\rho_0)^2}{\rho_0^3}-\frac{\nabla^2\rho_0}{\rho_0^2}\right)\tilde{\rho}\Bigg)\Bigg]\end{aligned} \tag{9.1.2}$$

where we have used the Euler-Lagrange equation (8.2.14) to simplify the expression.

Recalling that $\tilde{\rho}$ contains both first and second order components in the form (4.2.9)

$$\tilde{\rho}(\mathbf{r}) = \rho_1^{ik}(\mathbf{r})\,\epsilon_{ik} + \rho_2^{iklm}(\mathbf{r})\,u_{ik}u_{lm}$$

which we will use to separate components of the Lagrangian by order of the strain tensor.

Using variational calculus for the variable $\tilde{\rho}$ with the new normalisation condition (exactly the same as (4.2.10)) and expansion of the chemical potential (4.2.12), we can obtain the Euler-Lagrange equation for $\tilde{\rho}$. This is given by

$$L(\tilde{\rho}) = F(\rho_0, \mu_0, \mu_1^{ik}, \mu_2^{iklm}) \tag{9.1.3}$$

with

$$L(\tilde{\rho}) \equiv \frac{\hbar^2}{4m}\boldsymbol{\nabla}\cdot\left(\frac{\boldsymbol{\nabla}\tilde{\rho}}{\rho_0}\right) - U*\tilde{\rho} - \frac{\hbar^2}{4m}\frac{\tilde{\rho}}{\rho_0}\nabla^2\ln(\rho_0) - \frac{3}{2}g_{QF}\sqrt{\rho_0}\tilde{\rho} \tag{9.1.4}$$

and

$$\begin{aligned}F(\rho_0,\mu_0,\mu_1^{ik},\mu_2^{iklm}) \equiv &-\left(\mu_2^{iklm}+\mu_1^{ik}\delta_{lm}+\mu_0 M_{iklm}\right)u_{ik}u_{lm}\\&+\epsilon_{ik}\Bigg[-\mu_1^{ik}+\frac{\hbar^2}{4m}\left(2\frac{\partial_{ik}\rho_0}{\rho_0}-\frac{\partial_i\rho_0\partial_k\rho_0}{\rho_0^2}\right)\\&+\int_\Omega\left(f_{ik}(\mathbf{r}-\mathbf{r}')+\delta_{ik}U(\mathbf{r}-\mathbf{r}')\right)\rho_0(\mathbf{r}')\,\mathrm{d}\mathbf{r}'\Bigg].\end{aligned} \tag{9.1.5}$$

This is an integro-differential equation which can be solved in the same way as (5.2.15). This can be done using either Bloch's theorem or by direct translation of the mathematical operations to a matrix on a vector in the context of finite differencing.

In this work we solved these equations by writing the operations as finite differencing matrices on a vector, and then using an iterative matrix solver.

Once we have solved (9.1.3) and obtain the constant μ_1^{ik}, we can simplify the Lagrangians and collect them into first and second order components.

One can show that the first order component of the Lagrangian is

given by

$$
\begin{aligned}
-\mathcal{L}_1 = \epsilon_{ik} \Bigg[& \frac{\hbar^2}{4m} \left(\frac{(\nabla \rho_0)^2}{2\rho_0} \delta_{ik} - \frac{\partial_i \rho_0 \partial_k \rho_0}{\rho_0} \right) \\
& \left(\frac{1}{2} \delta \rho_0^2 + \frac{1}{2} \rho_0 (U * \rho_0) + \frac{2}{5} g_{QF} \rho_0 5/2 \right) \delta_{ik} \\
& + \frac{1}{2} \rho_0 \left(U * \rho_0 \delta_{ik} + f_{ik} * \rho_0 \right) + \mu_0 \rho_1^{ik} \Bigg]
\end{aligned}
\tag{9.1.6}
$$

which can be further simplified into

$$
-\mathcal{L}_1 = \rho_0 \left[\frac{1}{2} f_{ik} * \rho_0 - \frac{\hbar^2}{4m} \frac{\partial_i \rho_0 \partial_k \rho_0}{\rho_0^2} - \left(\frac{1}{2} \delta \rho_0 + \frac{3}{5} g_{QF} \rho_0^{3/2} \right) \delta_{ik} \right] \tag{9.1.7}
$$

from which we can obtain the pressure tensor P_{ik}. By following the differentiation rules outlined in Table 4.1, we find that

$$
P_{ik} = \frac{1}{|\Omega|} \int_\Omega \left[\left(\frac{1}{2} \delta \rho_0^2 + \frac{3}{5} g_{QF} \rho_0^{5/2} \right) \delta_{ik} + \frac{\hbar^2}{4m} \frac{\partial_i \rho_0 \partial_k \rho_0}{\rho_0} - \frac{1}{2} \rho_0 f_{ik} * \rho_0 \right] \mathrm{d}\mathbf{r} \tag{9.1.8}
$$

which is our expression for the pressure tensor.

N.B. That this expression has already been simplified to some extent. We used the ground-state Euler-Lagrange equation (8.2.14) to simplify terms with a single power of $\tilde{\rho}$ attached; this lives in the $\mu_0 \rho_1^{ik}$ term.

Similarly, we can write out the second-order component of the Lagrangian

$$
\begin{aligned}
-\mathcal{L}_2 = & \frac{\hbar^2}{4m} \left[\left(\Delta_{ik} + \chi_{ik} - \delta_{lm} \epsilon_{ik} \epsilon_{lm} \right) \frac{\partial_i \rho_0 \partial_k \rho_0}{\rho_0} \right] \\
& + \rho_0 \left[\frac{1}{2} U \delta_{ik} \delta_{lm} + f_{ik} \delta_{lm} + \frac{1}{2} W_{iklm} \right] * \rho_0 \epsilon_{ik} \epsilon_{lm} \\
& + \frac{1}{2} \rho_0 f_{ik} * \rho_0 \Delta_{ik} - \left(\frac{1}{2} \delta \rho_0^2 + \frac{3}{5} g_{QF} \rho_0^{5/2} \right) M_{iklm} u_{ik} u_{lm} \\
& + \frac{1}{2} \epsilon_{ik} \epsilon_{lm} \rho_1^{ik} \Bigg[\mu_1^{lm} + \frac{\hbar^2}{4m} \left(2 \frac{\partial_i \partial_k \rho_0}{\rho_0} - \frac{\partial_i \rho_0 \partial_k \rho_0}{\rho_0^2} \right) \\
& \qquad + \left(f_{ik} + \delta_{ik} U \right) * \rho_0 \Bigg]
\end{aligned}
\tag{9.1.9}
$$

From the above expression one can obtain the Cauchy elastic tensor like so

$$
B_{iklm} = \frac{\partial}{\partial \partial_i u_k} \frac{\partial}{\partial \partial_l u_m} \mathcal{L}_2 + P_{ik} \delta_{lm} - P_{im} \delta_{kl} \tag{9.1.10}
$$

Importantly, we must note that the phase diagram for the dipolar system has anisotropic ground states. Most notably, we expect the stripe state to have anisotropic elastic tensors. Specifically the pressure tensor, superfluid fraction tensor and Cauchy elastic tensors will be anisotropic.

where we find B_{iklm} is given by

$$\begin{aligned} B_{iklm} &= \frac{1}{|\Omega|}\int_\Omega b_{iklm}(\mathbf{r})\,\mathrm{d}\mathbf{r} \\ b_{iklm}(\mathbf{r}) &= +\frac{\hbar^2}{4m}\left(\frac{\partial_i\rho_0\partial_l\rho_0}{\rho_0}\delta_{km}+\frac{\partial_k\rho_0\partial_l\rho_0}{\rho_0}\delta_{im}-\frac{\partial_i\rho_0\partial_k\rho_0}{\rho_0}\delta_{lm}\right) \\ &\quad+\rho_0\Bigg[\delta_{ik}\delta_{lm}U+\frac{1}{2}\left(f_{il}\delta_{km}+f_{im}\delta_{kl}-f_{ik}\delta_{lm}\right) \\ &\qquad+2f_{ik}\delta_{lm}+W_{iklm}\Bigg]*\rho_0 \\ &\quad+\rho_1^{ik}\Bigg[\mu_1^{lm}+\frac{\hbar^2}{4m}\left(2\frac{\partial_{ik}\rho_0}{\rho_0}-\frac{\partial_i\rho_0\partial_k\rho_0}{\rho_0^2}\right) \\ &\qquad+\left(f_{lm}+\delta_{lm}U\right)*\rho_0\Bigg] \\ \text{with } (f*\rho)_{\mathbf{r}} &\equiv \int d\mathbf{r}' f(\mathbf{r}-\mathbf{r}')\rho(\mathbf{r}') \quad \text{for any function } f \text{ and } \rho\,, \end{aligned} \tag{9.1.11}$$

Note that although the contact potential does not directly appear in the Cauchy tensor, it is worth remembering that it appears in the equation for determining $\tilde{\rho}$ and μ_1^{ik}.

where f_{ik} and W_{iklm} are defined as

$$\begin{aligned} f_{ik}(\mathbf{r}) &\equiv \frac{r_i r_k}{|\mathbf{r}|}\frac{\partial U(|\mathbf{r}|)}{\partial|\mathbf{r}|} \\ W_{iklm}(\mathbf{r}) &\equiv \frac{r_i r_k r_l r_m}{2|\mathbf{r}|^2}\left(\frac{\partial^2 U}{\partial|\mathbf{r}^2|}-\frac{1}{|\mathbf{r}|}\frac{\partial U}{\partial|\mathbf{r}|}\right)\,. \end{aligned} \tag{9.1.12}$$

Note again that the functions f_{ik} and W_{iklm} are with reference to the U defined in (8.2.10), where the contact potential has been removed.

Importantly, the expression for B_{iklm} is exactly the same as that obtained for the system without the LHY correction, with the distinction that the ground-state density ρ_0 is altered by the existence of the LHY term, and that both $\tilde{\rho}$ and μ_1 both have the LHY term directly cooked in via the Euler-Lagrange equation for $\tilde{\rho}$.

The phase sector of the Lagrangian is exactly the same as that of a system without an LHY term, namely

$$\begin{aligned} L_\phi = &-\int_\Omega \hbar\rho_0\left(\partial_t\phi_0+\partial_t\phi_0\boldsymbol{\nabla}\cdot\mathbf{u}\right)+\frac{\hbar^2}{2m}\rho_0\left(\boldsymbol{\nabla}\phi_0\right)^2\mathrm{d}\mathbf{r} \\ &+|\Omega|\varrho_{ij}A_iA_j \end{aligned} \tag{9.1.13}$$

We shouldn't expect the phase sector of the Lagrangian to be any different, the addition of the LHY term is just a beyond-meanfield correction.

with

$$\varrho_{ij} = -\frac{1}{|\Omega|}\int_\Omega \rho_0\partial_i K_j\,\mathrm{d}\mathbf{r} \tag{9.1.14}$$

which can be interpreted as a correction to the superfluid phase stiffness.

A useful check to ensure that we have the correct elastic moduli is to compare our formulas against simpler techniques for obtaining elastic moduli in the case of a homogeneous BEC. In this regime, we can expect to find that $P = 1/2U_0n^2 + 3/5g_{QF}n^{5/2}$ and $K = nU_0 +$

$3/2n^{3/2}$, which our expression returns precisely (note U_0 is the value of the dipolar potential at $\mathbf{k} = 0$).

Continuing with the homogenisation procedure, we find an effective long-wavelength Lagrangian which describes the dynamics of the Goldstone modes carried by the fields ϕ and $\mathbf{u}$. Noting that the symmetry of the ground state will lead to isotropic ϱ_{ij} and B_{iklm} tensors, we can obtain

This is done by simply expanding $N \to N + \delta N$ and $V \to V + \delta V$ and collecting terms to second order. This works for the superfluid case as the convolution term is simple and the differential terms do not exist.

$$\begin{aligned} L = &- \mathcal{E} - \hbar n \dot{\phi} + \frac{\hbar^2}{2}\left[\frac{\dot{\phi}^2}{\mathcal{E}''} - \frac{n-\varrho}{m}\left(\boldsymbol{\nabla}\phi\right)^2\right] \\ &+ \frac{1}{2}\left[m\varrho\dot{\mathbf{u}}^2 - \left(B_{iklm} - \frac{\mu_1}{\mathcal{E}''}\mu_1\delta_{ik}\delta_{lm}\right)u_{ik}u_{lm}\right] \\ &- \hbar\left(n - \varrho + \frac{\mu_1}{\mathcal{E}''}\right)\dot{\phi}\boldsymbol{\nabla}\cdot\mathbf{u} \end{aligned} \tag{9.1.15}$$

which we note is exactly the same effective Lagrangian as that obtained previously, but now has considerably different coefficients owing to the existence of the LHY term. We must also stress that, as of now, the theory has not been specified to that of a dipolar BEC. The interaction is currently general, and we would expect the above analysis to hold for any interaction potential and subsequently any theory with a beyond-meanfield correction in the form of a LHY term.

Here we have decided to only study the isotropic phases (as they are a little more interesting), hence why the dynamic Lagrangian is of an isotropic form.

The spontaneously broken translational symmetry and the broken $U(1)$ symmetry mean that the system must have three different Goldstone modes, two of which are longitudinal and one of which is transverse. We expect the longitudinal modes to couple, and to be able to find the velocities of these excitations from homogenisation.

One can immediately obtain the velocities of the Goldstone modes by assuming that the fields ϕ and $\mathbf{u}$ take the form $\phi = \Phi e^{i\mathbf{k}\cdot\mathbf{x}-\omega t}$ and $\mathbf{u} = \mathbf{U}e^{i\mathbf{k}\cdot x-\omega t}$ respectively. Upon solving the Euler-Lagrange equations for the above Lagrangian, one finds

$$\omega^2 = \frac{A \pm D}{2m\varrho}\mathbf{k}^2 \tag{9.1.16}$$

with

$$\begin{aligned} A &= K + 2G + \left(n\mathcal{E}'' + 2\mu_1\right)\left(n - \varrho\right) \\ D^2 &= A^2 - 4\varrho(n-\varrho)\left[\mathcal{E}''(K+2G) - \mu_1^2\right] \end{aligned} \tag{9.1.17}$$

This is exactly the same process as in section 6.2.

for the two longitudinal velocities and $c_{shear} = \sqrt{\frac{G}{m\varrho}}$ for the transverse velocity.

An alternative technique to find the excitation velocities is to employ Bogoliubov theory, which for our case of a periodic lattice we must do in tandem with Bloch's theorem. A similar procedure was done in [72, 73] where the authors have a slightly different representation of the Bogoliubov-de-Gennes equations but are functionally

solving the same problem. One can show that the band structure is fully described by the equations

$$\begin{aligned}\left[-\omega^2+\left(\hat{T}^{\mathbf{k}}+\hat{U}^{\mathbf{k}}\right)\hat{T}^{\mathbf{k}}\right](\Phi)^{\mathbf{k}}=0\\ \left[-\omega^2+\hat{T}^{\mathbf{k}}\left(\hat{T}^{\mathbf{k}}+\hat{U}^{\mathbf{k}}\right)\right](\delta\psi)^{\mathbf{k}}=0\end{aligned} \tag{9.1.18}$$

with $\hat{T}$ and $\hat{U}$ defined as

Similarly, this follows virtually the same derivation as that of section 6.3, with the addition of the LHY term included.

$$\begin{aligned}\hat{T}^{\mathbf{k}}_{\mathbf{G},\mathbf{G}'}&=\left[\frac{1}{2}(\mathbf{G}+\mathbf{k})^2-\mu\right]\delta_{\mathbf{G},\mathbf{G}'}+U_{\mathbf{G}-\mathbf{G}'}\rho_{\mathbf{G}-\mathbf{G}'}+g_{QF}(\rho^{3/2})_{\mathbf{G}-\mathbf{G}'}\\ \hat{U}^{\mathbf{k}}_{\mathbf{G},\mathbf{G}'}&=2\sum_{\mathbf{G}''}\psi_{\mathbf{G}-\mathbf{G}''}U_{\mathbf{k}+\mathbf{G}''}\psi_{\mathbf{G}''-\mathbf{G}'}+3g_{QF}(\rho^{3/2})_{\mathbf{G}-\mathbf{G}'}\end{aligned} \tag{9.1.19}$$

with $U_{\mathbf{q}}$, $\psi_{\mathbf{q}}$ and $\rho_{\mathbf{q}}$ the fourier transforms of the interaction potential, the superfluid order parameter and the density respectively. We expect that the band structure obtained from solving these equations should find all the requisite Goldstone modes and that they should have the same velocities, which are given by $\mathrm{d}\omega/\mathrm{d}k|_\Gamma$ as predicted via homogenisation.

9.2 *Results*

In this chapter we chose to analyse the triangular and honeycomb phases numerically (but we stress that the theory is valid for any periodic ground state, which includes the stripe phase). We will analyse results along two lines in the phase space, one connecting the point (3a) $\rightarrow$ (3d) in the triangular region and the other connecting (3c) $\rightarrow$ (3f).

An immediately interesting result that we found is that the shear modulus is considerably smaller than the bulk modulus for all tested phases. Previously in the soft-core system we would see that $G \sim 0.4K$, where G is the shear modulus and K the bulk modulus. In the dipolar system, for phases with similar contrasts, the scaling was closer to $G \sim 0.01K$. This appears to be true in both the triangular and honeycomb phases.

Note that bulk deformations change the average density of the material, hence why the condensate $n_{k=0}$ is being shifted (bulk deformations also affect the $n_{k\neq 0}$ condensates). Shear deformations do not change $n_{k=0}$, which is why we primarily associate shear deformations with the tail of the dipolar interaction.

One possible explanation for this vast difference in the relative sizes of the shear and bulk modulus can be given by considering the dipolar potential. Consider again Fig. 8.3, where this time we are thinking about the energetic cost of distributing meanfield condensates along the tail of the dipolar interaction. As the tail of the potential flattens out, the difference in the potential landscape between a point k and $k+\delta k$ is very small. Consequently, any slight shifts in the momenta of the dipolar condensates at the tail of the potential is energetically cheap. Comparatively, if we consider the condensate

density at $k = 0$, in changing the value of $n_{k=0}$ there is a large energy cost. This can explain why the bulk moduli are significantly larger than the shear moduli.

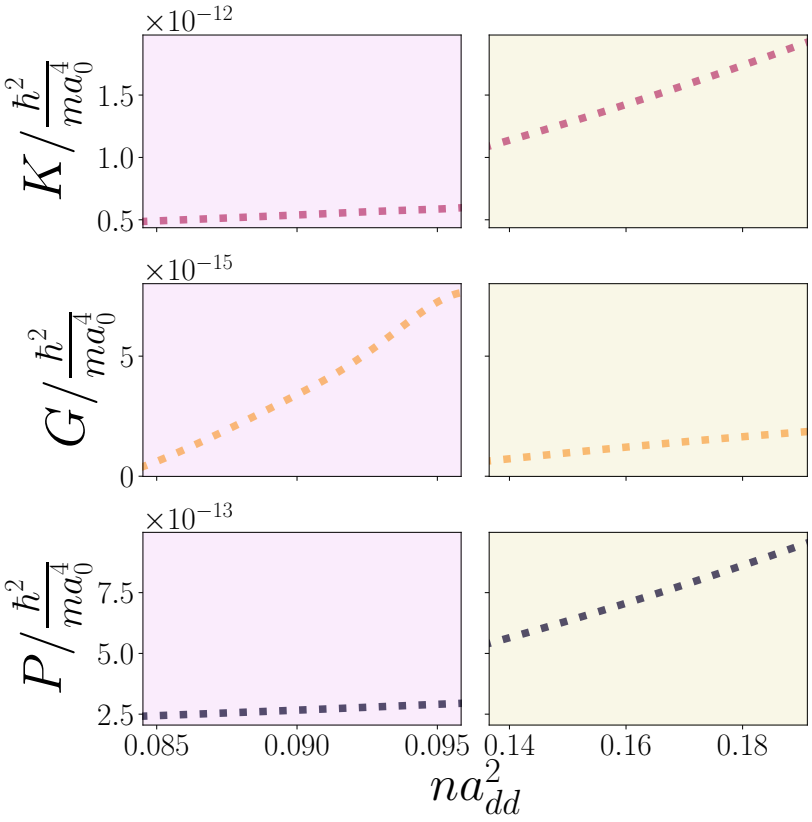


Fig. 9.1: Figure showing the bulk modulus (top row), shear modulus (middle row) and pressure (bottom row) for both the triangular (left column) and honeycomb (right column) phases over a range of points in the phase diagram. There is a strong indication that the bulk modulus and pressure for the honeycomb phases are significantly higher than the triangular phase, while the shear modulus is lower than in the triangular phase. In both phases the shear modulus is significantly smaller than both the bulk modulus and pressure, owing to the malleable nature of the dipolar BEC. An explanation for why the shear modulus is higher in the triangular phase than the honeycomb phase, but the bulk modulus and pressure are **lower** in the triangular phase than in the honeycomb phase, may possibly be arrived at by considering the superfluid-to-solid transition and how it affects the elastic constants. N.B. Lines shown are interpolated for ease of viewing.

Comparing the elastic constants in the triangular and honeycomb phases, we find that the typical values for the bulk modulus K and pressure P are larger in the honeycomb phases, in contrast to the shear modulus G which is larger in the triangular phase than the honeycomb phase. Again in both phases the shear modulus is approximately 2 orders of magnitude smaller than the bulk modulus, which is consistent with the fact that the pattern is quite malleable and can be easily deformed. As expected, the honeycomb phase also has a much larger superfluid fraction than the triangular phase.

The compressibility ratio for both phases is very close to 1, which marks a stark difference from the soft-core boson model where $\mathcal{R}$ was much closer to ≈ 1.4 for triangular phases of a similar contrast to those obtained in this work. This is most likely due to the fact that the supersolid phases in the dipolar system are considerably more malleable, in that they have significantly lower bulk and shear

One may initially question why the honeycomb phase appears to have a larger K and P but smaller G in comparison to the triangular phase, but it is worth recalling that the honeycomb phase is much closer to a superfluid phase than the triangular phase. In the supersolid phases which lie close to the superfluid-supersolid phase boundary, the bulk modulus and pressure are actually lower in the supersolid compared to the superfluid, whereas on the other hand the shear modulus gains a non-zero value. One can see that since the honeycomb phase is 'more superfluid' than the triangular phase, one can expect that the bulk and pressure are larger than the triangular phase, and the shear is smaller.

moduli compared to the soft-core system. Consequently, a possible explanation for this is that the energetic cost of dislocations is much smaller for the dipolar BECs, which can be expressed as

$$\left.\frac{\partial G}{\partial V}\right|_n \ll 1 \tag{9.2.1}$$

where the above inequality essentially states 'the dependence of the ordering wavevector on the geometry of the system is very small'. Recalling (7.1.6), one can then see that that resulting thermodynamic anomaly of these systems may be very small.

Given that in both phases the shear modulus is significantly smaller than the bulk modulus, one would therefore expect that the velocity of the shear mode should be significantly slower than the longitudinal modes. Interestingly, this is not the case.

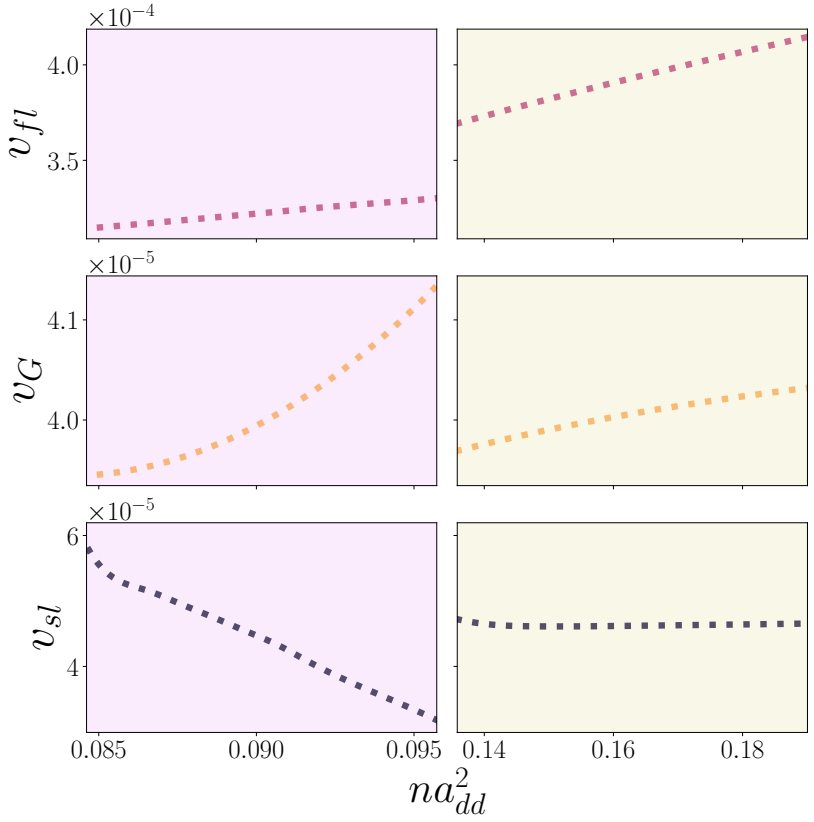


Fig. 9.2: Figure showing the velocities for the fast longitudinal mode (top row), shear mode (middle row) and slow longitudinal mode (bottom row) for the triangular (left column) and honeycomb (right column) phases. The fast longitudinal mode is consistently much faster in the honeycomb phase than the triangular phase, which is somewhat to be expected as the bulk modulus is also much higher in the honeycomb phase. Importantly, even though the shear modulus is several orders of magnitude lower than the bulk modulus, the velocity of the shear mode is only one order of magnitude slower than the fast longitudinal mode, and is actually comparable to the slow longitudinal mode. Interesting behaviour is observed in the inverted relationship of the shear and slow longitudinal speeds in the triangular phase; in the honeycomb phase both the shear and slow longitudinal velocities are constantly increasing as the superfluid fraction decreases (though note that the slow longitudinal mode increases much slower), while in the triangular phase the slow longitudinal mode **decreases**. Note again that lines are interpolated across data points for viewing ease.

Comparing the velocities in both the triangular and honeycomb sections of the phase diagram, we find that there is somewhat good agreement between the excitation velocities predicted by Bogoliubov theory and those obtained via homogenisation. The Bogoliubov technique agrees in the fast longitudinal and slow longitudinal phases

to accuracy comparable to the soft-core system, but consistently undervalues (compared to homogenisation) the shear velocity by about $5-10\%$. In our numerics, we found that the shear speed predicted by the Bogoliubov technique was highly dependent on finite size effects, and that as those effects were reduced the shear velocity would increase, while the two longitudinal modes were relatively stable. Comparatively, homogenisation was much less affected by finite size effects, which suggests that the two methods do agree in the limit of removing finite size effects, though more work needs to be done to conclusively illustrate this.

Using the results from homogenisation, we find that the fast longitudinal mode in the honeycomb phase is typically faster than in the triangular phase, and the slow longitudinal modes in both phases are comparable. The shear mode in the honeycomb phase is relatively constant, whereas the shear mode in the triangular phase appears to show significant variation across the phase diagram. Interestingly, the slow longitudinal mode is faster than the shear mode in the honeycomb phase.

An important point to note is that the triangular phase has considerably higher variation in superfluid fraction across the phase diagram. Whilst the honeycomb phases typically record a ϱ in the region of $15-20\%$, the triangular phases can have a ϱ as high as 70%.

We find a peculiar result pertaining to the shear speeds and slow longitudinal speeds in the triangular phases. Interestingly, we find that for certain parts of the phase diagram the shear mode is actually **slower** than the slow longitudinal mode. Here's why it's interesting:

- An important feature of a $2D$ triangular lattice is that there is a point in the Brillouin zone (other than Γ) where the transverse phonon and longitudinal phonon are degenerate, which is at the K point. In our context, this implies that there should be a band touching at K of the shear mode and the fast longitudinal mode.
- This is a symmetry protected feature of the triangular lattice, so it must always occur.
- The slow longitudinal mode is, by definition, slower than the fast longitudinal mode.
- Given that the shear mode is slower than the slow longitudinal mode, in order for the shear mode to touch the fast longitudinal mode at the K point, there must be some cross-over between the shear and slow longitudinal modes between the Γ and K points.
- This suggests that, at some arbitrary point in the Brillouin zone with potentially unremarkable symmetry properties, there should be a degeneracy or an avoided crossing between a longitudinal and transverse mode.

There's no such symmetry restriction at the K point for the honeycomb lattice, which means that there does not necessarily need to be a band degeneracy at any point.

An avoided crossing is when two bands approach each other, possess a matrix element between them that causes an interaction, and subsequently repel away, while still being able to transfer characteristics of the modes, i.e. if the lower mode is a transverse mode and the upper mode a longitudinal mode, it is possible that after the avoided crossing the upper mode can now be the the transverse mode and vice versa.

This is a new and interesting feature of supersolids that exists only because there is an additional Goldstone mode arising from the $U(1)$

phase. This extra Goldstone mode is not necessarily constrained by the same symmetry properties as the elastic modes, consequently allowing for band crossings/avoided crossings at non symmetry protected points.

It is necessary to consider whether it will be a true degeneracy or an avoided crossing; a band degeneracy indicates the existence of some previously unknown symmetry, whereas an avoided crossing only needs there to be some interactive component between the two modes. This potential band crossing can be seen in Fig. 9.3.

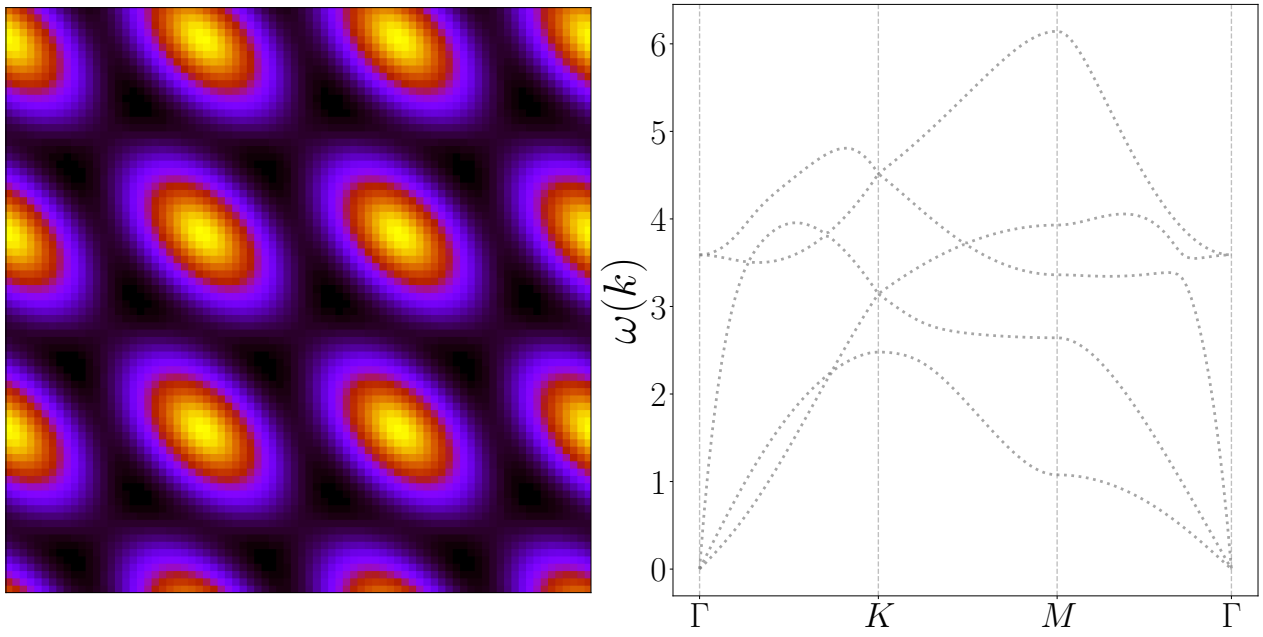


Fig. 9.3: Left figure shows a triangular supersolid state at $a_s = 0.769 a_{dd}$ and $n = 0.0886/a_{dd}^2$ with a lattice spacing $\sim 600 a_{dd}$, right figure shows the Bogoliubov band structure of the supersolid (units of ω scaled up from $\sim 10^{-9}$). This specific point in the phase diagram may look like a typical triangular supersolid, but it is actually one of the triangular phases which has the peculiar property of the shear mode being slower than the slow longitudinal mode. At about 2/3 of the way between the Γ and K point one can see that the two lowest bands apparently cross over. In this figure we have also included some of the higher bands as they also cross over with the fast longitudinal mode.

To the numerical resolution that we have been able to obtain it appears that this is a band degeneracy rather than an avoided band crossing, though we cannot conclusively rule out the possibility of a very small energy gap band crossing. We would need to conduct numerics with much higher resolution in order to be confident in our conclusion. Let us consider the implications of either an avoided crossing or band degeneracy.

The existence of a band degeneracy at a non symmetry protected point is extremely interesting as it implies there is an *accidental band degeneracy* existing in some supersolid structures. More specifically, it has been shown that accidental degeneracies can correspond with some hidden symmetry [74], which suggests that the structure of these phases contains richer physics than initial inspection may reveal.

Alternatively, an avoided crossing suggests some degree of interaction between the transverse shear mode and slow longitudinal mode, which itself may be interesting to study. We believe that it is more likely that there is some small energy gap avoided crossing between these two modes, but we note that this entirely unexpected result is completely open to further study.

What these accidental degeneracies mean for supersolids, how they arise and in what ways do they manifest themselves are all incredibly interesting questions that, unfortunately, are out of the scope of this thesis.

It is also interesting to consider the following question; given that I have a triangular phase in a dipolar BEC, when can I expect there to be an accidental degeneracy? This is an open question, and one for which we currently have no clear answer. One further interesting question to consider is what occurs when the ratio $v_G/v_{sl} = 1$?

Given that we know the shear mode is purely transversal at the Γ point, how can there be a degeneracy between longitudinal and transverse modes at a non symmetry protected point? An answer exists in that the longitudinal modes are only longitudinal at the Γ point not everywhere in the Brillouin zone. For example, the fast longitudinal mode and shear modes in a triangular lattice are longitudinal and transverse respectively at the Γ point, but are degenerate at K, which shows that the nature of the mode can change within the Brillouin zone.

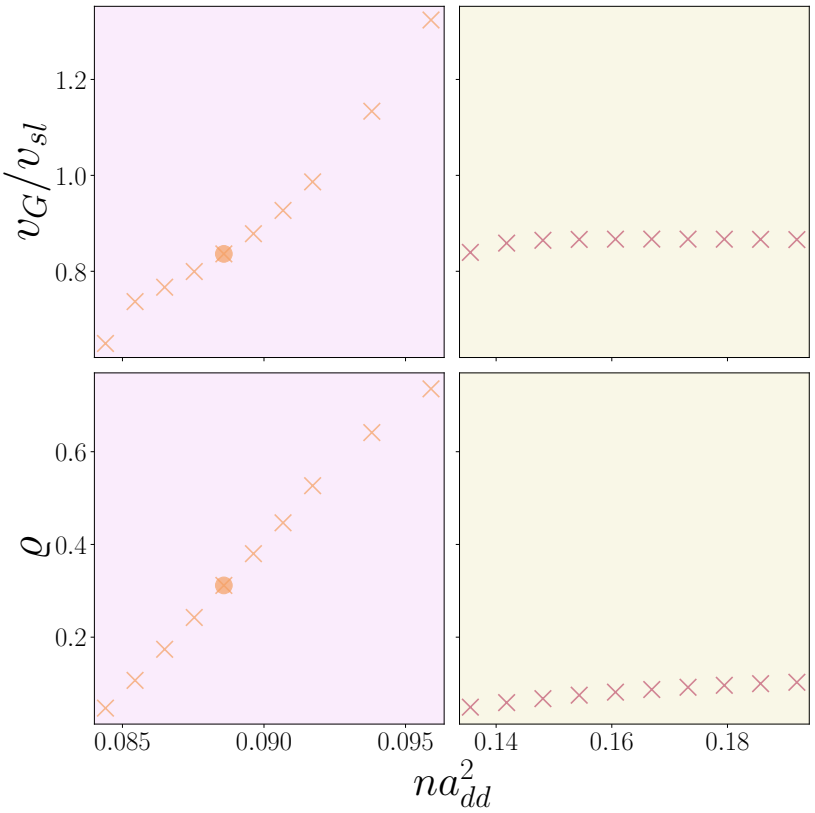


Fig. 9.4: Figure illustrating the ratio of the shear velocity v_G to the slow longitudinal velocity v_{sl} (top row) and the respective supersolid fraction ϱ (bottom row) for the triangular phases (left column) and honeycomb phases (right column). One can see that in the triangular phase there is a signicant variation in both the speed ratio and the supersolid fraction as one scans over the density na_{dd}^2, in contrast to the honeycomb phase which is relatively stable in both metrics. The circled point on the left column corresponds to the phase shown in Fig. 9.3 which possesses a band degeneracy, predicted first by homogenisation (as the ratio is less than unity and therefore the shear mode must cross through the slow longitudinal mode) and then shown conclusively by the Bogoliubov band structure.

Examining Fig. 9.4 in conjunction with Fig. 9.3, we see that homogenisation **can predict** the existence of an accidental band degeneracy. It is unclear at the moment whether there are any inter-

esting dynamics elucidated in the effective Lagrangian generated by homogenisation in these regions where we expect an accidental degeneracy, for two reasons. The first is that it is not obvious whether we should expect to see some hidden symmetry in the dynamic Lagrangian as it is a long-wavelength theory and the degeneracy, although it can be predicted by long-wavelength physics, only manifests itself at a shorter-wavelengths. Secondly, we have not had the time to study it conclusively, and so it is left for future research.

10 Closing Remarks

Over the course of this thesis we have introduced the notion of a supersolid, explained why it is an interesting physical system and provided a review of current experimental attempts to realise them.

We then provided some theoretical tools used to model and describe supersolids, illustrated how they could capture some details of supersolids, and demonstrated a technique to numerically solve the GPE.

We then began to lay out the framework for the homogenisation technique. We first used some results from elasticity theory to elucidate a key distinction between the Cauchy elastic tensor B_{iklm} and the coefficient of the second-order expansion of a Lagrangian under some strain tensor, given by A_{iklm}. This was later rederived in a completely separate way, and turns out to be crucial to the success of homogenisation.

Recall

$$B_{iklm} = A_{iklm} + P_{ik}\delta_{lm} - P_{im}\delta_{kl}$$

which was first defined in (4.1.15).

Following this, we defined an elastic deformation procedure, taking care to specify the effects of an elastic deformation on the curvature of the material frame of reference. We defined various key tensors associated with the derivatives and hence kinetic energy terms, Jacobians that are crucial to ensuring volume preservation, and normalisation conditions vital to preserving number conservation. Importantly, we defined a shift to the chemical potential which must be included in the expansion. We demonstrated how the interaction potential will be expanded under the elastic deformation, defining functions which would be akin to the first and second moments of our interaction. Finally, we also specified the particular form of the phase perturbation on our supersolid, and considered how it would couple to the strain perturbation.

While the chapters involving setting out the homogenisation framework and expanding and solving the Lagrangian were long and tiresome, they were significant.

We then undertook the long process of expanding the Lagrangian, beginning first with the phase component. We showed how the phase field picks up a material derivative term where the additional flow is the elastic deformation. We derived the Euler-Lagrange equation for the phase perturbation, and then simplified the Lagrangian using the solution to that equation to demonstrate the existence of a reduction to the phase stiffness ϱ_{ij}.

Moving on from the phase sector we turned to an expansion and solution of the elastic component of the Lagrangian. Following a long expansion procedure, we arrived at an equation for $\tilde{\rho}$, which we solved numerically. Crucially, there was also the task of determing the shifts to the chemical potential given by μ_1^{ik} and μ_2^{iklm}, which we also derived. Given these tools, we were able to simplify the elastic components of the Lagrangian and derived the tensors A_{iklm} and B_{iklm}.

We then described a process where one could arrive at these elastic results numerically using finite differencing. We verified that our homogenisation technique aligned with the numerical results, and plotted these parameters. Finally, we showed the homogenisation Lagrangian, which consisted simply of the long-wavelength response to both an elastic and phase perturbation.

The numerical verification of these results was a key step in our work; we needed to see that every elastic constant agreed to a good level of accuracy.

The final step in obtaining the correct dynamics of a supersolid came in considering the work done by an excitation on its surroundings. More specifically, we had to consider the effects of coupling unit cells with each other, and allowing number flow between them as well as other energetic effects (i.e. expansion of one unit cell leads to a compression of its neighbour). By including number density fluctuations in the homogenisation Lagrangian and adding in the additional energy due to an excitation interacting with its surroundings, we were able to derive a dynamic Lagrangian. This Lagrangian consisted of three variable fields δn (the number density fluctuations), u_{ik} the strain tensor and the phase field ϕ.

We then integrated out the δn variable, which left us with an effective Lagrangian that fully describe the long-wavelength dynamics of a supersolid. From this Lagrangian we calculated the excitation velocities, looked at the normal modes of the supersolid, and verified our results using a Bogoliubov technique.

We found this peculiar feature that there are now two separate definitions of compressibility in a supersolid, i.e. that the thermodynamic compressibility does not agree with the elastic one. While we are not absolutely certain of the origin of this phenomena, we offered an explanation in the form of supersolids being able to manifest a variety of lattice spacings at different densities, which may at least be approximately correct.

As far as we are aware, this is the only instance of this kind of thermodynamic anomaly being predicted.

We repeated this procedure for the dipolar LHY system, which has a considerably richer phase diagram containing triangular, stripe and honeycomb phases. We studied the triangular and honeycomb phases and found several unexpected results. The first was that the dipolar BEC had a significantly smaller shear modulus in comparison to similar phases in the soft-core system, which upon reflection made sense as the dipolar interaction is much more malleable at short wavelength

than the soft-core interaction. We also found that the thermodynamic anomaly in the dipolar system was considerably smaller than in the soft-core system, which we believe is a consequence of the dipolar phases having a reduced dependency on the lattice vector G.

More interestingly, we found the existence of a new phenomena in the triangular phase sector of dipolar BECs related to the shear mode and slow longitudinal modes. More specifically, we found the existence of phases where the shear mode was slower than the slow longitudinal mode, which did not exist in the soft-core system. As a result of triangular lattice symmetry, it is necessary that the shear and fast longitudinal modes are degenerate at the K point in the Brillouin zone, which in conjunction with the fact that the slow longitudinal mode outpaces the shear mode in these phases means that there must be either a degeneracy or an avoided band crossing between the two modes at some non symmetry protected point.

This symmetry constriction is not imposed on the honeycomb phase, but that doesn't rule out the existence of an accidental band degeneracy.

If it is a degeneracy, then this band crossing is known as an accidental band degeneracy, and it points to the existence of some hidden symmetry of the system. Alternatively, an avoided band crossing suggests some interaction between the two modes, which itself may generate interesting phenomenology.

While the existence and structure of this potentially hidden symmetry or interaction between modes is outside the scope of this work, we used homogenisation to predict if this band degeneracy would occur for a particular phase and then verified the existence of this degeneracy using Bogoliubov band structure theory (see Fig. 9.4 and Fig. 9.3 respectively). The exploration of this phenomena is incredibly interesting and, unfortunately, left to future work.

Supersolids are a fascinating quantum system; the idea that a single phase contains a rigid crystal structure but also the seemingly contradictory dissipationless flow characteristic of superfluids is yet another example of quantum mechanics being fundamentally **weird**. At first glance this phase of matter shouldn't exist, but it takes just a little bit of probing into the Gross-Pitaevskii equation to see that *maybe it can*. All it takes is a little bit of attraction and repulsion.

While the hunt for supersolid helium is still on-going, the experimental progress made in dipolar BEC systems is fantastic. It is there that we have seen this theoretical phase being made into reality, and while the experiments are relatively new and are still being perfected and extended, this is striking proof that such a weird and wonderful phase can exist.

With the coming of supersolid phases realised in dipolar BEC gases, the supersolid has ceased to be a purely academic material. Now comes the important question: how does it behave? To try to answer that you need to have a microscopic theory of a supersolid,

and although Gross-Pitaevskii theory is a meanfield approximation, it works strikingly well for BECs.

Our work has attempted to create a necessary bridge in the gap of knowledge for supersolid studies. On one side you have a microscopic theory, and on the other you have a whole host of techniques built on effective theories and phenomenological Lagrangians. We hope that our work will be able to give future researchers the microscopic foundations on which they build their new and fascinating phenomenological theories.

It is clear that a supersolid is not merely something that is solid + superfluid. It has shown behaviour that is unlike any mixture of these two materials could ever be; it is a type of intertwined order. There are other phases where intertwined order is visible too, most notably that of pair density waves in superconductors. I think that all the questions that one could ask about supersolids, one could also ask about pair density waves.

And there are many, many questions to ask about supersolids. How does one formulate the notion of a critical velocity in such a system? How does this system interact with heat? What kind of phases can we generate if we tune our interactions carefully? Can we make quasicrystals? What are vortices going to look like in this system, and are they even going to be quantised? What other strange thermodynamic features does this new phase of matter have?

I hope that this work has shortened the distance between ourselves and the answers to these questions.

Bibliography

[1] H. K. Onnes, "The superconductivity of mercury," Comm. Phys. Lab. Univ. Leiden, vol. 122, p. 124, 1911.

[2] P. Kapitza, "Viscosity of liquid helium below the λ-point," Nature, vol. 141, no. 3558, pp. 74–74, 1938.

[3] J. F. Allen and A. Misener, "Flow of liquid helium ii," Nature, vol. 141, no. 3558, pp. 75–75, 1938.

[4] V. Ginzburg and L. Landau, "Phenomenological theory," J. Exp. Theor. Phys. USSR, vol. 20, no. 1064, p. 17, 1950.

[5] L. Landau, "Theory of the superfluidity of helium ii," Physical Review, vol. 60, no. 4, p. 356, 1941.

[6] D. Thouless, "The flow of a dense superfluid," Annals of Physics, vol. 52, no. 3, pp. 403–427, 1969.

[7] A. Andreev and I. Lifshits, "Quantum theory of defects in crystals," Zhur Eksper Teoret Fiziki, vol. 56, no. 6, pp. 2057–2068, 1969.

[8] J. Nyéki, A. Phillis, A. Ho, D. Lee, P. Coleman, J. Parpia, B. Cowan, and J. Saunders, "Intertwined superfluid and density wave order in two-dimensional 4 he," Nature Physics, vol. 13, no. 5, pp. 455–459, 2017.

[9] D. Son, "Effective lagrangian and topological interactions in supersolids," Physical review letters, vol. 94, no. 17, p. 175301, 2005.

[10] C. Josserand, Y. Pomeau, and S. Rica, "Patterns and supersolids," The European Physical Journal Special Topics, vol. 146, no. 1, pp. 47–61, 2007.

[11] J. Ye, "Elementary excitation in a supersolid," Europhysics Letters, vol. 82, no. 1, p. 16001, 2008.

[12] P. Fulde and R. A. Ferrell, "Superconductivity in a strong spin-exchange field," Physical Review, vol. 135, no. 3A, p. A550, 1964.

[13] A. Larkin and Y. N. Ovchinnikov, "Nonuniform state of superconductors," Soviet Physics-JETP, vol. 20, no. 3, pp. 762–762, 1965.

[14] Q. Gu, J. P. Carroll, S. Wang, S. Ran, C. Broyles, H. Siddiquee, N. P. Butch, S. R. Saha, J. Paglione, J. S. Davis, et al., "Detection of a pair density wave state in ute2," Nature, vol. 618, no. 7967, pp. 921–927, 2023.

[15] D. F. Agterberg, J. S. Davis, S. D. Edkins, E. Fradkin, D. J. Van Harlingen, S. A. Kivelson, P. A. Lee, L. Radzihovsky, J. M. Tranquada, and Y. Wang, "The physics of pair-density waves: cuprate superconductors and beyond," Annual Review of Condensed Matter Physics, vol. 11, no. 1, pp. 231–270, 2020.

[16] W. Chen, W. Ren, N. Kennedy, M. Hamidian, S.-i. Uchida, H. Eisaki, P. D. Johnson, S. M. O'Mahony, and J. S. Davis, "Identification of a nematic pair density wave state in bi2sr2cacu2o8+ x," Proceedings of the National Academy of Sciences, vol. 119, no. 31, p. e2206481119, 2022.

[17] E. Kim and M. H.-W. Chan, "Probable observation of a supersolid helium phase," Nature, vol. 427, no. 6971, pp. 225–227, 2004.

[18] E. Kim and M. H.-W. Chan, "Observation of superflow in solid helium," Science, vol. 305, no. 5692, pp. 1941–1944, 2004.

[19] J. Day and J. Beamish, "Low-temperature shear modulus changes in solid 4 he and connection to supersolidity," Nature, vol. 450, no. 7171, pp. 853–856, 2007.

[20] D. Y. Kim and M. H. Chan, "Absence of supersolidity in solid helium in porous vycor glass," Physical Review Letters, vol. 109, no. 15, p. 155301, 2012.

[21] P. Nozieres, "Superfluidity, crystallization and localization," Journal of Low Temperature Physics, vol. 156, pp. 9–21, 2009.

[22] A. T. Dorsey, P. M. Goldbart, and J. Toner, "Squeezing superfluid from a stone: Coupling superfluidity and elasticity in a supersolid," Physical review letters, vol. 96, no. 5, p. 055301, 2006.

[23] T. Bland, E. Poli, C. Politi, L. Klaus, M. A. Norcia, F. Ferlaino, L. Santos, and R. N. Bisset, "Two-dimensional supersolid formation in dipolar condensates," Physical Review Letters, vol. 128, no. 19, p. 195302, 2022.

[24] N. Henkel, R. Nath, and T. Pohl, "Three-dimensional roton

excitations and supersolid formation in rydberg-excited bose-einstein condensates," Physical review letters, vol. 104, no. 19, p. 195302, 2010.

[25] L. Chomaz, D. Petter, P. Ilzhöfer, G. Natale, A. Trautmann, C. Politi, G. Durastante, R. Van Bijnen, A. Patscheider, M. Sohmen, et al., "Long-lived and transient supersolid behaviors in dipolar quantum gases," Physical Review X, vol. 9, no. 2, p. 021012, 2019.

[26] F. Böttcher, J.-N. Schmidt, M. Wenzel, J. Hertkorn, M. Guo, T. Langen, and T. Pfau, "Transient supersolid properties in an array of dipolar quantum droplets," Physical Review X, vol. 9, no. 1, p. 011051, 2019.

[27] L. Tanzi, E. Lucioni, F. Famà, J. Catani, A. Fioretti, C. Gabbanini, R. N. Bisset, L. Santos, and G. Modugno, "Observation of a dipolar quantum gas with metastable supersolid properties," Physical review letters, vol. 122, no. 13, p. 130405, 2019.

[28] L. Tanzi, J. Maloberti, G. Biagioni, A. Fioretti, C. Gabbanini, and G. Modugno, "Evidence of superfluidity in a dipolar supersolid from nonclassical rotational inertia," Science, vol. 371, no. 6534, pp. 1162–1165, 2021.

[29] M. Boninsegni and N. Prokof'ev, "Supersolid phase of hard-core bosons on a triangular lattice," Physical review letters, vol. 95, no. 23, p. 237204, 2005.

[30] M. Boninsegni, "Supersolid phases of cold atom assemblies," Journal of Low Temperature Physics, vol. 168, pp. 137–149, 2012.

[31] S. Wessel and M. Troyer, "Supersolid hard-core bosons on the triangular lattice," Physical review letters, vol. 95, no. 12, p. 127205, 2005.

[32] V. Heinonen, K. J. Burns, and J. Dunkel, "Quantum hydrodynamics for supersolid crystals and quasicrystals," Physical Review A, vol. 99, no. 6, p. 063621, 2019.

[33] M. Kunimi and Y. Kato, "Mean-field and stability analyses of two-dimensional flowing soft-core bosons modeling a supersolid," Phys. Rev. B, vol. 86, p. 060510, Aug 2012.

[34] T. D. Lee, K. Huang, and C. N. Yang, "Eigenvalues and eigenfunctions of a bose system of hard spheres and its low-temperature properties," Physical Review, vol. 106, no. 6, p. 1135, 1957.

[35] M. A. Norcia, C. Politi, L. Klaus, E. Poli, M. Sohmen, M. J. Mark,

R. N. Bisset, L. Santos, and F. Ferlaino, "Two-dimensional supersolidity in a dipolar quantum gas," Nature, vol. 596, no. 7872, pp. 357–361, 2021.

[36] G. During, C. Josserand, Y. Pomeau, and S. Rica, "Theory of real supersolids," arXiv preprint arXiv:1110.1323, 2011.

[37] N. Sepúlveda, C. Josserand, and S. Rica, "Nonclassical rotational inertia fraction in a one-dimensional model of a supersolid," Physical Review B, vol. 77, no. 5, p. 054513, 2008.

[38] A. S. C. Rittner and J. D. Reppy, "Observation of classical rotational inertia and nonclassical supersolid signals in solid he 4 below 250 mk," Physical review letters, vol. 97, no. 16, p. 165301, 2006.

[39] A. S. C. Rittner and J. D. Reppy, "Disorder and the supersolid state of solid he 4," Physical review letters, vol. 98, no. 17, p. 175302, 2007.

[40] M. Kondo, S. Takada, Y. Shibayama, and K. Shirahama, "Observation of non-classical rotational inertia in bulk solid 4 he," Journal of Low Temperature Physics, vol. 148, no. 5-6, pp. 695–699, 2007.

[41] Y. Aoki, J. Graves, and H. Kojima, "Oscillation frequency dependence of nonclassical rotation inertia of solid he 4," Physical Review Letters, vol. 99, no. 1, p. 015301, 2007.

[42] A. Penzev, Y. Yasuta, and M. Kubota, "ac vortex-dependent torsional oscillation response and onset temperature t o in solid he 4," Physical review letters, vol. 101, no. 6, p. 065301, 2008.

[43] B. Hunt, E. Pratt, V. Gadagkar, M. Yamashita, A. V. Balatsky, and J. Davis, "Evidence for a superglass state in solid 4he," Science, vol. 324, no. 5927, pp. 632–636, 2009.

[44] J. Day, O. Syshchenko, and J. Beamish, "Intrinsic and dislocation-induced elastic behavior of solid helium," Physical Review B—Condensed Matter and Materials Physics, vol. 79, no. 21, p. 214524, 2009.

[45] Y. Mukharsky, A. Penzev, and E. Varoquaux, "Low-frequency acoustics in solid h 4 e at low temperature," Physical Review B—Condensed Matter and Materials Physics, vol. 80, no. 14, p. 140504, 2009.

[46] X. Rojas, C. Pantalei, H. Maris, and S. Balibar, "Acoustic properties of solid 4he in the limit of zero impurity," Journal of Low Temperature Physics, vol. 158, no. 3, pp. 478–484, 2010.

[47] X. Lin, A. Clark, and M. H.-W. Chan, "Probable heat capacity signature of the supersolid transition," Nature, vol. 449, no. 7165, pp. 1025–1028, 2007.

[48] X. Lin, A. Clark, Z. Cheng, and M. Chan, "Heat capacity peak in solid he 4: Effects of disorder and he 3 impurities," Physical review letters, vol. 102, no. 12, p. 125302, 2009.

[49] N. Prokof'ev, "What makes a crystal supersolid?," Advances in Physics, vol. 56, no. 2, pp. 381–402, 2007.

[50] D. Ceperley and B. Bernu, "Ring exchanges and the supersolid phase of h e 4," Physical review letters, vol. 93, no. 15, p. 155303, 2004.

[51] M. Boninsegni, A. Kuklov, L. Pollet, N. Prokof'ev, B. Svistunov, and M. Troyer, "Fate of vacancy-induced supersolidity in he 4," Physical review letters, vol. 97, no. 8, p. 080401, 2006.

[52] M. Buzzacchi, D. Galli, and L. Reatto, "Variational monte carlo calculations of 4he adsorbed on graphite," Journal of low temperature physics, vol. 126, pp. 205–210, 2002.

[53] P. Corboz, M. Boninsegni, L. Pollet, and M. Troyer, "Phase diagram of h 4 e adsorbed on graphite," Physical Review B—Condensed Matter and Materials Physics, vol. 78, no. 24, p. 245414, 2008.

[54] J. Ahn, H. Lee, and Y. Kwon, "Prediction of stable c 7/12 and metastable c 4/7 commensurate solid phases for he 4 on graphite," Physical Review B, vol. 93, no. 6, p. 064511, 2016.

[55] M. Boninsegni and S. Moroni, "Superfluid transition of the second layer of 4he on graphite: Does substrate corrugation matter?," Results in Physics, vol. 44, p. 106186, 2023.

[56] S. Komineas and N. Cooper, "Vortex lattices in bose-einstein condensates with dipolar interactions beyond the weak-interaction limit," Physical Review A—Atomic, Molecular, and Optical Physics, vol. 75, no. 2, p. 023623, 2007.

[57] M. Wenzel, F. Böttcher, T. Langen, I. Ferrier-Barbut, and T. Pfau, "Striped states in a many-body system of tilted dipoles," Physical Review A, vol. 96, no. 5, p. 053630, 2017.

[58] D. Baillie and P. Blakie, "Droplet crystal ground states of a dipolar bose gas," Physical review letters, vol. 121, no. 19, p. 195301, 2018.

[59] Y. Guo, R. M. Kroeze, B. P. Marsh, S. Gopalakrishnan, J. Keeling,

and B. L. Lev, "An optical lattice with sound," Nature, vol. 599, no. 7884, pp. 211–215, 2021.

[60] P. B. Blakie, "Superfluid fraction tensor of a two-dimensional supersolid," arXiv preprint arXiv:2308.14001, 2023.

[61] M. Guo, F. Böttcher, J. Hertkorn, J.-N. Schmidt, M. Wenzel, H. P. Büchler, T. Langen, and T. Pfau, "The low-energy goldstone mode in a trapped dipolar supersolid," Nature, vol. 574, no. 7778, pp. 386–389, 2019.

[62] L. Chomaz, I. Ferrier-Barbut, F. Ferlaino, B. Laburthe-Tolra, B. L. Lev, and T. Pfau, "Dipolar physics: a review of experiments with magnetic quantum gases," Reports on Progress in Physics, vol. 86, no. 2, p. 026401, 2022.

[63] J. G. Verwer, W. H. Hundsdorfer, and B. P. Sommeijer, "Convergence properties of the runge-kutta-chebyshev method," Numerische Mathematik, vol. 57, pp. 157–178, 1990.

[64] R. C. Swanson, E. Turkel, and C.-C. Rossow, "Convergence acceleration of runge–kutta schemes for solving the navier–stokes equations," Journal of Computational Physics, vol. 224, no. 1, pp. 365–388, 2007.

[65] F. Bavaud, P. Choquard, and J.-R. Fontaine, "Statistical mechanics of elastic moduli," Journal of statistical physics, vol. 42, no. 3, pp. 621–646, 1986.

[66] L. D. Landau and E. M. Lifshitz, Theory of Elasticity: Volume 7. S.l: Butterworth-Heinemann, 3rd ed.. ed., 1984.

[67] L. D. Landau, E. M. Lifshitz, A. M. Kosevich, and L. P. Pitaevskii, Theory of elasticity: volume 7, vol. 7. Elsevier, 1986.

[68] Y. Pomeau and S. Rica, "Dynamics of a model of supersolid," Physical review letters, vol. 72, no. 15, p. 2426, 1994.

[69] A. P. Sutton, M. W. Finnis, D. G. Pettifor, and Y. Ohta, "The tight-binding bond model," Journal of Physics C: Solid State Physics, vol. 21, no. 1, p. 35, 1988.

[70] J.-R. Li, J. Lee, W. Huang, S. Burchesky, B. Shteynas, F. Ç. Top, A. O. Jamison, and W. Ketterle, "A stripe phase with supersolid properties in spin–orbit-coupled bose–einstein condensates," Nature, vol. 543, no. 7643, pp. 91–94, 2017.

[71] A. Aftalion, X. Blanc, and R. L. Jerrard, "Nonclassical rotational inertia of a supersolid," Physical review letters, vol. 99, no. 13, p. 135301, 2007.

[72] T. Ilg and H. P. Büchler, "Ground-state stability and excitation spectrum of a one-dimensional dipolar supersolid," Physical Review A, vol. 107, no. 1, p. 013314, 2023.

[73] S. M. Roccuzzo and F. Ancilotto, "Supersolid behavior of a dipolar bose-einstein condensate confined in a tube," Physical Review A, vol. 99, no. 4, p. 041601, 2019.

[74] J.-M. Hou and W. Chen, "Hidden antiunitary symmetry behind "accidental" degeneracy and its protection of degeneracy," Frontiers of Physics, vol. 13, pp. 1–4, 2018.

Copyright Permissions

American Physical Society
Reuse and Permissions License

12-Aug-2024

This license agreement between the American Physical Society ("APS") and Milan Rakic ("You") consists of your license details and the terms and conditions provided by the American Physical Society and SciPris.

Licensed Content Information

License Number:	**RNP/24/AUG/082204**
License date:	12-Aug-2024
DOI:	10.1103/PhysRevLett.128.195302
Title:	Two-Dimensional Supersolid Formation in Dipolar Condensates
Author:	T. Bland et al.
Publication:	Physical Review Letters
Publisher:	American Physical Society
Cost:	USD $ 0.00

Request Details

Does your reuse require significant modifications: No

Specify intended distribution locations:	UK & Commonwealth (excluding Canada)
Reuse Category:	Reuse in a thesis/dissertation
Requestor Type:	Student
Items for Reuse:	Figures/Tables
Number of Figure/Tables:	1
Figure/Tables Details:	Figure 3
Format for Reuse:	Electronic

Information about New Publication:

University/Publisher:	Imperial College London
Title of dissertation/thesis:	Intertwined Order in Strongly Correlated Quantum Systems
Author(s):	Milan Rakic
Expected completion date:	Aug. 2024

License Requestor Information

Name:	Milan Rakic
Affiliation:	Individual
Email Id:	milan.p.rakic@gmail.com
Country:	United Kingdom

American Physical Society
Reuse and Permissions License

TERMS AND CONDITIONS

The American Physical Society (APS) is pleased to grant the Requestor of this license a non-exclusive, non-transferable permission, limited to Electronic format, provided all criteria outlined below are followed.

1. You must also obtain permission from at least one of the lead authors for each separate work, if you haven't done so already. The author's name and affiliation can be found on the first page of the published Article.

2. For electronic format permissions, Requestor agrees to provide a hyperlink from the reprinted APS material using the source material's DOI on the web page where the work appears. The hyperlink should use the standard DOI resolution URL, http://dx.doi.org/{DOI}. The hyperlink may be embedded in the copyright credit line.

3. For print format permissions, Requestor agrees to print the required copyright credit line on the first page where the material appears: "Reprinted (abstract/excerpt/figure) with permission from [(FULL REFERENCE CITATION) as follows: Author's Names, APS Journal Title, Volume Number, Page Number and Year of Publication.] Copyright (YEAR) by the American Physical Society."

4. Permission granted in this license is for a one-time use and does not include permission for any future editions, updates, databases, formats or other matters. Permission must be sought for any additional use.

5. Use of the material does not and must not imply any endorsement by APS.

6. APS does not imply, purport or intend to grant permission to reuse materials to which it does not hold copyright. It is the requestor's sole responsibility to ensure the licensed material is original to APS and does not contain the copyright of another entity, and that the copyright notice of the figure, photograph, cover or table does not indicate it was reprinted by APS with permission from another source.

7. The permission granted herein is personal to the Requestor for the use specified and is not transferable or assignable without express written permission of APS. This license may not be amended except in writing by APS.

8. You may not alter, edit or modify the material in any manner.

9. You may translate the materials only when translation rights have been granted.

10. APS is not responsible for any errors or omissions due to translation.

11. You may not use the material for promotional, sales, advertising or marketing purposes.

12. The foregoing license shall not take effect unless and until APS or its agent, Aptara, receives payment in full in accordance with Aptara Billing and Payment Terms and Conditions, which are incorporated herein by reference.

13. Should the terms of this license be violated at any time, APS or Aptara may revoke the license with no refund to you and seek relief to the fullest extent of the laws of the USA. Official written notice will be made using the contact information provided with the permission request. Failure to receive such notice will not nullify revocation of the permission.

14. APS reserves all rights not specifically granted herein.

15. This document, including the Aptara Billing and Payment Terms and Conditions, shall be the entire agreement between the parties relating to the subject matter hereof.

SPRINGER NATURE LICENSE
TERMS AND CONDITIONS

Aug 13, 2024

This Agreement between Milan Rakic ("You") and Springer Nature ("Springer Nature") consists of your license details and the terms and conditions provided by Springer Nature and Copyright Clearance Center.

License Number	5846541250648
License date	Aug 12, 2024
Licensed Content Publisher	Springer Nature
Licensed Content Publication	Nature Physics
Licensed Content Title	Intertwined superfluid and density wave order in two-dimensional 4He
Licensed Content Author	Ján Nyéki et al
Licensed Content Date	Feb 6, 2017
Type of Use	Thesis/Dissertation
Requestor type	academic/university or research institute
Format	electronic
Portion	figures/tables/illustrations
Number of figures/tables/illustrations	2

Would you like a high resolution image with your order?	no
Will you be translating?	no
Circulation/distribution	1 - 29
Author of this Springer Nature content	no
Title of new work	Intertwined Order in Strongly Correlated Quantum Systems
Institution name	Imperial College London
Expected presentation date	Sep 2024
Portions	Figure 1, Figure 3
The Requesting Person / Organization to Appear on the License	Milan Rakic
Requestor Location	Mr. Milan Rakic 24B Percy Road London, W12 9QA United Kingdom Attn: Mr. Milan Rakic
Billing Type	Invoice
Billing Address	Mr. Milan Rakic 24B Percy Road London, United Kingdom W12 9QA Attn: Mr. Milan Rakic

Total 0.00 GBP

Terms and Conditions

Springer Nature Customer Service Centre GmbH Terms and Conditions

The following terms and conditions ("Terms and Conditions") together with the terms specified in your [RightsLink] constitute the License ("License") between you as Licensee and Springer Nature Customer Service Centre GmbH as Licensor. By clicking 'accept' and completing the transaction for your use of the material ("Licensed Material"), you confirm your acceptance of and obligation to be bound by these Terms and Conditions.

1. Grant and Scope of License

1. 1. The Licensor grants you a personal, non-exclusive, non-transferable, non-sublicensable, revocable, world-wide License to reproduce, distribute, communicate to the public, make available, broadcast, electronically transmit or create derivative works using the Licensed Material for the purpose(s) specified in your RightsLink Licence Details only. Licenses are granted for the specific use requested in the order and for no other use, subject to these Terms and Conditions. You acknowledge and agree that the rights granted to you under this License do not include the right to modify, edit, translate, include in collective works, or create derivative works of the Licensed Material in whole or in part unless expressly stated in your RightsLink Licence Details. You may use the Licensed Material only as permitted under this Agreement and will not reproduce, distribute, display, perform, or otherwise use or exploit any Licensed Material in any way, in whole or in part, except as expressly permitted by this License.

1. 2. You may only use the Licensed Content in the manner and to the extent permitted by these Terms and Conditions, by your RightsLink Licence Details and by any applicable laws.

1. 3. A separate license may be required for any additional use of the Licensed Material, e.g. where a license has been purchased for print use only, separate permission must be obtained for electronic re-use. Similarly, a License is only valid in the language selected and does not apply for editions in other languages unless additional translation rights have been granted separately in the License.

1. 4. Any content within the Licensed Material that is owned by third parties is expressly excluded from the License.

1. 5. Rights for additional reuses such as custom editions, computer/mobile applications, film or TV reuses and/or any other derivative rights requests require additional permission and may be subject to an additional fee. Please apply to journalpermissions@springernature.com or bookpermissions@springernature.com for these rights.

2. Reservation of Rights

Licensor reserves all rights not expressly granted to you under this License. You acknowledge and agree that nothing in this License limits or restricts Licensor's rights in or use of the Licensed Material in any way. Neither this License, nor any act, omission, or statement by Licensor or you, conveys any ownership right to you in any Licensed Material, or to any element or portion thereof. As between Licensor and you, Licensor owns and retains all right, title, and interest in and to the Licensed Material subject to the license granted in Section 1.1. Your permission to use the Licensed Material is expressly conditioned on you not impairing Licensor's or the applicable copyright owner's rights in the Licensed Material in any way.

3. Restrictions on use

3. 1. Minor editing privileges are allowed for adaptations for stylistic purposes or formatting purposes provided such alterations do not alter the original meaning or intention of the Licensed Material and the new figure(s) are still accurate and representative of the Licensed Material. Any other changes including but not limited to, cropping, adapting, and/or omitting material that affect the meaning, intention or moral rights of the author(s) are strictly prohibited.

3. 2. You must not use any Licensed Material as part of any design or trademark.

3. 3. Licensed Material may be used in Open Access Publications (OAP), but any such reuse must include a clear acknowledgment of this permission visible at the same time as the figures/tables/illustration or abstract and which must indicate that the Licensed Material is not part of the governing OA license but has been reproduced with permission. This may be indicated according to any standard referencing system but must include at a minimum 'Book/Journal title, Author, Journal Name (if applicable), Volume (if applicable), Publisher, Year, reproduced with permission from SNCSC'.

4. STM Permission Guidelines

4. 1. An alternative scope of license may apply to signatories of the STM Permissions Guidelines ("STM PG") as amended from time to time and made available at https://www.stm-assoc.org/intellectual-property/permissions/permissions-guidelines/.

4. 2. For content reuse requests that qualify for permission under the STM PG, and which may be updated from time to time, the STM PG supersede the terms and conditions contained in this License.

4. 3. If a License has been granted under the STM PG, but the STM PG no longer apply at the time of publication, further permission must be sought from the Rightsholder. Contact journalpermissions@springernature.com or bookpermissions@springernature.com for these rights.

5. Duration of License

5. 1. Unless otherwise indicated on your License, a License is valid from the date of

purchase ("License Date") until the end of the relevant period in the below table:

Reuse in a medical communications project	Reuse up to distribution or time period indicated in License
Reuse in a dissertation/ thesis	Lifetime of thesis
Reuse in a journal/ magazine	Lifetime of journal/magazine
Reuse in a book/ textbook	Lifetime of edition
Reuse on a website	1 year unless otherwise specified in the License
Reuse in a presentation/ slide kit/poster	Lifetime of presentation/slide kit/poster. Note: publication whether electronic or in print of presentation/slide kit/poster may require further permission.
Reuse in conference proceedings	Lifetime of conference proceedings
Reuse in an annual report	Lifetime of annual report
Reuse in training/CME materials	Reuse up to distribution or time period indicated in License
Reuse in newsmedia	Lifetime of newsmedia
Reuse in coursepack/ classroom materials	Reuse up to distribution and/or time period indicated in license

6. Acknowledgement

6. 1. The Licensor's permission must be acknowledged next to the Licensed Material in print. In electronic form, this acknowledgement must be visible at the same time as the figures/tables/illustrations or abstract and must be hyperlinked to the journal/book's homepage.

6. 2. Acknowledgement may be provided according to any standard referencing system and at a minimum should include "Author, Article/Book Title, Journal name/Book imprint, volume, page number, year, Springer Nature".

7. Reuse in a dissertation or thesis

7. 1. Where 'reuse in a dissertation/thesis' has been selected, the following terms apply: Print rights of the Version of Record are provided for; electronic rights for use only on institutional repository as defined by the Sherpa guideline (www.sherpa.ac.uk/romeo/) and only up to what is required by the awarding institution.

7. 2. For theses published under an ISBN or ISSN, separate permission is required. Please contact journalpermissions@springernature.com or bookpermissions@springernature.com for these rights.

7. 3. Authors must properly cite the published manuscript in their thesis according

to current citation standards and include the following acknowledgement: '*Reproduced with permission from Springer Nature*'.

8. License Fee

You must pay the fee set forth in the License Agreement (the "License Fees"). All amounts payable by you under this License are exclusive of any sales, use, withholding, value added or similar taxes, government fees or levies or other assessments. Collection and/or remittance of such taxes to the relevant tax authority shall be the responsibility of the party who has the legal obligation to do so.

9. Warranty

9. 1. The Licensor warrants that it has, to the best of its knowledge, the rights to license reuse of the Licensed Material. **You are solely responsible for ensuring that the material you wish to license is original to the Licensor and does not carry the copyright of another entity or third party (as credited in the published version).** If the credit line on any part of the Licensed Material indicates that it was reprinted or adapted with permission from another source, then you should seek additional permission from that source to reuse the material.

9. 2. EXCEPT FOR THE EXPRESS WARRANTY STATED HEREIN AND TO THE EXTENT PERMITTED BY APPLICABLE LAW, LICENSOR PROVIDES THE LICENSED MATERIAL "AS IS" AND MAKES NO OTHER REPRESENTATION OR WARRANTY. LICENSOR EXPRESSLY DISCLAIMS ANY LIABILITY FOR ANY CLAIM ARISING FROM OR OUT OF THE CONTENT, INCLUDING BUT NOT LIMITED TO ANY ERRORS, INACCURACIES, OMISSIONS, OR DEFECTS CONTAINED THEREIN, AND ANY IMPLIED OR EXPRESS WARRANTY AS TO MERCHANTABILITY OR FITNESS FOR A PARTICULAR PURPOSE. IN NO EVENT SHALL LICENSOR BE LIABLE TO YOU OR ANY OTHER PARTY OR ANY OTHER PERSON OR FOR ANY SPECIAL, CONSEQUENTIAL, INCIDENTAL, INDIRECT, PUNITIVE, OR EXEMPLARY DAMAGES, HOWEVER CAUSED, ARISING OUT OF OR IN CONNECTION WITH THE DOWNLOADING, VIEWING OR USE OF THE LICENSED MATERIAL REGARDLESS OF THE FORM OF ACTION, WHETHER FOR BREACH OF CONTRACT, BREACH OF WARRANTY, TORT, NEGLIGENCE, INFRINGEMENT OR OTHERWISE (INCLUDING, WITHOUT LIMITATION, DAMAGES BASED ON LOSS OF PROFITS, DATA, FILES, USE, BUSINESS OPPORTUNITY OR CLAIMS OF THIRD PARTIES), AND WHETHER OR NOT THE PARTY HAS BEEN ADVISED OF THE POSSIBILITY OF SUCH DAMAGES. THIS LIMITATION APPLIES NOTWITHSTANDING ANY FAILURE OF ESSENTIAL PURPOSE OF ANY LIMITED REMEDY PROVIDED HEREIN.

10. Termination and Cancellation

10. 1. The License and all rights granted hereunder will continue until the end of the applicable period shown in Clause 5.1 above. Thereafter, this license will be terminated and all rights granted hereunder will cease.

10. 2. Licensor reserves the right to terminate the License in the event that payment

is not received in full or if you breach the terms of this License.

11. General

11. 1. The License and the rights and obligations of the parties hereto shall be construed, interpreted and determined in accordance with the laws of the Federal Republic of Germany without reference to the stipulations of the CISG (United Nations Convention on Contracts for the International Sale of Goods) or to Germany´s choice-of-law principle.

11. 2. The parties acknowledge and agree that any controversies and disputes arising out of this License shall be decided exclusively by the courts of or having jurisdiction for Heidelberg, Germany, as far as legally permissible.

11. 3. This License is solely for Licensor's and Licensee's benefit. It is not for the benefit of any other person or entity.

Questions? For questions on Copyright Clearance Center accounts or website issues please contact springernaturesupport@copyright.com or +1-855-239-3415 (toll free in the US) or +1-978-646-2777. For questions on Springer Nature licensing please visit https://www.springernature.com/gp/partners/rights-permissions-third-party-distribution

Other Conditions:

Version 1.4 - Dec 2022

Questions? customercare@copyright.com.

SPRINGER NATURE LICENSE
TERMS AND CONDITIONS

Aug 13, 2024

This Agreement between Milan Rakic ("You") and Springer Nature ("Springer Nature") consists of your license details and the terms and conditions provided by Springer Nature and Copyright Clearance Center.

License Number	5846551206610
License date	Aug 12, 2024
Licensed Content Publisher	Springer Nature
Licensed Content Publication	Nature
Licensed Content Title	Probable observation of a supersolid helium phase
Licensed Content Author	E. Kim et al
Licensed Content Date	Jan 15, 2004
Type of Use	Thesis/Dissertation
Requestor type	academic/university or research institute
Format	electronic
Portion	figures/tables/illustrations
Number of figures/tables/illustrations	1

Would you like a high resolution image with your order?	no
Will you be translating?	no
Circulation/distribution	1 - 29
Author of this Springer Nature content	no
Title of new work	Intertwined Order in Strongly Correlated Quantum Systems
Institution name	Imperial College London
Expected presentation date	Sep 2024
Portions	Figure 2
The Requesting Person / Organization to Appear on the License	Milan Rakic
Requestor Location	Mr. Milan Rakic 24B Percy Road London, W12 9QA United Kingdom Attn: Mr. Milan Rakic
Billing Type	Invoice
Billing Address	Mr. Milan Rakic 24B Percy Road London, United Kingdom W12 9QA Attn: Mr. Milan Rakic

Total 0.00 GBP

Terms and Conditions

Springer Nature Customer Service Centre GmbH Terms and Conditions

The following terms and conditions ("Terms and Conditions") together with the terms specified in your [RightsLink] constitute the License ("License") between you as Licensee and Springer Nature Customer Service Centre GmbH as Licensor. By clicking 'accept' and completing the transaction for your use of the material ("Licensed Material"), you confirm your acceptance of and obligation to be bound by these Terms and Conditions.

1. Grant and Scope of License

1. 1. The Licensor grants you a personal, non-exclusive, non-transferable, non-sublicensable, revocable, world-wide License to reproduce, distribute, communicate to the public, make available, broadcast, electronically transmit or create derivative works using the Licensed Material for the purpose(s) specified in your RightsLink Licence Details only. Licenses are granted for the specific use requested in the order and for no other use, subject to these Terms and Conditions. You acknowledge and agree that the rights granted to you under this License do not include the right to modify, edit, translate, include in collective works, or create derivative works of the Licensed Material in whole or in part unless expressly stated in your RightsLink Licence Details. You may use the Licensed Material only as permitted under this Agreement and will not reproduce, distribute, display, perform, or otherwise use or exploit any Licensed Material in any way, in whole or in part, except as expressly permitted by this License.

1. 2. You may only use the Licensed Content in the manner and to the extent permitted by these Terms and Conditions, by your RightsLink Licence Details and by any applicable laws.

1. 3. A separate license may be required for any additional use of the Licensed Material, e.g. where a license has been purchased for print use only, separate permission must be obtained for electronic re-use. Similarly, a License is only valid in the language selected and does not apply for editions in other languages unless additional translation rights have been granted separately in the License.

1. 4. Any content within the Licensed Material that is owned by third parties is expressly excluded from the License.

1. 5. Rights for additional reuses such as custom editions, computer/mobile applications, film or TV reuses and/or any other derivative rights requests require additional permission and may be subject to an additional fee. Please apply to journalpermissions@springernature.com or bookpermissions@springernature.com for these rights.

2. Reservation of Rights

Licensor reserves all rights not expressly granted to you under this License. You acknowledge and agree that nothing in this License limits or restricts Licensor's rights in or use of the Licensed Material in any way. Neither this License, nor any act, omission, or statement by Licensor or you, conveys any ownership right to you in any Licensed Material, or to any element or portion thereof. As between Licensor and you, Licensor owns and retains all right, title, and interest in and to the Licensed Material subject to the license granted in Section 1.1. Your permission to use the Licensed Material is expressly conditioned on you not impairing Licensor's or the applicable copyright owner's rights in the Licensed Material in any way.

3. Restrictions on use

3. 1. Minor editing privileges are allowed for adaptations for stylistic purposes or formatting purposes provided such alterations do not alter the original meaning or intention of the Licensed Material and the new figure(s) are still accurate and representative of the Licensed Material. Any other changes including but not limited to, cropping, adapting, and/or omitting material that affect the meaning, intention or moral rights of the author(s) are strictly prohibited.

3. 2. You must not use any Licensed Material as part of any design or trademark.

3. 3. Licensed Material may be used in Open Access Publications (OAP), but any such reuse must include a clear acknowledgment of this permission visible at the same time as the figures/tables/illustration or abstract and which must indicate that the Licensed Material is not part of the governing OA license but has been reproduced with permission. This may be indicated according to any standard referencing system but must include at a minimum 'Book/Journal title, Author, Journal Name (if applicable), Volume (if applicable), Publisher, Year, reproduced with permission from SNCSC'.

4. STM Permission Guidelines

4. 1. An alternative scope of license may apply to signatories of the STM Permissions Guidelines ("STM PG") as amended from time to time and made available at https://www.stm-assoc.org/intellectual-property/permissions/permissions-guidelines/.

4. 2. For content reuse requests that qualify for permission under the STM PG, and which may be updated from time to time, the STM PG supersede the terms and conditions contained in this License.

4. 3. If a License has been granted under the STM PG, but the STM PG no longer apply at the time of publication, further permission must be sought from the Rightsholder. Contact journalpermissions@springernature.com or bookpermissions@springernature.com for these rights.

5. Duration of License

5. 1. Unless otherwise indicated on your License, a License is valid from the date of

purchase ("License Date") until the end of the relevant period in the below table:

Reuse in a medical communications project	Reuse up to distribution or time period indicated in License
Reuse in a dissertation/ thesis	Lifetime of thesis
Reuse in a journal/ magazine	Lifetime of journal/magazine
Reuse in a book/ textbook	Lifetime of edition
Reuse on a website	1 year unless otherwise specified in the License
Reuse in a presentation/ slide kit/poster	Lifetime of presentation/slide kit/poster. Note: publication whether electronic or in print of presentation/slide kit/poster may require further permission.
Reuse in conference proceedings	Lifetime of conference proceedings
Reuse in an annual report	Lifetime of annual report
Reuse in training/CME materials	Reuse up to distribution or time period indicated in License
Reuse in newsmedia	Lifetime of newsmedia
Reuse in coursepack/ classroom materials	Reuse up to distribution and/or time period indicated in license

6. Acknowledgement

6. 1. The Licensor's permission must be acknowledged next to the Licensed Material in print. In electronic form, this acknowledgement must be visible at the same time as the figures/tables/illustrations or abstract and must be hyperlinked to the journal/book's homepage.

6. 2. Acknowledgement may be provided according to any standard referencing system and at a minimum should include "Author, Article/Book Title, Journal name/Book imprint, volume, page number, year, Springer Nature".

7. Reuse in a dissertation or thesis

7. 1. Where 'reuse in a dissertation/thesis' has been selected, the following terms apply: Print rights of the Version of Record are provided for; electronic rights for use only on institutional repository as defined by the Sherpa guideline (www.sherpa.ac.uk/romeo/) and only up to what is required by the awarding institution.

7. 2. For theses published under an ISBN or ISSN, separate permission is required. Please contact journalpermissions@springernature.com or bookpermissions@springernature.com for these rights.

7. 3. Authors must properly cite the published manuscript in their thesis according

to current citation standards and include the following acknowledgement: '*Reproduced with permission from Springer Nature*'.

8. License Fee

You must pay the fee set forth in the License Agreement (the "License Fees"). All amounts payable by you under this License are exclusive of any sales, use, withholding, value added or similar taxes, government fees or levies or other assessments. Collection and/or remittance of such taxes to the relevant tax authority shall be the responsibility of the party who has the legal obligation to do so.

9. Warranty

9. 1. The Licensor warrants that it has, to the best of its knowledge, the rights to license reuse of the Licensed Material. **You are solely responsible for ensuring that the material you wish to license is original to the Licensor and does not carry the copyright of another entity or third party (as credited in the published version).** If the credit line on any part of the Licensed Material indicates that it was reprinted or adapted with permission from another source, then you should seek additional permission from that source to reuse the material.

9. 2. EXCEPT FOR THE EXPRESS WARRANTY STATED HEREIN AND TO THE EXTENT PERMITTED BY APPLICABLE LAW, LICENSOR PROVIDES THE LICENSED MATERIAL "AS IS" AND MAKES NO OTHER REPRESENTATION OR WARRANTY. LICENSOR EXPRESSLY DISCLAIMS ANY LIABILITY FOR ANY CLAIM ARISING FROM OR OUT OF THE CONTENT, INCLUDING BUT NOT LIMITED TO ANY ERRORS, INACCURACIES, OMISSIONS, OR DEFECTS CONTAINED THEREIN, AND ANY IMPLIED OR EXPRESS WARRANTY AS TO MERCHANTABILITY OR FITNESS FOR A PARTICULAR PURPOSE. IN NO EVENT SHALL LICENSOR BE LIABLE TO YOU OR ANY OTHER PARTY OR ANY OTHER PERSON OR FOR ANY SPECIAL, CONSEQUENTIAL, INCIDENTAL, INDIRECT, PUNITIVE, OR EXEMPLARY DAMAGES, HOWEVER CAUSED, ARISING OUT OF OR IN CONNECTION WITH THE DOWNLOADING, VIEWING OR USE OF THE LICENSED MATERIAL REGARDLESS OF THE FORM OF ACTION, WHETHER FOR BREACH OF CONTRACT, BREACH OF WARRANTY, TORT, NEGLIGENCE, INFRINGEMENT OR OTHERWISE (INCLUDING, WITHOUT LIMITATION, DAMAGES BASED ON LOSS OF PROFITS, DATA, FILES, USE, BUSINESS OPPORTUNITY OR CLAIMS OF THIRD PARTIES), AND WHETHER OR NOT THE PARTY HAS BEEN ADVISED OF THE POSSIBILITY OF SUCH DAMAGES. THIS LIMITATION APPLIES NOTWITHSTANDING ANY FAILURE OF ESSENTIAL PURPOSE OF ANY LIMITED REMEDY PROVIDED HEREIN.

10. Termination and Cancellation

10. 1. The License and all rights granted hereunder will continue until the end of the applicable period shown in Clause 5.1 above. Thereafter, this license will be terminated and all rights granted hereunder will cease.

10. 2. Licensor reserves the right to terminate the License in the event that payment

is not received in full or if you breach the terms of this License.

11. General

11. 1. The License and the rights and obligations of the parties hereto shall be construed, interpreted and determined in accordance with the laws of the Federal Republic of Germany without reference to the stipulations of the CISG (United Nations Convention on Contracts for the International Sale of Goods) or to Germany´s choice-of-law principle.

11. 2. The parties acknowledge and agree that any controversies and disputes arising out of this License shall be decided exclusively by the courts of or having jurisdiction for Heidelberg, Germany, as far as legally permissible.

11. 3. This License is solely for Licensor's and Licensee's benefit. It is not for the benefit of any other person or entity.

Questions? For questions on Copyright Clearance Center accounts or website issues please contact springernaturesupport@copyright.com or +1-855-239-3415 (toll free in the US) or +1-978-646-2777. For questions on Springer Nature licensing please visit https://www.springernature.com/gp/partners/rights-permissions-third-party-distribution

Other Conditions:

Version 1.4 - Dec 2022

Questions? customercare@copyright.com.

CCC Marketplace

This is a License Agreement between Milan Rakic ("User") and Copyright Clearance Center, Inc. ("CCC") on behalf of the Rightsholder identified in the order details below. The license consists of the order details, the Marketplace Permissions General Terms and Conditions below, and any Rightsholder Terms and Conditions which are included below.

All payments must be made in full to CCC in accordance with the Marketplace Permissions General Terms and Conditions below.

Order Date	13-Aug-2024	Type of Use	Republish in a thesis/ dissertation
Order License ID	1515295-1		
ISSN	0034-4885	Publisher	IOP Publishing
		Portion	Chart/graph/table/figure

LICENSED CONTENT

Publication Title	Reports on Progress in Physics	Country	United Kingdom of Great Britain and Northern Ireland
Author / Editor	Institute of Physics (Great Britain), Physical Society (Great Britain), Institute of Physics and the Physical Society., Institute of Physics Publishing.	Rightsholder	IOP Publishing, Ltd
		Publication Type	Journal
Date	01/01/1934		
Language	English		

REQUEST DETAILS

Portion Type	Chart/graph/table/figure	Distribution	U.K. and Commonwealth (excluding Canada)
Number of Charts / Graphs / Tables / Figures Requested	1	Translation	Original language of publication
Format (select all that apply)	Electronic	Copies for the Disabled?	Yes
		Minor Editing Privileges?	No
Who Will Republish the Content?	Academic institution	Incidental Promotional Use?	No
Duration of Use	Life of current edition	Currency	GBP
Lifetime Unit Quantity	Up to 499		
Rights Requested	Main product		

NEW WORK DETAILS

Title	Intertwined Order in Strongly Correlated Quantum Systems	Institution Name	Imperial College London
		Expected Presentation Date	2024-08-19
Instructor Name	Milan Rakic		

ADDITIONAL DETAILS

Order Reference Number	N/A

The Requesting Person / Organization to Appear on the License	Milan Rakic

REQUESTED CONTENT DETAILS

Title, Description or Numeric Reference of the Portion(s)	Figure 28	**Title of the Article / Chapter the Portion Is From**	N/A
Editor of Portion(s)	N/A	**Author of Portion(s)**	Institute of Physics (Great Britain); Physical Society (Great Britain); Institute of Physics and the Physical Society.; Institute of Physics Publishing.
Volume / Edition	N/A		
Page or Page Range of Portion	53	**Issue, if Republishing an Article From a Serial**	N/A
		Publication Date of Portion	2022-12-30

RIGHTSHOLDER TERMS AND CONDITIONS

These special terms and conditions are in addition to the standard terms and conditions for CCC's Republication Service and, together with those standard terms and conditions, govern the use of the Works. As the User you will make all reasonable efforts to contact the author(s) of the article which the Work is to be reused from, to seek consent for your intended use. Contacting one author who is acting expressly as authorised agent for their co-author(s) is acceptable. User will reproduce the following wording prominently alongside the Work: the source of the Work, including author, article title, title of journal, volume number, issue number (if relevant), page range (or first page if this is the only information available) and date of first publication; and a link back to the article (via DOI); and if practicable, and IN ALL CASES for new works published under any of the Creative Commons licences, the words "© IOP Publishing. Reproduced with permission. All rights reserved" Without the express permission of the author(s) and the Rightsholder of the article from which the Work is to be reused, User shall not use it in any way which, in the opinion of the Rightsholder, could: (i) distort or alter the author(s)' original intention(s) and meaning; (ii) be prejudicial to the honour or reputation of the author(s); and/or (iii) imply endorsement by the author(s) and/or the Rightsholder. This licence does not apply to any article which is credited to another source and which does not have the copyright line '© IOP Publishing Ltd'. User must check the copyright line of the article from which the Work is to be reused to check that IOP Publishing Ltd has all the necessary rights to be able to grant permission. User is solely responsible for identifying and obtaining separate licences and permissions from the copyright owner for reuse of any such third party material/figures which the Rightsholder is not the copyright owner of. The Rightsholder shall not reimburse any fees which User pays for a republication license for such third party content. This licence does not apply to any material/figure which is credited to another source in the Rightsholder's publication or has been obtained from a third party. User must check the Version of Record of the article from which the Work is to be reused, to check whether any of the material in the Work is third party material. Third party citations and/or copyright notices and/or permissions statements may not be included in any other version of the article from which the Work is to be reused and so cannot be relied upon by the User. User is solely responsible for identifying and obtaining separate licences and permissions from the copyright owner for reuse of any such third party material/figures where the Rightsholder is not the copyright owner. The Rightsholder shall not reimburse any fees which User pays for a republication license for such third party content. User and CCC acknowledge that the Rightsholder may, from time to time, make changes or additions to these special terms and conditions without express notification, provided that these shall not apply to permissions already secured and paid for by User prior to such change or addition. User acknowledges that the Rightsholder (which includes companies within its group and third parties for whom it publishes its titles) may make use of personal data collected through the service in the course of their business. If User is the author of the Work, User may automatically have the right to reuse it under the rights granted back when User transferred the copyright in the article to the Rightsholder. User should check the copyright form and the relevant author rights policy to check whether permission is required. If User is the author of the Work and does require permission for proposed reuse of the Work, User should select 'Author of requested content' as the Requestor Type. The Rightsholder shall not reimburse any fees which User pays for a republication license. If User is the author of the article which User wishes to reuse in User's thesis or dissertation, the republication licence covers the right to include the Version of Record of the article, provided it is not then shared or deposited online. User must include citation details. Where User wishes to share their thesis or dissertation online, they

should remove the Version of Record before uploading it. User may include a Preprint or the Accepted Manuscript (after the embargo period) in the online version of the thesis or dissertation, provided they do so in accordance with the Rightsholder's policies on sharing Preprints or Accepted Manuscripts. User may need to obtain separate permission for any third party content included within the article. User must check this with the copyright owner of such third party content. Any online or commercial use of User's thesis or dissertation containing the article, including publication via ProQuest, would need to be expressly notified in writing to the Rightsholder at the time of request and would require separate written permission from the Rightsholder. As well as CCC, the Rightsholder shall have the right to bring any legal action that it deems necessary to enforce its rights should it consider that the Work infringes those rights in any way. For content reuse requests that qualify for permission under the STM Permissions Guidelines, which may be updated from time to time, the STM Permissions Guidelines supplement the terms and conditions contained in this license.
If you are producing a new book or article to be published by another STM Signatory publisher, please choose "Reuse in a book under STM Guidelines" or "Reuse in a journal under STM Guidelines." You can consult the STM Guidelines website to see whether your new publisher is a signatory to the STM Permissions Guidelines.

Marketplace Permissions General Terms and Conditions

The following terms and conditions ("General Terms"), together with any applicable Publisher Terms and Conditions, govern User's use of Works pursuant to the Licenses granted by Copyright Clearance Center, Inc. ("CCC") on behalf of the applicable Rightsholders of such Works through CCC's applicable Marketplace transactional licensing services (each, a "Service").

1) **Definitions.** For purposes of these General Terms, the following definitions apply:

"License" is the licensed use the User obtains via the Marketplace platform in a particular licensing transaction, as set forth in the Order Confirmation.

"Order Confirmation" is the confirmation CCC provides to the User at the conclusion of each Marketplace transaction. "Order Confirmation Terms" are additional terms set forth on specific Order Confirmations not set forth in the General Terms that can include terms applicable to a particular CCC transactional licensing service and/or any Rightsholder-specific terms.

"Rightsholder(s)" are the holders of copyright rights in the Works for which a User obtains licenses via the Marketplace platform, which are displayed on specific Order Confirmations.

"Terms" means the terms and conditions set forth in these General Terms and any additional Order Confirmation Terms collectively.

"User" or "you" is the person or entity making the use granted under the relevant License. Where the person accepting the Terms on behalf of a User is a freelancer or other third party who the User authorized to accept the General Terms on the User's behalf, such person shall be deemed jointly a User for purposes of such Terms.

"Work(s)" are the copyright protected works described in relevant Order Confirmations.

2) **Description of Service.** CCC's Marketplace enables Users to obtain Licenses to use one or more Works in accordance with all relevant Terms. CCC grants Licenses as an agent on behalf of the copyright rightsholder identified in the relevant Order Confirmation.

3) **Applicability of Terms.** The Terms govern User's use of Works in connection with the relevant License. In the event of any conflict between General Terms and Order Confirmation Terms, the latter shall govern. User acknowledges that Rightsholders have complete discretion whether to grant any permission, and whether to place any limitations on any grant, and that CCC has no right to supersede or to modify any such discretionary act by a Rightsholder.

4) **Representations; Acceptance.** By using the Service, User represents and warrants that User has been duly authorized by the User to accept, and hereby does accept, all Terms.

5) **Scope of License; Limitations and Obligations.** All Works and all rights therein, including copyright rights, remain the sole and exclusive property of the Rightsholder. The License provides only those rights expressly set forth in the terms and conveys no other rights in any Works

6) **General Payment Terms.** User may pay at time of checkout by credit card or choose to be invoiced. If the User chooses to be invoiced, the User shall: (i) remit payments in the manner identified on specific invoices, (ii) unless otherwise specifically stated in an Order Confirmation or separate written agreement, Users shall remit payments upon receipt of

the relevant invoice from CCC, either by delivery or notification of availability of the invoice via the Marketplace platform, and (iii) if the User does not pay the invoice within 30 days of receipt, the User may incur a service charge of 1.5% per month or the maximum rate allowed by applicable law, whichever is less. While User may exercise the rights in the License immediately upon receiving the Order Confirmation, the License is automatically revoked and is null and void, as if it had never been issued, if CCC does not receive complete payment on a timely basis.

7) **General Limits on Use.** Unless otherwise provided in the Order Confirmation, any grant of rights to User (i) involves only the rights set forth in the Terms and does not include subsequent or additional uses, (ii) is non-exclusive and non-transferable, and (iii) is subject to any and all limitations and restrictions (such as, but not limited to, limitations on duration of use or circulation) included in the Terms. Upon completion of the licensed use as set forth in the Order Confirmation, User shall either secure a new permission for further use of the Work(s) or immediately cease any new use of the Work(s) and shall render inaccessible (such as by deleting or by removing or severing links or other locators) any further copies of the Work. User may only make alterations to the Work if and as expressly set forth in the Order Confirmation. No Work may be used in any way that is unlawful, including without limitation if such use would violate applicable sanctions laws or regulations, would be defamatory, violate the rights of third parties (including such third parties' rights of copyright, privacy, publicity, or other tangible or intangible property), or is otherwise illegal, sexually explicit, or obscene. In addition, User may not conjoin a Work with any other material that may result in damage to the reputation of the Rightsholder. Any unlawful use will render any licenses hereunder null and void. User agrees to inform CCC if it becomes aware of any infringement of any rights in a Work and to cooperate with any reasonable request of CCC or the Rightsholder in connection therewith.

8) **Third Party Materials.** In the event that the material for which a License is sought includes third party materials (such as photographs, illustrations, graphs, inserts and similar materials) that are identified in such material as having been used by permission (or a similar indicator), User is responsible for identifying, and seeking separate licenses (under this Service, if available, or otherwise) for any of such third party materials; without a separate license, User may not use such third party materials via the License.

9) **Copyright Notice.** Use of proper copyright notice for a Work is required as a condition of any License granted under the Service. Unless otherwise provided in the Order Confirmation, a proper copyright notice will read substantially as follows: "Used with permission of [Rightsholder's name], from [Work's title, author, volume, edition number and year of copyright]; permission conveyed through Copyright Clearance Center, Inc." Such notice must be provided in a reasonably legible font size and must be placed either on a cover page or in another location that any person, upon gaining access to the material which is the subject of a permission, shall see, or in the case of republication Licenses, immediately adjacent to the Work as used (for example, as part of a by-line or footnote) or in the place where substantially all other credits or notices for the new work containing the republished Work are located. Failure to include the required notice results in loss to the Rightsholder and CCC, and the User shall be liable to pay liquidated damages for each such failure equal to twice the use fee specified in the Order Confirmation, in addition to the use fee itself and any other fees and charges specified.

10) **Indemnity.** User hereby indemnifies and agrees to defend the Rightsholder and CCC, and their respective employees and directors, against all claims, liability, damages, costs, and expenses, including legal fees and expenses, arising out of any use of a Work beyond the scope of the rights granted herein and in the Order Confirmation, or any use of a Work which has been altered in any unauthorized way by User, including claims of defamation or infringement of rights of copyright, publicity, privacy, or other tangible or intangible property.

11) **Limitation of Liability.** UNDER NO CIRCUMSTANCES WILL CCC OR THE RIGHTSHOLDER BE LIABLE FOR ANY DIRECT, INDIRECT, CONSEQUENTIAL, OR INCIDENTAL DAMAGES (INCLUDING WITHOUT LIMITATION DAMAGES FOR LOSS OF BUSINESS PROFITS OR INFORMATION, OR FOR BUSINESS INTERRUPTION) ARISING OUT OF THE USE OR INABILITY TO USE A WORK, EVEN IF ONE OR BOTH OF THEM HAS BEEN ADVISED OF THE POSSIBILITY OF SUCH DAMAGES. In any event, the total liability of the Rightsholder and CCC (including their respective employees and directors) shall not exceed the total amount actually paid by User for the relevant License. User assumes full liability for the actions and omissions of its principals, employees, agents, affiliates, successors, and assigns.

12) **Limited Warranties.** THE WORK(S) AND RIGHT(S) ARE PROVIDED "AS IS." CCC HAS THE RIGHT TO GRANT TO USER THE RIGHTS GRANTED IN THE ORDER CONFIRMATION DOCUMENT. CCC AND THE RIGHTSHOLDER DISCLAIM ALL OTHER WARRANTIES RELATING TO THE WORK(S) AND RIGHT(S), EITHER EXPRESS OR IMPLIED, INCLUDING WITHOUT LIMITATION IMPLIED WARRANTIES OF MERCHANTABILITY OR FITNESS FOR A PARTICULAR PURPOSE. ADDITIONAL RIGHTS MAY BE REQUIRED TO USE ILLUSTRATIONS, GRAPHS, PHOTOGRAPHS, ABSTRACTS, INSERTS, OR OTHER PORTIONS OF THE WORK (AS OPPOSED TO THE ENTIRE WORK) IN A MANNER CONTEMPLATED BY USER; USER UNDERSTANDS AND AGREES THAT NEITHER CCC NOR THE RIGHTSHOLDER MAY HAVE SUCH ADDITIONAL RIGHTS TO GRANT.

13) **Effect of Breach.** Any failure by User to pay any amount when due, or any use by User of a Work beyond the scope of the License set forth in the Order Confirmation and/or the Terms, shall be a material breach of such License. Any breach not cured within 10 days of written notice thereof shall result in immediate termination of such License without further notice. Any unauthorized (but licensable) use of a Work that is terminated immediately upon notice thereof may be liquidated by payment of the Rightsholder's ordinary license price therefor; any unauthorized (and unlicensable) use that is not terminated immediately for any reason (including, for example, because materials containing the Work cannot reasonably be recalled) will be subject to all remedies available at law or in equity, but in no event to a payment of less than three times the Rightsholder's ordinary license price for the most closely analogous licensable use plus Rightsholder's and/or CCC's costs and expenses incurred in collecting such payment.

14) **Additional Terms for Specific Products and Services.** If a User is making one of the uses described in this Section 14, the additional terms and conditions apply:

a) ***Print Uses of Academic Course Content and Materials (photocopies for academic coursepacks or classroom handouts).*** For photocopies for academic coursepacks or classroom handouts the following additional terms apply:

i) The copies and anthologies created under this License may be made and assembled by faculty members individually or at their request by on-campus bookstores or copy centers, or by off-campus copy shops and other similar entities.

ii) No License granted shall in any way: (i) include any right by User to create a substantively non-identical copy of the Work or to edit or in any other way modify the Work (except by means of deleting material immediately preceding or following the entire portion of the Work copied) (ii) permit "publishing ventures" where any particular anthology would be systematically marketed at multiple institutions.

iii) Subject to any Publisher Terms (and notwithstanding any apparent contradiction in the Order Confirmation arising from data provided by User), any use authorized under the academic pay-per-use service is limited as follows:

A) any License granted shall apply to only one class (bearing a unique identifier as assigned by the institution, and thereby including all sections or other subparts of the class) at one institution;

B) use is limited to not more than 25% of the text of a book or of the items in a published collection of essays, poems or articles;

C) use is limited to no more than the greater of (a) 25% of the text of an issue of a journal or other periodical or (b) two articles from such an issue;

D) no User may sell or distribute any particular anthology, whether photocopied or electronic, at more than one institution of learning;

E) in the case of a photocopy permission, no materials may be entered into electronic memory by User except in order to produce an identical copy of a Work before or during the academic term (or analogous period) as to which any particular permission is granted. In the event that User shall choose to retain materials that are the subject of a photocopy permission in electronic memory for purposes of producing identical copies more than one day after such retention (but still within the scope of any permission granted), User must notify CCC of such fact in the applicable permission request and such retention shall constitute one copy actually sold for purposes of calculating permission fees due; and

F) any permission granted shall expire at the end of the class. No permission granted shall in any way include any right by User to create a substantively non-identical copy of the Work or to edit or in any other way modify the Work (except by means of deleting material immediately preceding or following the entire portion of the Work copied).

iv) Books and Records; Right to Audit. As to each permission granted under the academic pay-per-use Service, User shall maintain for at least four full calendar years books and records sufficient for CCC to determine the numbers of copies made by User under such permission. CCC and any representatives it may designate shall have the right to audit such books and records at any time during User's ordinary business hours, upon two days' prior notice. If any such audit shall determine that User shall have underpaid for, or underreported, any photocopies sold or by three percent (3%) or more, then User shall bear all the costs of any such audit; otherwise, CCC shall bear the costs of any such audit. Any amount determined by such audit to have been underpaid by User shall immediately be paid to CCC by User, together with interest thereon at the rate of 10% per annum from the date such amount was

originally due. The provisions of this paragraph shall survive the termination of this License for any reason.

b) ***Digital Pay-Per-Uses of Academic Course Content and Materials (e-coursepacks, electronic reserves, learning management systems, academic institution intranets).*** For uses in e-coursepacks, posts in electronic reserves, posts in learning management systems, or posts on academic institution intranets, the following additional terms apply:

i) The pay-per-uses subject to this Section 14(b) include:

A) **Posting e-reserves, course management systems, e-coursepacks for text-based content,** which grants authorizations to import requested material in electronic format, and allows electronic access to this material to members of a designated college or university class, under the direction of an instructor designated by the college or university, accessible only under appropriate electronic controls (e.g., password);

B) **Posting e-reserves, course management systems, e-coursepacks for material consisting of photographs or other still images not embedded in text,** which grants not only the authorizations described in Section 14(b)(i)(A) above, but also the following authorization: to include the requested material in course materials for use consistent with Section 14(b)(i)(A) above, including any necessary resizing, reformatting or modification of the resolution of such requested material (provided that such modification does not alter the underlying editorial content or meaning of the requested material, and provided that the resulting modified content is used solely within the scope of, and in a manner consistent with, the particular authorization described in the Order Confirmation and the Terms), but not including any other form of manipulation, alteration or editing of the requested material;

C) **Posting e-reserves, course management systems, e-coursepacks or other academic distribution for audiovisual content,** which grants not only the authorizations described in Section 14(b)(i)(A) above, but also the following authorizations: (i) to include the requested material in course materials for use consistent with Section 14(b)(i)(A) above; (ii) to display and perform the requested material to such members of such class in the physical classroom or remotely by means of streaming media or other video formats; and (iii) to "clip" or reformat the requested material for purposes of time or content management or ease of delivery, provided that such "clipping" or reformatting does not alter the underlying editorial content or meaning of the requested material and that the resulting material is used solely within the scope of, and in a manner consistent with, the particular authorization described in the Order Confirmation and the Terms. Unless expressly set forth in the relevant Order Conformation, the License does not authorize any other form of manipulation, alteration or editing of the requested material.

ii) Unless expressly set forth in the relevant Order Confirmation, no License granted shall in any way: (i) include any right by User to create a substantively non-identical copy of the Work or to edit or in any other way modify the Work (except by means of deleting material immediately preceding or following the entire portion of the Work copied or, in the case of Works subject to Sections 14(b)(1)(B) or (C) above, as described in such Sections) (ii) permit "publishing ventures" where any particular course materials would be systematically marketed at multiple institutions.

iii) Subject to any further limitations determined in the Rightsholder Terms (and notwithstanding any apparent contradiction in the Order Confirmation arising from data provided by User), any use authorized under the electronic course content pay-per-use service is limited as follows:

A) any License granted shall apply to only one class (bearing a unique identifier as assigned by the institution, and thereby including all sections or other subparts of the class) at one institution;

B) use is limited to not more than 25% of the text of a book or of the items in a published collection of essays, poems or articles;

C) use is limited to not more than the greater of (a) 25% of the text of an issue of a journal or other periodical or (b) two articles from such an issue;

D) no User may sell or distribute any particular materials, whether photocopied or electronic, at more than one institution of learning;

E) electronic access to material which is the subject of an electronic-use permission must be limited by means of electronic password, student identification or other control permitting access solely to students and instructors in the class;

F) User must ensure (through use of an electronic cover page or other appropriate means) that any person, upon gaining electronic access to the material, which is the subject of a permission, shall see:

- a proper copyright notice, identifying the Rightsholder in whose name CCC has granted permission,
- a statement to the effect that such copy was made pursuant to permission,
- a statement identifying the class to which the material applies and notifying the reader that the material has been made available electronically solely for use in the class, and
- a statement to the effect that the material may not be further distributed to any person outside the class, whether by copying or by transmission and whether electronically or in paper form, and User must also ensure that such cover page or other means will print out in the event that the person accessing the material chooses to print out the material or any part thereof.

G) any permission granted shall expire at the end of the class and, absent some other form of authorization, User is thereupon required to delete the applicable material from any electronic storage or to block electronic access to the applicable material.

iv) Uses of separate portions of a Work, even if they are to be included in the same course material or the same university or college class, require separate permissions under the electronic course content pay-per-use Service. Unless otherwise provided in the Order Confirmation, any grant of rights to User is limited to use completed no later than the end of the academic term (or analogous period) as to which any particular permission is granted.

v) Books and Records; Right to Audit. As to each permission granted under the electronic course content Service, User shall maintain for at least four full calendar years books and records sufficient for CCC to determine the numbers of copies made by User under such permission. CCC and any representatives it may designate shall have the right to audit such books and records at any time during User's ordinary business hours, upon two days' prior notice. If any such audit shall determine that User shall have underpaid for, or underreported, any electronic copies used by three percent (3%) or more, then User shall bear all the costs of any such audit; otherwise, CCC shall bear the costs of any such audit. Any amount determined by such audit to have been underpaid by User shall immediately be paid to CCC by User, together with interest thereon at the rate of 10% per annum from the date such amount was originally due. The provisions of this paragraph shall survive the termination of this license for any reason.

c) ***Pay-Per-Use Permissions for Certain Reproductions (Academic photocopies for library reserves and interlibrary loan reporting) (Non-academic internal/external business uses and commercial document delivery).*** The License expressly excludes the uses listed in Section (c)(i)-(v) below (which must be subject to separate license from the applicable Rightsholder) for: academic photocopies for library reserves and interlibrary loan reporting; and non-academic internal/external business uses and commercial document delivery.

i) electronic storage of any reproduction (whether in plain-text, PDF, or any other format) other than on a transitory basis;

ii) the input of Works or reproductions thereof into any computerized database;

iii) reproduction of an entire Work (cover-to-cover copying) except where the Work is a single article;

iv) reproduction for resale to anyone other than a specific customer of User;

v) republication in any different form. Please obtain authorizations for these uses through other CCC services or directly from the rightsholder.

Any license granted is further limited as set forth in any restrictions included in the Order Confirmation and/or in these Terms.

d) ***Electronic Reproductions in Online Environments (Non-Academic-email, intranet, internet and extranet).*** For "electronic reproductions", which generally includes e-mail use (including instant messaging or other electronic transmission to a defined group of recipients) or posting on an intranet, extranet or Intranet site (including any display or performance incidental thereto), the following additional terms apply:

i) Unless otherwise set forth in the Order Confirmation, the License is limited to use completed within 30 days for

any use on the Internet, 60 days for any use on an intranet or extranet and one year for any other use, all as measured from the "republication date" as identified in the Order Confirmation, if any, and otherwise from the date of the Order Confirmation.

ii) User may not make or permit any alterations to the Work, unless expressly set forth in the Order Confirmation (after request by User and approval by Rightsholder); provided, however, that a Work consisting of photographs or other still images not embedded in text may, if necessary, be resized, reformatted or have its resolution modified without additional express permission, and a Work consisting of audiovisual content may, if necessary, be "clipped" or reformatted for purposes of time or content management or ease of delivery (provided that any such resizing, reformatting, resolution modification or "clipping" does not alter the underlying editorial content or meaning of the Work used, and that the resulting material is used solely within the scope of, and in a manner consistent with, the particular License described in the Order Confirmation and the Terms.

15) **Miscellaneous.**

a) User acknowledges that CCC may, from time to time, make changes or additions to the Service or to the Terms, and that Rightsholder may make changes or additions to the Rightsholder Terms. Such updated Terms will replace the prior terms and conditions in the order workflow and shall be effective as to any subsequent Licenses but shall not apply to Licenses already granted and paid for under a prior set of terms.

b) Use of User-related information collected through the Service is governed by CCC's privacy policy, available online at www.copyright.com/about/privacy-policy/.

c) The License is personal to User. Therefore, User may not assign or transfer to any other person (whether a natural person or an organization of any kind) the License or any rights granted thereunder; provided, however, that, where applicable, User may assign such License in its entirety on written notice to CCC in the event of a transfer of all or substantially all of User's rights in any new material which includes the Work(s) licensed under this Service.

d) No amendment or waiver of any Terms is binding unless set forth in writing and signed by the appropriate parties, including, where applicable, the Rightsholder. The Rightsholder and CCC hereby object to any terms contained in any writing prepared by or on behalf of the User or its principals, employees, agents or affiliates and purporting to govern or otherwise relate to the License described in the Order Confirmation, which terms are in any way inconsistent with any Terms set forth in the Order Confirmation, and/or in CCC's standard operating procedures, whether such writing is prepared prior to, simultaneously with or subsequent to the Order Confirmation, and whether such writing appears on a copy of the Order Confirmation or in a separate instrument.

e) The License described in the Order Confirmation shall be governed by and construed under the law of the State of New York, USA, without regard to the principles thereof of conflicts of law. Any case, controversy, suit, action, or proceeding arising out of, in connection with, or related to such License shall be brought, at CCC's sole discretion, in any federal or state court located in the County of New York, State of New York, USA, or in any federal or state court whose geographical jurisdiction covers the location of the Rightsholder set forth in the Order Confirmation. The parties expressly submit to the personal jurisdiction and venue of each such federal or state court.

Last updated October 2022

American Physical Society
Reuse and Permissions License

13-Aug-2024

This license agreement between the American Physical Society ("APS") and Milan Rakic ("You") consists of your license details and the terms and conditions provided by the American Physical Society and SciPris.

Licensed Content Information

License Number:	**RNP/24/AUG/082239**
License date:	13-Aug-2024
DOI:	10.1103/PhysRevA.108.053321
Title:	Two-dimensional supersolidity in a planar dipolar Bose gas
Author:	B. T. E. Ripley, D. Baillie, and P. B. Blakie
Publication:	Physical Review A
Publisher:	American Physical Society
Cost:	USD $ 0.00

Request Details

Does your reuse require significant modifications: No

Specify intended distribution locations:	UK & Commonwealth (excluding Canada)
Reuse Category:	Reuse in a thesis/dissertation
Requestor Type:	Student
Items for Reuse:	Figures/Tables
Number of Figure/Tables:	2
Figure/Tables Details:	Figure 1, Figure 2
Format for Reuse:	Electronic

Information about New Publication:

University/Publisher:	Imperial College London
Title of dissertation/thesis:	Intertwined Order in Strongly Correlated Quantum Systems
Author(s):	Milan Rakic
Expected completion date:	Aug. 2024

License Requestor Information

Name:	Milan Rakic
Affiliation:	Individual
Email Id:	milan.p.rakic@gmail.com
Country:	United Kingdom

American Physical Society
Reuse and Permissions License

TERMS AND CONDITIONS

The American Physical Society (APS) is pleased to grant the Requestor of this license a non-exclusive, non-transferable permission, limited to Electronic format, provided all criteria outlined below are followed.

1. You must also obtain permission from at least one of the lead authors for each separate work, if you haven't done so already. The author's name and affiliation can be found on the first page of the published Article.

2. For electronic format permissions, Requestor agrees to provide a hyperlink from the reprinted APS material using the source material's DOI on the web page where the work appears. The hyperlink should use the standard DOI resolution URL, http://dx.doi.org/{DOI}. The hyperlink may be embedded in the copyright credit line.

3. For print format permissions, Requestor agrees to print the required copyright credit line on the first page where the material appears: "Reprinted (abstract/excerpt/figure) with permission from [(FULL REFERENCE CITATION) as follows: Author's Names, APS Journal Title, Volume Number, Page Number and Year of Publication.] Copyright (YEAR) by the American Physical Society."

4. Permission granted in this license is for a one-time use and does not include permission for any future editions, updates, databases, formats or other matters. Permission must be sought for any additional use.

5. Use of the material does not and must not imply any endorsement by APS.

6. APS does not imply, purport or intend to grant permission to reuse materials to which it does not hold copyright. It is the requestor's sole responsibility to ensure the licensed material is original to APS and does not contain the copyright of another entity, and that the copyright notice of the figure, photograph, cover or table does not indicate it was reprinted by APS with permission from another source.

7. The permission granted herein is personal to the Requestor for the use specified and is not transferable or assignable without express written permission of APS. This license may not be amended except in writing by APS.

8. You may not alter, edit or modify the material in any manner.

9. You may translate the materials only when translation rights have been granted.

10. APS is not responsible for any errors or omissions due to translation.

11. You may not use the material for promotional, sales, advertising or marketing purposes.

12. The foregoing license shall not take effect unless and until APS or its agent, Aptara, receives payment in full in accordance with Aptara Billing and Payment Terms and Conditions, which are incorporated herein by reference.

13. Should the terms of this license be violated at any time, APS or Aptara may revoke the license with no refund to you and seek relief to the fullest extent of the laws of the USA. Official written notice will be made using the contact information provided with the permission request. Failure to receive such notice will not nullify revocation of the permission.

14. APS reserves all rights not specifically granted herein.

15. This document, including the Aptara Billing and Payment Terms and Conditions, shall be the entire agreement between the parties relating to the subject matter hereof.